

Utah State University

DigitalCommons@USU

All Graduate Theses and Dissertations

Graduate Studies

12-2017

Measurement of Agriculture-Related Air Pollutant Emissions using Point and Remote Sensors

Kori D. Moore
Utah State University

Follow this and additional works at: <https://digitalcommons.usu.edu/etd>



Part of the [Civil and Environmental Engineering Commons](#)

Recommended Citation

Moore, Kori D., "Measurement of Agriculture-Related Air Pollutant Emissions using Point and Remote Sensors" (2017). *All Graduate Theses and Dissertations*. 6907.
<https://digitalcommons.usu.edu/etd/6907>

This Dissertation is brought to you for free and open access by the Graduate Studies at DigitalCommons@USU. It has been accepted for inclusion in All Graduate Theses and Dissertations by an authorized administrator of DigitalCommons@USU. For more information, please contact digitalcommons@usu.edu.



MEASUREMENT OF AGRICULTURE-RELATED AIR
POLLUTANT EMISSIONS USING POINT
AND REMOTE SENSORS

by

Kori D. Moore

A dissertation submitted in partial fulfillment
of the requirements for the degree

of

DOCTOR OF PHILOSOPHY

in

Civil and Environmental Engineering

Approved:

Randal Martin, Ph.D.
Major Professor

David Stevens, Ph.D.
Committee Member

Rhonda Miller, Ph.D.
Committee Member

Jiming Jin, Ph.D.
Committee Member

Michael Wojcik, Ph.D.
Committee Member

Mark R. McLellan, Ph.D.
Vice President for Research and
Dean of the School of Graduate Studies

UTAH STATE UNIVERSITY
Logan, Utah

2017

Not Copyrighted

Data collection funded by the Agriculture Research
Service, United States Department of Agriculture

ABSTRACT

Measurement of Agriculture-Related Air Pollutant

Emissions using Point and Remote Sensors

by

Kori D. Moore, Doctor of Philosophy

Utah State University, 2017

Major Professor: Dr. Randal S. Martin
Department: Civil and Environmental Engineering

Measuring air pollution emissions from agricultural sources is complicated by their size and variability. Traditional point sensors may not adequately characterize plumes as variability in the plume transport may affect which sensors are impacted. Remote sensors, such as a scanning light detection and ranging (lidar) system, provide advantages due to their large sampling volumes, temporal resolution, and spatial scales. Both point and remote sensors were used to characterize plumes and estimate emissions from multiple agricultural operations. The purposes of this work were to further develop methodologies for measuring agricultural air pollution emissions and to report emissions for several varying types of operations.

The body of this dissertation is comprised of five chapters, where each chapter is a separate paper submitted for publication in a peer-reviewed journal. Their topics

include: an in-depth discussion of the mass conversion factor used to convert optical measurements, such as backscatter lidar, to particulate matter (PM) mass concentrations; calculating the PM emissions control efficiency of two conservation management practices (CMP) over the traditional management practices using lidar, particle size distribution, and filter-based PM data; the use of passive diffusion sampler and open path-Fourier transform infrared spectrometer measurements to estimate ammonia (NH_3) emissions from an open-lot dairy; and the development, initial testing, and first application of a backwards Lagrangian stochastic (bLS) dispersion model for use in inverse modeling that allows particle behavior to deviate from the surrounding flow.

These papers contribute to emissions measurement methodologies for area sources through the publication of the deposition-enabled bLS tested for near-source inverse modeling and its impact on emissions estimates, the lidar-based methods used in the tillage CMP studies, and the use of a scanning OP-FTIR system to measure NH_3 levels downwind of a dairy. Calculated emissions were published for multiple tillage activities, resulting in CMP reductions ranging from 25% to 90% over traditional practices. Summer time emissions of NH_3 from an open-lot dairy and PM_{10} from a beef feedlot were calculated through inverse modeling and were similar to summer emissions found in literature. Including particle behavior in the bLS increased PM_{10} emissions by 8-20% over the diurnal cycle.

PUBLIC ABSTRACT

Measurement of Agriculture-Related Air Pollutant

Emissions using Point and Remote Sensors

Kori D. Moore

Measuring air pollution emissions from agricultural activities is usually difficult because of their large area and variability. Traditional air quality sensors, called point samplers, measure conditions in one location, which may not adequately measure a plume. Remote sensors, instruments that measure pollution along a line rather than at a single point, are better able to measure conditions around large areas. This dissertation reports on four agricultural air emissions studies that used both point and remote sensors for comparison. The methods used to calculate the emissions are based on previous work and are further developed in these studies. In particular, an atmospheric dispersion model was developed and tested that can account for a particle behaving different than the surrounding gas due to gravity and inertia and depositing out of the flow. Particulate matter (PM) emissions values are reported for two agricultural tillage conservation management practices (CMPs) and the corresponding traditional tillage methods in order to determine how well the CMP reduces emissions. In addition, gas-phase ammonia (NH_3) emissions for a dairy operation and PM emissions from a feedlot operation are reported. These studies can help us better measure emissions from agricultural operations and understand how much air pollution is being emitted.

ACKNOWLEDGMENTS

I thank the Utah State University Research Foundation, Space Dynamics Laboratory, Agriculture Research Service, Texas A&M AgriLife Research, and Utah Water Research Laboratory for providing project funding and additional support. I also thank the Space Dynamics Laboratory for the SDL Fellowship, as well as the Rocky Mountain Section of the Air & Waste Management Association for a scholarship.

I wish to thank my committee members, Dr. Randy Martin, Dr. David Stevens, Dr. Michael Wojcik, Dr. Rhonda Miller, and Dr. Jiming Jin, for their support, comments, and suggestions throughout this entire process. A very special thank you is in order for my major professor, Dr. Randy Martin, for his guidance, support, and example.

The following individuals deserve recognition for their support during this work: Brooke McKenna and Scott Anderson with the Space Dynamics Laboratory; Dr. Gail Bingham and Dr. Christian Marchant, formerly with the Space Dynamics Laboratory; Jeff Muhs, formerly with the Energy Dynamics Laboratory; and Dr. Jerry Hatfield and Dr. John Prueger with the Agriculture Research Service. I would like to acknowledge and give thanks to the individuals too numerous to name involved in sample collection, data processing, and support activities, particularly those involved in the long, off-site field studies. Those field studies would not have been possible without the permission and support from forward thinking agricultural producers and agricultural advocates.

I would particularly like to thank my wife, Liz, for her continued support, love, encouragement, and prayers. I also thank our five children, Spencer, Matthew, Olette, Conrad, and Lucy, for their constant encouragement and love. My family has been key to my accomplishments. I acknowledge the continued encouragement of extended family, especially from my parents, Daryl and Treena Moore and David and Becky Cook. I would also like to thank my friends and peers for their encouragement. I must express my gratitude towards my Heavenly Father – I am grateful for this blessing and journey.

Kori D. Moore

CONTENTS

	Page
ABSTRACT	iii
PUBLIC ABSTRACT	v
ACKNOWLEDGMENTS	vi
LIST OF TABLES	x
LIST OF FIGURES	xiii
EXECUTIVE SUMMARY	xvi
CHAPTER	
I. INTRODUCTION	1
Background	3
Objective	6
Instrumentation	8
Calculating Emissions	11
Manuscript Summaries	13
Literature Review	22
References	25
II. DERIVATION AND USE OF SIMPLE EMPIRICAL RELATIONSHIPS BETWEEN AERODYNAMIC AND OPTICAL PARTICLE MEASUREMENTS	32
Abstract	32
Introduction	33
Methodology	35
Results and Discussion	47
Summary and Conclusions	64
Acknowledgments	65
References	66

III. PARTICULATE EMISSIONS CALCULATIONS FROM FALL TILLAGE OPERATIONS USING POINT AND REMOTE SENSORS	70
Abstract	70
Introduction	71
Materials and Methods	74
Results and Discussion	84
Conclusions	98
Acknowledgments	99
References	100
IV. PARTICULATE MATTER EMISSIONS ESTIMATES FROM AGRICULTURAL SPRING TILLAGE OPERATIONS USING LIDAR AND INVERSE MODELING	103
Abstract	103
Introduction	104
Methodology	107
Results and Discussion	129
Conclusions	149
Acknowledgments	150
References	151
V. AMMONIA MEASUREMENTS AND EMISSIONS FROM A CALIFORNIA DAIRY USING POINT AND REMOTE SENSORS	157
Abstract	157
Introduction	158
Materials and Methods	160
Results and Discussion	185
Conclusions	209
Acknowledgments	210
References	211
VI. USING A DEPOSITION-ENABLED BACKWARD LAGRANGIAN STOCHASTIC MODEL TO ESTIMATE PARTICULATE MATTER AREA SOURCE EMISSIONS THROUGH INVERSE MODELING	217
Abstract	217

	Page
Introduction	218
Model Formulation	222
Model Testing	230
Results and Discussion	241
Conclusions	257
Acknowledgments	259
References	259
VII. CONCLUSIONS	264
VIII. ENGINEERING SIGNIFICANCE	269
APPENDICES	271
Appendix A: Data	272
Appendix B: Journal Copyright Releases	273
Appendix C: Permission-to-Use Letters.....	280
Appendix D: List of Acronyms and Symbols	296
Appendix E: Vitae	303

LIST OF TABLES

Table		Page
1-1	Major field deployments within the Ag Program.....	6
2-1	Conditions during each field campaign for which the mass conversion factor (MCF) has been calculated and included in this manuscript.....	45
2-2	Statistical measures of the intra- and inter-instrument comparability test datasets (including outliers) conducted in March 2004 and July 2007.....	62
3-1	Sample schedule and sample period tillage and meteorological characteristics.....	76
3-2	Manufacturer, precision, and accuracy information for deployed meteorological instrumentation.	78
3-3	Comparison of average particulate matter (PM) mass concentrations with respective 95% confidence intervals (CI) about the mean as reported by collocated MiniVol PM samplers, optical particle counters (OPCs), and lidar (light detection and ranging) at an upwind and downwind location for the 23 Oct. sample period.	90
3-4	Mean emissions rates (ER) \pm 95% confidence intervals (CIs) calculated using inverse modeling with AERMOD and filter-based particulate matter (PM) measurements and the mass balance technique applied to PM calibrated lidar data.....	91
3-5	Mean emission factors (EF) \pm 95% confidence intervals (CIs) calculated via inverse modeling with AERMOD and filter-based particulate matter (PM) measurements and the mass balance technique with PM calibrated lidar data for each operation, as well as the calculated control efficiencies of the Combined Operations CMP method.	92
4-1	Information for each sample period regarding tillage operations, equipment used, tractor operation time, area worked, and sample time.....	111

Table	Page
4-2 Manufacturer, precision, and accuracy information for deployed meteorological instrumentation.	116
4-3 Period-averaged meteorological measurements $\pm 1\sigma$ made at the upwind meteorological tower.	131
4-4 Mass conversion factors (MCFs) used to convert optical particle measurements to mass concentrations for each sample day and averaged for the whole campaign.	136
4-5 Comparison of period average PM mass concentrations as reported by collocated MiniVol filter samplers and OPCs, as well as the adjacent lidar bin, at measurement heights of 9 m agl at upwind and downwind tower locations for the 18 June sample period.	144
4-6 Average particulate matter (PM) emission factors and 95% confidence intervals (CI) estimated for the conventional and conservation tillage management practices.	146
5-1 Animal count, average animal mass, average feed characteristics, and estimated manure and nitrogen excreted for cattle on this dairy during the study period.	162
5-2 Meteorological instruments employed in this study.	169
5-3 Comparison of average meteorological conditions (± 1 SD) measured at the dairy from 13-20 June 2008 and at a site in Kings County for the same period, the full month of June 2008, and June from 1998-2007.	187
5-4 Statistics of emission factors (EFs) calculated for both NH ₃ measurement datasets using the following three optimization procedures: Unconstrained – EF values for pen and liquid manure system (LMS) are unconstrained; Constrained – constraints are imposed on the minimum values for pen and LMS EFs, based on minimum values found in literature; and Sequential – pen EF estimated first from samples impacted only by pens, then the LMS EF is estimated from samples impacted by both pens and LMS.	198

Table		Page
5-5	Comparison of dairy NH ₃ emission factors (EFs) estimated from this study with EFs reported in literature.	201
6-1	The d_p and the average v_s values used in configuration testing of the LS models.	246
6-2	Comparison of feedlot PM ₁₀ emissions(Q_{PM10}) and surface fluxes calculated in this study with some found in literature.	256

LIST OF FIGURES

Figure	Page
1-1 The Aglite Lidar with the 532 nm laser beam visible.	9
2-1 Scatter plots of data from V_k and PM_k for the following values of k : a) 1.0 μm , b) 2.5 μm , c) 10 μm , and d) TSP.	48
2-2 A box and whisker plot of period averaged MCF_k values.	50
2-3 Time series of PM_{10} concentrations measured immediately downwind of a dairy farm over two days as measured by a collocated MiniVol and OPC.	54
2-4 Example of PM_{10} concentrations calculated from a single lidar scan through the use of the MCF.	55
2-5 Comparison of $PM_{2.5}$ and PM_{10} concentrations reported by the MiniVols and the respective FRM samplers.	60
3-1 Sample layouts for particulate matter (PM) and meteorological measurements made during a) conventional tillage operations in Field A and b) the combined operations conservation management practice operations in Field B.	79
3-2 Period-averaged PM_{10} concentrations ($\mu\text{g m}^{-3}$) resulting from the tillage activity on 23 Oct. along the vertical downwind lidar scanning plane as a) estimated by lidar (average downwind minus average upwind) and b) predicted by AERMOD using the Lidar-derived emission rate for this sample period.	88
3-3 Lidar measured downwind PM_{10} concentrations ($\mu\text{g m}^{-3}$) from a single vertical scan on 23 Oct; a tillage plume is seen crossing the lidar scan at a range of 600 m and centered at 50 m above ground level.	96
4-1 Map of fields under study and the sample layout for each field.	110
4-2 Process diagram for lidar PM calibration algorithm.	123

Figure	Page
4-3	Wind rose for the hourly averaged wind observations during the days on which samples were collected. 130
4-4	Sample period-averaged upwind and downwind PSDs as measured by OPCs for (a) 17 May, strip-till operation, Field 5, (b) 18 May, chisel operation, Field 4, (c) 5 June, plant operation, Field 4, and (d) 7 June, plant and fertilize operation, Field 5. 134
4-5	Time series of PM ₁₀ concentrations as reported by the collocated OPC, MiniVol filter sampler, and lidar at 9 m agl on the downwind side of the tillage activity for the 18 June sample period (14:00 – 16:10). 139
4-6	Lidar-derived PM ₁₀ in a time versus distance from the lidar concentration map (top) and a time series average concentration versus distance from the lidar graph (bottom). 141
4-7	Image of plumes in a vertical scan on 5 June. 142
5-1	Map of dairy pens, storage, and sampling locations. 163
5-2	Hourly average wind conditions measured at the dairy during the measurement periods, 13-20 June 2008. 187
5-3	NH ₃ concentration (ppbv) measured by both the upwind and downwind OP-FTIR instruments at ~ 2m agl. 190
5-4	Estimated diurnal emissions profiles for the pens, liquid manure system (LMS), and the entire facility based on 2 h averaged OP-FTIR data. 207
6-1	Satellite image of the feedlot under study with particle and meteorological measurement locations shown, as well as the facility and pen borders. 232
6-2	Measured values for wind speed (u) and direction (θ) and calculated values for shear velocity (u^*) and the inverse of Monin-Obukov length ($1/L$) as 30 min averages throughout the collection period. 242

Figure	Page
6-3	PM ₁₀ concentrations measured at the feedlot by the upwind (Site 7) and downwind (Sites 1, 2, 4, and 6) TEOMs as 30 min averages..... 243
6-4	(a) Example particle size distributions (PSDs) measured by the OPS at Site 3 averaged over 30 min periods and (b) the PM ₁₀ concentration calculated from the OPS PSD measured at Site 3 compared with TEOM PM ₁₀ from adjacent sites 2 and 4..... 244
6-5	Touchdown and deposition counts as a function of d_p for the fLS model and two bLS model runs with different particle release heights (z_{rel}). 247
6-6	Histograms of touchdowns and depositions versus distance from the source volume at $[0,0,z_{rel}]$ for bLS models with $z_{rel} = 2.0$ m and 0.205 m and the fLS with $z_{rel} = 0.205$ m for $d_p = 10$ μ m and a bin width of 100 m..... 249
6-7	The relative fLS $(C/Q_{Vol})_{sim}$ values for randomly selected sample periods for particles with d_p of (a) 0 μ m, (b) 1 μ m, (c) 2.5 μ m, (d) 5.0 μ m, (e) 10 μ m, (f) 20 μ m, (g) 30 μ m, (h) 40 μ m, and (i) 50 μ m. 251
6-8	Emission rates ($Q_{m, count}$) calculated from the (a) fLS and (b) bLS models as applied to the Texas feedlot for a subset of 30 sample periods and assuming a particle concentration of 1.0 particles m ⁻³ for each d_p 252
6-9	Diurnal pattern of calculated Deposition feedlot PM ₁₀ emissions (Q_{PM10}) and Non-deposition Q_{PM10} as two hour averages (left axis) and the number of Q_{PM10} values in each half hour sampling period throughout the day (right axis)..... 254

EXECUTIVE SUMMARY

The purposes of the work described in this dissertation were to contribute to the information on and methodologies for measuring air pollution emissions from large area sources, specifically targeted toward agricultural facilities but also applicable to other difficult to characterize area sources, and to provide emissions values for several different agricultural processes/operations. The size and temporally and spatially variable nature of these systems can significantly complicate efforts to quantify emissions. Point sensors may be challenged to adequately represent concentrations inside large plumes using relatively few sampling points at ground level. Remote sensors, such the scanning light detection and ranging (lidar) and open-path Fourier transform infrared spectrometer (OP-FTIR) systems employed herein, have an advantage due to their large sampling volumes, spatial extents, and temporal resolution. This work utilizes both point and remote sensors to measure plume concentrations and estimate emissions from multiple agricultural operations.

The body of this dissertation is comprised of five chapters, where each chapter is a separate paper that was submitted for publication in a peer-reviewed journal. The first paper presents an in-depth discussion of the mass conversion factor (MCF) used to convert optical particle measurements to particulate matter (PM) mass concentrations. Examples of information gained through its application were provided, including observations of PM dynamics at finer temporal and spatial scales and greater spatial

extents. Specifically, vertical PM-calibrated lidar scans mapped the concentrations in plumes observed above the point sensor array.

The second and third papers utilized PM-calibrated lidar and optical particle counter data to estimate the emissions control efficiency (η) of two conservation management practices (CMP) over the traditional management practices. Emissions were calculated with a mass balance method applied to vertical lidar scans and through inverse modeling with point sensor data. The first study presented the first known investigation of reductions from a combined operations CMP, calculating η of 29%, 60%, and 25% for PM_{2.5}, PM₁₀, and TSP, respectively. The second study examined emissions from a spring tillage conservation tillage CMP and found η of approximately 90% for PM_{2.5}, PM₁₀, and TSP, similar to a previous conservation tillage CMP η measurement.

The fourth paper reported an NH₃ emissions study of an open-lot dairy in the San Joaquin Valley (SJV) of California, the first known summer time measurements in that climate. Concentration measurements were made using multiple passive samplers and a scanning system to achieve multiple OP-FTIR beam paths in a repeating series. This was the first known implementation of such a system with OP-FTIR. Emissions were estimated through inverse modeling with both datasets, yielding $140.7 \pm 42.5 \text{ g d}^{-1} \text{ animal}^{-1}$ ($113.5 \pm 34.3 \text{ g d}^{-1} \text{ AU}^{-1}$) for the passive sampler data and $199.2 \pm 22.0 \text{ g d}^{-1} \text{ animal}^{-1}$ ($160.8 \pm 17.8 \text{ g d}^{-1} \text{ AU}^{-1}$) for OP-FTIR data. These values were within the range of emissions in the literature for an open-lot dairy.

The fifth manuscript presented the formulation and initial testing of a Lagrangian stochastic (LS) atmospheric dispersion model for near-field inverse modeling that allows for a particle's movement in the air to deviate from the air motion due to settling velocity and deposition. It is the first publication of a deposition-enabled LS model being tested in a backward-in-time (bLS) configuration. A bLS has significant computational and run time advantages over the forward-in-time (fLS) versions for an area source. Initial evaluation of the modified bLS with a validation dataset yielded good results in a non-depositional case. In addition, the modified fLS and bLS were applied to a PM dataset from a commercial feedlot. Testing showed very consistent results between the two for particle sizes $\leq 20 \mu\text{m}$. Using the modified bLS produced PM_{10} emissions between 8% and 20% higher than the non-deposition model throughout the diurnal cycle, with total daily emissions being 12% larger at $62.5 \pm 12.4 \text{ g animal}^{-1} \text{ day}^{-1}$.

This collection of papers fulfills the purposes of this work to contribute to the field of emissions measurement methodology for large area sources and publication of emissions values for various agricultural operations. First-of-a-kind data were published on the deposition-enabled bLS for near-source inverse modeling, the η of a combined operations CMP for the fall tillage sequence, the use of a scanning OP-FTIR system to measure NH_3 levels downwind of a dairy, and NH_3 emissions from a SJV dairy during summer. Additionally, the conservation tillage CMP η for spring tillage supported the findings of the only other known study. PM_{10} emissions calculated from the feedlot using the modified bLS were high compared to most in the literature but in line with

another summer time measurement. The ability of the lidar to observe and measure plumes not well sampled by point sensors or reproduced in the air dispersion model was demonstrated in both tillage studies.

CHAPTER 1

INTRODUCTION

Over 100 epidemiological studies published over the past 30 years have linked both short-term and long-term ambient air pollution exposure to a long and growing list of increased human health and welfare risks, including increased hospitalization and mortality rates (see Pope, 1989; Dockery et al., 1993; Davidson et al., 2005; Pope and Dockery, 2006; Qian et al., 2007; Geer et al., 2012; Pope et al., 2013; O'Neal et al., 2017; Turner et al., 2017; and many others). Exposure to air pollutants can also lead to acute and chronic effects in animals, plants, and ecosystems. These effects have led governments worldwide to set ambient concentration (C) and/or exposure limits for many air pollutants. The limits in the United States are called the National Ambient Air Quality Standards (NAAQS) and are set by the Environmental Protection Agency (EPA). Currently, there are NAAQS for particulate matter (PM) with aerodynamic equivalent diameters (d_a) $\leq 2.5 \mu\text{m}$ ($\text{PM}_{2.5}$) and with $d_a \leq 10 \mu\text{m}$ (PM_{10}), nitrogen dioxide (NO_2), sulfur dioxide (SO_2), ozone (O_3), lead (Pb), and carbon monoxide (CO) (EPA, 2017). If these are exceeded, local air regulatory authorities are required to develop and implement pollution remediation strategies to reduce concentrations to below the NAAQS. Among other things, this necessitates a robust understanding of the emissions (Q) of significant air pollutant sources.

Since the passage of the Clean Air Act in 1970, most anthropogenic pollutant sources have been investigated and their emissions drastically reduced (Cooper and

Alley, 2002). The agricultural sector is one of few air pollution source categories not highly regulated. However, impacts and potential reductions from agricultural sources are increasingly being investigated as the cost of emissions reductions in non-agricultural sectors grow. Agricultural sources of air pollution have been investigated for their impact on local, regional, and global atmospheric pollution loadings since the 1990s. Studies have documented the following pollutants emitted from various agricultural sources: particles of various sizes suspended in the air, also referred to as PM; ammonia (NH_3); hydrogen sulfide (H_2S); oxides of nitrogen (NO_x); oxides of sulfur (SO_x); methane (CH_4); carbon monoxide (CO); carbon dioxide (CO_2); nitrous oxide (N_2O); and volatile non-methane organic hydrocarbons (NMHCs) (Casey et al., 2006). None of these pollutants are exclusive to agricultural activities – all are emitted by other anthropogenic and natural sources.

Agricultural operations, however, may present challenges to determining emissions generally not found in other air pollution sources. Difficulties arise due to large spatial extents of the source(s), temporal and spatial variations in emissions, and influences of meteorological and process conditions on measuring a source's impact on air pollutant levels in an often ill-defined plume. Typical approaches that have been developed for estimating emissions of such large and open sources are the inverse modeling, flux-gradient profiling, eddy covariance, and flux chamber methods. The first three use the difference between measurements of upwind and downwind concentrations and relate that value to emissions through different methods of

estimating or measuring the strength of atmospheric mixing. The fourth samples a small portion of the source surface to measure emissions directly in multiple locations and assumes the sample locations are representative of the source.

Another complication may arise from the use of point samplers due to their relatively small sample volume and limited numbers feasibly deployed. Remote sensors, such as light detection and ranging (lidar) and open path Fourier transform infrared spectroscopy (OP-FTIR) systems, offer an advantage over point sensors in that they can measure pollutant concentrations over a much greater volume, distance, and, usually, time. This allows for a greater characterization of the downwind plume and emissions. The work described in this dissertation includes developments and applications of emissions quantification using both point and remote sensors to measure pollutant levels. In addition, a modified air dispersion model that has not previously been reported is detailed and tested against both validation and real-world datasets.

Background

The National Research Council (NRC) released a report in 2003 focusing on the state of the science and future needs in livestock agriculture air pollutant emissions (NRC, 2003). This document lists 13 findings and sets of recommendations, one of which highlighted gaps in emissions measurement methodologies:

“FINDING 7: Scientifically sound and practical protocols for measuring air concentrations, emission rates, and fates are needed for the various elements (nitrogen, carbon, sulfur), compounds (e.g., ammonia [NH₃], CH₄, H₂S), and particulate matter.

RECOMMENDATIONS:

- Reliable and accurate calibration standards should be developed, particularly for ammonia.
- Standardized sampling and compositional analysis techniques should be provided for PM, odor, and their individual components.”

- NRC (2003)

Several research efforts have been carried out in response to the NRC report, such as the National Agriculture Emissions Monitoring Study (NAEMS, Heber et al., 2008). A research effort to address the measurement methodology gap began in 2004 by the U.S. Department of Agriculture’s (USDA) Agricultural Research Service (ARS), Utah State University Research Foundation’s Space Dynamics Laboratory (SDL), and Utah State University (USU). A portion of the research efforts of this program, referred to as “the Ag Program”, will be the focus of this dissertation.

SDL entered into a Cooperative Agreement with the ARS with the following objectives:

“1) Develop new methods and improve existing methods to measure emissions of particulate matter and gases from animal feeding operations; 2) Develop and determine the effectiveness of management practices and control technologies to reduce emissions; and 3) Develop tools to predict emissions and their dispersion across a range of animal production systems, management practices, and environmental conditions.”

- Specific Cooperative Agreement, No. 58-3625-4-121

SDL and USU have worked to accomplish these objectives in cooperation with the ARS and under the direction of Dr. Jerry Hatfield, Laboratory Director for the National Laboratory for Agriculture and the Environment, USDA ARS.

Through the Ag Program, a collection of both point and remote sensors were assembled into a system capable of measuring PM and gaseous concentrations around large, open agricultural sources. The main gaseous species of interest was NH_3 , though capabilities were tested for NO_x and methane (CH_4). The PM size fractions the system was capable of measuring were PM with $d_a \leq 1.0 \mu\text{m}$ (PM_{10}), $\text{PM}_{2.5}$, PM_{10} , and total suspended PM (TSP). These measurement systems were deployed in 12 field studies between 2005 and 2012, as shown in Table 1-1.

Methods to estimate emissions have been developed or enhanced as part of the Ag Program efforts and applied to most of the datasets in Table 1-1. One focus of the Ag Program was to publish these methods and calculated emissions values in peer-reviewed journals and books in order to contribute to the body of knowledge on agricultural air pollutant emissions. To date, one book chapter has been published (Wojcik et al., 2012) and nine papers (Bingham et al., 2009; Marchant et al., 2009, 2011; Martin et al., 2008; Moore et al., 2013, 2014, 2015a, 2015b; and Zavyalov et al., 2009). In addition, results from most of these tests have been presented at various scientific conferences and meetings.

Table 1-1. Major field deployments within the Ag Program.

Measurement Period	State	Facility/Operation Studied	Pollutant(s) Measured
August – September 2005	IA	Finishing swine facility	PM, NH ₃
November 2005	UT	Research dairy	PM, NH ₃
September – October 2006	CA	Almond harvesting	PM
December 2006	CA	Cotton ginning	PM
September – October 2007	ID	Wastewater holding ponds on a commercial dairy	NH ₃
October 2007	CA	Fall tillage	PM
May – June 2008	CA	Spring tillage	PM
June 2008	CA	Commercial dairy	PM, NH ₃
June 2009	UT	Chemical/biological simulant release	PM
October 2009	UT	Hydrocarbon production wastewater evaporation treatments	PM, NO _x , CH ₄
July 2011	UT	Chemical/biological simulant release	PM
August 2012	CA	Commercial dairy	PM

Objective

The objective of this dissertation work is to advance the state of the science regarding methods to quantify air pollutant emissions from agricultural sources and to contribute to the body of literature on emissions values. These were accomplished using Ag Program activities involving both point and remote sensors. Specifically, this work will demonstrate:

- 1) the development and/or application of variations on emission measurement techniques not previously employed in either the Ag Program or by others;

- 2) the establishment of in depth descriptions of the techniques used by the Ag Program; and
- 3) the publication of air pollutant emissions from various agricultural activities in internationally-recognized scientific journals.

The body of this work is a collection of five manuscripts that have been submitted for publication in scientific journals. Four have already been accepted and published and the fifth was submitted in April 2017 for consideration. The manuscript topics include: (1) a detailed description of the relation between the optical and aerodynamic PM measurement techniques, referred to as the mass conversion factor (MCF), and examples of how it has been used in Ag Program studies to monitor PM levels and emissions in greater temporal and spatial scales versus using traditional sensors; (2) differences in PM emissions between a traditional tillage management practice and a combined operations conservation management practice (CMP) as measured in the 2007 fall tillage study; (3) differences in PM emissions between a traditional spring tillage management practice and a conservation tillage CMP as measured in the 2008 spring tillage study; (4) dairy NH_3 emissions based on NH_3 concentration datasets from both point and remote sensing measurement techniques employed in the 2008 commercial dairy study; and (5) the development and initial testing of a backward Lagrangian stochastic (bLS) model, including algorithms for size-dependent deposition, for particles that can be used in estimating PM emission rates through inverse modeling. Chapters 2 through 6 of this dissertation present the

manuscripts as published (papers 1 through 4) or submitted (paper 5). Each contributes new information on measuring plume concentrations and estimating emissions from area sources and fulfills at least one stated objective in the Cooperative Agreement.

Instrumentation

This section provides a summary description of the instruments used in the Ag Program to measure ambient air pollutant levels. The next section describes, generally, how these measurements have been employed in the emissions calculation techniques. Each field study utilized a different combination of sensors, configurations, and emission estimation methodologies, as described in the following chapters.

The signature instrument of the Ag Program is Aglite, a custom-built elastic lidar system described by Marchant et al. (2009) and shown in Figure 1-1. Aglite emits pulses of light at three different wavelengths (355 nm, 532 nm, and 1,064 nm) simultaneously and measures the amount of energy returned to the instrument from the particles and molecules in the atmosphere, which is referred to as backscatter. Combining backscatter data from the three wavelengths in a single analysis potentially allows for a greater understanding of the physical and optical properties of the particles and molecules in the beam. The lidar return signals were calibrated to PM concentrations through an algorithm developed as part of the Ag program and described by Zavyalov et al. (2009). In summary, the algorithm uses particle size distribution (PSD) data to calibrate the lidar return signal to the PSD and the cumulative particle volume



Figure 1-1. The Aglite Lidar with the 532 nm laser beam visible.

concentrations (V_k), up to a particle diameter k . V_k is multiplied by MCF_k to yield PM_k , where MCF_k is a simple scalar value relating PM_k and V_k . This relationship is the subject of Chapter 2.

The PSDs were measured by battery-powered optical particle counters (OPCs) (Aerosol Profilers, Model 9712, Met One Instruments, Inc., Grants Pass, OR). These OPCs have eight size bins with lower bin limits ranging from 0.3 μm to 10.0 μm . An OPC reports number of particles detected in each size bin over a sample period, usually set at 20 seconds for Ag Program activities. An OPC measures optical diameter (d_{op}) with a laser, utilizing the same measurement principle as an elastic lidar.

MiniVol Portable Air Samplers (Models 4.2 and 5.0, Airmetrics, Eugene, OR) were used to measure PM_k in Ag Program deployments. It is a portable, battery-powered unit that collects ambient aerosol onto filters; PM_k is calculated by measuring mass accumulation on exposed filters and dividing by the volume of sampled air. Separation of particles greater than a desired cumulative size k is accomplished by an impactor plate assembly upstream of the filter. These systems can be configured to measure $PM_{1,}$ $PM_{2.5}$, PM_{10} , or TSP.

Gaseous NH_3 was measured using both passive samplers and an OP-FTIR. The passive samplers employed were from Ogawa USA, Inc. (Pompano Beach, FL), which utilize a filter infused with citric acid to collect gaseous NH_3 for analysis through ion chromatography (IC). The mass of detected NH_3 is related to a period-averaged concentration through the diffusion equations described by Roadman et al (2003).

The OP-FTIR was a monostatic unit manufactured by MDA used to measure NH_3 levels within the units beam path (Model ABB-Bomen MB-100, Atlanta, GA, now Cerex Monitoring Solutions, LLC, Atlanta, GA). A monostatic unit has the source, interferometer, and detector at one end of the path and a retroreflecting mirror at the other end to direct the beam back to the detector. A scanning system was designed for use with this OP-FTIR with multiple retroreflectors in order to determine NH_3 levels along multiple path lines from a single instrument location. Quantification of the path-length averaged concentration was performed using a partial least squares regression

technique with instrument-specific calibration parameters (Griffiths et al., 2009; Shao et al., 2010).

Meteorological parameters monitored during system deployments include vertical and horizontal wind speeds, wind direction, temperature, relative humidity, and incoming solar radiation. This was accomplished through an assortment of instrumentation that varied slightly between field studies. Specific configurations are described in each paper.

Calculating Emissions

The pollutant concentration data were used to derive pollutant emission rates (ERs) and emission factors (EFs). The definition of ER and EF generally vary by operation type. In the case of the manuscripts, there are two ER and EF definitions utilized. For those studies estimating emissions from agricultural tillage operations, EFs are emissions based on a quantity of field processed (e.g., g m^{-2}) and ERs are emissions that include a time factor (e.g., $\text{g m}^{-2} \text{sec}^{-1}$). In the studies estimating emissions from the dairy and feedlot operations, EFs are emission values on a per animal or per animal unit (AU) and per unit time basis (i.e., $\text{g d}^{-1} \text{animal}^{-1}$, $\text{kg yr}^{-1} \text{AU}^{-1}$), while ERs are based on time but not per animal (i.e., kg d^{-1} , $\text{g m}^{-2} \text{sec}^{-1}$). References to an ER or EF are generic through this section and do not have a specific set of associated units.

ERs and EFs were calculated in the Ag Program using inverse modeling and a mass balance method. Inverse modeling uses an initial estimate of the emission rate

(Q_{sim}) in an atmospheric dispersion model to predict the resulting downwind concentration (C_{sim}). The $(C/Q)_{sim}$ ratio is then used in the following equation with the concentrations measured at the facility to calculate the observed emission rate (Q_{calc}):

$$Q_{calc} = \frac{C_{downwind} - C_{upwind}}{(C/Q)_{sim}} \quad (1-1)$$

In this equation, C_{upwind} is subtracted from $C_{downwind}$ to determine concentrations resulting from the source(s). It is this difference that is compared against the modeled $(C/Q)_{sim}$ ratio because the models do not generally account for C_{upwind} , unless a background concentration is explicitly used as an input.

In cases where the dispersion model used yields a proportionally linear response in C_{sim} to changes in Q_{sim} , the initial estimate of Q_{sim} will not affect Q_{calc} as the $(C/Q)_{sim}$ ratio describes the slope of the line relating the two terms and has neither local maxima nor minima. In cases where the C_{sim} response is not necessarily linear, local maxima or minima are possible, requiring a wide range of Q_{sim} to be tested.

There were two atmospheric dispersion models used to estimate $(C/Q)_{sim}$. Most studies used the American Meteorological Society/US Environmental Protection Agency Regulatory Model (AERMOD), which is described by Cimorelli et al. (2005) and is a current EPA-recommended regulatory model. The other model was a bLS model modified from that described by Flesch et al. (2004) to account for particle settling velocity (v_s) and deposition. The development and initial testing of this model are the subject of Chapter 6 in this dissertation. Flesch et al. validated their model for emissions

estimation through inverse modeling, a test that has not yet been applied to AERMOD and reported in literature. Application of the model utilized in each emissions estimation effort is described in the respective chapters.

The second method of calculating area source emissions in the Ag Program was a mass balance approach applied to the PM-calibrated lidar data. Average upwind levels were subtracted from those calculated in and around detected plumes in the downwind vertical scans. The difference was multiplied by the component of the average wind perpendicular to the vertical scanning plane to calculate the horizontal flux of PM through the sampling plane. Fluxes were summed across the plane and averaged over the length of the sample period to determine the net flux of particles through the lidar measurement area. The emissions were related to the observed operation by dividing the flux by a characteristic property (i.e., number of cattle on the feedlot). This method of calculating emissions using lidar is described in detail in Bingham et al. (2009).

Manuscript Summaries

A brief summary of the papers comprising chapters 2 through 6 is provided in this section, with new contributions to science highlighted. The reader is referred to each chapter for detailed descriptions of the relevant published literature, the concentration measurement and emissions estimation methodologies used, the results, and the conclusions for each study. Note that the manuscripts are not presented in chronological publication order. The paper describing calculation and use of the MCF_k is

first to provide a stronger foundation for the two papers using this relationship in converting lidar data to PM_k . The other four papers are listed in chronological order of data collection. The document styles vary slightly as the journal-specific formats have been maintained for each paper.

Field studies reported in Chapters 3 through 5 were conducted in California's San Joaquin Valley (SJV) and the data reported in Chapter 6 were collected at a commercial beef feedlot in the panhandle of Texas. Both regions have a very large agricultural economy (USDA, 2009). The SJV also has a history of air pollution problems tied to agricultural activities (Battye et al., 2003; Chow et al., 1992, 1993).

The SJV was a non-attainment area for the PM_{10} NAAQS from 1991 to 2008 (EPA, 1991, 2008). Designation as a non-attainment area requires an area's air quality governing body to develop and implement plans to reduce anthropogenic emissions to the point that ambient pollutant levels meet the NAAQS. In the SJV, rules were put into place mandating the use of CMPs, but the η of most CMPs were estimated as they had not previously been measured. The two tillage studies in the SJV were conducted to quantify η for more CMPs. The NH_3 emissions study was conducted because NH_3 directly contributes to PM levels through photochemistry, and such measurements had not yet been conducted in the summer climate of the SJV (Cassel et al., 2005; Finlayson-Pitts and Pitts, 1999). The reductions in emissions achieved by various rules contributed greatly to lowering ambient PM_{10} below the NAAQS and the change in the SJV's PM_{10} status to attainment/maintenance in 2008. However, just one year later it was

designated as non-attainment for PM_{2.5}, requiring a PM_{2.5} attainment plan be created and implemented (EPA, 2009).

The data collected in the panhandle of Texas was from a 2015 study designed to test the ability of a backscatter lidar to quantify PM levels in feedlot plumes. After a successful demonstration, additional funding is being sought for studies to quantify the η of various CMPs to reduce feedlot emissions.

Chapter 2, Paper #1

Title: *Derivation and use of simple empirical relationships between aerodynamic and optical particle measurements*

Journal: Journal of Environmental Engineering

Manuscript Status: Published 2015 (Moore et al., 2015a)

Description: Several instruments measure optical properties of aerosols and use empirical relationships based on historical data to convert to PM concentrations.

However, differences between the measured aerosol and the historical data aerosol may significantly bias the reported PM mass-based levels. This paper presented a simple empirical method internally developed for converting optical measurements to PM for each individual sample period and locale. This relationship is referred to as the MCF and was very briefly described in Zavyalov et al. (2009). However, a more in depth discussion was needed. This paper describes the OPC data treatment, how the MCF is calculated, what it represents, the potential influential variables it encompasses, and how it has

been used to create more temporally and spatially resolved PM level datasets. Issues and anomalies found while using this approach are discussed. In the Ag Program, the MCF is necessary to convert the lidar V_k data to PM_k , which allows for the quantitative assessment of particle size-based fluxes and facility/operation emissions. The MCF is also used to convert OPC V_k into PM_k to examine concentration and emissions trends on a much more temporally resolved scale than is possible with the MiniVols. In addition to the MCF, this paper also presents results verifying that the MiniVols yield PM concentrations similar (usually within $\pm 10\%$) to Federal Reference Method (FRM) samplers under tested conditions.

Chapter 3, Paper #2

Title: *Particulate emissions calculations from Fall tillage operations using point and remote sensors*

Journal: Journal of Environmental Quality

Manuscript Status: Published 2013 (Moore et al., 2013)

Description: A rule targeting reductions in primary PM_{10} emissions from agricultural operations in the SJV, Rule 4550, Conservation Management Practices, was adopted in 2004 and required the use of approved CMPs (SJVAPCD, 2006). However, very little literature data were available concerning the actual reductions from the CMPs for crop production tillage activities. SDL and ARS partnered with the EPA Office of Research and Development, National Exposure Research Laboratory to study the η of the combined

operations tillage CMP. The η is the decrease in emissions realized by utilization of the CMP instead of the traditional management practice, relative to the emissions from the traditional method. The combined operations CMP reduces the number of passes across the field by combining two or more operations. Calculating η required deriving EF values for both the conventional tillage management practice and the CMP. Measurements made in October 2007 yielded η values for the CMP of 29% for $PM_{2.5}$, 60% for PM_{10} , and 25% for TSP based on lidar data. The filter based dataset was not sufficiently complete to estimate η . These emissions reduction values were the first available in literature for the combined operations CMP. Additionally, lidar measurements showed a significant portion of the plumes were lofted above the point sensors, with some even detached completely from the surface, and AERMOD did not effectively reproduce these elevated plumes. This comparison study is the type of test meeting the second objective of the Cooperative Agreement between ARS and SDL.

Chapter 4, Paper #3

Title: *Particulate matter emission estimates from agricultural Spring tillage operations using lidar and inverse modeling*

Journal: Journal of Applied Remote Sensing

Manuscript Status: Published 2015 (Moore et al., 2015b)

Description: A companion study to the Fall tillage CMP study was funded by the San Joaquin Valleywide Air Pollution Study Agency to examine η from a Spring tillage CMP.

Field measurements were collected in May and June of 2008. The selected CMP was the conservation tillage CMP, which reduces the extent of disturbed soil. The conservation tillage CMP in this study consisted of three operations totaling three passes across the field. In comparison, the conventional tillage method had nine different operations totaling 13 passes. Improper maintenance of the MiniVol sampler size separation assemblies through the first portion of the study, combined with the short duration, high intensity dust plumes resulting from the tillage activity, led to the rejection of most of the downwind filter samples during the May sample periods. Therefore, EFs were only estimated from filter-based samples for about half of the sample periods. The OPCs deployed on the downwind side of the fields were not overloaded. The upwind MiniVol and OPC samples, which were not compromised by the tillage plumes, were used to calculate daily average MCF_k values to convert both downwind OPC and lidar data to PM_k data. The η values calculated based on OPC and lidar data were 85% and 91% for $PM_{2.5}$, 87% and 94% for PM_{10} , and 90% and 91% for TSP, respectively. These values were similar to the only other conservation tillage CMP study in the literature. Like the previous tillage CMP study, this study directly meets the second objective of the Cooperative Agreement.

Chapter 5, Paper #4

Title: *Ammonia measurements and emissions from a California dairy using point and remote sensors*

Journal: Transactions of the ASABE (American Society of Agricultural and Biological Engineers)

Manuscript Status: Published 2014 (Moore et al., 2014)

Description: A significant portion of the PM_{2.5} and PM₁₀ in the SJV is ammonium nitrate (NH₄NO₃), which is formed through photochemical reactions in the atmosphere involving NH₃, NO_x, and other compounds (Chow et al., 1992, 1993; Finlayson-Pitts and Pitts, 1999). However, only wintertime NH₃ emission levels had previously been estimated under the SJV climactic conditions. The Ag Program conducted a summer PM and NH₃ emissions study on a commercial dairy in the SJV, in part to fill this gap in knowledge. The passive Ogawa samplers and scanning OP-FTIR system were deployed. The results of the PM study were published in Marchant et al. (2011). This paper presents the results of the NH₃ measurements and emissions calculations. Significant improvements to data treatment, modeling inputs, and inverse modeling EF calculation methodology were made in this paper compared to previous work in the Ag Program. Also, this constitutes the first NH₃ EF study published in peer reviewed literature based on the scanning OP-FTIR system. A diurnal pattern in downwind NH₃ was observed, with the highest levels reported in the afternoon despite greater mixing and dilution. EFs averaged $140.5 \pm 42.5 \text{ g d}^{-1} \text{ animal}^{-1}$ from the passive sampler data and $199.2 \pm 22.0 \text{ g d}^{-1} \text{ animal}^{-1}$ from OP-FTIR data, which are within the range of summer values from other studies with similar housing and manure management practices in other locations.

Emissions exhibited a diurnal cycle similar to concentrations, with peak afternoon values at least a factor of 10 higher than observed in the morning.

Chapter 6, Paper #5

Title: *Using a deposition-enabled backward Lagrangian stochastic model to estimate particulate matter area source emissions through inverse modeling*

Journal: Atmospheric Environment

Manuscript Status: Submitted, April 2017

Description: Simulation of atmospheric dispersion using most dispersion models, including AERMOD, assumes the molecule/particle of interest is inert and follows the behavior of the carrier fluid. However, this assumption does not always hold with large particles ($d_p \geq 5 \mu\text{m}$) due to effects of gravitational and momentum forces. Large particles may have significant v_s compared to the vertical wind velocity (w), causing them to continually decrease in vertical position (z) relative to the associated carrier fluid, thereby affecting both vertical and horizontal dispersion. In addition, particles may be removed from the flow through deposition. Accounting for these deviations from the carrier flow could be important. A type of model called the Lagrangian stochastic model (LS) was used to account for v_s and deposition in near-field (generally $< 1,000 \text{ m}$) inverse modeling.

An LS attempts to mimic atmospheric turbulence by simulating the movement of marked fluid elements (MFEs) in a domain with known mean flow and by adding

random variations to the MFE movement to simulate the stochastic nature of turbulence (Lin, 2012). Running the LS for thousands of MFEs provides a statistical representation of the simulated dispersion and yields the $(C/Q)_{sim}$ ratio required to calculate Q_{calc} using Eq. 1-1. LS models may be run forward in time (fLS), from the source to the receptor, or backward in time (bLS), from the receptor towards the source. The bLS has been shown to be much more computationally efficient than the fLS, often by an order of magnitude or more. Flesch et al. (2004) validated a bLS model (that does not take into account v_s or deposition) for calculating emissions through inverse modeling. This model has been used by many researchers to estimate agricultural emissions for various pollutants in recent years (Bjorneberg et al., 2009; Bonifacio et al., 2013; Flesch et al., 2009; Todd et al., 2008; Leytem et al., 2011, 2013; Yang et al., 2017; and others). Others have accounted for v_s and deposition in fLS models (Sawford and Guest, 1991; McGinn et al., 2010; Wang et al., 1995, 2008; etc.), but no bLS accounting for particle behavior was previously found in literature.

The last paper in this dissertation presents a modified bLS that allows for particle depositional behavior to be taken into account. It is based on the model of Flesch et al. (2004) with modifications from several papers on fLS models with v_s and deposition. The non-depositional case of this model ($v_s = 0.0 \text{ m s}^{-1}$) was tested against a portion of the validation dataset published by Flesch et al. and found to yield similar results with the same uncertainty value. The modified bLS and fLS models were compared for a subset of sample periods from a Texas panhandle cattle feedlot dataset collected in 2015 by

Texas A&M AgriLife Research and SDL. The modified bLS yielded slightly higher emissions values at $d_p \leq 20 \mu\text{m}$ with relative results remaining nearly constant across sample periods. The modified bLS was assumed to be valid for estimating emissions for particles with $d_p < 20 \mu\text{m}$, the size range of interest for $Q_{PM2.5}$ and Q_{PM10} (regulated particle classifications). The modified bLS estimated Q_{PM10} from the full feedlot dataset at $62.5 \text{ g animal}^{-1} \text{ day}^{-1}$ when accounting for v_s and deposition, 12% higher than in the non-depositional case. Significant contributions to the science of measuring emissions from large area sources include another validation of the bLS for use in estimating emissions, the description of a modified bLS that can account for v_s and deposition for $d_p < 20 \mu\text{m}$ while yielding results consistent with the fLS, and the results of the model's first tests.

Literature Review

A literature review is provided in each chapter of the relevant publications. To avoid duplication, only relevant literature published or found since the papers were finalized are presented in this section. No additional papers are presented for the modified bLS paper as it was submitted for publication consideration in April 2017.

No new discussions on the MCF or mass conversion algorithms has been published recently. However, a conference paper by Shao et al (2016) reported on the development and testing of an OPC that utilized instrument response at specific angles relative to illumination to size particles. Particle density was not accounted for in the

mass calculation; instead, they focused on better measuring the optical diameter because the effect of density scales linearly on PM while diameter scales to the third power. Initial testing with a reference PM_{2.5} instrument showed very good correlations.

The number of publications on estimates of agricultural tillage emissions remains small. Only one additional paper was found since Moore et al. (2015b) was published. Agricultural tillage PM_{2.5} and PM₁₀ emissions in northeastern China were estimated by Chen et al. (2017) for planting, harvesting, and a combined operations CMP for spring tillage. They estimated emissions with the flux profile method described by Holmén et al. (2001) coupled with optical sensors utilizing a mass conversion algorithm to produce PM_{2.5} and PM₁₀ concentrations. Spring tillage CMP emissions ranged from 9 to 119 mg m⁻² for PM₁₀ and 3 to 33 mg m⁻² for PM_{2.5}, with lower values associated with higher soil moisture content. These values were in the same range as those reported for PM_{2.5} in Table 4-6 in Chapter 4, but lower for PM₁₀. Reported planting emissions had smaller ranges than CMP tillage, 4 to 17 mg m⁻² for PM₁₀ and 3 to 4 mg m⁻² for PM_{2.5}, and were smaller than those presented in Table 4-6. Harvesting emissions ranged from 18 to 33 mg m⁻² for PM₁₀ and 6 to 11 mg m⁻² for PM_{2.5}.

A few papers were found and/or published since publication of Moore et al. (2014) on the topic of NH₃ emissions from dairies. First, a very good review was given by Hristov et al. (2011), covering NH₃ sources, emissions mechanisms and processes, and measurements from both dairy and beef feedlot operations. Included is a table comparing dairy NH₃ emissions from 26 published studies, many of which were not

directly listed in Table 5-5 in Chapter 5 from Moore et al., but some were included in the review performed by Arogo et al. (2006). Only four of the studies listed by Hristov et al. were from open-lot dairies, the type of facility investigated herein, and all were in Table 5-5. The mean \pm 1 standard deviation (σ) for the values in Hristov et al. was 58.8 ± 65.0 g animal⁻¹ day⁻¹.

An open-lot dairy NH₃ emissions study was carried out in the High Plains area of New Mexico and reported by Todd et al. (2015). They measured summer time NH₃ levels with tunable diode laser systems, and combined them with inverse modeling using WindTrax to estimate emissions. They found a daily emission of 321 g animal⁻¹ day⁻¹, higher than most other published studies except Leytem et al. (2013). A contributing factor was postulated to be the herd at this dairy was entirely mature, which differs from the study in Chapter 5 that had a mixed herd of calves, heifers, and mature cows. Todd et al. found pen emissions dominated the total emissions like in Moore et al., accounting for 95% of the total emissions.

Yang et al. (2016) reported NH₃ emissions measurements from pen surfaces at two dairies near Beijing, China. The dairies were open-lot with a brick base and had weekly manure removal. NH₃ concentrations were measured using a tunable diode laser system and emissions were estimated with WindTrax in inverse modeling. They found average summer time emissions of 210.8 and 177.6 g animal⁻¹ day⁻¹, similar to those reported in Chapter 5. The yearly averages were 139.7 and 122.1 g animal⁻¹ day⁻¹.

Liu et al. (2017) performed a meta-analysis study of NH₃ emissions from beef feedlots and dairy housing. They found positive correlations between both air temperature and dietary crude protein content and NH₃ emissions. They also observed that the method used to measure emissions could affect the results, with flux chamber methods usually underestimating emissions and the nitrogen balance method overestimating them. Another meta-analysis study reported by Bougouin et al. (2016) found that the greatest factor affecting NH₃ emissions from dairy housing was flooring type, followed by season and diet factors. An open-lot dairy was found to produce the highest emissions of flooring type.

References

- Auvermann, B., R. Bottcher, A. Heber, D. Meyer, C.B. Parnell, B. Shaw, and J. Worley. 2006. "Particulate matter emissions from animal feeding operations." In Rice, J.M., D.F. Caldwell, and F.J. Humenik (eds.), *Animal agriculture and the environment: National Center for Manure and Animal Waste Management white papers*, American Society of Agricultural and Biological Engineers, St. Joseph, Michigan, 435-468.
- Battye, W., V.P. Aneja, and P.A. Roelle. 2003. Evaluation and improvement of ammonia emissions inventories. *Atmospheric Environment*, 37:3873-3883.
- Bingham, G.E., C.C. Marchant, V.V. Zavyalov, D.J. Ahlstrom, K.D. Moore, D.S. Jones, T.D. Wilkerson, L.E. Hipps, R.S. Martin, P.J. Silva, and J.L. Hatfield. 2009. Lidar based emissions measurements at the whole facility scale: method and error analysis. *Journal of Applied Remote Sensing*, 3(1); 033510.
- Bjorneberg, D.L., A.B. Leytem, D.T. Westermann, P.R. Griffiths, L. Shao, and M.J. Pollard. 2009. Measurement of atmospheric ammonia, methane, and nitrous oxide at a concentrated dairy production facility in southern Idaho using open-path FTIR spectrometry. *Transactions of the ASABE*, 52:1749-1756.

- Bonifacio, H.F., R.G. Maghirang, E.B. Razote, S.L. Trabue, and J.H. Prueger. 2013. Comparison of AERMOD and WindTrax dispersion models in determining PM₁₀ emission rates from a beef cattle feedlot. *Journal of the Air and Waste Management Association*, 63:545-556.
- Bougouin, A., A. Leytem, J. Dijkstra, R.S. Dungan, and E. Kebreab. 2016. Nutritional and environmental effects on ammonia emissions from dairy cattle housing: a meta-analysis. *Journal of Environmental Quality*, 45:1123-1132.
- Casey, K.D., J.R. Bicudo, D.R. Schmidt, A. Singh, S.W. Gay, R. Gates, L.D. Jacobson, and S. Hoff. 2006. "Air quality and emissions from livestock and poultry production/waste management systems." In Rice, J.M., D.F. Caldwell, and F.J. Humenik (eds.), *Animal agriculture and the environment: National Center for Manure and Animal Waste Management white papers*, American Society of Agricultural and Biological Engineers, St. Joseph, Michigan, 1-40.
- Cassel, T., L. Ashbaugh, and R. Flocchini. 2005. Ammonia emission factors for open-lot dairies: direct measurements and estimation by Nitrogen intake. *Journal of the Air and Waste Management Association*, 55:826-833.
- Chen, W., D.Q. Tong, S. Zhang, X. Zhang, and H. Zhoa. 2017. Local PM₁₀ and PM_{2.5} emissions inventories from agricultural tillage and harvest in northeastern China. *Journal of Environmental Sciences*, in press.
- Chow, J.C., J.G. Watson, D.H. Lowenthal, P.A. Solomon, K.L. Magliano, S.D. Ziman, and L.W. Richards. 1992. PM₁₀ source apportionment in California's San Joaquin Valley. *Atmospheric Environment*, 26:3335-3354.
- Chow, J.C., J.G. Watson, D.H. Lowenthal, P.A. Solomon, K.L. Magliano, S.D. Ziman, and L.W. Richards. 1993. PM₁₀ and PM_{2.5} Compositions in California's San Joaquin Valley. *Aerosol Science and Technology*, 18:105-128.
- Cimorelli, A.J., S.G. Perry, A. Venkatram, J.C. Weil, R.J. Paine, R.B. Wilson, R.F. Lee, W.D. Peters, and R.W. Brode. 2005. AERMOD: a dispersion model for industrial source applications. Part I: general model formulation and boundary layer characterization. *Journal of Applied Meteorology*, 44:682-693.
- Cooper, D.C., and F.C. Alley. 2002. *Air pollution control: A design approach*. 3rd ed. Waveland Press Inc. Prospect Heights.

- Davidson, C.I., R.F. Phalen, and P.A. Solomon. 2005. Airborne particulate matter and human health: a review. *Aerosol Science and Technology*, 39:737-749.
- Dockery, D.W., C.A. Pope, X. Xu, J.D. Spengler, J.H. Ware, M.E. Fay, B.G. Ferris, and F.E. Speizer. 1993. An association between air pollution and mortality in six U.S. cities. *The New England Journal of Medicine*, 329:1753-1759.
- Environmental Protection Agency (EPA). 1991. Designations and classifications for initial PM-10 nonattainment areas. *Federal Register*, 56(51):11101-11105.
- EPA. 2008. Approval and Promulgation of Implementation Plans; Designation of Areas for Air Quality Planning Purposes; State of California; PM-10; Revision of Designation; Redesignation of the San Joaquin Valley Air Basin PM-10 Nonattainment Area to Attainment; Approval of PM-10 Maintenance Plan for the San Joaquin Valley Air Basin; Approval of Commitments for the East Kern PM-10 Nonattainment Area. *Federal Register*, 73(219):66,759-66,775.
- EPA. 2009. Air Quality Designations for the 2006 24-Hour Fine Particle (PM_{2.5}) National Ambient Air Quality Standards. *Federal Register*, 74(218):58,688-58,781.
- EPA. 2017. Criteria Air Pollutants. Last modified: March 10, 2017. Accessed: April 2, 2017. Available: <https://www.epa.gov/criteria-air-pollutants>.
- Finlayson-Pitts, B. J. and J. N. Pitts, Jr. 1999. Chemistry of the upper and lower atmosphere: theory, experiments, and applications. Academic Press, San Diego, California.
- Flesch, T.K., J.D. Wilson, L.A. Harper, B.P. Crenna, and R.R. Sharpe. 2004. Deducing ground-to-air emissions from observed trace gas concentrations: a field trial. *Journal of Applied Meteorology*, 43: 487-502.
- Flesch, T.K., L.A. Harper, J.M. Powell, and J.D. Wilson. 2009. Inverse-dispersion calculation of ammonia emissions from Wisconsin dairy farms. *Transactions of the ASABE*, 52:253-265.
- Geer, L.A., J. Weedon, and M.L. Bell. 2012. Ambient air pollution and term birth weight in Texas from 1998 to 2004. *Journal of the Air and Waste Management Association*, 62:1285-1295.
- Grimm, H., and D.J. Eatough. 2009. Aerosol measurement: The use of optical light scattering for the determination of particulate size distribution, and particulate

mass, including the semi-volatile fraction. *Journal of the Air and Waste Management Association*, 59:101-107.

Griffiths, P.R., L. Shao, and A.B. Leytem. 2009 Completely automated open-path FT-IR spectrometry. *Analytical and Bioanalytical Chemistry*, 393:45-50.

Heber, A.J., B.W. Bogan, J.-Q. Ni, T.T. Lim, E.L. Cortus, J.C. Ramirez-Dorransoro, C.A. Diehl, S.M. Hanni, C. Xiao, K.D. Casey, C.A. Gooch, L.D. Jacobson, J.A. Koziel, F.M. Mitloehner, P.M. Ndegwa, W.P. Robarge, L. Wang, and R. Zhang. 2008. The National Air Emissions Monitoring Study: Overview of barn sources. ASAE Paper No. 701P0408. In *Proc. 8th International Livestock Environment Symposium*, 199-205. St. Joseph, Mich.: ASABE.

Hinds, W.C. 1999. *Aerosol technology: properties, behavior, and measurement of airborne particles*, 2nd ed. Wiley-Interscience, New York, New York.

Holmén, B.A., T.A. James, L.L. Ashbaugh, and R.G. Flocchini. 2001. Lidar-assisted measurement of PM₁₀ emissions from agricultural tilling in California's San Joaquin Valley – Part I: lidar. *Atmospheric Environment*, 35:3251-3264.

Hristov, A.N., M. Hanigan, A. Cole, R. Todd, T.A. McAllister, P.M. Ndegwa, and A. Rotz. 2011. Review: Ammonia emissions from dairy farms and beef feedlots. *Canadian Journal of Animal Science*, 91:1-35.

Leytem, A.B., R.S. Dungan, D.L. Bjorneberg, and A.C. Koehn. 2011. Emissions of ammonia, methane, carbon dioxide, and nitrous oxide from dairy cattle housing and manure management systems. *Journal of Environmental Quality*, 40:1383-1394.

Leytem, A.B., R.S. Dungan, D.L. Bjorneberg, and A.C. Koehn. 2013. Greenhouse gas and ammonia emissions from an open-freestall dairy in southern Idaho. *Journal of Environmental Quality*, 42:10-20.

Lin, J., D. Brunner, C. Gerbig, A. Stohl, A. Luhar, and P. Webley. 2012. *Lagrangian Modeling of the Atmosphere*, Geophysical Monograph Series 200. American Geophysical Union, Washington, DC.

Liu, Z., Y. Liu, X. Shi, J.P. Murphy, and R. Maghirang. 2017. Variations of ammonia emissions from cattle operations: effects of air temperature and dietary crude protein content. *Transactions of the ASABE*, 60:215-227.

- Marchant, C.C., T.D. Wilkerson, G.E. Bingham, V.V. Zavyalov, J.M. Andersen, C.B. Wright, S.S. Cornelsen, R.S. Martin, P.J. Silva, and J.L. Hatfield. 2009. Aglite lidar: A portable elastic lidar system for investigating aerosol and wind motions at or around agricultural production facilities. *Journal of Applied Remote Sensing*, 3(1):033511.
- Marchant, C.C., K.D. Moore, M.D. Wojcik, R.S. Martin, R.L. Pfeiffer, J.H. Prueger, and J.L. Hatfield. 2011. Estimation of dairy particulate matter emission rates by lidar and inverse modeling. *Transactions of the ASABE*, 54(4):1453-1463.
- Martin, R.S., P.J. Silva, K. Moore, M. Erupe, and V.S. Doshi. 2008. Particle composition and size distributions in and around a deep pit swine operation. *Journal of Atmospheric Chemistry*, 59(2), 135-150.
- McGinn, S.M., T.K. Flesch, D. Chen, B. Crenna, O.T. Denmead, T. Naylor, D. Rowell. 2010. Coarse particulate matter emissions from cattle feedlots in Australia. *Journal of Environmental Quality*, 39:791-798.
- Moore, K.D., M.D. Wojcik, R.S. Martin, C.C. Marchant, G.E. Bingham, R.L. Pfeiffer, J.H. Prueger, and J.L. Hatfield. 2013. Particulate emissions calculations from fall tillage operations using point and remote sensors. *Journal of Environmental Quality*, 42:1029-1038.
- Moore, K.D., E. Young, C. Gurell, M.D. Wojcik, R.S. Martin, G.E. Bingham, R.L. Pfeiffer, J.H. Prueger, J.L. Hatfield. 2014. Ammonia measurements and emissions from a California dairy using point and remote sensors. *Transactions of the ASABE*, 57:181-198.
- Moore, K.D., R.S. Martin, W.J. Bradford, C.C. Marchant, D.S. Jones, M.D. Wojcik, R.L. Pfeiffer, J.H. Prueger, and J.L. Hatfield. 2015a. Derivation and use of simple relationships between aerodynamic and optical aerosol measurements. *Journal of Environmental Engineering*, 141:04014078.
- Moore, K.D., M.D. Wojcik, R.S. Martin, C.C. Marchant, D.S. Jones, W.J. Bradford, G.E. Bingham, R.L. Pfeiffer, J.H. Prueger, and J.L. Hatfield. 2015b. Particulate-matter emission estimates from agricultural spring-tillage operations using LIDAR and inverse modeling. *Journal of Applied Remote Sensing*, 9:096066.
- O'Neal, W.T., E.Z. Soliman, J.T. Efird, V.J. Howard, G. Howard, and L.A. McClure. 2017. Fine particulate air pollution and premature ventricular contractions: the

- REasons for Geographic And Racial Differences in Stroke (REGARDS) Study. *Environmental Research*, 154:115-119.
- Pope, C.A. 1989. Respiratory disease associated with community air pollution and a steel mill, Utah Valley. *American Journal of Public Health*, 79:623-628.
- Pope, C.A., and D.W. Dockery. 2006. Health effects of fine particulate air pollution: lines that connect. *Journal of the Air and Waste Management Association*, 56:709-742.
- Pope, C.A., M. Ezzati, and D.W. Dockery. 2013. Fine particulate air pollution and life expectancies in the United States: the role of influential observations. *Journal of the Air and Waste Management Association*, 63:129-132.
- Qian, Z., Q. He, H.-M. Lin, L. Kong, D. Liao, N. Yang, C.M. Bentley, and S. Xu. 2007. Short-term effects of gaseous pollutants on cause-specific mortality in Wuhan, China. *Journal of the Air & Waste Management Association*, 57:785-793.
- Roadman, M. J., J. R. Scudlark, J. J. Meisinger, and W. J. Ullman. 2003. Validation of Ogawa passive samplers for the determination of gaseous ammonia concentrations in agricultural settings. *Atmospheric Environment*, 37:2317-2325.
- San Joaquin Valley Air Pollution Control District (SJVAPCD). 2006. Conservation Management Practices Program Report, San Joaquin Valley Air Pollution Control District (SJVAPCD). Available: <https://www.valleyair.org/rules/currentrules/r4550.pdf>. Accessed: 7 April 2017.
- Shao, L., P.R. Griffiths, and A.B. Leytem. 2010. Advances in data processing for open-path fourier transform infrared spectrometry of greenhouse gases. *Analytical Chemistry*, 82:8027-8033.
- Shao, W., H. Zhang, and H. Zhou. 2016. "A new particle sensor based on true RMS value measurement," in *Instrumentation and Measurement Technology Conference Proceedings, 2016 IEEE International*, New York, New York.
- Sawford, B.L., and F.M. Guest. 1991. Lagrangian statistical simulation of the turbulent motion of heavy particles. *Boundary Layer Meteorology*, 54:147-166.
- Todd, R.W., N.A. Cole, R.N. Clark, T.K. Flesch, L.A. Harper, and B.H. Baek. 2008. Ammonia emissions from a beef cattle feedyard on the southern High Plains. *Atmospheric Environment*, 42:6797-6805.

- Todd, R.W., N.A. Cole, G.R. Hagevoort, K.D. Casey, and B.W. Auvermann. 2015. Ammonia losses and nitrogen partitioning at a southern High Plains open lot dairy. *Atmospheric Environment*, 110:75-83.
- Turner, M.C., A. Cohen, R.T. Burnett, M. Jerrett, W.R. Diver, S.M. Gapstur, D. Krewski, J.M. Samet, and C.A. Pope. 2017. Interactions between cigarette smoking and ambient PM_{2.5} for cardiovascular mortality. *Environmental Research*, 154:304-310.
- United States Department of Agriculture (USDA). 2009. 2007 Census of Agriculture: United States Summary and State Data. AC-07-A-51.
- Wang, Y., D.R. Miller, D.E. Anderson, and M.L. McManus. 1995. A Lagrangian stochastic model for aerial spray transport above an oak forest. *Agricultural and Forest Meteorology*, 76:277-291.
- Wang, J., A.L. Hiscox, D.R. Miller, T.H. Meyer, T.W. Sammis. 2008. A dynamic Lagrangian, field-scale model of dust dispersion from agricultural tilling operations. *Transactions of the ASABE*, 51:1763-1774.
- Wojcik, M.D., R.S. Martin, and J.L. Hatfield. "Using lidar to characterize particles from point and diffuse sources in an agricultural field," pp. 299-332, in N.B. Chang (ed.), *Environmental Remote Sensing and Systems Analysis*. CRC Press, Boca Raton, FL, USA.
- Yang, Y., W. Liao, X. Wang, C. Liu, Q. Xie, Z. Gao, W. Ma, and Y. He. 2016. Quantification of ammonia emissions from dairy and beef feedlots in the Jing-Jin-Ji district, China. *Agriculture, Ecosystems and Environment*, 232:29-37.
- Zavalyov, V.V., C.C. Marchant, G.E. Bingham, T.D. Wilkerson, J.L. Hatfield, R.S. Martin, P.J. Silva, K.D. Moore, J. Swasey, D.J. Ahlstrom, and T.L. Jones. 2009. Aglite lidar: Calibration and retrievals of well characterized aerosols from agricultural operations using a three-wavelength elastic lidar. *Journal of Applied Remote Sensing*, 3(1):033522.

CHAPTER 2
DERIVATION AND USE OF SIMPLE EMPIRICAL RELATIONSHIPS
BETWEEN AERODYNAMIC AND OPTICAL
PARTICLE MEASUREMENTS¹

Abstract

A simple relationship, referred to as a mass conversion factor (MCF), is presented to convert optically-based particle measurements to mass concentration. It is calculated from filter-based samples and optical particle counter (OPC) data on a daily or sample period basis. The MCF allows for greater temporal and spatial mass concentration information than typical filter-based measurements. Results of MCF calculations from several field studies are summarized. Pairwise comparisons from a collocated study with multiple OPCs and mass samplers suggest the minimum variability of the MCF is 5 to 10%. The variability of the MCF within a sample period during a field study with distributed samplers averaged 17 to 21%. In addition, the precision of the Airmetrics MiniVol Portable Air Sampler for particulate matter (PM) was found to be typically < 10%. Comparisons with federal reference method (FRM) samplers showed that MiniVols yield PM_{2.5} concentrations essentially equivalent to FRMs with slightly greater deviations from the FRM for PM₁₀ under tested ambient conditions.

¹ Citation: Moore, K.D., R.S. Martin, W.J. Bradford, C.C. Marchant, D.S. Jones, M.D. Wojcik, R.L. Pfeiffer, J.H. Prueger, and J.L. Hatfield. 2015. Derivation and use of simple relationships between aerodynamic and optical particle measurements. *Journal of Environmental Engineering*, 141:04014078.

Introduction

Many different properties can be used to describe a single particle. These include shape, chemical speciation, density, index of refraction, aerodynamic diameter, optical diameter, etc. Numerous measurement techniques have been developed to quantify various properties, though most are capable of measuring only one or two properties. Comparisons between simultaneous measurements of an aerosol mixture made using different techniques may provide valuable information about relationships between the measurement methodologies and the measured properties, as well as additional information not measured.

Estimating specific particle properties even from a combination of measurement techniques may be challenging both theoretically and in practice. For example, Schmid et al. (2007) provides a detailed explanation of mathematical relationships between density, shape, effective density, and various equivalent diameters for spherical and non-spherical particles. Deriving a property from such methods requires significant investment in equipment, as well as knowledge or assumptions of other pertinent particle properties. However, comparisons between two or more measurement techniques may be made in order to derive an empirical relationship that incorporates all applicable properties into a more simple expression. While this method does not provide insight into the values of specific properties, it can be very useful in calibrating the output of a sensor to provide information not directly measured, such as the

calibration of an optical particle counter (OPC) to provide particulate matter (PM) mass concentration. A significant advantage of an OPC over typical filter-based mass samplers is that the OPC can provide a much more temporally resolved dataset and may yield valuable information about changes in concentration.

Binnig et al. (2007) describes the calibration of an OPC to yield concentrations of PM with an aerodynamic diameter (d_a) $\leq 2.5 \mu\text{m}$ ($\text{PM}_{2.5}$) for a well-defined aerosol utilizing known particle density and assuming uniform composition across the size range. This procedure, however, should not be applied in situations with significant fractions of particles that are not well-defined, as is often the case in ambient measurements. Instead, researchers tend to rely on historical data to develop these empirical relationships for converting optical measurements to PM mass concentrations (Grimm and Eatough 2009). Several commercially available ambient PM monitors currently utilize mass conversion relationships based on historical data to report PM concentrations from optical systems, such as the Aerosol Spectrometer series by GRIMM Technologies, Inc. (Ainring, Germany), the TSI Inc. DustTrak series (Shoreview, MN, USA), and the Palas GmbH Fidas System (Karlsruhe, Germany).

The accuracy of PM concentrations calculated from optical data and converted using relationships based on historical data is strongly influenced by how closely the properties of the monitored aerosol match the properties of the historical dataset. For instance, errors in PM estimates at a clean background site, rural site, or a site heavily impacted by a single source could be significant if the employed PM calibration was

created from measurements in an urban area, all of which have different aerosol sources and, thus, optical properties. Estimating this relationship based on measurements of the aerosol of interest through an in situ calibration, referred to by the authors as the mass conversion factor (MCF), can decrease the error due to dissimilar aerosols. This method may also be used to provide a sample period PM calibration for instruments that do not have a historical dataset. Zavyalov et al. (2009) touched very briefly on how the MCF is calculated and potential uses. In this paper we provide more details on calculating the MCF, present data collected during field measurements that have been used to calculate MCFs, and give examples of how the MCFs have been used to estimate PM mass concentrations from optical sensors on finer timescales than filter-based measurements. In addition, results of multiple comparison studies between the filter-based PM samplers used in these studies to Federal Reference Method (FRM) samplers are presented.

Methodology

Instrumentation and Analysis

PM mass concentration data were collected using filter-based MiniVol Portable Air Samplers from Airmetrics (Eugene, OR, USA). These are portable, battery operated instruments with programmable sample times. Air is pulled into the sample head at a nominal flow rate of 5.0 L min^{-1} where size separation occurs based on particle inertia through the use of a removable impactor plate assembly. This inertial particle

separation method is the same principle as that used in FRM samplers for PM with $d_a \leq 10 \mu\text{m}$ (PM₁₀) and PM_{2.5}, although the design is different and the collection efficiency curve of the MiniVol assembly is not as steep as that of the FRM samplers (Hill et al. 1999). The MiniVol can sample PM₁₀, PM_{2.5}, or PM with $d_a \leq 1 \mu\text{m}$ (PM₁), depending on the impactor assembly used; total suspended particulate matter (TSP) may be collected if the impactor assembly is not used. Impaction plates were coated with a thin layer of high vacuum silicone grease to prevent particles removed from the airstream from being re-entrained in the sample flow. A filter holder is located downstream of the size separator to collect particles remaining in the airstream.

Sample flow is not actively maintained at 5.0 L min^{-1} by the MiniVol. Instead, it is set using a calibrated rotameter before each run and verified during sample retrieval. Flow calibrations were conducted yearly and prior to deployment for each instrument used. The calibration equations and estimated sample period average pressure and ambient temperature (T_{amb}) were used to calculate the sample period specific rotameter settings necessary to achieve a sample flow of 5.0 L min^{-1} . Occasional sampling or handling irregularities occurred with MiniVol samples, all of which were noted. Any sample with a noted issue was excluded from further calculations.

Teflon filters 47 mm in diameter were used to collect all samples herein reported. Filters were pre-conditioned according to the protocols outlined in Title 40, Part 50, Appendix J of the U.S. Code of Federal Regulations (40 CFR 50 Appendix J). Final average filter weights for both pre- and post-test were calculated from three stable

weights within $\pm 5 \mu\text{g}$ determined using a microbalance, Type MT5 (Mettler-Toledo, Inc., Columbus, OH, USA). Calculated concentration values represent a sample period average. Balance accuracy was verified every 10 filter measurements using a 1.000 mg calibration weight.

Aerosol Profilers, Model #9722 (Met One Instruments, Inc., Grants Pass, OR, USA) were used to measure the optical diameter (d_{op}) of individual particles. These OPCs measure the amount of light scattered by a particle and compare that quantity to light scattered by calibration particles of various sizes to determine the particle's d_{op} . Measured d_{op} are grouped into eight bins with the following size ranges: 1) 0.3–0.5 μm , 2) 0.5–0.6 μm , 3) 0.6–1.0 μm , 4) 1.0–2.0 μm , 5) 2.0–2.5 μm , 6) 2.5–5.0 μm , 7) 5.0–10.0 μm , and 8) $> 10.0 \mu\text{m}$. The OPC produces total particle counts per size bin over the sample period of duration t , ranging from 2 sec to 60 sec. Note that PM mass concentration calibrations based on historical data have not been developed for these OPCs. OPC flow measurements, usually made before and after experiments using a soap bubble displacement system (Gilian Gilibrator2 Calibration System, Sensidyne, LP, Clearwater, FL, USA), reported that average flow rates (q) ranged from 0.8 to 1.2 L min^{-1} between OPCs but that the q for a given OPC was very stable. Sampled aerosol was not preconditioned to control temperature or relative humidity (RH) in measurements herein reported as they were made in dry climates. However, preconditioning is suggested as high RH may have substantial effects on particle properties and measurements, particularly for hygroscopic particles.

For a specific OPC (j), number concentration (N_{ij}) per bin (i) is a function of raw particle counts (p_{ij}), the measured average flow rate (q_j), and the sample time (t) as shown in Eq. 2-1.

$$N_{ij} = \frac{p_{ij}}{q_j t} \quad (2-1)$$

In this equation the units for N are # cm⁻³, p is number (#), q is cm³ min⁻¹, and t is min.

Inter-calibration of OPC particle counts was performed in post analysis to ensure comparability between deployment sites. The inter-calibration equations, referred to by the authors as Counting Correction Factors (CCFs), were calculated based on data collected either as a collocated group before or after an experiment or, if a collocated dataset did not exist, from multiple periods over the deployment during which the source under study was not active and OPCs were measuring a consistent, uniform background aerosol. As instrument response for each upper bin limit in each OPC must be factory calibrated individually, so too the CCFs must be calculated for each bin of each OPC. A CCF_{ij} is estimated through comparison of the average particle number concentration (\check{N}_{ij}) over the identified period with the average particle number concentration across all OPCs (\check{N}_i). CCFs were applied to all N_{ij} prior to further analysis.

Both scalar and linear function ($y = mx + b$) CCFs have been found to greatly decrease inter-instrument variability. As an example, the variability between \check{N}_{ij} prior to CCF application to a collocated dataset was 18.0%, calculated as the relative standard deviation (RSD). Application of scalar CCF_{ij} values reduced the RSD to 6.8%, and

application of linear function CCFs yielded a RSD of 6.5%. Other types of CCF equations may be used as deemed appropriate.

The volume concentration (V) of sampled particles based on N may be calculated based on the following simplifying assumptions: 1) the particles are spheres, and 2) the maximum measured d_{op} is 20 μm . The assumption of a maximum measured d_{op} provides an upper bound for the largest-sized channel. The geometric mean d_{op} per bin (GMD_i) was selected as the representative diameter of the particles in a given bin i with the assumption of a log-normal distribution of particle counts. The cumulative V (V_k) up to a particle diameter k (d_k) may be calculated using Eq. 2-2:

$$V_k = \frac{\pi}{6} \int_0^{d_k} n(d) d^3 dd \quad (2-2)$$

where $n(d)$ is the number concentration at diameter d . For application to the collected OPC data, Eq. 2-2 is discretized and expressed in the following terms that have been previously defined:

$$V_k = \frac{\pi}{6} \sum_{i=1}^{\text{GMD}_i \leq d_k} \text{GMD}_i^3 N_i \quad (2-3)$$

where GMD_i is expressed in μm , N_i is in $\# \text{cm}^{-3}$, and V_k is in units of $\mu\text{m}^3 \text{cm}^{-3}$. In this case, the V_k definition is similar to PM_k concentrations: the total volume of particles whose d_{op} is $\leq k = 1 \mu\text{m}$, $2.5 \mu\text{m}$, $10 \mu\text{m}$, and ∞ for TSP.

MCF Calculations

The MCF is calculated from optical and aerodynamic particle measurements. The V_k data, as calculated in Eq. 2-3, are averaged over the corresponding MiniVol sample time. The MCF, with units of density (g cm^{-3}), for each PM size fraction k is calculated as shown in Eq. 2-4.

$$MCF_k = \frac{PM_k}{V_k} \quad (2-4)$$

The MCF is typically averaged across sample locations. Note that this MCF is different from the MCF described by Binnig et al. (2007). Binnig et al. include particle shape factor and density, which must be supplied by the user. However, this MCF incorporates the many properties from the particles, the environment, and the measurement techniques that influence the reported PM_k and V_k values without requiring explicit consideration. Including these factors in the MCF may lead to significantly different values and larger variability in MCF_k across sample periods and instrumentation than other conversion factors or mean density correction methods report.

Properties of particles that may influence optical and aerodynamic measurements include, but are not limited to, chemical composition, effective density, shape, and index of refraction, which are interdependent to varying degrees. Chemical composition affects both the index of refraction and effective density. As OPC measurements are influenced by a particle's index of refraction, differences in indices of

refraction between measured ambient and calibration particles may result in significant differences between a particle's physical diameter (d_p) and d_{op} , leading to potentially significant differences between calculated and actual V and V_k . The OPC d_{op} sizing calibrations were performed by the manufacturer with polystyrene latex (PSL) spheres. These calibrations were used for all sample periods. No attempts were made to calibrate the OPCs to local aerosol mixtures due to their complex and changing natures. This may result in positive or negative biases in sizing, with the degree of impact varying with ambient aerosol d_p and chemical composition.

Particle properties also influence filter-based measurements. The MiniVol impactor assembly separates particles based on d_a , which is influenced by d_p , effective density, and shape, among other factors. Combining optical and aerodynamic measurements in calculating the MCF also combines the effects of particle properties, with varying impacts. For instance, if a particle has a d_a larger than a MiniVol assembly cut point but a d_{op} smaller than the lower bin limit of the OPC channel corresponding to the MiniVol assembly cut point, it may be included in V_k as a smaller particle but not in PM_k , leading to a smaller MCF_k . The inverse situation with d_{op} and d_a may also occur, resulting in a larger MCF_k .

Additional complications may arise from the past and current ambient environments in which the particle(s) has (have) been suspended. For instance, T_{amb} may affect chemical composition as volatile and semi-volatile compounds are found as both gasses and particles over the typical range of T_{amb} . Also, some compounds common

in ambient particles, such as ammonium sulfate ((NH₄)₂SO₄) and ammonium nitrate (NH₄NO₃), readily absorb water at RH conditions above their deliquescence point, which varies between compounds and with T_{amb}, and thus increase the particle size and change the chemical composition (Finlayson-Pitts and Pitts 1999). Effects of T_{amb} and RH will be different between optical- and filter-based samplers and may be large, particularly for hygroscopic particles, depending on the similarity of sample period T_{amb} and RH conditions to those used in filter conditioning. The MCF envelops all of these effects without requiring their quantification.

The sampling properties of the instruments used to measure PM_k and V_k also influence the MCF. One factor is particle aspiration effectiveness, particularly for large particles. This refers to how well particles of a given size are drawn into the system at the inlet. It is a strong function of a particle's inertia and d_a and the inlet design. Marchant et al. (2011), based on conversations with Met One Instruments, Inc., stated that particles with d_a larger than about 25 μm are not likely to enter the OPC inlet and that the aspiration efficiency of particles down to 5 μm may be affected at wind speeds greater than ~3 m s⁻¹. Baldauf et al. (2001) reported that aspiration efficiencies for MiniVols for particles with $d_a = 10$ μm vary from 100% at a wind speed of 1.4 m s⁻¹ to ~70% at a wind speed of 16.7 m s⁻¹.

One factor affecting mass measurement systems is the effectiveness of the size selection mechanism. The FRM PM₁₀ and PM_{2.5} size segregation sample heads have been designed to mimic the particle removal efficiency of the human respiratory

system, with most utilizing a particle's inertia for separation if it is above the designed d_a cut point. The removal efficiencies can be represented by an S-curve with some particles smaller than the targeted cut point being removed, half the particles at the cut point being removed, and some particles larger than the cut point passing through the removal mechanism. The MiniVol impactor removal efficiency is designed to be similar to FRMs, though the slope is not as steep (Hill et al. 1999). Significant particle loading on the MiniVol impactor plate may lead to particles impacting the surface and returning to the airstream for collection on the filter. This is known as "particle bounce" and may result in higher PM_k being reported than is actually present. The manufacturer suggests the use of a thin grease film on the impactor plate as a preventative measure, with a cleaning and film renewal cycle based on sampling frequency and sampled concentrations. If cleaning and renewal cycles are too infrequent, particle buildup may occur and result in particle bounce (Tropp et al. 1998).

MCF values have been calculated from data collected during six field studies conducted in the San Joaquin Valley (SJV) of California, in the Cache Valley along the border between Utah and Idaho, and on the Colorado Plateau in eastern Utah. Measurements were taken during summer and fall seasons between 2007 and 2012 under the meteorological and potential PM source conditions listed in Table 2-1. Field study average T_{amb} were above 20 °C during all but one, and average RH values were in the 30% to 40% range. Maximum RH values were between 60% and 80% and occurred for short periods of time in early morning when T_{amb} was lowest. Typical point sensor

deployment on these field studies consisted of collocating an OPC with one to four MiniVol samplers. Sampler inlets were arranged at approximately the same elevation above ground level (AGL) and within a circle of radius ≤ 1.5 m with a minimum separation distance between inlets of 0.3 m to prevent interference. Samples were collected between 2 m and 10 m AGL. MiniVol sample periods ranged from 1 to 24 hr, depending on sampling objectives, while OPCs recorded data continuously in 20 sec intervals. Proper maintenance of the MiniVol impactor plate surface was a priority in each deployment.

MiniVol Accuracy and Precision Tests

Several collocated ambient tests were conducted in which multiple MiniVols and one or two FRM samplers were deployed to determine the precision and accuracy of the MiniVols. The FRM instruments used were Anderson Regulated Air Sampler (RAS) units operated by the authors for PM₁₀, a Partisol Plus Model 2025 Sequential Air Sampler operated by the State of Utah Division of Air Quality (UDAQ) for PM_{2.5}, and a Partisol FRM Model 2000 Air Sampler operated by UDAQ for PM₁₀, all of which were manufactured by Rupprecht and Patashnick Co., Inc. (now Thermo Fisher Scientific, Inc., Waltham, MA, USA). All filter samples collected by the authors were conditioned and weighed as previously discussed. Filter treatment by UDAQ followed established U.S. National Ambient Air Quality Standards (NAAQS) monitoring protocols. Samples were

Table 2-1. Conditions during each field campaign for which the mass conversion factor (MCF) has been calculated and included in this manuscript. Meteorological values are those recorded during sample periods only.

Location	Month(s) & Year	Sample Periods	Meteorological Conditions			Potential PM Sources	References	
			Avg ± SD	Min	Max			
Cache Valley, Utah, USA	July 2007	5	T _{amb} (°C)	25 ± 7	11	36	Combustion, small industrial processes, agriculture, construction, mobile	NA
			RH (%)	40 ± 22	12	86		
Colorado Plateau, Utah, USA	October 2009	4	T _{amb} (°C)	9 ± 5	-4	18	Long range transport (Malm et al., 2004), windblown dust, mobile, unpaved roads	NA
			RH (%)	41 ± 15	17	71		
San Joaquin Valley, Cal., USA	October 2007	7	T _{amb} (°C)	23 ± 4	14	30		Moore et al., 2013
			RH (%)	38 ± 14	17	79		
	May & June 2008	13	T _{amb} (°C)	30 ± 4	18	37	Samples collected around agricultural operations	NA
			RH (%)	28 ± 10	11	64		
	June 2008	7	T _{amb} (°C)	28 ± 7	15	39	Others: Combustion, industrial processes, construction, mobile, and others (Held et al., 2004)	Marchant et al., 2011
			RH (%)	39 ± 17	13	77		
	August 2012	5	T _{amb} (°C)	28 ± 6	13	37		NA
			RH (%)	39 ± 18	20	85		

Note: Avg = average, °C = degrees Celsius, Max = maximum, Min = minimum, NA = not applicable, PM = particulate matter, RH = relative humidity, SD = standard deviation

collected over 23 or 24 hr sample periods, with samplers arrayed to minimize horizontal and vertical spread while maintaining a minimum of 0.5 m distance between samplers.

A PM_{2.5} comparison test was conducted in early March 2004 utilizing 15 MiniVol samplers and UDAQ's PM_{2.5} FRM over four days. A PM₁₀ comparison test was then

conducted in late March 2004 over four sample periods with six MiniVols and the Anderson RAS PM₁₀ FRM. Samples were collected every two to three days to allow for filter deployment and collection. Another comparison study was carried out in July 2007 over five consecutive days. In this test, 20 MiniVol samplers were arranged adjacent to the UDAQ PM_{2.5} and PM₁₀ FRMs. Three MiniVols sampled PM₁, seven sampled PM_{2.5}, seven sampled PM₁₀, and three sampled TSP. The UDAQ FRMs had multiple filter cassettes with automated switching, allowing them to run nearly continuously. The MiniVols, however, required manual filter swapping between each sample. Therefore, the MiniVols sampled from 0:30 to 23:30, with the 1 hr break to allow time to switch sample heads, record elapsed sample run time, and adjust sampler flows. Verified PM_{2.5} and PM₁₀ values were obtained from UDAQ for all sample dates.

The accuracy and precision tests were carried out in the Cache Valley. Silva et al. (2007) showed that periods of elevated PM_{2.5} in Cache Valley in early 2004 were dominated by secondary particles, mostly NH₄NO₃, (NH₄)₂SO₄, and organic carbon (OC), with 90% of the mass present in the submicron range. Cache Valley and other nearby mountain valleys experience episodic events of air pollution levels above NAAQS limits during winter due to a combination of topographical, meteorological, and source characteristics (Malek et al. 2006; Silva et al. 2007; Silcox et al. 2012; Lareau et al. 2013). Summertime elevated PM has typically occurred due to impacts from wildfire or windblown dust events.

Results and Discussion

Field Study MCF Results

Six field deployments have resulted in a total of 95 samples for comparison between reported OPC and MiniVol values for PM₁, 380 for PM_{2.5}, 394 for PM₁₀, and 208 for TSP. Fig. 2-1 presents scatter plots of all the data, separated into the four size fractions. PM_k was almost always greater than V_k as few points are below the 1-to-1 dashed line. Linear trends were evident in the k = 1 μm, 10 μm, and TSP graphs, with slopes between 1.2 and 1.6 and 0.78 < R² < 0.82. The linear fit to k = 2.5 μm data had a slope of 1.4 but did not represent the data well (R² = 0.06) due to a collection of low V_{2.5} values (< 10 μm³ cm⁻³) paired with high PM_{2.5} concentrations (> 100 μg m⁻³). The majority of the high PM_{2.5}/low V_{2.5} pairings come from a single field study. The cause of these unusual values and their grouping is discussed at the end of this subsection. The k = 2.5 μm values from this field study were removed and the remaining data were plotted in the graph inset in Fig. 2-1b. The linear fit is significantly more representative (R² = 0.66) with a slope of 2.4 (n = 279).

PM chemical composition analyses were performed on select PM_{2.5} samples from two of the six datasets and on select PM_{2.5}, PM₁₀, and TSP filters from one dataset, all collected in the SJV. Water-soluble ions were quantified for all samples, while OC and elemental carbon (EC) were quantified in PM_{2.5} samples only based on the assumption that the majority of OC and EC were present in the PM_{2.5} fraction. The results showed

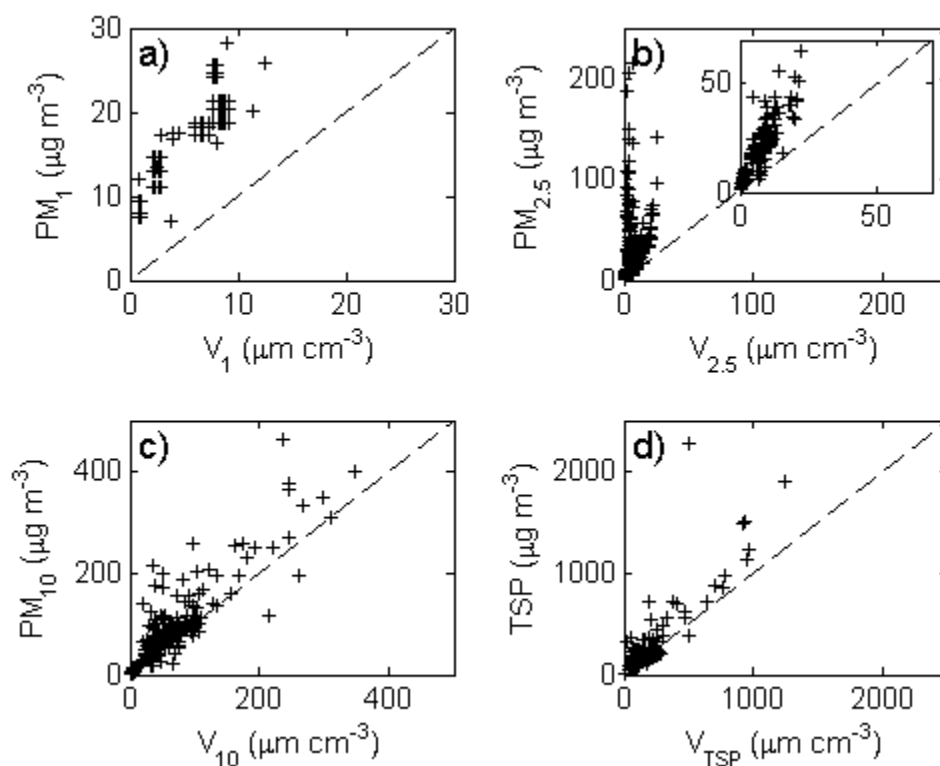


Figure 2-1. Scatter plots of V_k and PM_k for the following values of k : a) 1.0 μm , b) 2.5 μm , c) 10 μm , and d) TSP. The plot inset in (b) shows the $V_{2.5}/PM_{2.5}$ pairs after excluding data from one field study.

that most of the mass in analyzed samples (50-85%) was composed of elements/compounds not in the list of analytes. Malm and Hand (2007) used six particle composition classes to represent $PM_{2.5}$ dry mass based on the Interagency Monitoring of Protected Visual Environments (IMPROVE) protocols: NH_4NO_3 , $(\text{NH}_4)_2\text{SO}_4$, OC, EC, crustal, and sea salt. As NH_4NO_3 , $(\text{NH}_4)_2\text{SO}_4$, and sea salt were quantified in the water-soluble ion test, the majority of PM during these field studies in the SJV was, therefore,

assumed to be associated with crustal material. Particle chemical composition for the remaining three field studies is unknown.

A statistical summary of sample period average MCF_k values for all periods with more than two collocated comparisons is presented as a box and whisker plot in Fig. 2-2. As points of reference, the average density of soil is 2.65 g cm^{-3} , the density of mercury is 13.5 g cm^{-3} , and Peters (2006) provided several ambient PM density values derived from field studies that range from 1.77 to 2.64 g cm^{-3} (USDA NRCS 2007). Note that the y-axis in this figure has been limited in order to show details at the lower values—one sample period had an average $MCF_{2.5}$ of 23.5 g cm^{-3} . Outliers are shown as plus signs and calculated as greater than (less than) the 75th (25th) percentile value plus (minus) 1.5 times the interquartile range (IQR). The IQR is calculated as the difference between the 25th and 75th percentiles, which are shown by the top and bottom lines of the boxes. The whiskers extend to the most distant data values from the box edges within 1.5 times the IQR. The MCF_{10} and MCF_{TSP} values were more tightly grouped than the MCF_1 and $MCF_{2.5}$ values, as indicated by the smaller IQRs. This is also supported by the locations of the mean values for MCF_{10} and MCF_{TSP} , shown by the dots within circles, being much closer to the median, shown by the center line in the boxes. The overall mean \pm one standard deviation (SD) and the median of the period average values, respectively, were as follows: $MCF_1 = 4.3 \pm 2.2 \text{ g cm}^{-3}$ and 3.2 g cm^{-3} ($n = 5$); $MCF_{2.5} = 5.0 \pm 1.1 \text{ g cm}^{-3}$ and 3.2 g cm^{-3} ($n = 36$); $MCF_{10} = 1.6 \pm 0.3 \text{ g cm}^{-3}$ and 1.5 g cm^{-3} ($n = 38$); and $MCF_{TSP} = 1.6 \pm 0.4 \text{ g cm}^{-3}$ and 1.3 g cm^{-3} ($n = 33$). The absence of outliers for MCF_1 is

likely due the calculations being based on just five data points from a single field deployment.

The RSD between MCF values from different sample locations within a sample period averaged between 17% and 21% for $MCF_{2.5}$, MCF_{10} , and MCF_{TSP} , with maximum and minimum values for each size around 60% and 5%, respectively. Samplers were spread around various facilities/operations for five studies. The sixth study was conducted as a part of the MiniVol precision and accuracy test in July 2007 and had lower variability than the others. Seven OPCs were deployed with 20 MiniVols, providing

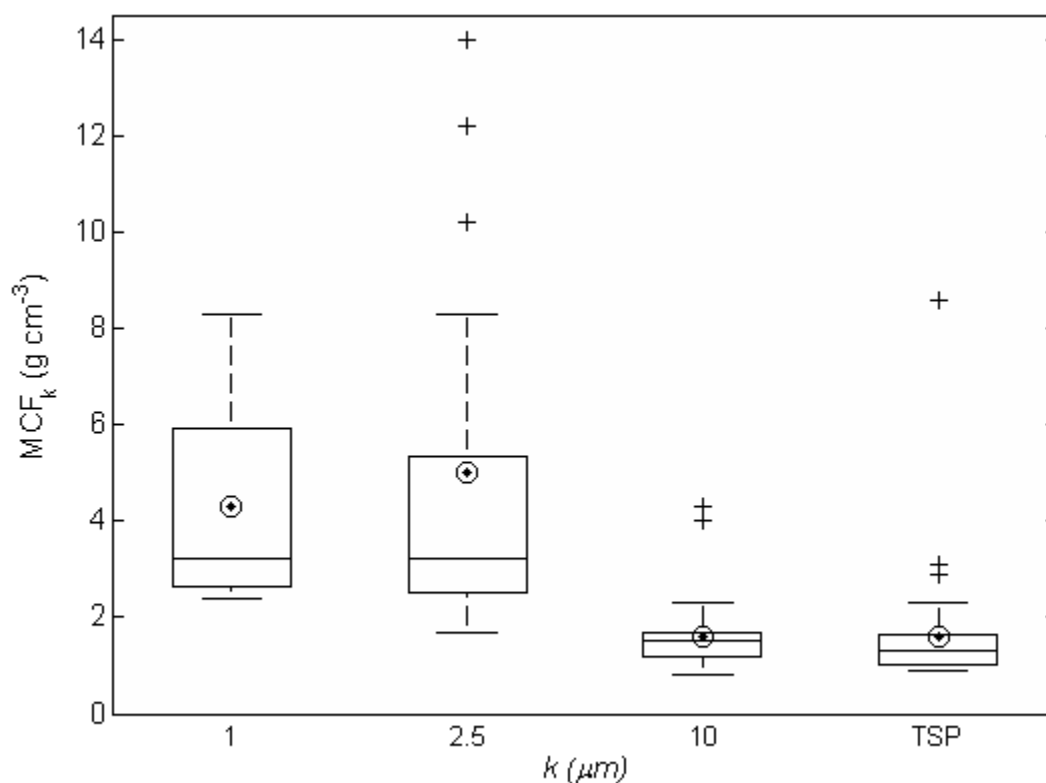


Figure 2-2. A box and whisker plot of period averaged MCF_k values.

multiple pairwise collocated comparisons to determine the minimum variability of the calculated MCFs. The RSD averages were 10% for MCF_1 , 8% for $MCF_{2.5}$, and 5% for both MCF_{10} and MCF_{TSP} with maximum values of 17%, 11%, 8%, and 6% for MCF_1 , $MCF_{2.5}$, MCF_{10} , and MCF_{TSP} , respectively. The data from all deployments show that calculated MCF values can be expected to have a minimum RSD of 5–10%, an average RSD \leq 25%, and maximum RSDs can be $>$ 50%. High RSDs were found across the range of average MCF values and the amount of variability was different across size fractions within a sample period.

High individual MCF values were calculated during multiple field studies, but were usually limited to the $MCF_{2.5}$. Some factors potentially contributing to variations in MCF_k were discussed earlier, including the properties of the particles, past and present environmental conditions, and sampling methodologies. Sample period average MCF_k values were graphically compared (not shown) with sample period average T_{amb} , RH, wind speed, and percent of OC, EC, ionic, and unknown chemical composition. Trends were not evident in any of these plots.

Sampling errors or irregularities may also influence the MCF. The majority of $MCF_{2.5}$ values above 5 g cm^{-3} , including the maximum of 66.1 g cm^{-3} , were from the field study referenced previously with the high $PM_{2.5}$ /low $V_{2.5}$ pairs. The cause of this grouping of high $MCF_{2.5}$ values is unclear, though sampling irregularities are suspected. Meteorological conditions were hot and dry throughout, minimizing potential effects of water absorption by hygroscopic particles. There was not a significant $PM_{2.5}$

composition difference between periods with higher and lower MCFs within this study. MCF_{10} and MCF_{TSP} patterns tended to follow $MCF_{2.5}$, having correlation coefficients (r) of 0.64 and 0.84, respectively, but with much smaller changes in amplitude. Comparing MCF values with sample duration produced good negative correlations ($-0.69 \leq r \leq -0.64$) for all MCF_k , which means that MCF_k tended to increase as sample duration decreased. Contamination during filter handling and storage is a possible cause, one to which samples with smaller mass catch, i.e. samplers with $PM_{2.5}$ impactor configurations and/or shorter sample times, would be more sensitive. Field and lab blanks, unfortunately, were not taken to monitor for and quantify contamination. Contamination mitigation and monitoring strategies have since been developed and successfully implemented. It is believed that a poor quality $PM_{2.5}$ dataset resulted in the unusually high $MCF_{2.5}$ values for a portion of this study.

The MCF method should be applied carefully and the quality of the data used in its calculation should be verified, as shown in the example above. In cases with poor quality data, the authors have occasionally chosen not to use the calculated MCF and instead used density values for the dominant particulate chemical component. In the example above, the average density of soil (2.65 g cm^{-3} , USDA NRCS, 2007) replaced the calculated $MCF_{2.5}$ values as measurements were being made of agricultural tillage plumes. If all the MCF_k values for this field study were removed, the mean \pm one SD and median values become 3.2 ± 0.6 and 2.7 g cm^{-3} for $MCF_{2.5}$ ($n = 27$), 1.4 ± 0.3 and 1.3 g

cm^{-3} for MCF_{10} ($n = 28$), and 1.1 ± 0.2 and 1.1 g cm^{-3} for MCF_{TSP} ($n = 21$). MCF_1 statistics do not change as PM_1 measurements were not made during this study.

Application of the MCF

Calculated MCF_k values have been used to convert V_k data collected by multiple optical instruments into PM_k . The MCFs were applied to OPC data, allowing the examination of temporal changes in mass loadings unresolved by filter-based MiniVols. For example, PM_{10} concentrations measured by a collocated MiniVol and OPC downwind of a commercial dairy over two days are shown in Fig. 2-3. The MiniVol collected integrated samples from 00:30 to 23:30 each day, yielding a single average concentration per sample period. The OPC provided a data point every 20 sec, which have been averaged up to 5 min and 23 hr, corresponding to the MiniVol sample time, and multiplied by the average MCF_{10} for both days of 1.3 g cm^{-3} . Note that the diurnal PM_{10} patterns easily shown by the 5 min averaged OPC data are not evident in the 23 hr average data that span the same time period. However, the influence of the evening peak is included in the 23 hr average concentrations as they are higher than the OPC 5 min average levels throughout most of the sample period. Applying the MCF in this case allows for the analysis of PM_{10} at much smaller temporal scales, which may help to explain emissions patterns and lead to more effective and efficient mitigation strategies.

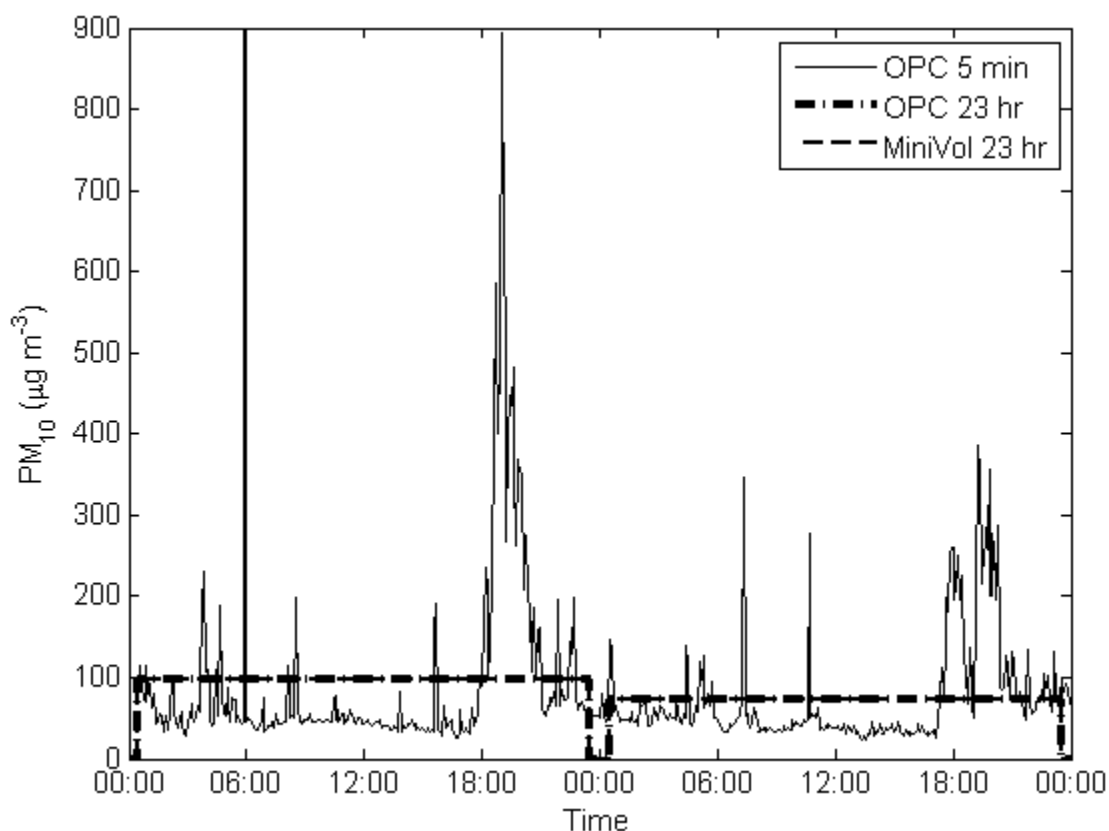


Figure 2-3. Time series of PM_{10} concentrations measured immediately downwind of a dairy farm over two days as measured by a collocated MiniVol and OPC.

A main objective of most of the field deployments was to estimate PM emissions from a source. In all such cases, an emissions estimation methodology was employed that used the difference between downwind and upwind MiniVol concentrations. OPC data may also be used for this after the conversion to mass concentration and on a finer temporal scale. For instance, Moore et al. (2011) estimated emissions during a wind erosion event based on OPC PM_k .

Another optical instrument to which the MCF has been applied is the Aglite elastic light detection and ranging (lidar) system, as described by Marchant et al. (2009).

The Aglite lidar is a three wavelength system capable of scanning in both horizontal and vertical directions that measures laser pulse returns from particles in the atmosphere. The lidar data analysis algorithm, described by Zavyalov et al. (2009), utilizes OPC data collected during the lidar operation to calibrate the lidar return signal, with the final product being an estimate of V_k in each lidar bin. The MCF_k values are then used to convert lidar V_k to PM_k , as shown in Fig. 2-4.

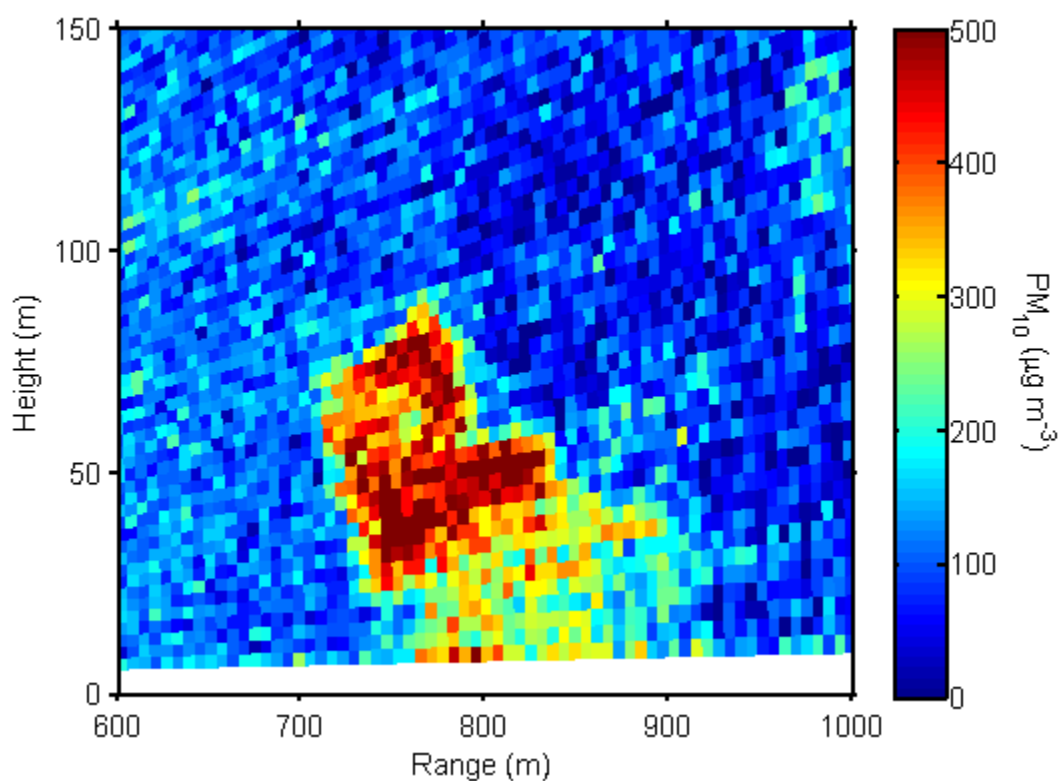


Figure 2-4. Example of PM_{10} concentrations calculated from a single lidar scan through the use of the MCF. This vertical scan was taken along the downwind edge of an agricultural field being tilled.

Comparisons between lidar and OPC data converted to PM_k with the MCF_k and MiniVol PM_k measurements have been made in most of the field campaigns involving the lidar (Bingham et al., 2009; Zavyalov et al., 2009; Marchant et al., 2011; Moore et al., 2013). In summary, the results have shown good agreement between the three at upwind locations with more variability between the lidar and the other two point measurements downwind of sources, particularly non-stationary ones such as agricultural tillage operations. A large factor contributing to the observed differences is that the lidar is normally operated in a scanning mode and, thereby, collects coincident data at the downwind OPC and MiniVol location for only 5-10% of a given time period. OPC PM_k values have usually been closer to MiniVol measurements due to collocation throughout the measurement period. For instance, the OPC 5 min average data in Fig. 2-3 were averaged over the 23 hr MiniVol sample periods and plotted. As can be seen, the 23 hr average OPC PM_{10} values are indistinguishable from the MiniVol reported concentrations, being only 2% higher. Refer to Moore et al. (2013) for more explanation of possible reasons for differences between the three measurements.

Note that the SD of PM_k is calculated as follows (Berthouex and Brown, 2002):

$$\frac{SD_{PMk}^2}{PM_k^2} = \frac{SD_{MCFk}^2}{MCF_k^2} + \frac{SD_{V_k}^2}{V_k^2} \quad \text{or} \quad (RSD_{PMk})^2 = (RSD_{MCFk})^2 + (RSD_{V_k})^2. \quad (2-5)$$

In the case of the MCF datasets presented herein, the RSD_{PMk} for the sample period average minimum RSD_{MCFk} (5%), RSD_{MCFk} for an arrayed deployment (20%), and maximum RSD_{MCFk} (50%) were calculated as 21%, 28%, and 54%, respectively, assuming

a RSD_{V_k} value of 20%. If a RSD_{V_k} value of 10% is used, the RSD_{PM_k} values drop to 11%, 22%, and 51%, respectively.

Mass calibrated lidar data have also been used to estimate source emissions through the application of a mass balance. Bingham et al. (2009) provide a description of the sampling and analysis methodology utilized to perform the mass balance emission calculations. Several papers have estimated emissions based on this technique (Bingham et al. 2009; Marchant et al. 2011; Moore et al. 2011, 2013). A scanning, mass calibrated lidar system such as this can provide PM concentration and emissions data over a large area in time steps on the order of seconds or minutes, allowing the identification of spatial inhomogeneity and temporal fluctuations and patterns on horizontal and vertical extents not achievable through point measurements.

If one desires to use this MCF technique to provide a mass concentration calibration for optical systems, it is recommended that the reliability and reproducibility of the particle measurement systems be sufficiently characterized, particularly the optical systems. The authors use calibrations in concert with collocated tests in typical deployment conditions to accomplish this objective. The development and use of the CCF_{ij} has proven key in normalizing OPC count data to RSD values of $\leq 10\%$ —the variability in counts between the OPCs employed by the authors during a collocated test challenges the confidence in any one of them to provide the true absolute particle count. While this reduces the confidence in calculated V and V_k , the MCF_k provides a

stable point of reference for PM_k . Additionally, the MCF should be applied with care as described above.

MiniVol Precision and Accuracy Test Results

Collocated comparison tests between filter-based PM sensors were conducted in three separate studies, each with replicate MiniVol samplers over four to five sample periods. $PM_{2.5}$ concentrations measured by the FRM units ranged from $7.4 \mu\text{g m}^{-3}$ to $53.4 \mu\text{g m}^{-3}$, while PM_{10} levels ranged from $4.0 \mu\text{g m}^{-3}$ to $40.7 \mu\text{g m}^{-3}$. The maximum and minimum PM_{10} concentrations being lower than the $PM_{2.5}$ values are not of concern—all but one of the PM_{10} comparison tests were conducted on separate days from the $PM_{2.5}$ tests and, in the case of the coincident test, the reported PM_{10} level was higher than the $PM_{2.5}$ level. All data were screened for noted sample handling and collection errors.

Fig. 2-5 presents both $PM_{2.5}$ and PM_{10} comparisons with the MiniVol data along the x-axis and the FRM data along the y-axis. As can be seen from this graph, most of the MiniVol data are fairly well clustered, with most cluster cores within $\pm 10\%$ of the 1-to-1 line across the range of observed values. However, there are several points significantly outside of the clusters. The extreme value test was used to determine if these points were statistical outliers. Nineteen points were found to be statistical outliers and have been marked on the graph by a dot inside the marker. Note that all but two of the outliers were found in the $PM_{2.5}$ dataset, and that 12 of those were in the $PM_{2.5}$ comparison test carried out in March 2004. Out of the four sample periods in this

study, one sampler contributed four statistical outliers, a second contributed three outliers, and a third contributed two outliers. Multiple outliers resulting from a single sampler is suggestive of sampler operational issues. Therefore, all data from these samplers were removed from further analysis and the outlier analysis for this PM_{2.5} dataset was performed again, resulting in only three identified as statistical outliers for a total of 10 from all datasets. All other samplers with outlier data points had just one each. The following linear regression equations were developed based on the remaining points: $FRM = 0.99 \times \text{MiniVol} + 0.31$, $R^2 = 0.962$, for PM_{2.5}; and $FRM = 0.83 \times \text{MiniVol} + 3.90$, $R^2 = 0.918$, for PM₁₀.

Potential causes of variability and outliers between the MiniVol samples may include, but are not limited to, the following: 1) recording errors during weighing or operation logging, 2) improper setting of the sample flow, 3) sample contamination, 4) improper assembly of the sampler head, 5) non-uniform PM levels across the inlets, and 6) random variability in sampler operation and mass catch determination. Preventative measures were taken to decrease the likelihood of the first five listed causes. Personnel were trained on proper instrument assembly, instrument operation, sample handling, filter weighing, and datalogging procedures to minimize human error. Filter exposure during handling and transport was minimized to prevent contamination. Samplers were deployed close together, in the ambient air, and within areas of uniform surface and source conditions to maximize uniformity in average PM concentrations. Random

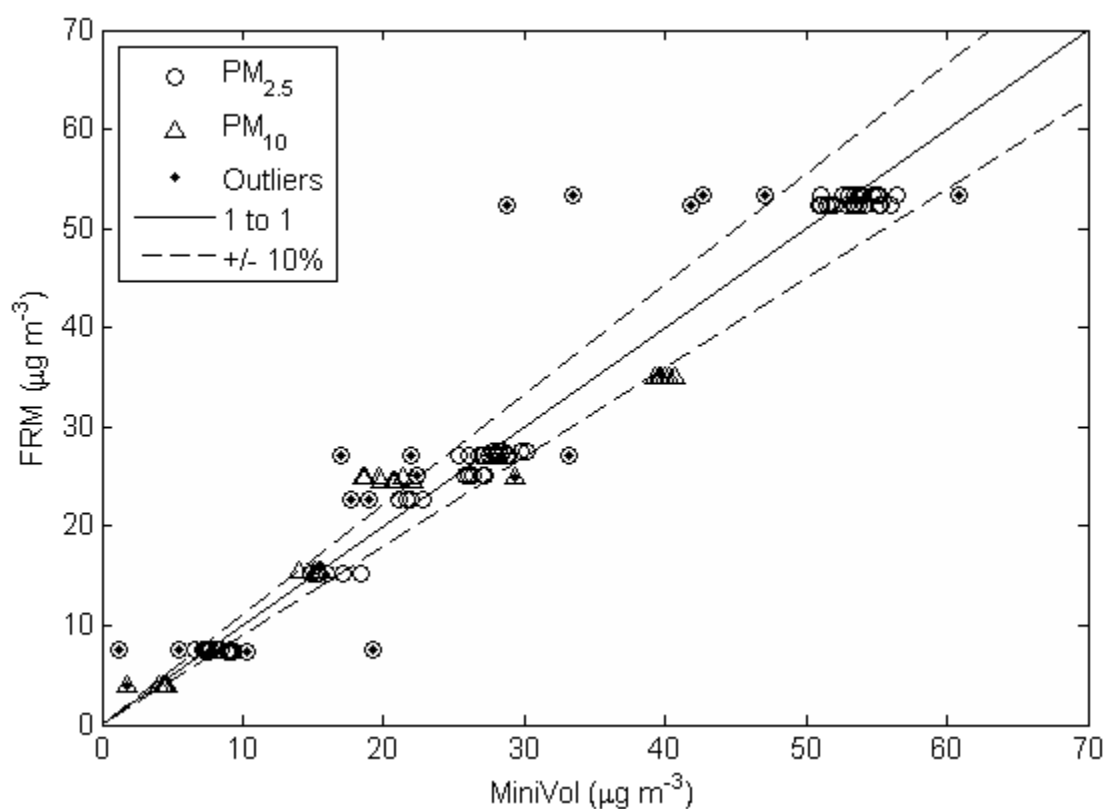


Figure 2-5. Comparison of $\text{PM}_{2.5}$ and PM_{10} concentrations reported by the MiniVols and the respective FRM samplers.

variability in sampler operation would likely result in relatively small variations in reported concentrations, not the large differences seen in the case of some outliers. The outliers seen in this study and not removed due to sampler operational issues, as previously discussed, are likely the result of a combination of human error, instrument operation anomalies, or random variations in PM concentration, though the exact cause(s) were not identifiable. Unless otherwise noted, these data were not excluded from further calculations due to the lack of an identified cause.

Table 2-2 lists various statistical measures of the variability between the MiniVol samplers for each size fraction in each study. The variability of reported PM concentrations between the MiniVols within a sample period, expressed as the RSD, ranged from 1% to 27%. The variability between MiniVols was generally smaller across all size ranges during the 2007 study compared to the 2004 studies with all average RSDs below 10%. The bias of the MiniVols was calculated by subtracting the sample period FRM concentration from the average MiniVol concentration and averaging across the sample periods within each study. The average PM_{2.5} biases were less than $\pm 1 \mu\text{g m}^{-3}$, but the PM₁₀ biases averaged $-1.9 \mu\text{g m}^{-3}$ during the March 2004 study and $+4.9 \mu\text{g m}^{-3}$ for the single PM₁₀ sample period in the July 2007 study with a corresponding FRM sample. The results of the FRM and MiniVol comparison from these collocated sample periods are presented in Table 2-2 as a ratio. An FRM/MiniVol ratio of 1.0 shows the MiniVol reported the same PM concentration as the FRM, while a ratio greater than 1.0 results from higher MiniVol concentrations and vice versa for ratios less than 1.0. The average ratios from the two PM_{2.5} tests \pm the 95% confidence interval (CI) were 1.03 ± 0.04 and 0.96 ± 0.04 for the 2004 and 2007 studies, respectively. These show the MiniVols were, on average, in very good agreement with the PM_{2.5} FRM under these conditions, even that the 95% CIs bound the value 1.00 in both cases. The PM₁₀ ratios showed a higher deviation from 1.00 with 1.15 ± 0.14 and 0.88 ± 0.01 for the two studies, though the average values are still within 15% of 1.00.

Table 2-2. Statistical measures of the intra- and inter-instrument comparability test datasets (including outliers) conducted in March 2004 and July 2007.

Statistic	Statistic	Units	March 2004		July 2007			
			PM _{2.5}	PM ₁₀	PM ₁	PM _{2.5}	PM ₁₀	TSP ^a
Sample Periods		count	4		5			
FRM PM Concentration								
Range	Min	µg m ⁻³	7.6	4.0	---	7.4	35.0 ^b	---
	Max	µg m ⁻³	53.4	24.9	---	27.6	---	---
MiniVol PM Concentration								
Range	Min	µg m ⁻³	6.6	1.8	7.4	7.6	17.9	45.3
	Max	µg m ⁻³	56.5	29.3	25.5	30.2	49.5	78.8
RSD	Avg	%	10	13	8	7	4	3
	Min	%	5	4	3	3	1	3
	Max	%	14	27	14	10	8	3
Bias	Avg	µg m ⁻³	-0.5	-1.9	---	+0.6	+4.9 ^b	---
	SD	µg m ⁻³	0.7	1.9	---	1.4	---	---
Samples		count	48	18	15	33	33	12
Outliers		count	3	2	0	5	0	0
FRM/MiniVol Ratio								
Avg		Unitless	1.03	1.15	---	0.96	0.88	---
SD		Unitless	0.16	0.31	---	0.11	0.01	---
95% CI		Unitless	0.04	0.14		0.04	0.01	

Note: Avg = average, CI = confidence interval, Min = minimum, Max = maximum, RSD = relative standard deviation, SD = standard deviation, --- = no data or insufficient data

^a Based on only two sample periods with three valid samples each

^b Only one PM₁₀ sample collected by the Federal Reference Method (FRM) sampler

Several previous MiniVol precision and accuracy studies have been reported in multiple PM sampling configurations. Heal et al. (2000), Baldauf et al. (2001), and Chen et al. (2007) reported very good MiniVol precision. Baldauf et al. (2001), Chow et al. (2002), and Chen et al. (2011) found the MiniVols yielded PM levels very similar to the

comparison sampling systems. Hill et al. (1999) found that the PM_{2.5} MiniVol was statistically “equivalent” to an FRM only when results were field blank corrected. Chow et al. (2006) found differences between PM_{2.5} MiniVols and FRMs at multiple sites ranging from 1.23 to 1.41 and had an overall average of 1.32. Heal et al. (2000) reported the MiniVol correlated very well with a FRM PM₁₀ sampler in indoor environments with PM₁₀ levels $\sim 10 \mu\text{g m}^{-3}$, but on average reported mass concentrations 23% greater. Salter and Parsons (1999) found a MiniVol did not correlate well in comparisons with a tapered element oscillating microbalance (TEOM; Rupprecht & Patashnick Co. Inc., now Thermo Fisher Scientific, Inc., Waltham, MA, USA) and a Partisol. Kingham et al. (2006) found weak PM₁₀ correlations with data from both a TEOM and a DustTrak during one series of measurements and good correlations during a second series of measurements.

Insights gained through these tests and analyses with respect to obtaining accurate and precise PM measurements with MiniVols (or any other PM system) should be noted. First, proper maintenance and regular inspection of the MiniVol is required, with particular focus on flow calibration and the impactor assembly. Second, occasional collocated tests are suggested for comparisons between multiple MiniVols and, if possible, an FRM to monitor for operational issues. If possible, these tests should be carried out under conditions typical of deployments. Third, proper personnel training is key to reducing human error.

Summary and Conclusions

Currently available PM monitoring systems based on optical measurements generally use calibration factors calculated from historical data to estimate PM concentrations. However, the applicability of these calibrations may be questionable when properties of the measured aerosol are different from properties of the aerosols used to estimate the calibration factor. In this paper we have presented a simple, on-site procedure to determine the MCF_k that may be used to convert data from an optical instrument into PM_k levels based on the actual measurement conditions. This procedure may also be used with an optical system for which a PM calibration has not been developed. Data from field measurements have been presented to demonstrate typical MCF_k values for $k = 1 \mu\text{m}$, $2.5 \mu\text{m}$, $10 \mu\text{m}$, and TSP. MCF_1 and $MCF_{2.5}$ values tend to be higher than MCF_{10} and MCF_{TSP} within a sample period. The average RSDs were about 20% for arrayed measurements made during multiple field studies and $< 10\%$ for collocated measurements. The MCF_k has been key in converting optical instrument data to mass concentration, which has allowed for examination of concentration and emissions data on much smaller time scales and, in the case of a scanning lidar, over much greater spatial scales.

Results from studies examining the precision and accuracy of the MiniVol PM sampler are given. The sample period RSDs were usually $< 10\%$ for PM_1 , $PM_{2.5}$, PM_{10} , and TSP size fractions. Comparisons at the $PM_{2.5}$ size fraction between MiniVols and

FRMs showed excellent agreement with average FRM/MiniVol ratios \pm 95% CI of 1.03 ± 0.04 and 0.96 ± 0.04 and average biases $< \pm 1 \mu\text{g m}^{-3}$. Results of the PM_{10} comparisons were not as strong with average ratios of 1.15 ± 0.14 and 0.88 ± 0.01 and biases of $-1.9 \mu\text{g m}^{-3}$ and $+4.9 \mu\text{g m}^{-3}$. In conclusion, the MiniVols yielded $\text{PM}_{2.5}$ values that were essentially equivalent to $\text{PM}_{2.5}$ concentrations reported by FRM samplers under these test conditions, and PM_{10} values were in good agreement with PM_{10} FRM measurements.

Acknowledgments

This material is partially based upon work supported by the U.S. Department of Agriculture, Cooperative Agreement # 58-3625-9-743. Any opinions, findings, conclusions, or recommendations expressed in this publication are those of the authors and do not necessarily reflect the view of the U.S. Department of Agriculture. The State of Utah, Department of Environmental Quality also provided funding and equipment support for some of the data collection. The authors thank the teams involved in conducting the field work. Mention of a trademark, proprietary product, or vendor is for information purposes only and does not constitute an endorsement by the U.S. Department of Agriculture, State of Utah, Utah State University, or Space Dynamics Laboratory.

References

- Baldauf, R. W., Lane, D. D., Marotz, G. A., and Wiener, R. W. (2001). "Performance evaluation of the portable MiniVOL particulate matter sampler." *Atmos. Environ.*, 35, 6087-6091. doi: 10.1016/S1352-2310(01)00403-4.
- Berthouex, P. M., and Brown, L. C. (2002). "Precision of calculated values." *Statistics for Environmental Engineers, 2nd Ed.* Lewis Publishers, Boca Raton, FL, 87-95.
- Bingham, G. E., Marchant, C. C., Zavyalov, V. V., Ahlstrom, D. J., Moore, K. D., Jones, D. S., Wilkerson, T. D., Hipps, L. E., Martin, R. S., Hatfield, J. L., Prueger, J. H., and Pfeiffer, R. L. (2009). "Lidar based emissions measurement at the whole facility scale: Method and error analysis." *J. Appl. Rem. Sens.*, 3(1), 033510. doi: 10.1117/12.829411.
- Binnig, J., Meyer, J., and Kasper, G. (2007). "Calibration of an optical particle counter to provide PM_{2.5} mass for well-defined particle materials." *J. Aerosol Sci.*, 38, 325-332. doi: 10.1016/j.jaerosci.2006.12.001.
- Chen, F.-L., Williams, R., Svendsen, E., Yeatts, K., Creason, J., Scott, J., Terrell, D., and Case, M. (2007). "Course particulate matter concentrations from residential outdoor sites associated with the North Carolina Asthma and Children's Environment Studies (NC-ACES)." *Atmos. Environ.*, 41, 1200-1208. doi: 10.1016/j.atmosenv.2006.09.049.
- Chen, F.-L., Vanderpool, R., Williams, R., Dimmick, F., Grover, B. D., Long, R., and Murdoch, R. (2011). "Field evaluation of portable and central site PM samplers emphasizing additive and differential mass concentration estimates." *Atmos. Environ.*, 45, 4522-4527. doi: 10.1016/j.atmosenv.2011.02.006.
- Chow, J.C., Watson, J.G., Edgerton, S. A., Vega, E., and Ortiz, E. (2002). "Spatial differences in outdoor PM₁₀ mass and aerosol composition in Mexico City." *J. Air Waste Manage. Assoc.*, 52, 423-434. doi: 10.1080/10473289.2002.10470791.
- Chow, J.C., Watson, J. G., Lowenthal, D. H., Chen, L.-W.A., Tropp, R. J., Park, K., and Magliano, K. A. (2006). "PM_{2.5} and PM₁₀ mass measurements in California's San Joaquin Valley." *Aerosol Sci. Technol.*, 40, 796-810. doi: 10.1080/02786820600623711.

- Finlayson-Pitts, B. J., and Pitts, J. N., Jr. (1999). *Chemistry of the upper and lower atmosphere: theory, experiments, and applications*. Academic Press, San Diego, CA.
- Grimm, H., and Eatough, D. J. (2009). "Aerosol measurement: The use of optical light scattering for the determination of particulate size distribution, and particulate mass, including the semi-volatile fraction." *J. Air Waste Manage. Assoc.*, 59, 101-107. doi: 10.3155/1047-3289.59.1.101.
- Heal, M. R., Beverland, I. J., McCabe, M., Hepburn, W., and Agius, R. M. (2000). "Intercomparison of five PM₁₀ monitoring devices and the implications for exposure measurement in epidemiological research." *J. Environ. Monit.*, 2, 455-461.
- Held, T., Ying, Q., Kaduwela, A., Kleeman, M. (2004). "Modeling particulate matter in the San Joaquin Valley with a source-oriented externally mixed three-dimensional photochemical grid model." *Atmos. Environ.*, 38, 3689-3711. doi:10.1016/j.atmosenv.2004.02.053.
- Hill, J. S., Patel, P. D., and Turner, J. R. (1999). "Performance characterization of the MiniVol PM_{2.5} Sampler." *Proc., Air and Waste Management Association's 92nd Annual Meeting*, Air and Waste Management Association, Pittsburgh, PA, Paper 99-617.
- Kingham, S., Durand, M., Aberkane, T., Harrison, J., Wilson, J. G., and Epton, M. (2006). "Winter comparison of TEOM, MiniVol and DustTrak PM₁₀ monitors in a woodsmoke environment." *Atmos. Environ.*, 40, 338-347. doi:10.1016/j.atmosenv.2005.09.042.
- Lareau, N. P., Crosman, E., Whiteman, C. D., Horel, J. D., Hoch, S. W., Brown, W. O., and Horst, T.W. (2013). "The persistent cold-air pool study." *Bull. Amer. Metero. Soc.*, 93, 51-63. doi: 10.1175/BAMS-D-11-00255.1.
- Malek, E., Davis, T., Martin, R. S., and Silva, P. J. (2006). "Meteorological and environmental aspects of one of the worst national air pollution episodes (January, 2004) in Logan, Cache Valley, Utah, USA." *Atmos. Res.*, 79, 108-122. doi:10.1016/j.atmosres.2005.05.003.
- Malm, W. C., and Hand, J. L. (2007). "An examination of the physical and optical properties of aerosols collected in the IMPROVE program." *Atmos. Environ.*, 41, 3407-3427. doi: 10.1016/j.atmosenv.2006.12.012.

- Malm, W. C., Schichtel, B. A., Pitchford, M. L., Ashbaugh, L. L., and Eldred, R. A. (2004). "Spatial and monthly trends in speciated fine particle concentration in the United States." *J. Geophys. Res.*, 109, D03306. doi: 10.1029/2003JD003739.
- Marchant, C. C., Wilkerson, T. D., Bingham, G. E., Zavyalov, V. V., Andersen, J. M., Wright, C. B., Cornelsen, S. S., Martin, R. S., Silva, P. J., and Hatfield, J. L. (2009). "Aglite lidar: A portable elastic lidar system for investigating aerosol and wind motions at or around agricultural production facilities." *J. Appl. Rem. Sens.*, 3(1), 033511. doi: 10.1117/12.829412.
- Marchant, C. C., Moore, K. D., Wojcik, M. D., Martin, R. S., Pfeiffer, R. L., Prueger, J. H., and Hatfield, J.L. (2011). "Estimation of dairy particulate matter emission rates by lidar and inverse modeling." *Trans. ASABE*, 54, 1453-1463.
- Moore, K. D., Wojcik, M. D., Marchant, C. C., Martin, R. S., Pfeiffer, R. L., Prueger, J. H., and Hatfield, J. L. (2011). "Comparisons of measurements and predictions of PM concentrations and emission rates from a wind erosion event." *Proc., Int. Symp. on Erosion and Landscape Evolution*, American Society of Agricultural and Biological Engineers, St. Joseph, MI, Paper 11020.
- Moore, K. D., Wojcik, M. D., Martin, R. S., Marchant, C. C., Bingham, G. E., Pfeiffer, R. L., Prueger, J. H., and Hatfield, J. L. (2013). "Particulate emissions calculations from fall tillage operations using point and remote sensors." *J. Environ. Qual.*, 42, 1029-1038. doi:10.2134/jeq2013.01.0009.
- Peters, T. M. (2006). "Use of the Aerodynamic Particle Sizer to measure ambient PM_{10-2.5}: the coarse fraction of PM₁₀." *J. Air Waste Manage. Assoc.*, 56, 411-416.
- Salter, L. F., and Parsons, B. (1999). "Field trials of the TEOM® and Partisol for PM₁₀ monitoring in the St. Austell china clay area, Cornwall, UK." *Atmos. Environ.*, 33, 2111-2114.
- Schmid, O., Karg, E., Hagen, D. E., Whitefield, P. D., and Ferron, G. A. (2007). "On the effective density of non-spherical particles as derived from combined measurements of aerodynamic and mobility equivalent size." *J. Aerosol Sci.*, 38, 431-443. doi:10.1016/j.jaerosci.2007.01.002.
- Silcox, G. D., Kelly, K. E., Crosman, E. T., Whiteman, C. D., and Allen, B. L. (2012). "Wintertime PM_{2.5} concentrations during persistent, multi-day cold-air pools in a

mountain valley." *Atmos. Environ.*, 46, 17-24. doi:
10.1016/j.atmosenv.2011.10.041.

Silva, P. J., Vawdrey, E. L., Corbett, M., and Erupe, M. (2007). "Fine particle concentrations and composition during wintertime inversions in Logan, Utah, USA." *Atmos. Environ.*, 41, 5410-5422. doi: 10.1016/j.atmosenv.2007.02.016.

Tropp, R., Jones, K., Kuhn, G., and Berg, N. (1998). "Comparison of PM_{2.5} saturation samplers with prototype PM_{2.5} Federal Reference Method samplers." *Proc. Air and Waste Management Association's 91st Annual Meeting*, Air and Waste Management Association, Pittsburgh, PA, Paper 98-TA31A.04.

U.S. Department of Agriculture, Natural Resources Conservation Service (USDA NRCS). (2007). *National Soil Survey Handbook*, 430-VI, <<http://soils.usda.gov/technical/handbook/>> (Dec. 20, 2007).

Zavalyov, V. V., Marchant, C. C., Bingham, G. E., Wilkerson, T. D., Hatfield, J. L., Martin, R. S., Silva, P. J., Moore, K. D., Swasey, J., Ahlstrom, D. J., and Jones, T.L. (2009). "Aglite lidar: Calibration and retrievals of well characterized aerosols from agricultural operations using a three-wavelength elastic lidar." *J. Appl. Rem. Sens.*, 3(1), 033522. doi: 10.1117/12.833365.

CHAPTER 3

PARTICULATE EMISSIONS CALCULATIONS FROM FALL TILLAGE

OPERATIONS USING POINT AND REMOTE SENSORS¹**Abstract**

Soil preparation for agricultural crops produces aerosols that may significantly contribute to seasonal atmospheric particulate matter (PM). Efforts to reduce PM emissions from tillage through a variety of conservation management practices (CMP) have been made but the reductions from many of these practices have not been measured in the field. A study was conducted in California's San Joaquin Valley to quantify emissions reductions from fall tillage CMPs. Emissions were measured from conventional tillage methods and a "Combined Operations" CMP, which combines several implements to reduce tractor passes. Measurements were made of soil moisture, bulk density, meteorological profiles, filter-based TSP (total suspended PM), PM₁₀ (PM with an equivalent aerodynamic diameter $\leq 10 \mu\text{m}$), and PM_{2.5} (PM with an equivalent aerodynamic diameter $\leq 2.5 \mu\text{m}$) concentrations, and aerosol size distribution. A mass-calibrated, scanning, three wavelength lidar estimated PM through a series of algorithms. Emissions were calculated via inverse modeling with mass

¹ Citation: Moore, K.D., M.D. Wojcik, R.S. Martin, C.C. Marchant, G.E. Bingham, R.L. Pfeiffer, J.H. Prueger, and J.L. Hatfield. 2013. Particulate emissions calculations from fall tillage operations using point and remote sensors. *Journal of Environmental Quality*, 42:1029-1038.

concentration measurements and applying a mass balance to lidar data. Inverse modeling emission estimates were higher, often with statistically significant differences. Derived PM₁₀ emissions for conventional operations generally agree with literature values. Sampling irregularities with a few filter-based samples prevented calculation of a complete set of emissions through inverse modeling; however, the lidar-based emissions dataset was complete. The CMP control effectiveness was calculated based on lidar-derived emissions to be 29% ± 2%, 60% ± 1%, and 25% ± 1% for PM_{2.5}, PM₁₀, and TSP size fractions, respectively. Implementation of this CMP provides an effective method for the reduction of PM emissions.

Introduction

Agricultural air emissions of gaseous species and particles, such as ammonia (NH₃), volatile organic compounds (VOCs), and particulate matter (PM), are being increasingly evaluated for their contributions to local and regional atmospheric loading and their effects on air quality. Sources of these emissions include animal husbandry, waste management, harvesting, and tillage operations. The USEPA has set National Ambient Air Quality Standards (NAAQS) for ambient concentrations of designated criteria pollutants (CO, NO_x, O₃, SO_x, PM₁₀ and PM_{2.5}, and Pb). Air quality regulatory agencies use the NAAQS to regulate emissions of pollutants that contribute to the concentration of criteria pollutants, with more stringent emissions requirements in areas determined to be in “nonattainment” with the NAAQS.

The San Joaquin Valley Air Basin was classified as being in nonattainment for PM₁₀ until November 2008, and as such, the San Joaquin Valley Air Pollution Control District (SJVAPCD) was required to implement emission controls for all significant PM₁₀ sources in order to reduce primary PM₁₀ emissions. Agricultural operations above a specified size that grow crops and/or have animal feeding operations were included in the list of significant sources required to reduce emissions and subject to SJVAPCD Rule 4550, Conservation Management Practices (CMPs), passed in August 2004. In order to meet targeted PM emissions reductions, producers were required to choose at least one CMP from a list of several options for each applicable management area, submit the planned CMP strategy, and implement it once the plan was approved. The small amount of data available in the literature concerning the variety of CMPs for tillage activities required that most control efficiencies were estimated from emissions measurements of other operations (SJVAPCD, 2006). While the San Joaquin Valley Air Basin is currently classified as in attainment with the PM₁₀ NAAQS, its maintenance plan requires the same strategies employed to bring it back into attainment continue to be applied. In addition, other PM₁₀ non-attainment areas such as Imperial Valley, CA and Phoenix, AZ have CMP or best management practice (BMP) rules in place for agricultural tillage practices.

Previous research on PM emissions from agricultural tillage operations (Flocchini et al., 2001; Holmen et al., 1998, 2001a, 2001b; Kasumba et al., 2011; Madden et al., 2008; Wang et al., 2010) have focused almost exclusively on PM₁₀ emission rates (ERs)

and factors (EFs). A significant conclusion from Flocchini et al. (2001) found emission factors were significantly influenced by environmental conditions, e.g., near-ground temperature profile, relative humidity, and soil moisture, and the potential variability of emissions from the same implement under opposing extreme environmental conditions may be larger than the variation from the type of crop or equipment used for tilling. Holmen et al. (1998) used elastic lidar (light detection and ranging) data collected during tillage emissions measurements to track plume movements in the downwind vertical plane and demonstrate plume depths were greater than the elevated point sensors located downwind at 10 m above ground level (agl). They suggested the best method for sampling fugitive dust includes a combination of elastic lidar and strategically placed point samplers. Marchant et al. (2011) utilized point sensors and a mass calibrated lidar to investigate fugitive dust emissions from a dairy. Madden et al. (2008) is the only one to report PM₁₀ emissions from standard tillage operations and a CMP (strip-till). The California Air Resource Board (ARB) developed area source PM₁₀ emission inventory calculation methodologies for agricultural tillage and harvesting operations based on the report by Flocchini et al. (California ARB, 2003a, 2003b).

A Regional Applied Research Effort (RARE) grant was awarded to the USEPA Office of Research and Development, National Exposure Research Laboratory (NERL) in order to investigate the control effectiveness of one or more of the listed SJVAPCD CMPs using advanced measurement technologies in a field scale setting. The research questions this study was designed to address were: 1) what are the magnitude, flux, and

transport of PM emissions produced by agricultural practices for row crops where tillage CMPs are being implemented vs. the magnitude, flux, and transport of PM emissions produced by agricultural practices where CMPs are not being implemented?; 2) what are the control efficiencies of equipment being used to implement the “combined operations” CMP?; and 3) can these CMPs for a specific crop be quantitatively compared, controlling for soil type, soil moisture, and meteorological conditions? It is important to note that the main focus of this research was to quantify the control effectiveness of the selected CMP, which required the emissions to be quantified, and it was not an effort to provide representative emission factors for any one of the agricultural operations involved. This paper summarizes the results of the PM measurements made during a field experiment, the calculated ERs, and addresses these research questions. A full report detailing all of the sampling methodology and results is given in Williams et al. (2012).

Materials and Methods

The fall tillage sequence after harvest of a row crop (cotton) was selected for this comparison study. The experiment was carried out near Los Banos, California, during October 2007 on two adjacent fields with nearly identical crop and irrigation treatment over the previous several years. They were both planted in cotton for the 2007 growing season, which had been harvested prior to tillage activities with the stalks shredded and left on the ground (cooperating producer, personal communication, 2007). The site was

chosen based on producer cooperation, historically dominant northwest winds, and field layout. The surrounding landscape was flat and dominated by agricultural crop production. USDA-NRCS soil survey data list the soil in both fields as being dominated by nearly identical distributions of three clay loam classifications: 103 – Alros clay loam, partially drained; 139 – Bolfar clay loam, partially drained; and 170 – Dos Palos clay loam, partially drained (Soil Survey Staff, 2007).

The CMP selected for investigation was the Combined Operations method, which reduces the number of passes by combining multiple operations into one. The CMP implement used was the Optimizer 5000 (Tillage Management, Tulare, California), which incorporates all forms of conventional tillage into a single pass. The CMP was applied to Field B (51.8 ha) and standard practices were used in Field A (25.5 ha). The sampling schedule is given in Table 3-1, providing the date, operation, sample time, total tractor time, total area tilled, and tillage rate. Most of the operations had two tractor and implement pairs working the field at one time; total tractor time is the sum of time spent by each tractor and implement pair tilling the field. Less than the full field was tilled in each measurement period due to environmental, temporal, and equipment factors. For example, there were two samples collected for the Disc 2 pass – farm equipment malfunctions during the Disc 2A sample period halted the operation and it was resumed the following day when the remainder of the field was tilled in the Disc 2B sample period.

Table 3-1. Sample schedule and sample period tillage and meteorological characteristics. Meteorological parameters measured at 5 m above ground level.

Date	Tillage Operation	Sample time hr	Total tractor time hr _{tractor}	Total area tilled ha	Tillage rate ha hr _{tractor} ⁻¹	Mean temp ± 1σ C	Mean wind speed ± 1σ m s ⁻¹	Mean wind direction ± 1σ °
<u>Combined Operations Practice – Field B</u>								
19 Oct.	Chisel	5.33	8.5	22.0	2.6	20.5 ± 2.8	1.1 ± 0.3	43 ± 62
20 Oct.	Optimizer	2.85	4.36	20.0	4.7	16.8 ± 1.3	6.9 ± 2.0	320 ± 1
<u>Conventional Practice – Field A</u>								
23 Oct.	Disc 1	7.27	11.0	24.8	2.3	26.1 ± 2.6	1.6 ± 0.6	320 ± 7
25 Oct.	Chisel	4.24	6.5	19.5	3.0	27.4 ± 1.8	1.2 ± 0.8	338 ± 9
26 Oct.	Disc 2A	5.52	3.4	10.5	3.0	22.0 ± 1.9	2.9 ± 0.8	328 ± 5
27 Oct.	Disc 2B	4.09	5.75	14.2	2.5	22.7 ± 1.9	3.1 ± 1.3	10 ± 33
	Total Disc 2	9.61	9.16	24.7	2.7	---	---	---
29 Oct.	Land Plane	3.49	3.33	8.0	2.4	23.5 ± 1.6	1.7 ± 0.9	1 ± 19

Sample Layout

Sensors for PM and meteorology were distributed to measure upwind and downwind conditions based on the historically dominant northwest wind.

Meteorological characterizations were performed at upwind, downwind, and crosswind

locations with the instrumentation in Table 3-2. Vertical temperature, humidity, and wind speed profiles were measured using two 15.3 m towers, one upwind and one downwind as shown in Figure 3-1. Each tower had five humidity/temperature sensors at 1.5, 2.5, 3.9, 6.2, and 9.7 m above ground level (agl) of and 3-cup anemometers at 2.5, 3.9, 6.2, 9.7, and 15.3 m agl. Wind direction was measured at 15.3 m using a wind vane. Wind direction measurements were made at 15.3 m agl on the towers instead of 10 m, as is typical, due to fact that lidar measurements were made at higher elevations (up to 200 m agl) and the 15.3 m measurement height was reasoned to provide a better representation of both ground level and higher elevation wind direction than the 10 m height. A meteorological station monitored wind speed, wind direction, temperature, relative humidity, precipitation, barometric pressure, and solar radiation at 5 m agl at the air quality (AQ) trailer locations in Figure 3-1. Four pairs of three-dimensional sonic anemometers and infrared gas analyzers were deployed around the fields to characterize upwind and downwind turbulence, as well as vertical fluxes of latent heat (evaporation), sensible heat, carbon dioxide, and horizontal momentum. Bulk density and soil moisture were quantified prior to each operation, with calculations performed as described in Doran and Janis (1996).

Particulate matter was characterized by 30 MiniVol Portable Air Samplers (AirMetrics, Eugene, Oregon), a filter-based mass concentration sampler, and by nine Aerosol Profilers (model 9722, Met One Instruments, Grants Pass, Oregon), also known as optical particle counters (OPCs). The MiniVol is a portable, programmable, filter-

Table 3-2. Manufacturer, precision, and accuracy information for deployed meteorological instrumentation.

Instrument Model	Manufacturer	Measured Parameter	Accuracy
HMP45C	Vaisala, Oulu, Finland	temperature relative humidity	± 0.2 C at 20 C $\pm 2\%$ for values in the range 0% to 90% and $\pm 3\%$ for values in the range 90% to 100%
Gill 3-cup anemometer	RM Young Co., Traverse City, Michigan	horizontal wind speed	± 0.2 m s ⁻¹ over 1 m s ⁻¹ , threshold speed = 0.5 m s ⁻¹
024A Wind Vane	Met One Instruments, Grants Pass, Oregon	wind direction	$\pm 5^\circ$
Vantage Pro2 Plus Weather Station	Davis Instruments, Inc., Hayward, California	temperature relative humidity horizontal wind speed wind direction precipitation barometric pressure solar radiation	± 0.5 C for values greater than -7 C, ± 1.0 C for values less than -7 C $\pm 3\%$ for values 0% to 90% and $\pm 4\%$ for values 90% to 100% ± 1 m s ⁻¹ or 5%, whichever is greater $\pm 3^\circ$ $\pm 3\%$ or 0.02 mm per event, whichever is greater ± 0.8 mm Hg at 25°C $\pm 5\%$ of full scale
CSAT	Campbell Scientific, Inc., Logan, Utah	three dimensional wind vector	Offset error $< \pm 8$ cm s ⁻¹ Gain error for wind vector within 20° of horizontal $< \pm 6\%$ of reading
7500 Infrared Gas Analyzer	LI-COR, Lincoln, Nebraska	gaseous H ₂ O and CO ₂ concentrations	Dependent on calibration and environmental conditions

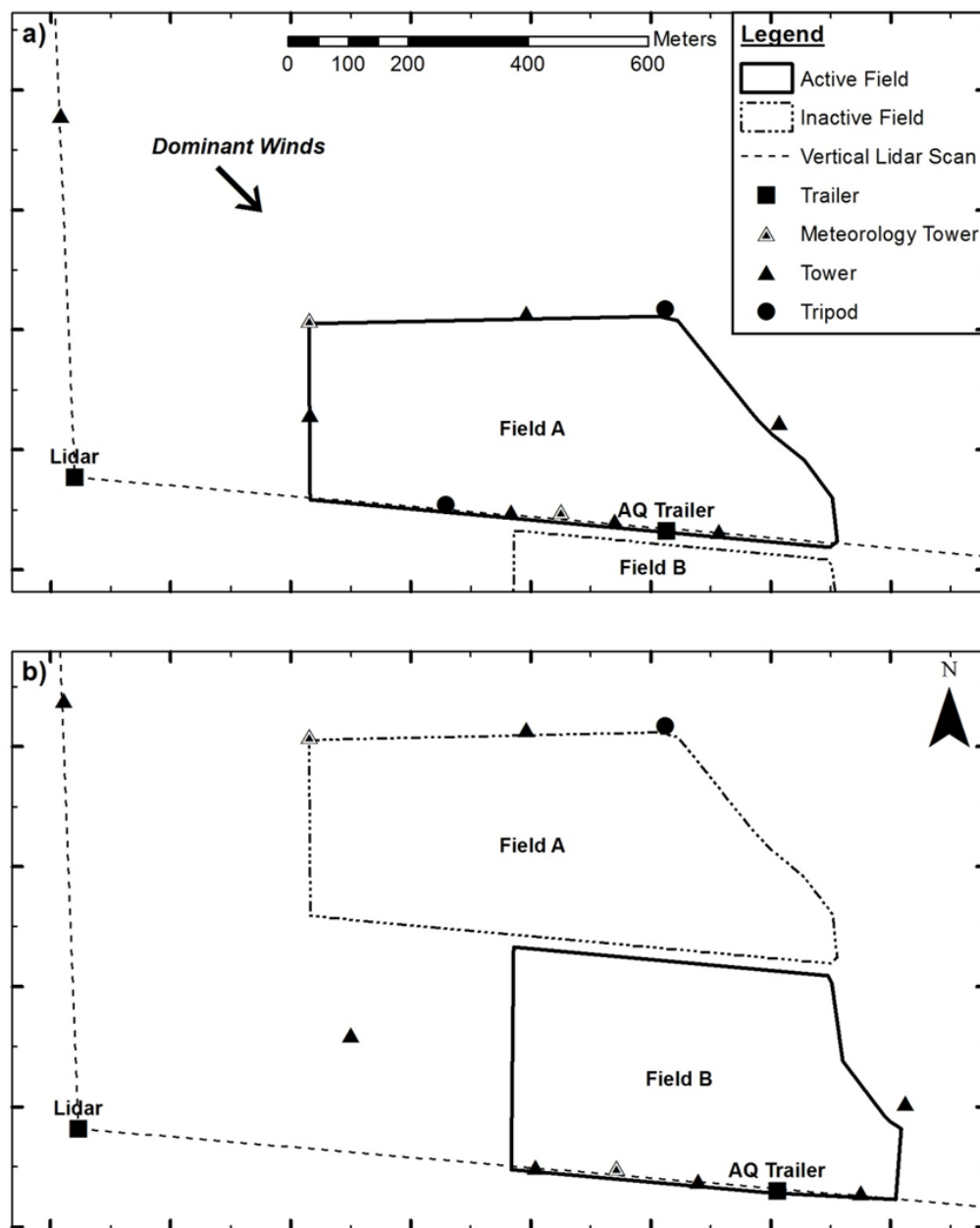


Figure 3-1. Sample layouts for particulate matter (PM) and meteorological measurements made during a) conventional tillage operations in Field A and b) the combined operations conservation management practice operations in Field B.

based sampler that yields mass concentration averaged over the sample time, with an impactor plate assembly employed for a single-sized particle fractionation for $PM_{2.5}$, PM_{10} , and TSP. MiniVol flow calibration was performed prior to deployment. Pre- and post-weights for the 47 mm Teflon filters used in the MiniVols were quantified using a calibrated microbalance (Type MT5, Mettler-Toledo, Inc., Columbus, Ohio) at the Utah Water Research Laboratory in Logan, UT. Filter conditioning was carried out in accordance with guidance in 40 CFR 50 Appendix J (USEPA, 1987). The OPCs sums particle counts in eight size bins over nominal 20 s sample periods with lower bin limits of 0.3, 0.5, 0.6, 1.0, 2.0, 2.5, 5.0, and 10.0 μm ; the last channel counts particles greater than 10.0 μm . OPC flow and count calibrations were performed on-site and applied in post-analysis. These instruments were deployed in a sampling array surrounding the field of interest, at 2 and 9 m agl. At most of the locations, multiple MiniVols with different size-fractionation configurations and an OPC were collocated in order to characterize particle size and mass distributions.

Particle volume concentrations (V_k) for each size fraction (k) were calculated from OPC particle counts assuming a spherical shape. MiniVol-measured mass concentrations in each size fraction (PM_k) were divided by the corresponding period-averaged V_k on a location-by-location basis. This ratio was termed a mass conversion factor (MCF) by Zavyalov et al. (2009) and is a simple scalar representation of a complex and varying relationship between optical and aerodynamic measurements. It incorporates many factors, such as particle shape, porosity, density, indices of refraction

different from OPC calibration aerosols, and instrument sampling efficiencies, into a single value. Average MCFs were calculated across sampling locations for each size fraction on each day.

In addition to the point sensors, the Aglite lidar system was employed in characterizing particulate emissions from each tillage activity. The Aglite lidar is a portable system using a micro-pulsed Nd:YAG laser with three wavelengths (355 nm, 532nm, and 1064 nm) with the capability to scan 280° in azimuth and from -5° to +40° in elevation. The effective range is 500 m to 15 km range bin size of 6 m. The Aglite lidar was placed in a crosswind position 400+ m away from the nearest tillage area border. It continuously performed vertical scans on the upwind and downwind sides of the field, horizontal scans over the field, and calibration stares throughout tillage observation periods. A calibration stare refers to short periods (60-120 s) when the lidar beam is held adjacent to the upwind calibration tower, which is instrumented with collocated OPC and MiniVols; calibration stares were performed routinely throughout the sample period at 15-20 min intervals. In post-processing, lidar return signals were calibrated to particle size distribution and particle volume concentrations based on upwind calibration stares through Klett's inversion (Marchant et al., 2009). Conversion from particle volume concentration to mass concentration was accomplished through the use of MCFs. This calibration method converts lidar data points along the beam path to mass concentration, which allows a scanning lidar to estimate PM concentrations in the volume of air surrounding an area of interest. Detailed descriptions of the lidar system,

inversion technique, and data analysis are provided by Marchant et al. (2009) and Zavyalov et al. (2009).

Emission Calculation Methods

The ERs and EFs were calculated using two different methods from the collected filter and lidar data in order to estimate the control efficiency of the combined operations CMP in this study. The PM_{2.5}, PM₁₀, and TSP concentrations measured by the MiniVols were coupled with an air dispersion model through inverse modeling. In inverse modeling, the measured concentration attributable to the activity is known (measured downwind concentrations minus upwind/background concentrations) while the ER is unknown. The ER supplied to the model is adjusted in order to best match the modeled concentrations to the measured contributions from the activity. AERMOD, the current USEPA-recommended steady-state air dispersion model, was utilized to perform the inverse modeling estimation of observed emission rates through AERMOD View, a commercially available user-interface from Lakes Environmental, Inc. (Waterloo, Ontario, Canada), with AERMOD version 07026. On-site measured wind speed, wind direction, temperature, humidity, and solar radiation were used by AERMET, the meteorological pre-processor for AERMOD, to create both surface and elevated meteorological input files. In addition, percent cloud cover was set to zero based on visual observations during the measurement periods and default agricultural land autumn values of noon-time albedo (0.18) and surface roughness length (0.05 m) were

selected. A Bowen ratio value of 1.0 was used instead of the default autumn value of 0.7 due to the dry, bare soil surface. Tillage areas and sampler locations were measured by a hand-held GPS unit and included as AERMOD inputs. Modeled plume edge effects on the ER were avoided by eliminating locations with modeled concentrations less than 10% of the maximum modeled concentration from calculations, as per Arya (1998).

The second ER and EF calculation approach was a mass balance applied to the mass concentration-calibrated lidar data. Assuming uniform background aerosol levels, average upwind concentrations were subtracted from concentrations in and around detected plumes in the downwind vertical scans. The difference was multiplied by the component of the minute-averaged wind perpendicular to the beam, which is a function of elevation, to calculate the horizontal flux of PM through the vertical plane. Fluxes were summed across the vertical plane, averaged over the length of the sample period, and then divided by the size of the tilled area to calculate the mean EF of PM from the field surface. The EF was further divided by the total tractor time to calculate the mean ER of each operation. This method of calculating ERs and EFs using lidar are provided in detail in Bingham et al. (2009).

Vertical wind speed profiles up to 250 m agl were calculated to estimate the horizontal flux of PM through the downwind vertical lidar scanning plane, though most sample periods did not require data more than 150 m agl. Profiles were developed using cup anemometer measurements from the tower in the northwest corner of Field A and the following power law, as given by Cooper and Alley (2002):

$$u_2 = u_1 \left(\frac{z_2}{z_1} \right)^p \quad (3-1)$$

where z_1 is the lower elevation with units of m, z_2 is the higher elevation in m, u_1 and u_2 are the wind speeds in m s^{-1} at the lower and higher elevations, respectively, and p is a dimensionless number that varies with atmospheric stability. Cooper and Alley list $p \approx 0.5$ for very stable conditions and $p \approx 0.15$ for very unstable conditions. Values of p used to calculate vertical profiles were estimated by solving the above equation for p and using average wind speeds, nominally from the 2.5 and 9.7 m measurement elevations. Estimated period-average p values ranged between 0.16 and 0.22 and averaged 0.20. Vertical profiles were calculated with u_1 values taken from measurements at $z_1 = 9.7$ m.

Wind direction over the vertical profile was assumed to be constant. Though wind direction is known to change in a vertical profile, the influencing factors may be complex and the magnitude and direction of change highly variable. Therefore, in the absence of measured data, the assumption that wind direction didn't change with increasing elevation over the 250 m profile was used. Wind direction as measured by the sonic anemometer on the northwest corner of Field A at 11.3 m agl was used for these analyses.

Results and Discussion

Observed wind conditions throughout the field study were very similar to the conditions observed during the month of October for previous years at Station #56 of

the California Irrigation Management Information System (CIMIS) located near Los Banos, CA with dominant winds from the northwest. Mean temperature, wind speed, and wind direction values $\pm 1\sigma$ for each sample period are given in Table 3-1.

Unfortunately, light and variable winds delayed and/or impacted sampling on several occasions; one example of an impacted period is the 19 Oct. sample period, which had an average wind speed of 1.1 m s^{-1} and a high wind direction standard deviation of 62° . In addition, two precipitation events were recorded immediately prior to the first sample period and one between the last two sample periods that affected soil surface conditions. Evapotranspiration calculations from the downwind latent heat flux measurements suggested no residual water was present in the soil from precipitation events prior to the first sample period. However, it did suggest residual water was present in the soil during the last sample period (land plane operation) from the rainfall two days prior.

Soil bulk densities measured in the furrows and ridges averaged $\pm 1\sigma$ $1.47 \pm 0.02 \text{ g cm}^{-3}$ and $1.37 \pm 0.03 \text{ g cm}^{-3}$, respectively, for field B (Combined Methods CMP treatment) and $1.52 \pm 0.06 \text{ g cm}^{-3}$ and $1.34 \pm 0.05 \text{ g cm}^{-3}$, respectively, for field A (traditional treatment). Higher average soil moisture conditions $\pm 1\sigma$ were present in furrows, at $10.3 \pm 0.49 \%$ for Field B and $11.34 \pm 0.61\%$ for Field A, while the ridges were drier at $9.45 \pm 0.06\%$ and $8.08 \pm 0.08\%$ for fields B and A, respectively. Soil moisture was highest in both fields prior to any tillage activity and decreased as the number of tillage operations increased.

MiniVol sampler-measured $PM_{2.5}$ concentrations ranged from 5.8 to 52.9 $\mu\text{g m}^{-3}$; PM_{10} concentrations ranged from 16.3 to 165.3 $\mu\text{g m}^{-3}$; TSP concentrations ranged from 60.5 to 203.3 $\mu\text{g m}^{-3}$. Filter samples were passed through a rigorous QA/QC process that included examination of the filters during handling, of sampler run data, and of calculated concentrations to identify potential data outliers. Only those filters that passed QA/QC were used in emissions calculations.

Time-series OPC data were used to examine potential impacts on upwind samplers. The majority of observed impacts on upwind samples were due to unpaved road traffic associated with logistical support for the tillage operations. However, significantly elevated PM levels of short duration were detected during a few periods of variable wind conditions and an absence of nearby unpaved road traffic. These anomalies are likely due to tillage plumes from the field under study being transported to upwind sample locations. Most impacted upwind samples were removed from further calculations. However, there were three sample periods in which non-impacted background samples did not exist. In these instances, background PM levels for emission calculation purposes were estimated through multiplication of the impacted MiniVol concentration by a ratio of OPC V_k data (average V_k excluding time periods with impacts divided by the period-average V_k). The assumption is that this ratio would remain constant between volume and mass concentration and is based on similar chemical compositions between the background and plume aerosols, as shown in chemical analyses performed on collected particulates not herein reported, and supported by

similar MCFs calculated across all sites. These OPC V_k ratios averaged $\pm 1\sigma$ 0.98 ± 0.02 for $PM_{2.5}$, 0.82 ± 0.12 for PM_{10} , and 0.84 ± 0.13 for TSP over the three sample periods.

Period average MCFs for the $PM_{2.5}$ size fraction ranged from 2.16 to 4.90 $g\ cm^{-3}$ with a mean $\pm 1\sigma$ of $2.95 \pm 1.25\ g\ cm^{-3}$. MCFs for the PM_{10} size fraction had a mean of $1.44 \pm 0.44\ g\ cm^{-3}$, with a range of 1.29 to 1.71 $g\ cm^{-3}$, and TSP MCFs ranged from 0.63 to 2.77 $g\ cm^{-3}$ with a mean of $1.53 \pm 0.90\ g\ cm^{-3}$. Day to day variation in the MCF is not fully understood, but is likely due to changes in background aerosol sources and composition, as the point samplers collected ambient aerosol for a much larger period of the time than the non-stationary tillage plume. Lidar and OPC data were converted from particle volume concentration to particle mass concentration using the sample period average MCF values. An example of a downwind lidar scan with a tillage plume present is given in Figure 3-2.

Comparisons of PM levels measured or estimated by collocated MiniVols, OPCs, and the lidar bin adjacent to the tower were made at both upwind and downwind elevated locations to verify estimated lidar and OPC PM concentrations. An example of these comparisons is presented in Table 3-3. As can be seen in this example, the calculated concentrations agree fairly well for $PM_{2.5}$ and TSP at the upwind location, though upwind PM_{10} lidar levels were 130% of the adjacent PM sampler concentrations and 85% of the adjacent OPC values. Reported downwind concentrations were significantly different at all size fractions, with the lidar greater than the adjacent PM sampler by 421%, 257%, and 147% for $PM_{2.5}$, PM_{10} , and TSP, respectively, and greater

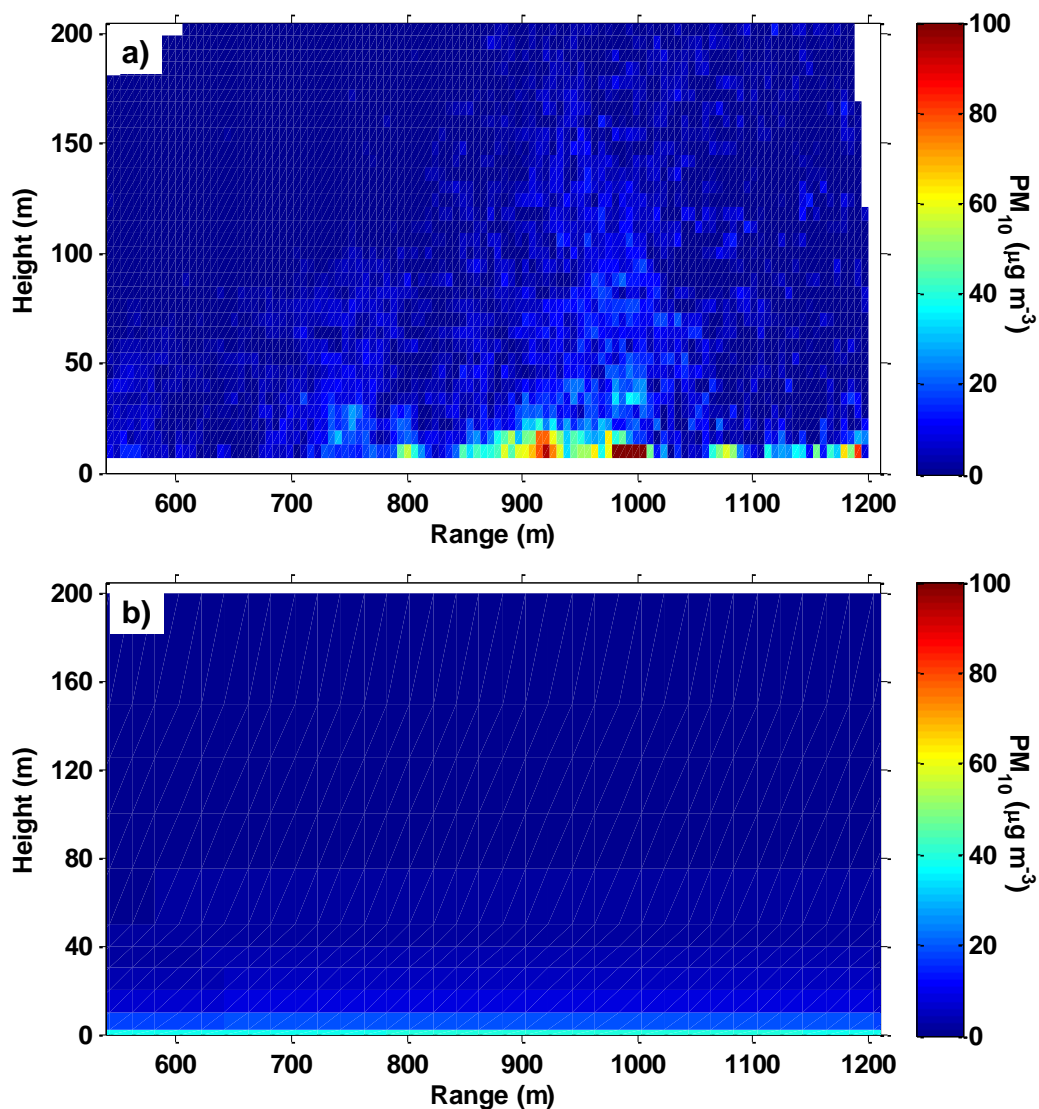


Figure 3-2. Period-averaged PM_{10} concentrations ($\mu\text{g m}^{-3}$) resulting from the tillage activity on 23 Oct. along the vertical downwind lidar scanning plane as a) estimated by lidar (average downwind minus average upwind) and b) predicted by AERMOD using the Lidar-derived emission rate for this sample period. Note that the minimum elevation measurement of the lidar was 8 m due to safety concerns.

than the adjacent OPC by 326%, 305%, and 307% for $PM_{2.5}$, PM_{10} , and TSP, respectively.

Differences, particularly in downwind values, may be attributed to several factors,

including but not limited to, the following: sample volume differences (OPCs - 1 L min^{-1} ; MiniVols - 5 L min^{-1} ; lidar - 6 m bin length x $\sim 1 \text{ m}$ beam diameter sampled at 10 kHz with data averaged over 0.5 s), sampling frequency at the comparison location (MiniVol and OPC - continuous; lidar - upwind: $\sim 2 \text{ min}$ per 15 min, and downwind: $\sim 10 \text{ s}$ per 15 min), lidar sample timing/frequency with respect to plume location (i.e., simultaneous presence of both the lidar beam and transient plume in the bin of interest adjacent to the tower versus the total time the plume impacted the instrumented tower), and the differences between the MCF values calculated at the comparison site and the average MCF across all measurement sites used to convert OPC and lidar particle volume concentrations to mass concentration.

Emissions Calculations

The average MiniVol-measured upwind PM concentrations were subtracted from the individual downwind concentrations in order to determine the impact of the operation on measured PM. Only downwind samples with levels greater than the average upwind concentration plus the corresponding 67% confidence interval (CI), selected to correspond with 1 standard deviation away from the mean, were used in emissions calculations. This statistical difference was not achieved by any downwind $\text{PM}_{2.5}$ measurements from two sample periods: the chisel pass of the combined operations treatment (19 Oct.) and the Disc 1 pass of the traditional treatment (23 Oct.). Therefore, no $\text{PM}_{2.5}$ emissions based on inverse modeling were calculated for these

Table 3-3. Comparison of average particulate matter (PM) mass concentrations with respective 95% confidence intervals (CI) about the mean as reported by collocated MiniVol PM samplers, optical particle counters (OPCs), and lidar (light detection and ranging) at an upwind and downwind location for the 23 Oct. sample period.

Measured Concentrations	PM _{2.5}	PM ₁₀	TSP
	----- $\mu\text{g m}^{-3}$ -----		

<u>Upwind</u>			
PM sampler	17.0	35.9	60.5
Upwind PM sampler average \pm 95% CI	16.1 \pm 1.2	39.6 \pm 7.2	60.5
OPC \pm 95% CI	13.9 \pm 0.2	54.5 \pm 3.9	65.6 \pm 6.3
Lidar \pm 95% CI	13.8 \pm 0.2	45.9 \pm 0.9	60.1 \pm 1.4
<u>Downwind</u>			
PM sampler	9.9	75.5	203.3
Downwind PM sampler average \pm 95% CI	11.8 \pm 2.5	59.7 \pm 8.4	203.3
OPC \pm 95% CI	12.8 \pm 0.2	63.5 \pm 3.1	97.0 \pm 13.0
Lidar \pm 95% CI	41.7 \pm 9.0	193.7 \pm 47.7	297.7 \pm 76.6

operations. Only two downwind PM₁₀ samples passed this statistical comparison from the chisel pass of the traditional tillage treatment on 25 Oct. and statistical measures about the mean were omitted for that period.

A ratio of the measured over the modeled impact at each location with valid measured values was calculated and then averaged across all locations. The average ratio is the required scalar adjustment to the initial ER provided to the dispersion model in order to yield an average measured-over-modeled ratio of 1.0, which then becomes the estimated ER for that operation. This method was applied to all size fractions with statistically significant measured differences between upwind and downwind for all

tillage operations using the AERMOD dispersion model. Average estimated ER values, in units of mass per unit area per unit time, for each operation are listed in Table 3-4. EFs in units of mass per unit area tilled were calculated by multiplying the ERs by total tillage time and are listed in Table 3-5.

It should be noted that the PM_{2.5} and PM₁₀ ERs and EFs for the Disc 2 pass are averages over two sample periods, October 26th and 27th. Tillage equipment malfunctions on the 26th delayed completion of the operation until the following day. Additionally, due to the absence of a valid downwind TSP sample for October 26th and the model predicted concentration at the downwind TSP sample location being about 7% of the maximum predicted concentration on October 27th, the TSP EF for the Disc 2

Table 3-4. Mean emissions rates (ER) ± 95% confidence intervals (CIs) calculated using inverse modeling with AERMOD and filter-based particulate matter (PM) measurements and the mass balance technique applied to PM calibrated lidar data.

Operation	PM _{2.5} ER		PM ₁₀ ER		TSP ER	
	AERMOD	Lidar	AERMOD	Lidar	AERMOD	Lidar
----- μg s ⁻¹ m ⁻² -----						
-						
<u>Combined Operations CMP Method</u>						
Chisel	-	1.5 ± 0.4	5.2 ± 4.6***	2.3 ± 0.7***	9.1	8.7 ± 2.5
Optimizer	4.5 ± 7.0***	2.1 ± 0.3***	6.6 ± 7.7***	2.7 ± 0.4***	24.6	10.8 ± 1.7
<u>Conventional Method</u>						
Disc 1	-	0.5 ± 0.1	3.2 ± 1.5***	2.5 ± 0.3***	25.7	4.0 ± 0.5
Chisel	1.5 ± 4.9ns†	1.5 ± 0.3ns	7.2	3.4 ± 0.6	18.1	10.0 ± 1.7
Disc 2	0.7 ± 0.2***	1.2 ± 0.3***	4.5 ± 2.8***	2.4 ± 0.6***	36.7	4.5 ± 1.2
Land plane	1.5	1.2 ± 0.3	3.4 ± 0.9***	1.8 ± 0.5***	3.2	2.8 ± 0.8

*** Difference between emission calculation methods is significant at the 0.001 probability level

† ns, nonsignificant at the 0.20 probability level

Table 3-5. Mean emission factors (EF) \pm 95% confidence intervals (CIs) calculated via inverse modeling with AERMOD and filter-based particulate matter (PM) measurements and the mass balance technique with PM calibrated lidar data for each operation, as well as the calculated control efficiencies of the Combined Operations CMP method.

Operation	PM _{2.5} EF		PM ₁₀ EF		TSP EF	
	AERMOD	Lidar	AERMOD	Lidar	AERMOD	Lidar
----- mg m ⁻² -----						
<u>Combined Operations CMP Method</u>						
Chisel	-	45.3 \pm 13.1	158.9 \pm 140.1***	69.0 \pm 19.9***	278.0	265.9 \pm 76.6
Optimizer	71.2 \pm 109.6***	32.5 \pm 5.1***	103.5 \pm 121.0***	42.7 \pm 6.6***	385.4	169.9 \pm 26.2
Sum	-	77.8 \pm 14.0	262.4 \pm 185.1***	111.6 \pm 20.9***	663.4	435.8 \pm 80.9
<u>Conventional Method</u>						
Disc 1	-	20.4 \pm 2.6	125.6 \pm 57.9***	99.7 \pm 12.5***	1018.2	159.8 \pm 20.0
Chisel	34.5 \pm 115.1ns†	35.8 \pm 5.9ns	167.5	79.5 \pm 13.1	423.2	235.1 \pm 38.8
Disc 2	23.3 \pm 7.4***	39.5 \pm 11.2***	149.2 \pm 91.8***	80.7 \pm 20.5***	1210.0	149.3 \pm 40.3
Land plane	18.4	13.8 \pm 3.9	41.3 \pm 10.6***	21.9 \pm 6.2***	38.9	33.4 \pm 9.4
Sum	-	109.5 \pm 13.5	483.6	281.9 \pm 28.0	2690.2	577.6 \pm 60.1
<u>Control Effectiveness</u>						
----- % -----						
$\eta \pm 1\sigma$	-	28.9 \pm 1.6	45.7	60.4 \pm 0.7	75.3	24.6 \pm 1.3

*** Differences between emission calculation methods is significant at the 0.001 probability level

† ns, nonsignificant at the 0.20 probability level

pass was calculated by assuming that the PM₁₀/TSP EF ratio observed during the Disc 1 pass of 0.12 was representative of disc passes under similar conditions and then dividing the Disc 2 PM₁₀ EF of 149.2 mg m⁻² by 0.12 to yield a TSP EF of 1,210.0 mg m⁻² for the operation.

Emissions from lidar measurements were estimated using a simple mass balance technique. Average flux values for each tillage operation were calculated, multiplied by total tillage time, and divided by total area tilled to yield EF values in mass per unit area tilled. These are presented in Table 3-5 with their associated 95% CIs. The EFs were then divided by total tractor time to yield ERs in mass per unit area tilled per unit time of operation and are given in Table 3-4. The reported Disc 2 ERs/EFs are weighted averages of the two sample periods, with the weights calculated based on the number of total valid downwind scans collected each day.

The lowest EF among the investigated operations for each PM size fractions and EF calculation methodologies was derived for the land plane operation in the conventional tillage method. EFs available in literature for land planing are generally higher than all other activities by a factor of 10. This relationship between the EF for land planing and discing/tilling/chiseling was not seen in this study. The much lower EFs for land planing are likely due to the water remaining in the soil surface from the precipitation event that occurred two days prior, as calculated from downwind latent heat measurements.

Statistical comparisons between the mean reported ERs and EFs from the two emission estimation techniques and within a PM size fraction and operation were made via independent t-tests for all pairs in which $n > 2$ for the inverse modeling technique, i.e., all pairs reporting confidence intervals about both average values. The results are presented in Table 3-4 and Table 3-5, showing that the differences between all but one

pair of averages with sufficient data points were statistically significant at the 0.001 probability level. The difference between the lone pair was found to not be significant at the 0.20 probability level. Only one instance of tillage method sums with sufficient statistical measures to perform an independent t-test exists in this dataset, the Combined Operations CMP Method for the PM₁₀ size fraction; the differences between the summed emissions for the two techniques were found to be statistically significant at the 0.001 probability level. For those pairs without sufficiently large n for the inverse modeling technique to report a confidence interval, a more qualitative comparison may be made between the inverse modeling estimates with the average lidar values \pm the 95% CI. In the majority of such cases, the estimated inverse modeling value was greater than the average lidar-based emission value plus the 95% CI, a pattern present throughout the dataset. This pattern of higher inverse modeling emissions estimates than lidar estimates is similar to the findings of Marchant et al. (2011) who investigated PM emissions from a dairy using inverse modeling with AERMOD and mass balance applied to lidar data.

While inverse modeling emissions are usually a factor of two to three higher, two inverse modeling TSP ERs and EFs are significantly higher by factors of six (disc 1 operation) and eight (disc 2 operation). These large differences in the two disc operation EFs lead to a much larger difference between emission estimation techniques in TSP EF sums for the conventional tillage method than for the combined operations CMP method, which in turn cause a large difference in calculated TSP control efficiencies

between emission calculation methodologies. In addition, ERs across tillage operations for a given PM fraction and ER calculation method do not generally vary by more than a factor of three, with the exception of the land plane TSP ER estimated through inverse modeling. The ERs measured and reported for the Optimizer pass of the combined operation CMP are among the higher values for each PM fraction herein reported, though not always the highest. When the total tractor time is accounted for in the EF calculation, the Optimizer emissions move toward the lower end of the measured EF values due to its tillage rate being approximately twice that of the other operations (see Table 3-1).

Methodology limitations may contribute, in part, to the differences observed between reported ERs and EFs. First, the lidar was unable to monitor plumes below 8 m agl in this test due to laser safety concerns, and may have thus underestimated emissions due to the unmeasured PM leaving the field below 8 m agl. Second, the ability of the model to simulate observed vertical dispersion appears to have been limited in some cases, as demonstrated in Figure 3-2. These images compare average PM₁₀ concentrations along the vertical downwind lidar scanning plane as calculated from lidar return signal for the 23 Oct. measurement period and as predicted by AERMOD using the lidar-derived PM₁₀ ER from the same period. While the model predicts PM levels decreasing exponentially with height, the lidar detected significant PM above 50 m agl. The highest concentrations in some plumes were measured far above the surface, as seen in Figure 3-3. This limited simulation of observed vertical dispersion decreases

predicted concentrations relative to the actual measured impact at elevations above the release height, leading to higher inverse modeling estimated emissions to better match elevated MiniVol measurements.

PM₁₀ EFs for conventional tillage operations estimated during this study are occasionally in agreement with values reported by Flocchini et al (2001), Kasumba et al. (2011), Madden et al. (2008), and Wang et al. (2010), as well as those given by the California ARB (2003a). While the values from all the previously published studies are generally not in close agreement, they are within the range of the variability expected

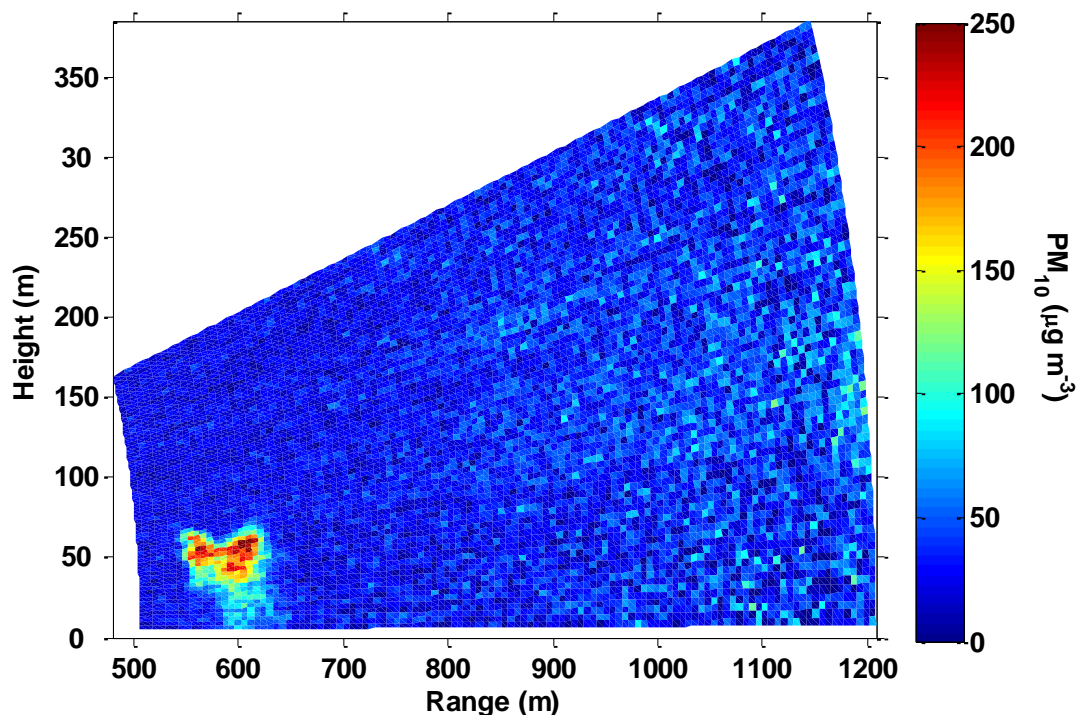


Figure 3-3. Lidar measured downwind PM₁₀ concentrations ($\mu\text{g m}^{-3}$) from a single vertical scan on 23 Oct; a tillage plume is seen crossing the lidar scan at a range of 600 m and centered at 50 m above ground level. Note that the minimum elevation measurement of the lidar was 8 m due to safety concerns.

from measurements made under different meteorological and soil conditions, as demonstrated by the wide range of values from Flocchini et al. (2001).

The EFs for each tillage method were quantified in order to compare the control effectiveness (η) of the CMP, as calculated from the following equation based on the approach described by Cooper and Alley (2002):

$$\eta = \frac{EF_{CT} - EF_{COT}}{EF_{CT}}, \quad (3-2)$$

where EF_{CT} is the summed EF for the conventional tillage method and EF_{COT} is the summed EF for the combined operations tillage method. Calculated values of η are listed in Table 3-5 for each size fraction. The lack of a complete $PM_{2.5}$ EF dataset from the inverse modeling method prevents this comparison and the singular TSP data point for each operation in the same method excludes statistical measure estimates.

However, emissions values based on lidar data are complete and were therefore used to represent the CMP control efficiency for all size fractions. The particulate emissions control efficiency of the Combined Operations CMP $\pm 1\sigma$, as monitored by lidar in this study, were $29\% \pm 2\%$, $60\% \pm 1\%$, and $25\% \pm 1\%$ for $PM_{2.5}$, PM_{10} , and TSP, respectively.

Another important result of this investigation is the assessment of the utility of lidar for measuring and AERMOD for simulating particulate emissions in an agricultural setting. These lidar measurements clearly indicate that lidar is an effective tool for visualizing plumes from tillage operations. When mass calibrated, it functions as a virtual broad array of fast response point samplers. Specifically, the lidar captured far

more particulate matter suspended at heights above 20 m than AERMOD predicts (Fig. 3-2). This poses larger questions about the role of PM entrainment and transport away from the tillage site, a question that is beyond the scope of this manuscript. Also, it is difficult to accurately simulate the emission characteristics from these tillage studies with AERMOD because it is being used at the limit of its designed performance. The analysis of the emissions between the two methods differs in that a point sampler-based model uses a mathematical function to estimate plume characteristics based on a handful of data points whereas the lidar directly sums the results from all bins to determine the extent and concentration of the plume and the strength of the source. It is clear that the incorporation of lidar measurements is an important complement to ground based sensors because ground based sensors cannot measure elevated plumes.

Conclusions

Aerosol concentrations resulting from traditional agricultural tillage activities and the combined operations CMP were successfully measured with both point sensors and a mass-calibrated, scanning lidar system. ERs and EFs for TSP, PM₁₀, and PM_{2.5} were calculated based on both point and the remote sensor datasets in order to quantify the control effectiveness of the CMP. These EFs were generally in agreement with and within the variability of those found in the literature, except for the EFs estimated for the land plane operation. The estimated emissions from the inverse modeling methodology were usually higher than those calculated from lidar data; most

differences between the two techniques were statistically significant where a statistical comparison was possible. The CMP control effectiveness per PM size fraction was estimated based on lidar-derived ERs due to dataset completeness. The control effectiveness values $\pm 1\sigma$ were $29\% \pm 2\%$, $60\% \pm 1\%$, and $25\% \pm 1\%$ for $PM_{2.5}$, PM_{10} , and TSP, respectively.

The mass-calibrated lidar proved very effective in detecting downwind plumes and, in combination with wind vector and upwind PM measurements, quantifying dust emissions from the tillage activities. Downwind plumes of significant concentration were frequently detected by Aglite at elevations much greater than that predicted by AERMOD, even up to 200 m. This suggests that application of such air dispersion models to activities similar in spatial and temporal variability to agricultural tillage should be done carefully and conservatively.

Acknowledgments

The Space Dynamics Laboratory would like to thank the individuals and groups whose efforts made this study and subsequent analysis possible. Funding was provided by a USEPA Regional Applied Research Effort (RARE) grant. Cooperators include: the USDA-ARS, National Laboratory for Agriculture and the Environment; Utah State University; USEPA Region 9; USEPA Office of Research and Development, National Exposure Research Laboratory; the San Joaquin Valleywide Air Pollution Study Agency, the San Joaquin Valley Ag Technical Group, the San Joaquin Valley Air Pollution Control

District, California Air Resources Board, and the cooperative agricultural producers and industry representatives. Mention of tradenames does not constitute endorsement by the USDA-ARS, USEPA, Space Dynamics Laboratory, or Utah State University.

References

- Arya, S.P. 1998. Air pollution meteorology and dispersion. Oxford University Press, New York.
- Bingham, G.E., C.C. Marchant, V.V. Zavyalov, D.J. Ahlstrom, K.D. Moore, D.S. Jones, et al. 2009. Lidar based emissions measurement at the whole facility scale: Method and error analysis. *J. Appl. Remote Sens.*3(1):033510. doi: 10.1117/1.3097919
- California Air Resources Board (ARB). 2003a. Area source methods manual, section 7.4: Agricultural land preparation. California ARB. www.arb.ca.gov/ei/areasrc/fullpdf/full7-4.pdf (7 Nov. 2011).
- California ARB. 2003b. Area source methods manual, section 7.5: Agricultural harvest operations. California ARB. www.arb.ca.gov/ei/areasrc/fullpdf/full7-5.pdf (7 Nov. 2011).
- Cooper, D.C., and F.C. Alley. 2002. Air pollution control: A design approach. 3rd ed. Waveland Press Inc. Prospect Heights.
- Doran, J.W., and A. Jones. 1996. Methods for assessing soil quality. SSSA Special Publication Number 49. Soil Science Society of America, Madison.
- Flocchini, R.G., T.A. James, L.L. Ashbaugh, M.S. Brown, O.F. Carvacho, B.A. Holmen, et al. 2001. Interim report: Sources and sinks of PM₁₀ in the San Joaquin Valley. Crocker Nuclear Laboratory, UC-Davis, CA. www.arb.ca.gov/research/apr/reports/I2022.pdf (7 Nov. 2011).
- Holmen, B.A., W.E. Eichinger, and R.G. Flocchini. 1998. Application of elastic LIDAR to PM₁₀ emissions from agricultural nonpoint sources. *Environ. Sci. and Technol.* 32:3068-3076.

- Holmen, B.A., T.A. James, J.L. Ashbaugh, and R.G. Flocchini. 2001a. LIDAR-assisted measurement of PM₁₀ emissions from agricultural tilling in California's San Joaquin Valley—Part I. LIDAR. *Atmos. Environ.* 35:3251-2364.
- Holmen, B.A., T.A. James, J.L. Ashbaugh, and R.G. Flocchini. 2001b. LIDAR-assisted measurement of PM₁₀ emissions from agricultural tilling in California's San Joaquin Valley—Part II: Emission factors. *Atmos. Environ.* 35:3265-3277.
- Kasumba, J., B.A. Holmen, A. Hiscox, J. Wang, and D. Miller. 2011. Agricultural PM₁₀ emissions from cotton field disking in Las Cruces, NM. *Atmos. Environ.* 45:1668-1674.
- Madden, N.M., R.J. Southard, and J.P. Mitchell. 2008. Conservation tillage reduces PM₁₀ emissions in dairy forage rotations. *Atmos. Environ.* 42:3795-3808.
- Marchant, C.C., T.D. Wilkerson, G.E. Bingham, V.V. Zavyalov, J.M. Andersen, C.B. Wright, et al. 2009. Aglite lidar: A portable elastic lidar system for investigating aerosol and wind motions at or around agricultural production facilities. *J. Appl. Remote Sens.* 3(1):033511. doi: 10.1117/1.3097928
- Marchant, C.C., K.D. Moore, M.D. Wojcik, R.S. Martin, R.L. Pfeiffer, J.H. Prueger, et al. 2011. Estimation of dairy particulate matter emission rates by lidar and inverse modeling. *Trans. ASABE* 54:1453-1463.
- San Joaquin Valley Air Pollution Control District (SJVAPCD). 2006. Conservation management practices program report for 2005. San Joaquin Valley Air Pollution Control District, Fresno.
http://www.valleyair.org/farmpermits/updates/cmp_program_report_for_2005.pdf (accessed 7 Nov. 2011).
- Soil Survey Staff. 2007. Web Soil Survey 2.0. USDA-NRCS.
<http://websoilsurvey.nrcs.usda.gov/app/> (accessed 2 Oct. 2007).
- USEPA. 1987. 40 CFR Appendix J to Part 50: Reference method for the determination of particulate matter as PM₁₀ in the atmosphere. *Fed. Reg.* 54: 24664.
- Wang, J., D.R. Miller, T.W. Sammis, A.L. Hiscox, W. Yang, and B.A. Holmen. 2010. Local Dust Emission Factors for Agricultural Tilling Operations. *Soil Sci.* 175(4):194-200.
- Williams, D.J., S. Chilingaryan, and J. Hatfield. 2012. Los Banos, CA Fall 2007 Tillage Campaign: Data Analysis. USEPA Rep. EPA/600/R-12/734. U.S. Gov. Print. Office,

Washington, D.C. Available:

http://cfpub.epa.gov/si/si_public_record_report.cfm?dirEntryId=248752.

Zavalyov, V.V., C.C. Marchant, G.E. Bingham, T.D. Wilkerson, J.L. Hatfield, R.S. Martin, et al. 2009. Aglite lidar: Calibration and retrievals of well characterized aerosols from agricultural operations using a three-wavelength elastic lidar. *J. Appl. Remote Sens.* 3(1):033522. doi: 10.1117/1.3122363

CHAPTER 4

PARTICULATE MATTER EMISSION ESTIMATES FROM AGRICULTURAL SPRING
TILLAGE OPERATIONS USING LIDAR AND INVERSE MODELING¹**Abstract**

Particulate matter (PM) emissions from a typical spring agricultural tillage sequence and a strip-till conservation tillage sequence in California's San Joaquin Valley were estimated to calculate the emissions control efficiency (η) of the strip-till conservation management practice (CMP). Filter-based PM samplers, PM-calibrated optical particle counters (OPCs), and a PM-calibrated light detection and ranging (lidar) system were used to monitor upwind and downwind PM concentrations during May and June 2008. Emission rates were estimated through inverse modeling coupled with the filter and OPC measurements and through applying a mass balance to the PM concentrations derived from lidar data. Sampling irregularities and errors prevented the estimation of emissions from 42% of the sample periods based on filter samples. OPC and lidar datasets were sufficiently complete to estimate emissions and the strip-till CMP η , which were $\sim 90\%$ for all size fractions in both datasets. Tillage time was also reduced by 84%. Calculated emissions for some operations were within the range of

¹ Citation: Moore, K.D., M.D. Wojcik, R.S. Martin, C.C. Marchant, D.S. Jones, W.J. Bradford, G.E. Bingham, R.L. Pfeiffer, J.H. Prueger, and J.L. Hatfield. 2015. Particulate-matter emission estimates from agricultural spring-tillage operations using LIDAR and inverse modeling. *Journal of Applied Remote Sensing*, 9: 096066.

values found in published studies, while other estimates were significantly higher than literature values. The results demonstrate that both PM emissions and tillage time may be reduced by an order of magnitude through the use of a strip-till conservation tillage CMP when compared to spring tillage activities.

Introduction

As aerosols have been shown to have detrimental effects on human health and visibility¹, many governments have set regulations on allowable ambient concentrations. In the U.S., the Environmental Protection Agency (EPA) has established National Ambient Air Quality Standards (NAAQS) for particulate matter (PM) with aerodynamic equivalent diameters $\leq 10 \mu\text{m}$ (PM₁₀) and PM with aerodynamic equivalent diameters $\leq 2.5 \mu\text{m}$ (PM_{2.5}). If an area exceeds the NAAQS, the area's air quality governing body is required to identify the causes and restrict anthropogenic emissions in order to reduce PM levels below the standard.

The San Joaquin Valley of California, USA, was designated as noncompliant with the PM₁₀ NAAQS in 1991 and given a "serious" classification in 1993^{2,3}. Rule 4550, one of the regulations enacted by the San Joaquin Valley Air Pollution Control District (SJVAPCD) to reduce ambient PM₁₀ levels in the San Joaquin Valley, required agricultural production operations to select several conservation management practices (CMPs) from a provided list, submit their selections for SJVAPCD approval, and implement approved CMPs. The CMPs were designed to reduce PM₁₀ emissions from agricultural

animal and crop production activities. However, the small amount of data available in the literature concerning the emissions reductions from the CMPs for crop production tillage activities required that the control efficiency (η) of most tillage CMPs was estimated from emissions measurements of other operations⁴. The η of a CMP is the amount of particle emission reduction achieved relative to the conventional management practice. While the San Joaquin Valley Air Basin has since been classified as in attainment with the PM₁₀ NAAQS, its maintenance plan requires the same strategies employed to bring it back into attainment continue to be applied. In addition, other PM₁₀ non-attainment areas such as Imperial Valley, CA and Phoenix, AZ have CMP or best management practice (BMP) rules in place for agricultural tillage practices that are based on limited emissions measurements.

Previous agricultural tillage PM emissions studies⁵⁻¹² have focused almost exclusively on measuring PM₁₀ emission rates (ERs) and factors (EFs) from conventional tillage operations. For this discussion, EFs are emissions based on a quantity of production (e.g., g m⁻²) and ERs are emissions that include a time factor (e.g., g m⁻² s⁻¹). The California Air Resource Board (ARB) developed area source PM₁₀ emission inventory calculation methodologies for agricultural tillage and harvesting operations based on the report by Ref. 5^{13,14}. References 10 and 11 are the only instances of reporting PM emissions from standard tillage operations and a CMP (strip-till conservation tillage and combined operations, respectively). Reference 6 used elastic lidar (light detection and ranging) data collected during tillage emissions measurements to track plume

movements in the downwind vertical plane and demonstrated plume depths were greater than the elevated point sensors located downwind at 10 m above ground level (agl). The report suggested the best method for sampling fugitive dust includes a combination of elastic lidar and strategically placed point samplers. Reference 11 used both filter-based mass concentration point samplers and a lidar system to monitor tillage emissions and estimated EFs from both datasets.

The study described in Ref. 11 was initiated specifically to provide more emissions η data with respect to a CMP in Rule 4550. The focus was on a typical fall tillage operation after a row crop harvest. A companion study funded by the San Joaquin Valleywide Air Pollution Study Agency was conducted to measure η of a spring tillage CMP using the same point sensor and lidar methodology. Research questions which this study was designed to address include: 1) what are the magnitude, flux, and transport of PM emissions produced by agricultural practices for row crops where tillage CMPs are being implemented vs. the magnitude, flux, and transport of PM emissions produced by agricultural practices where CMPs are not being implemented?; 2) what are the values of η of equipment being used to implement the “combined operations” CMP?; and 3) can these CMPs for a specific crop be quantitatively compared, controlling for soil type, soil moisture, and meteorological conditions? It is important to note that the main focus of this research was to quantify η of the selected CMP, which required the emissions to be quantified, and it was not an effort to provide representative emission factors for any one of the agricultural operations involved. This paper summarizes the results of the PM

measurements made during the field experiment, the calculated ERs, and addresses these research questions. A full report detailing all of the sampling methodology and results is given in Ref. 15.

Methodology

Site and Operation Description

This CMP η study was performed during the spring tillage sequence following the harvest of a winter wheat crop in preparation for planting of corn. It was carried out in the San Joaquin Valley of California during May and June 2008. Two adjacent fields were used with identical crop and flood irrigation treatment over the previous several years. Both fields were cultivated in winter wheat in late 2007 and were to be planted in corn for the 2008 summer growing season. The wheat was harvested while still green for silage four days before the tillage processes began, resulting in standing stubble but little plant material left on the surface. The site was chosen based on producer cooperation, historically dominant northwest winds, and field layout.

The surrounding landscape was topographically flat and dominated by agricultural production, including grain and corn fields, almond orchards, grape vineyards, and commercial dairy operations. Both fields were surrounded on all sides by roads. These roads, with the exception of one, were unpaved roads used for field access by farm machinery. The paved road, which was downwind of the fields during all measurements, was heavily travelled. Railroad tracks were located to the north of this

site, with two to three trains passing by per day with a varying numbers of cars. USDA NRCS soil survey data list the soil in both fields as soil type 130 – Kimberlina fine sandy loam, saline-alkali¹⁶.

The CMP selected for this study was the Conservation Tillage method. As described in Ref. 4, this CMP “involves using a system in which the soil is being tilled or cultivated to a lesser extent compared to a conventional system” and it is “intended to reduce primary soil disturbance operation such as plowing, discing, ripping, and chiseling.” The Conservation Tillage CMP under study was a strip-till method which combines multiple operations to reduce the number of passes required and only disturbs the soil in strips 0.2 m wide centered every 0.8 m instead of disturbing the entire surface. Strip-till reduced both the number of passes and the tilled surface by about 75%, as well as left most of the wheat stubble still standing for ground cover. The strip-till implement used in this study was the Orthman 1-tRIPr. The cooperating farm had been using the Orthman 1-tRIPr for seedbed preparation on all of its fields for several years, with the exception of Field 4 which was prepared by conventional tillage methods.

The conservation tillage CMP applied in this study consisted of three tillage activities totaling three operations across the field, excluding the building and removal of ditches. All three were monitored in separate sample periods. In comparison, the conventional tillage method as applied here had nine different tillage activities totaling 13 operations, excluding the building and removal of a ditch and field edge borders.

Monitoring of 12 of the operations occurred over nine sample periods. Note that not all operations were active throughout sample periods in which multiple operations occurred. Also, not all of the conventional tillage operations are intended to work the entire field, such as breaking down in-field borders. The term in-field borders as used here applies to low ridges of soil that separate the field into smaller areas for flood irrigation. The conventional tillage method was employed in Field 4, shown in Fig. 4-1, and the conservation tillage CMP was used in Field 5. The operations that were performed in each management practice are shown in order in Table 4-1, with their corresponding dates, equipment utilized, number of passes over a given area, tractor run time, total area worked, and sample period length. In cases where multiple tractors and implements were used within a sample period, they are listed in the order of use with the area worked and tractor time being summed. The lister, also called a double plow, prepares the soil for planting by creating furrows and ridges. The cultivator passes in the conventional tillage sequence function as mechanical weed control, whereas a chemical weed control (herbicide) is used in the CMP sequence.

During the first part of the lister operation, plant material not harvested along in-field borders caused clogging of the lister, decreasing effectiveness. A second tractor with the disc set was brought in to repeat the effort along the border lines to further reduce the size of residual plant material. Also note that the cultivator passes 1 and 2 and the roller pass for the first sample period on 5 June were not finished when planting in Field 4 began and the second sample period was started. The combination of the

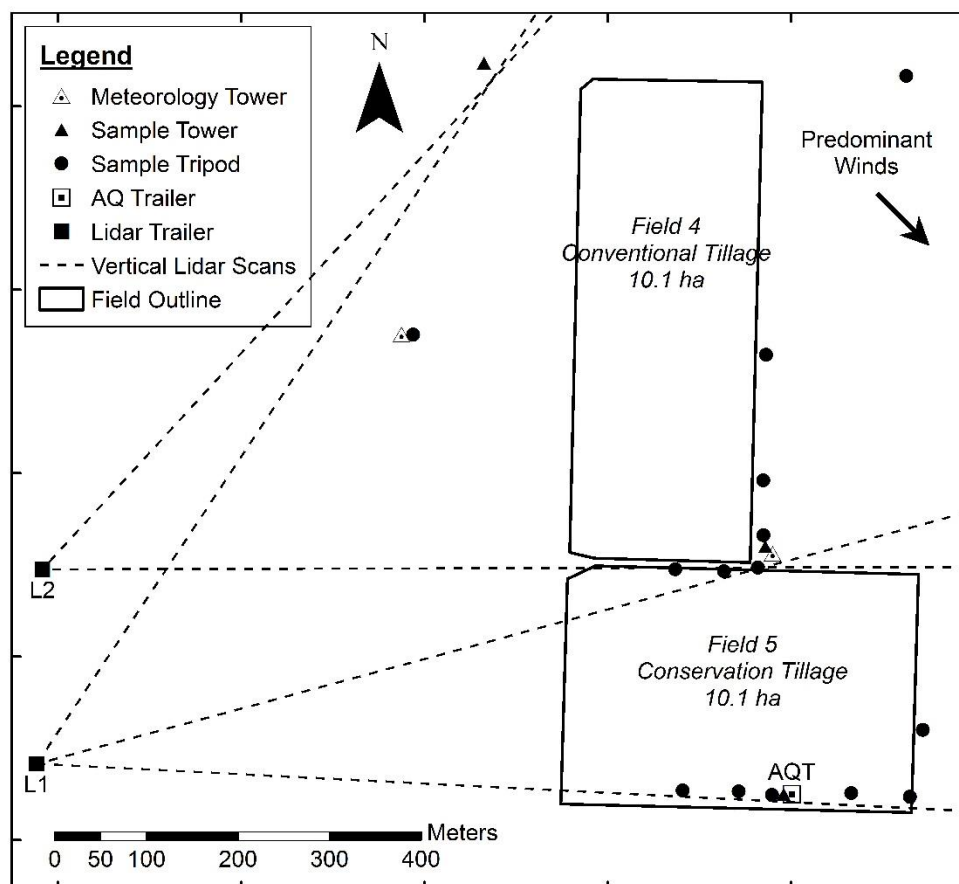


Figure 4-1. Map of fields under study and the sample layout for each field. L1 and L2 represent lidar locations used during sampling and dashed lines emanating from L1 and L2 show positions of vertical lidar scans.

cultivator and roller positions and meteorological conditions prevented significant impacts from these operations on downwind samples located near the southern end of the field.

Additionally, cultivator pass 4 was carried out the day after cultivator pass 3, but the emissions were not measured due to scheduling conflicts. It is assumed, in calculating the total PM emissions, that the ERs of both passes 3 and 4 were equal. In

Table 4-1. Information for each sample period regarding tillage operations, equipment used, tractor operation time, area worked, and sample time.

Date	Tillage Operation	Tractor Make and Model	Implement Make and Model	Number of Passes	Sample Time (hr)	Tractor Time (hr _{tractor})	Area Worked (ha)	Tractor Operation Rate (hr _{tractor} /ha)
<i>Conservation Tillage (Field 5)</i>								
17 May	Strip-Till	Case MX255	Orthman 1-tRIPr, 6 row, 0.8 m spacing	1	3.92	3.05	9.1	0.34
7 June	Plant and Fertilize	Case MX255	Monosem Twin-Row Planter Model 6x2, 6 rows, 0.8 m spacing	1	5.33	3.82	9.1	0.42
11 June	Herbicide Application	Kubota B-Series	Hardi ATV Sprayer, 12.2 m boom	1	1.58	0.93	9.1	0.10
<i>Conventional Tillage (Field 4)</i>								
17 May	Break down in-field irrigation borders	Case Puma 195	Custom border buster (2 sets of 3 discs that move soil from center to edges)	2, in-field border areas only	0.92	0.92	2.0	0.46
18 May	Chisel	Case MX255	Custom chisel, 4.0 m wide, 0.6 m depth, w/ edged roller	1	6.58	6.18	8.5	0.73
19 May	Disc 1	Case Puma 195	International Offset Disc, 5.8 m wide, pulling a single axle (2 smooth road tires), pulling a 5.8 m wide spiked roller	1	4.92	4.83	10.1	0.48

Table 4-1 (continued)

Date	Tillage Operation	Tractor Make and Model	Implement Make and Model	Number of Passes	Sample Time (hr)	Tractor Time (hr _{tractor})	Area Worked (ha)	Tractor Operation Rate (hr _{tractor} /ha)
19 May	Disc 2	Case Puma 195	International Offset Disc, 5.8 m wide, pulling a single axle (2 smooth tires) pulling a 5.8 m wide spiked roller	1	5.25	4.73	10.1	0.47
20 May	Lister	Case MX255	Custom lister, 6 row, 1.0 m spacing	1	3.83	5.07	12.5	0.41
		Case Puma 195	International Offset Disc, 5.8 m wide	3, only in-field border areas				
5 June	Break down ditch and field-edge borders, Cultivator passes 1 and 2, and Roller	Kubota M8030DT	Custom 1-way disc (1 set of 3 discs that move soil from one side to the other)	8, east side edge only	7.25	7.43	23.9	0.31
		Case 870	Custom border buster (2 sets of 3 discs that move soil from center to edges)	4, east and west side edges only				
		Case Puma 195	Lilliston Rolling Cultivator, 6 rows wide, 1.0 m spacing	2				
		Case 2290	Flat roller, 6 rows wide	1				

Table 4-1 (continued)

Date	Tillage Operation	Tractor Make and Model	Implement Make and Model	Number of Passes	Sample Time (hr)	Tractor Time (hr _{tractor})	Area Worked (ha)	Tractor Operation Rate (hr _{tractor} /ha)
5 June	Plant	Case Puma 195	Lilliston Rolling Cultivator, 6 rows wide, 1.0 m spacing	2	2.00	3.82	13.2	0.29
		Case 2290	Flat roller, 6 rows wide	1				
		John Deere 4055	John Deere MaxEmerge 2 Row Planter, single row, 6 rows wide, 1.0 m spacing	1				
18 June	Fertilize	Case 2290	Custom side-dress fertilizer, 6 rows wide, 1.0 m spacing, pulling a fertilizer tank (1 axle, 2 small smooth tractor tires)	1	2.17	1.08	3.8	0.28
25 June	Cultivator pass 3	Case 1370	Lilliston Rolling Cultivator, 6 rows wide, 1.0 m spacing	1	4.25	4.02	10.1	0.40

general, two cultivator passes are performed in sequence in opposite directions down the rows to ensure adequate weed control.

Ditches and field-edge borders were built and then broken down in both fields between 20 May and 5 June to allow for flood irrigation prior to planting. Water for irrigation was taken from the earthen holding pond of the adjacent dairy; drainage ditches on the east side of both fields returned excess water to the same holding pond. As the ditch and field-edge border construction and removal were not measured in the CMP field, the corresponding step for the conventional tillage method was not considered in the total emissions per method. Prior to any spring tillage activities, both Fields 4 and 5 had in-field borders running in roughly an east/west direction. The in-field borders in Field 5 were not broken down and smoothed out, but instead were used for the summer corn crop. However, in Field 4 they were removed and the irrigation water moved in the furrows created by the lister.

Field personnel observed operations continually and recorded notes on tractor operation times, potential contamination issues due to traffic on surrounding dirt roads and wind-blown dust, general meteorological observations, etc.

Instrumentation and Sample Layout

A very dominant northwest wind was found in historical data for the months of May and June from a representative meteorological monitoring station in Stratford, CA, in the California Irrigation Management Information System (CIMIS). Therefore, the PM

and meteorology sampling layouts were configured to measure upwind conditions to the north and west and downwind conditions to the south and east.

Meteorological measurements were made at upwind and downwind locations with the instrumentation in Table 4-2. Vertical temperature, humidity, and wind speed profiles were measured using two 15.3 m towers, one upwind and one downwind as shown in Fig. 4-1. Each tower had five humidity/temperature sensors at 1.5, 2.5, 3.9, 6.2, and 9.7 m agl and 3-cup anemometers at 2.5, 3.9, 6.2, 9.7, and 15.3 m agl. Wind direction was measured at 15.3 m using a wind vane instead of the typical 10 m due to fact that lidar measurements were made at higher elevations (up to 200 m agl) and the 15.3 m measurement height was reasoned to provide a better representation of both ground level and higher elevation wind direction than the 10 m height. Additionally, a meteorological station monitored wind speed, wind direction, temperature, relative humidity, precipitation, barometric pressure, and incoming solar radiation at 5 m agl at the air quality trailer (AQT) location. Three pairs of three-dimensional sonic anemometers and infrared gas analyzers were deployed, one at an upwind location and one each downwind of the two fields of interest, to characterize upwind and downwind turbulence, as well as vertical fluxes of latent heat (evaporation), sensible heat, carbon dioxide, and horizontal momentum. Bulk density and soil moisture were quantified several times throughout the study, with calculations performed as described in Ref. 17.

Table 4-2. Manufacturer, precision, and accuracy information for deployed meteorological instrumentation.

Instrument Model	Manufacturer	Measured Parameter	Accuracy
HMP45C	Vaisala, Oulu, Finland	temperature relative humidity	± 0.2 C at 20 C $\pm 2\%$ for values in the range 0% to 90% and $\pm 3\%$ for values in the range 90% to 100%
Gill 3-cup anemometer	RM Young Co., Traverse City, Michigan	horizontal wind speed	± 0.2 m s ⁻¹ over 1 m s ⁻¹ , threshold speed = 0.5 m s ⁻¹
024A Wind Vane	Met One Instruments, Grants Pass, Oregon	wind direction	$\pm 5^\circ$
Vantage Pro2 Plus Weather Station	Davis Instruments, Inc., Hayward, California	temperature relative humidity horizontal wind speed wind direction precipitation barometric pressure solar radiation	± 0.5 C for values greater than -7 C, ± 1.0 C for values less than -7 C $\pm 3\%$ for values 0% to 90% and $\pm 4\%$ for values 90% to 100% ± 1 m s ⁻¹ or 5%, whichever is greater $\pm 3^\circ$ $\pm 3\%$ or 0.02 mm per event, whichever is greater ± 0.8 mm Hg at 25°C $\pm 5\%$ of full scale
CSAT	Campbell Scientific, Inc., Logan, Utah	three dimensional wind vector	Offset error $< \pm 8$ cm s ⁻¹ Gain error for wind vector within 20° of horizontal $< \pm 6\%$ of reading
7500 Infrared Gas Analyzer	LI-COR, Lincoln, Nebraska	gaseous H ₂ O and CO ₂ concentrations	Dependent on calibration and environmental conditions

PM mass concentrations were monitored by 20 MiniVol Portable Air Samplers (models 4.2 and 5.0, AirMetrics, Eugene, Oregon), referred to hereafter as MiniVols. They are a portable, programmable, filter-based sampler that is battery-powered and yields an integrated sample over the exposure period. Filters were exposed for the duration of each sample period (see Table 4-1), yielding a single mass concentration measurement per sampler per sample period. Cumulative samples of particles up to PM_{2.5} or PM₁₀ is accomplished via an impactor plate assembly inserted just upstream of the filter; TSP may be sampled without an impactor assembly in place. The MiniVol impactor assembly is designed to operate a flow of 5.0 L min⁻¹, though the flow rate is neither actively monitored nor actively controlled by the system. It is set prior to deployment by the user via a calibrated rotameter. Rotameter flow calibration was performed prior to deployment. While several studies have found that PM_{2.5} and PM₁₀ levels reported by MiniVols are very similar to concentrations measured by federal reference method (FRM, see 40 CFR 50.6 and 50.7) monitors, the slope of the particle removal efficiency versus particle size curve of the MiniVol impactor assembly is less steep than required by FRM samplers¹⁸⁻²¹. Therefore, PM levels reported by the MiniVols should be considered as close approximations to those that would be given by FRM samplers.

Pre- and post-weights for the 47 mm Teflon filters used to collect particles were quantified using a calibrated microbalance (Type MT5, Mettler-Toledo, Inc., Columbus, Ohio). Filter conditioning was carried out in accordance with guidance in 40 CFR 50

Appendix J. Sample period average mass concentrations were calculated by dividing the total mass catch (average post-weight minus average pre-weight) by the volume of air sampled.

Particle size distribution (PSD) was measured by eight Aerosol Profilers (model 9722, Met One Instruments, Grants Pass, Oregon), also known as optical particle counters (OPCs). The OPC sums particle counts in eight size bins over nominal 20 s sample periods. The particle diameters (d_p) for lower bin limits were 0.3, 0.5, 0.6, 1.0, 2.0, 2.5, 5.0, and 10.0 μm , with the last channel counting all particles $\geq 10.0 \mu\text{m}$. The factory calibrations of signal strength versus particle size using polystyrene latex (PSL) beads of known size were used due to varying atmospheric aerosol composition. The sample flows were not conditioned prior to passing through the sampling chamber during these measurements due to the dry conditions, though this is suggested in atmospheres with high relative humidity. OPC flow measurements and inter-OPC count calibrations were performed on-site and applied in post analysis. Particle volume concentrations (V) per bin were calculated from the counts, assuming spherical particles and using the geometric mean diameter (GMD) as the representative d_p . Values of V in bins up to $d_p = k$ were summed to estimate the cumulative volume concentration (V_k).

The MiniVols and OPCs were deployed on towers and tripods upwind and downwind of the fields, as shown in Fig. 4-1. Most downwind sensors were moved between the downwind layouts, depending on the field being tilled. The AQT and the associated samplers did not move. The AQT is a 5 m x 2.5 m x 2.5 m cargo trailer used as

the base of operations and equipped with tables, a refrigerator and dessicator for sample storage, and a rooftop platform for sensor deployment. Samplers were placed on tripods at 2 m agl at all locations except for those on top of the AQT at 5 m and those at the top of the towers at 9 m. Not all sample sites shown for a given setup were used in each sample period due to instrument availability limitations. However, samples were collected at a minimum of two upwind and six downwind locations during each sample period.

At most of the locations, multiple MiniVols with different impactor configurations and an OPC were collocated in order to characterize particle size and mass distributions. These data were used to calculate mass conversion factors (MCFs) for each size fraction (k), as described in detail by Ref. 21. In summary, the MCF_k is calculated using PM_k reported by MiniVols and V_k , averaged over the MiniVol sample time, from each sample location through the following equation:

$$MCF_k = \frac{PM_k}{V_k} \quad (4-1)$$

where the units for PM_k are $\mu\text{g m}^{-3}$, V_k are $\mu\text{m}^3 \text{cm}^{-3}$, and MCF_k are g cm^{-3} . Daily average MCFs were calculated across sampling locations.

The MCF is a simplified method to account for several complex and possibly interdependent variables that affect how an aerosol mixture is measured/detected based on both optical and aerodynamic properties. It incorporates many factors, such as particle shape, density, indices of refraction different from OPC calibration aerosols, and

instrument sampling efficiencies, into a single scalar value. The MCF also includes effects due to optical systems measuring particles in ambient conditions while mass concentrations are calculated based on conditioned filters. This effect may be significant in humid environments, but the effect is assumed to be negligible in warm and dry conditions such as those found during this study. The MCF_k values were used to convert the OPC V_k into PM_k to examine concentrations on a much finer temporal scale than possible with the filter data.

The Aglite lidar system was deployed to characterize PM concentrations in addition to point sensors. The Aglite lidar is a portable system using a micro-pulsed Nd:YAG laser with three wavelengths (λ), 355 nm, 532nm, and 1064 nm. It has the capability to scan 280° in azimuth and from -10° to +45° in elevation. The effective range is 500 m to 15 km with each range bin approximately 6 m in length²². The lidar was placed in crosswind positions 550 m away from the nearest tillage area border. It was at L1, as shown in Fig. 4-1, from 17 May through 11 June and at L2 for the 18 June sample period. Critical component failures prevented its use for the 25 June sample period.

The lidar continuously performed vertical scans on the upwind and downwind sides of the field, horizontal scans over the field, and calibration stares throughout tillage observation periods. Lines of approximate vertical scan locations are shown in Fig. 4-1 by the dashed lines emanating from L1 and L2; horizontal scans moved between upwind and downwind vertical scan positions at 0.75 degrees from horizontal. Vertical scans started at 0.75 degrees and extended up to between 15 to 45 degrees. The

maximum vertical angle varied between sample periods but was usually ≤ 25 degrees. Images resulting from vertical scans were monitored throughout each sample period to ensure that the maximum vertical extent of the plumes were entirely captured; modifications to the maximum vertical extent were made as needed. The lidar beam was about 10 m agl at the closest edge of the fields at 0.75 degrees in elevation. The beam was kept at or above this level due to eye safety concerns. The lidar system did not measure plumes below this level and, therefore, may underestimate PM flux.

A calibration stare refers to short periods (60-120 s) when the lidar beam is held adjacent to an upwind tower with collocated point sensors. Calibration stares were performed routinely throughout the sample period at 10-20 min intervals. In post-processing, lidar return signals collected during calibration stares were calibrated to PSD and V_k measurements. The process used to accomplish this is described in detail by Refs. 23 and 24 and will now be summarized. The calibration process is illustrated in Fig. 4-2 and was carried out through the following steps:

1. The raw lidar signal was preprocessed to yield range (R) and background corrected return power with R .
2. Relationships between backscatter (β), extinction (α), and V_k of the aerosol components were established based on OPC data from both upwind and downwind locations. The PSD of both the background and plume aerosol as a function of time were calculated, after which the α and β coefficients at the calibration range (R_c) at each lidar λ were calculated using Mie scattering

- theory applied to the PSDs. Assumptions made in these calculations were 1) all particles were spherical and 2) the bulk aerosol had a complex index of refraction equivalent to a mineral particle type (1.53 – 0.008i; Ref. 25).
3. The inversion of the lidar data was performed using a form of Klett's solution^{25.a} for two scatterers where α is proportional to β using the relationships found in step 2, resulting in α and β as function of R and λ ($\alpha(R,\lambda)$, $\beta(R,\lambda)$). The backward integration Klett method was applied to $R < R_c$ and the forward integration method was used for $R > R_c$. The backward integration method yields more stable solutions than the forward integration method and is, therefore, preferred. The calibration point R_c was placed at the farthest range possible within property ownership/field of view limitations to maximize the extent of the range of interest subject to backward integration.
 4. The relationships from step 2 were used to convert $\beta(R, \lambda)$ into $V_k(R)$ through a least-squares method in the aerosol concentration retrieval step.
 5. Conversion from $V_k(R)$ to $PM_k(R)$ was accomplished through the use of MCF_k .

This calibration method allows a scanning lidar to estimate PM_k concentrations surrounding an area/source of interest at a much finer spatial scale than possible with point sensors.

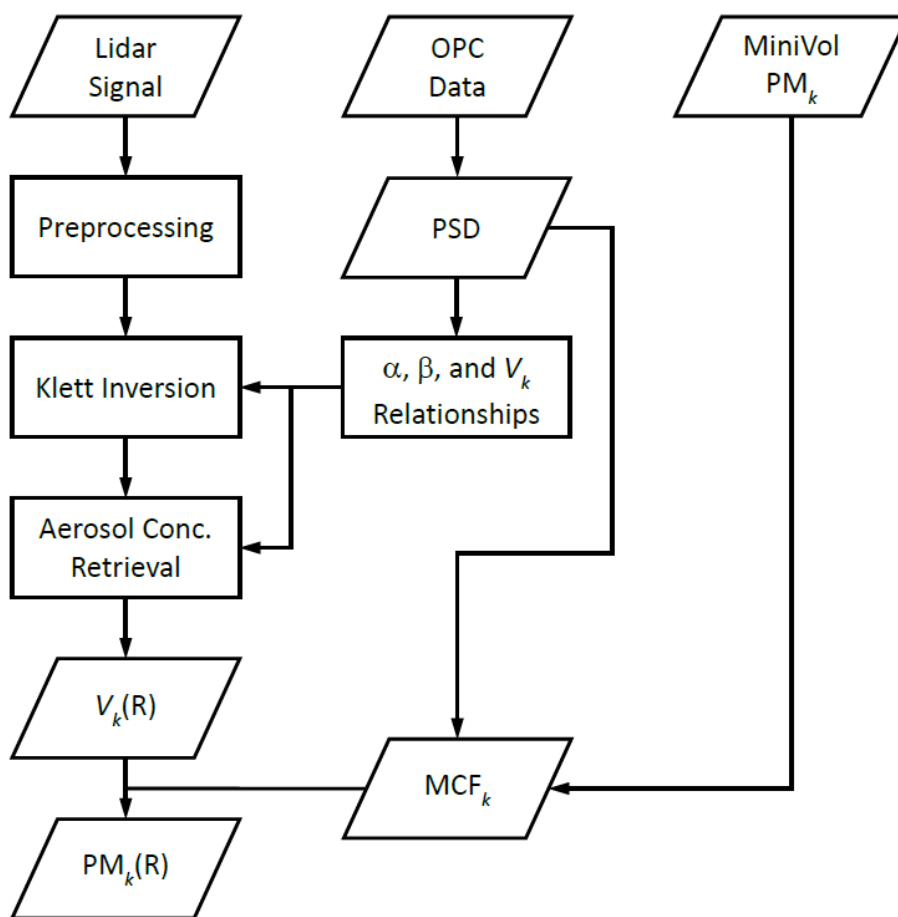


Figure 4-2. Process diagram for lidar PM calibration algorithm.

Emission Calculation Methods

The PM_k data from the point sensors and lidar were used to estimate η of the conservation tillage CMP in this study. The point sensor PM_k concentrations were coupled with an air dispersion model through inverse modeling. In typical air dispersion model applications, a source ER is supplied to a model which then calculates the resulting concentration (C_{sim}) at a given receptor location. Inverse modeling involves

using a dispersion model and concentrations measurements around a source activity ($C_{downwind}$, C_{upwind}) in order to estimate the observed ER (Q_{meas}). An initial ER (Q_{sim}) is supplied to the model to calculate C_{sim} , then the following equation is used to calculate Q_{meas} :

$$Q_{meas} = \frac{C_{downwind} - C_{upwind}}{(C/Q)_{sim}} \quad (4-2)$$

If the model used has a proportionally linear response in C_{sim} to changes in Q_{sim} , the ratio $(C/Q)_{sim}$ is a scalar value independent of the given Q_{sim} value, i.e. there are no local maxima or minima that might influence the resulting value of Q_{meas} .

AERMOD (American Meteorological Society and U.S. EPA Regulatory Model), a Gaussian air dispersion model that estimates C_{sim} at a given receptor point based on meteorological conditions, source strength, and the horizontal and vertical distance of the receptor from the source, was selected to perform the inverse modeling estimation of Q_{meas} ²⁶. It is an air dispersion model currently recommended for regulatory modeling by the U.S. EPA. It operates in one hour time steps, has a proportionally linear response in C_{sim} to changes in Q_{sim} , and assumes steady-state conditions, continuous emissions during a time step, conservation of mass, and C_{sim} resulting from multiple sources are additive. Pollutant distribution is modeled as Gaussian in the stable boundary layer in both the horizontal and vertical directions. In the convective boundary layer, horizontal dispersion is modeled as Gaussian while vertical pollutant distribution is modeled as bi-Gaussian. The spatial resolution of C_{sim} is controlled by the user through discrete and/or

gridded receptor points. The commercially available user-interface AERMOD View from Lakes Environmental, Inc. (Waterloo, Ontario, Canada), with AERMOD version 13350, was employed.

On-site measured wind speed, wind direction, temperature, humidity, and solar radiation were used by AERMET, the meteorological pre-processor for AERMOD, to create both surface and elevated meteorological input files. Wind, temperature, and humidity data were used from the upwind meteorology tower dataset, with wind speed from 9.7 m agl and temperature and relative humidity from 2.5 m agl. Incoming solar radiation was measured at the AQT location. Percent cloud cover was set to zero based on visual observations during the measurement periods.

The land use classification on all sides of the site was cultivated land. Values provided to AERMET for midday albedo and Bowen ratio of 0.18 and 1.5, respectively, were suggested as average summer values under dry conditions for a fallow agricultural field in Ref. 27. The surface roughness length (z_0), also required by AERMET, was calculated based on wind profile measurements at the upwind meteorological tower using the following equation which relates wind speeds (u_1, u_2 in m s^{-1}) at two heights (z_1, z_2 in m) and was derived from the integrated logarithmic wind speed profile equation:

$$\frac{u_2}{u_1} = \frac{\ln\left(\frac{z_2}{z_0}\right)}{\ln\left(\frac{z_1}{z_0}\right)} \quad (4-3)$$

A least sum of squares of residuals methodology was used to determine the value of z_0 that best fit measured wind speeds at the higher elevation of two paired wind speed time series over the study period. A z_0 value of 0.02 m was calculated as the arithmetic average of the values that best fit six pairings of wind speeds measured at 2.5 m, 3.9 m, 6.2 m, and 9.7 m agl, i.e. 2.5 m and 3.9 m, 2.5 m and 6.2 m, 2.5 m and 9.7 m, 3.9 m and 6.2 m, 3.9 m and 9.7 m, and 6.2 m and 9.7 m. The cup anemometer at 15.3 m malfunctioned during this deployment, rendering the data unusable for this analysis. The upwind location was selected for this analysis as the downwind tower was removed on 12 June to support another study nearby. The AQT was also removed from the southern edge of Field 5 at this same time.

Tillage operations were modeled as ground level area sources with initial plume heights of 0 m and areal extents equal to the actual tilled portions of the field. Most operations covered all or most of the field within a sample period, but some, such as the break down in-field borders operation, were intended to only work a small portion of the field surface. Tilled areas and sampler locations were measured using a hand-held GPS unit. The Q_{sim} values for each modeled operation were based on a preliminary average ER value across all tillage operations from Ref. 11 of $8.6 \mu\text{g s}^{-1} \text{m}^{-2}$ per operation

per pass multiplied by the number of passes over the field within a sample period. Sources were activated or deactivated in hourly time steps throughout a simulated sample period according to the tractor operation times as monitored by on-site personnel. Discrete receptors were set at each sampling location to yield C_{sim} for inverse modeling comparisons. Uniform Cartesian receptor grids at 2 m agl and 15 m spacing between points were set from upwind sampling locations to several hundred meters downwind of the fields to visualize predicted plume movement, shape, and concentration. Hourly C_{sim} values were averaged over the modeled sample period. Modeled plume edge effects were avoided by eliminating those locations with C_{sim} less than 10% of the maximum C_{sim} , adapted from suggestions by Ref. 28, from emissions calculations.

The second ER and EF calculation approach was a mass balance applied to the lidar PM_k data. Assuming uniform background aerosol levels, average upwind concentrations were subtracted from concentrations in and around detected plumes in the downwind vertical scans. The difference was multiplied by the component of the wind perpendicular to the beam to calculate the horizontal flux of PM through the downwind vertical scanning plane. Fluxes were summed across the vertical plane, averaged over the length of the sample period, and then divided by the size of the tilled area to calculate the mean EF of PM_k from the field surface. The EF was further divided by the total tractor time to calculate the mean ER of each operation. This method of calculating ERs and EFs using lidar is described in detail in Ref. 29.

Vertical profiles of PM mass concentration, horizontal wind speed, and wind direction are required to use the mass balance approach. The PM profile was provided by the lidar PM_k data. Profiles of wind speed were calculated using the wind speed power law, as given by Ref. 30

$$u_2 = u_1 \left(\frac{z_2}{z_1} \right)^p, \quad (4-4)$$

where z_1 and z_2 are the lower and upper elevations (m), respectively, p is a dimensionless number that varies with atmospheric stability, and u_1 , u_2 , z_1 , and z_2 , have been defined previously. Ref. 30 lists $p \approx 0.5$ for very stable conditions and $p \approx 0.15$ for very unstable conditions. The horizontal wind speeds recorded at the upwind tower were used to find the values of p that best fit the time series of measured profiles up to 9.7 m agl, with imposed minimum and maximum limits of 0.1 and 0.6, respectively. Derived values of p across all sample periods ranged from 0.10 to 0.60 and averaged 0.19. These p values were then combined with the minute-averaged wind speeds in the wind speed power law to calculate the vertical profile of horizontal wind speed up to 250 m agl, though most sample periods did not require data more than 150 m agl.

Wind direction over the vertical profile was assumed to be constant. Though wind direction is known to change in a vertical profile, the influencing factors may be complex and the magnitude and direction of change highly variable. Therefore, in the absence of measured data, the assumption that wind direction didn't change with increasing elevation over the 250 m profile was used.

Results and Discussion

Results of the soil analyses were almost identical between the two fields, suggesting little to no difference in the influence of soil properties on airborne PM emissions. Bulk densities averaged $1.57 \pm 0.05 \text{ g cm}^{-3}$ for Field 4 and $1.57 \pm 0.08 \text{ g cm}^{-3}$ for Field 5. Unless otherwise noted, error values represent one standard deviation (σ). Average soil moisture values in both fields measured immediately prior to May sample periods varied between 1.0% and 3.3%, showing very little change across operations. However, average soil moisture measured on June 5 in Field 4 was 6.1% and 8.2% in Field 5 on June 7. This increase was likely due to flood irrigation in both fields shortly after the May 20 sample period. A precipitation event occurred shortly after irrigation, but the quantity was not measured and the effect was assumed to be masked by the flood irrigation.

Wind conditions were favorable for the designed sampling layouts throughout the study period, as shown in Fig. 4-3 and Table 4-3. The median, minimum, and maximum values for sample period average winds were 4.0, 1.9, and 5.6 m s^{-1} , respectively, for speed and 321, 315, and 335° , respectively, for direction. Sample periods were generally hot and dry, with median, minimum, and maximum sample period average temperatures and relative humidity values of 31.4, 24.7, and 36.8°C and 27, 16, and 40%, respectively.

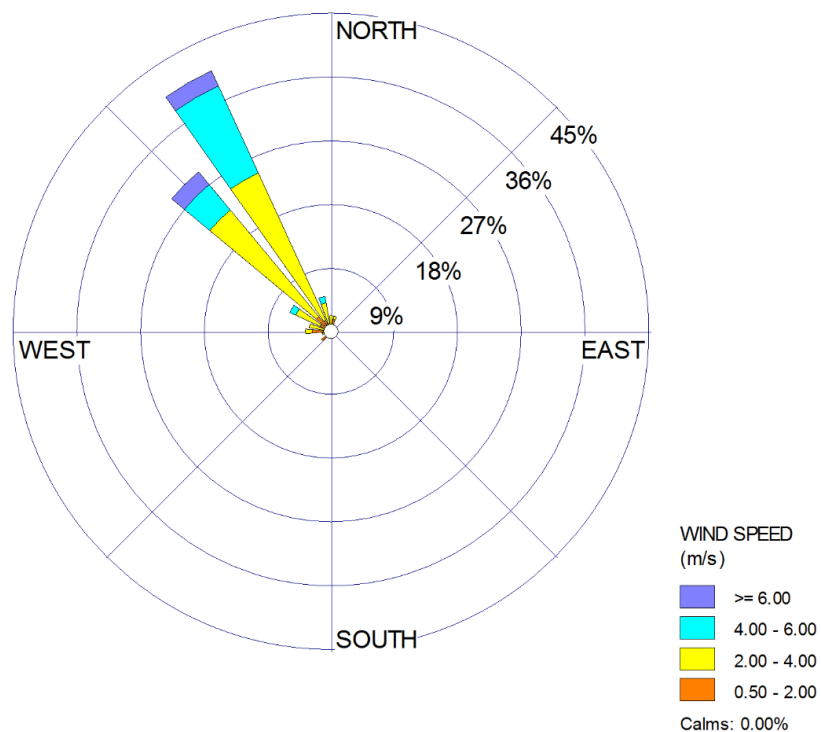


Figure 4-3. Wind rose for the hourly averaged wind observations during the days on which samples were collected.

PM Concentration Measurements

A total of 296 filter samples were collected: 116 PM_{2.5} (39%), 116 PM₁₀ (39%), and 64 TSP (22%). Calculated PM_{2.5} concentrations based on filter catch ranged from 23.2 to 3244.9 $\mu\text{g m}^{-3}$; PM₁₀ concentrations ranged from 38.1 to 1458.4 $\mu\text{g m}^{-3}$; TSP concentrations ranged from 73.6 to 2276.9 $\mu\text{g m}^{-3}$. The average method detection limit (MDL, $n = 13$), calculated based on sample period duration, the targeted flow of 5.0 L min^{-1} , and the minimum detectable difference between pre- and post-test filter weights

Table 4-3. Period-averaged meteorological measurements $\pm 1\sigma$ made at the upwind meteorological tower. Temperature, relative humidity, and wind speed were measured at 9.7 m agl and wind direction was measured at 15.3 m agl.

Date	Operation, Field	Ambient Temperature (C)	Relative Humidity (%)	Wind Speed (m/s)	Wind Direction (°)
17 May	Strip-till, Field 5	32.3 \pm 2.1	33 \pm 4	3.6 \pm 0.6	321 \pm 15
17 May	Break down in-field borders, Field 4	36.8 \pm 0.2	24 \pm 0.3	4.3 \pm 0.6	321 \pm 8
18 May	Chisel, Field 4	33.8 \pm 2.8	29 \pm 4	4.3 \pm 1.2	325 \pm 16
19 May	Disc 1, Field 4	31.4 \pm 2.5	27 \pm 3	2.9 \pm 0.8	318 \pm 22
19 May	Disc 2, Field 4	35.3 \pm 1.5	21 \pm 3	3.3 \pm 0.5	319 \pm 16
20 May	Lister, Field 4	29.1 \pm 2.2	30 \pm 10	5.1 \pm 1.1	320 \pm 10
5 June	Break down ditch, Cultivator 1 and 2, and Roller, Field 4	24.7 \pm 2.6	34 \pm 7	3.3 \pm 1.3	320 \pm 30
5 June	Plant, Field 4	27.6 \pm 0.5	26 \pm 2	4.0 \pm 0.9	315 \pm 7
7 June	Plant and Fertilize, Field 5	22.5 \pm 2.7	40 \pm 9	4.0 \pm 1.0	335 \pm 20
11 June*	Herbicide, Field 5	29.1 \pm 0.1	19 \pm 1	3.8 \pm 0.6	326 \pm 17
18 June	Fertilize, Field 4	34.1 \pm 0.3*	16 \pm 1*	5.6 \pm 0.7	326 \pm 4
25 June*	Cultivator 3	30.2 \pm 2.5	29 \pm 5	1.9 \pm 0.8	328 \pm 29

* Data taken from downwind tower due to missing data at upwind tower

of 5 μg , was 6.6 \pm 4.9 $\mu\text{g m}^{-3}$ and the median was 4.3 $\mu\text{g m}^{-3}$, with a range of 2.3 $\mu\text{g m}^{-3}$ for a run length of 7.3 hr to 17.3 $\mu\text{g m}^{-3}$ for a run length of 1.0 hr.

Of the 296 filter samples collected, 98 (33%) did not pass quality analysis (QA) checks applied to the dataset. QA checks included visual inspection of filter surfaces,

sample log inspection for noted problems, OPC time series examination for contamination (used mostly at upwind sites), concentration consistency across sampling locations, and concentration comparisons between PM_{2.5}, PM₁₀, and TSP at each sample location. In-depth descriptions of the QA checks are found in Ref. 15. An investigation into the cause(s) of this high rate of failure was conducted and a summary of conclusions is provided in the following paragraph. A large number of failures of near-source, downwind samples relative to the total number of downwind samples collected were found in the sample periods from May 18 to May 20. This, when combined with the results from the investigation into the large number of failures, cast doubt on the validity of the remaining near-source downwind samples from those runs. Therefore, all near-source downwind MiniVol samples for these sample periods were removed from MCF and ER calculations, rendering the upwind and far-source downwind samples that passed QA unusable for estimating PM emissions. The filter dataset used to calculate ERs and EFs totaled 131 samples (44%). Concentration ranges for this dataset were 26.7 to 149.8 $\mu\text{g m}^{-3}$ for PM_{2.5}, 47.4 to 489.4 $\mu\text{g m}^{-3}$ for PM₁₀, and 102.9 to 1,896.9 $\mu\text{g m}^{-3}$ for TSP. The size fraction distribution of filters used to estimate emissions was nearly identical to the total sample set: 51 (39%) were PM_{2.5}, 50 (38%) were PM₁₀, and 30 (23%) were TSP.

Filters that did not pass QA were found to have been contaminated during one or more of the following stages: sampling, filter handling, and filter storage. Evidence of “particle bounce” was found on many PM_{2.5} and PM₁₀ samples collected during May

sample periods. Particle bounce occurs when particles that collide with the impactor plate are re-entrained in the airstream and collected on the filter downstream and result in higher reported levels than actually existed. This issue is most likely due to exposing the MiniVol samplers to dust plumes exceeding the maximum recommended exposure level and improper instrument maintenance and cleaning through the May sample periods. Corrective action in the form of inspection after each deployment and cleaning, if needed, was taken during the June sample periods; no issues associated with particle bounce were observed in the second portion of the study. Additionally, some particles were observed on top of and imbedded into the plastic annular ring around the Teflon filter material – the plastic ring is covered by the filter holder assembly during deployment. This was likely due to contamination during on-site filter storage or handling. Efforts were made to minimize this issue throughout, especially during the June sample periods. However, windblown dust did impact the handling and storage area on May 20.

The collected OPC data were used to calculate PSD, V , and V_k values. Unlike the downwind MiniVol samplers, the downwind OPCs were not overwhelmed by the dust plumes from the tillage activities – the manufacturer specified range of the OPC of 0 to 3.18×10^8 particles m^{-3} was never exceeded – and thus provided usable data throughout all sample periods. Background and downwind PSD and V profiles varied throughout the study, as shown in Fig. 4-4. The particle concentrations in this figure were calculated as the change in number (N) per change in natural logarithm of d_p ($dN/d(\ln(d_p))$) where d_p

is the GMD per bin. The particles emitted by the tillage activities were generally large ($d_p > 5 \mu\text{m}$) and, therefore, strongly dominated the volume and mass contributions of the activity to near-source atmospheric particle loadings. Three to four OPCs were in positions immediately downwind of the field under study in each sample period, with between one and four OPCs in upwind locations.

OPC time series data at upwind locations were examined for contamination from upwind activities, such as unpaved road traffic. Contamination was found in six of the 12

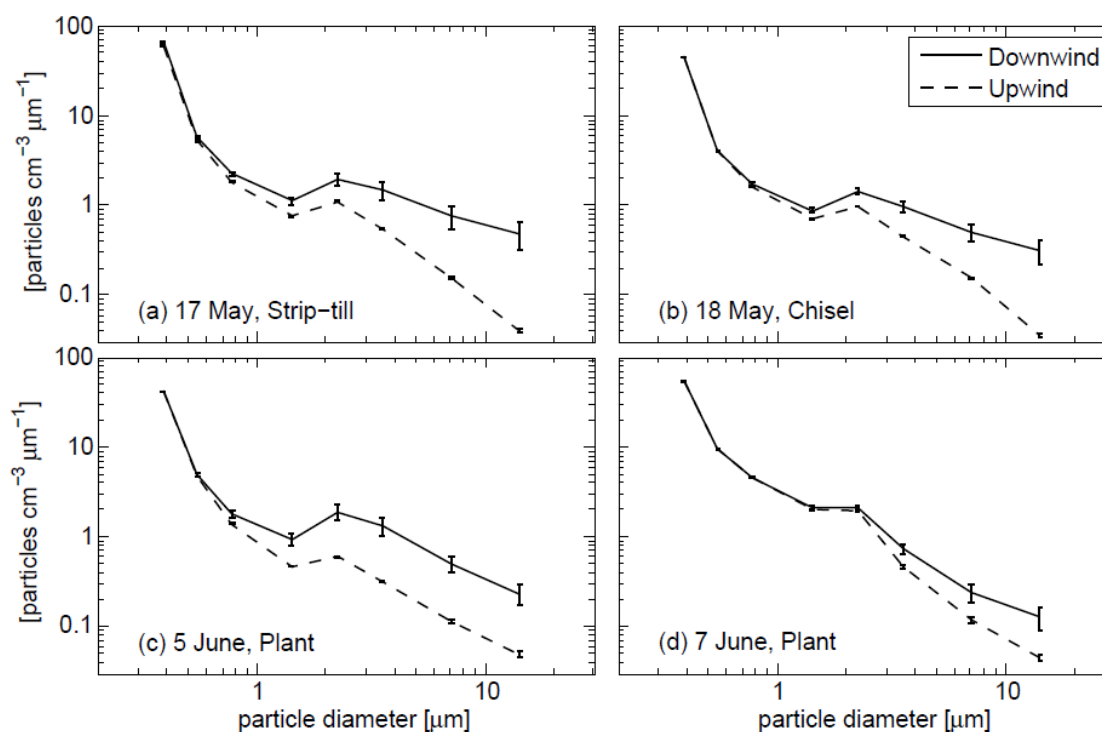


Figure 4-4. Sample period-averaged upwind and downwind PSDs as measured by OPCs for (a) 17 May, strip-till operation, Field 5, (b) 18 May, chisel operation, Field 4, (c) 5 June, plant operation, Field 4, and (d) 7 June, plant and fertilize operation, Field 5. Error bars represent the 95% confidence intervals about the average.

sample periods, with five of those occurring at the sample site adjacent to the upwind meteorological tower and immediately downwind of an unpaved road. Large, short-duration spikes indicative of contamination were removed from the upwind data in these instances to estimate the background aerosol concentration. In each instance this was performed, the estimated background levels were in very good agreement with those measured by an OPC at a different, uncontaminated upwind location. Filter samples collected at upwind locations with contamination indicated by OPC data were removed from ER estimation.

Those filter samples that passed QA, including the upwind and far-source downwind samples from May 18 to May 20, were used to estimate MCF_k values if collected adjacent to an OPC. Most of the daily average MCF_{10} and MCF_{TSP} values were within the expected range of 1 to 3 $g\ cm^{-3}$. However, the daily average $MCF_{2.5}$ values were much larger than expected, with individual values ranging from 3.2 $g\ cm^{-3}$ to 28.2 $g\ cm^{-3}$, having a mean of $14.6 \pm 3.7\ g\ cm^{-3}$ and a median of 10.1 $g\ cm^{-3}$. For comparison, the densities of pure nickel and mercury are 8.9 $g\ cm^{-3}$ and 13.5 $g\ cm^{-3}$, respectively. In past field campaigns $MCF_{2.5}$ has generally been higher than MCF_{10} and MCF_{TSP} values, but these $MCF_{2.5}$ values were much higher than those seen before and account for the majority of values above 5 $g\ cm^{-3}$ reported in Ref. 21. Due to the non-physically large numbers, the calculated $MCF_{2.5}$ were not used. Instead, the average soil density of 2.65 $g\ cm^{-3}$ given in the USDA NRCS National Soil Survey Handbook was used as a constant $MCF_{2.5}$ for all sample periods³¹. Using a constant $MCF_{2.5}$ may affect the accuracy of

calculated $PM_{2.5}$ concentrations, ERs, and EFs and the value of $\eta_{2.5}$. However, as will be shown later, the effect on $\eta_{2.5}$ was assumed to be small as the values were very close to those of η_{10} and η_{TSP} . Table 4-4 presents the daily MCF_k values used to convert V_k calculated from lidar and OPC measurements to PM_k .

The cause of the high $MCF_{2.5}$ values is unknown. No significant differences in $PM_{2.5}$ chemical composition were observed between sample periods with higher and lower $MCF_{2.5}$. While PSDs varied between sample periods, no trends in PSDs sufficient to explain high/low $MCF_{2.5}$ groupings were observed. Higher average $MCF_{2.5}$ values were not restricted to sample periods in which evidence of particle bounce was found (18-20May); those filters exhibiting evidence of particle bounce were removed prior to MCF

Table 4-4 Mass conversion factors (MCFs) used to convert optical particle measurements to mass concentrations for each sample day and averaged for the whole campaign. Error values represent the 95% confidence interval for $n \geq 3$. A constant $MCF_{2.5}$ value equal to the average density of soil was used due to non-physically high values calculated for most of the sample days³¹.

Date	$MCF_{2.5}$		MCF_{10}		MCF_{TSP}	
	Avg	n	Avg \pm 95% CI	n	Avg \pm 95% CI	n
	(g cm ⁻³)	count	(g cm ⁻³)	count	(g cm ⁻³)	count
17 May	2.65	---	2.6 \pm 1.3	9	4.4 \pm 4.0	7
18 May	2.65	---	1.6	2	1.6 \pm 0.1	3
19 May	2.65	---	1.7 \pm 0.3	5	1.6 \pm 0.3	8
20 May	2.65	---	1.6 \pm 0.5	5	1.4 \pm 0.2	4
5 June	2.65	---	1.8 \pm 0.3	5	1.5	2
7 June	2.65	---	1.5 \pm 0.3	5	1.4 \pm 0.2	4
11 June	2.65	---	4.3 \pm 1.2	4	2.9 \pm 0.5	4
18 June	2.65	---	1.8 \pm 0.5	6	2.3 \pm 1.0	4
25 June	2.65	---	2.0 \pm 0.3	6	2.2 \pm 0.6	5
All	---	---	2.1 \pm 0.3	49	2.3 \pm 0.7	44

calculations. MCF_{10} and MCF_{TSP} patterns tended to follow $MCF_{2.5}$ patterns, having correlation coefficients (r) of 0.64 and 0.84, respectively, but with much smaller changes in amplitude. Good negative correlations ($-0.69 \leq r \leq -0.64$) were found when comparing all MCF_k with sample duration. This means that MCF_k tended to increase as sample duration decreased.

One potential explanation consistent with these relationships is contamination during filter handling and storage. If filters were equally contaminated, the greatest effect would be found on those samples with the smallest mass catch, i.e. samplers with $PM_{2.5}$ impactor configurations or shorter sample times. Unfortunately, field and lab blanks were not collected to monitor for and quantify such contamination; this oversight has been corrected in subsequent studies.

An alternate contamination test is a comparison with independent and proximate PM measurements, though conclusions from this test are limited by comparability of sample characteristics. The closest independent monitoring site was a suburban monitoring station operated by the SJVAPCD, which reported 24-hr average PM_{10} concentrations on three days during which tillage monitoring occurred. The SJVAPCD 24-hr average PM_{10} and study site mean background PM_{10} pairs were, respectively, 38 and 38 $\mu\text{g m}^{-3}$ for 18 May, 34 and 47 $\mu\text{g m}^{-3}$ for 5 June, and 38 and 163 $\mu\text{g m}^{-3}$ on 11 June. Differences in sample period (24-hr vs. 1.5-hr to 7.5-hr and limited to daylight hours only), location setting and local sources (suburban vs. rural), and instrumentation (FRM vs. MiniVol) existed between the two datasets and contributed to

observed differences. The differences in concentration between the two sites on 18 May and 5 June were within the range of expected values and do not support the sample contamination hypothesis. At first glance, the large difference on 11 June may be interpreted to support this hypothesis. However, all filters collected during this sample period easily passed the visual filter inspection for particle bounce and particles on and/embedded into the annular ring. If filter contamination did occur during this field study, it does not appear to have been consistent based on the comparison with proximate PM_{10} measurements nor evident in the applied QA tests. Therefore, the cause of the high $MCF_{2.5}$ values is unknown and no further data exclusions were made.

Sample period-averaged OPC PM_k data ranged from 4.3 to 60.2 $\mu\text{g m}^{-3}$ for $PM_{2.5}$, 41.2 to 641.1 $\mu\text{g m}^{-3}$ for PM_{10} , and 95.3 to 3,271.9 $\mu\text{g m}^{-3}$ for TSP. OPC PM_k values at the native 20 s averaging period had much higher ranges across all k as the plumes emitted by the roving tillage activities impacted the point samplers in short bursts, the impact of which was reduced when averaged with intervals measuring lower levels. Lidar-derived PM_k also had a high variability for the same reason. This is evident in Fig. 4-5, which presents PM_{10} reported by all three systems at 9 m agl at the downwind tower for the 18 June sample period (14:00 – 16:10). The dashed black line represents the sample period average PM_{10} value based on the MiniVol filter sample, the red line represents the PM_{10} based on 20 s OPC data, and the blue markers represent the lidar-derived PM_{10} for each 0.5 s signal averaging period. The higher temporal sampling frequency of the optical systems show the timing and magnitude of individual plumes impacting the

collocated group not resolved by the single MiniVol sample. The lidar beam was not continuously adjacent to the point sensors as it was performing upwind calibration stares and downwind vertical scans, leading to the gaps seen the in the lidar time series. The lidar reported elevated PM_{10} levels when collocated during plume impaction events. It also reported elevated levels when the point sensors did not – this was due to part of a plume being within the 6 m long lidar bin but not significantly impacting the tower. Negative PM_k values were occasionally reported by the lidar, as seen here. These were artifacts of the optimization in the calibration procedure and are not real – negative PM concentrations are not possible.

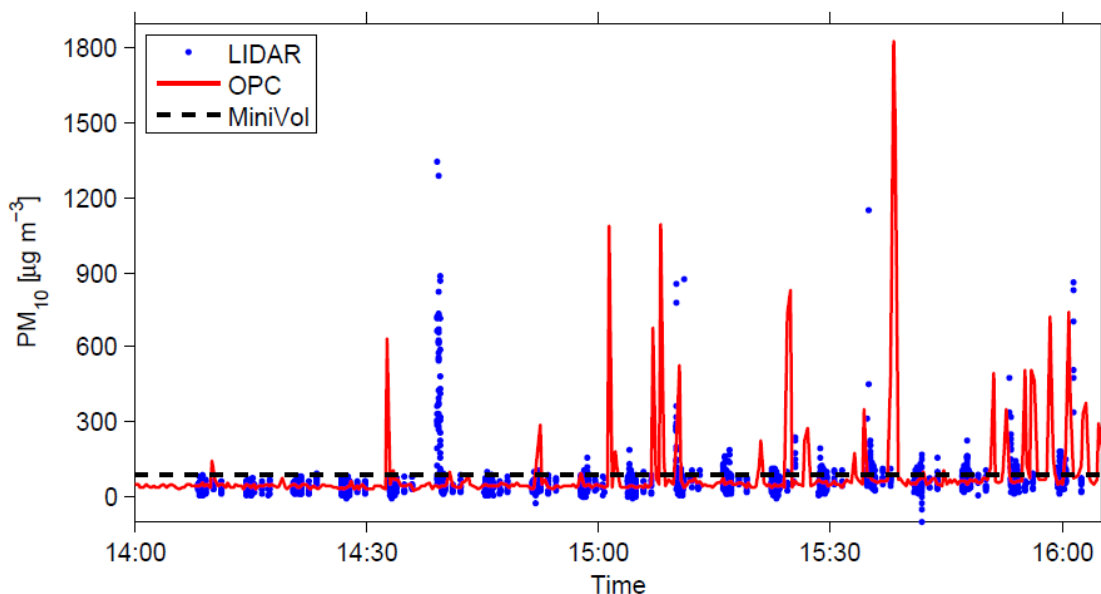


Figure 4-5. Time series of PM_{10} concentrations as reported by the collocated OPC, MiniVol filter sampler, and lidar at 9 m agl on the downwind side of the tillage activity for the 18 June sample period (14:00 – 16:10).

While the scanning lidar was at a disadvantage compared to the point sensors in monitoring PM continuously at a given location in Fig. 4-5, a significant advantage of the lidar over the point sensors is its ability to monitor plumes over a line or area. For instance, the data shown in Fig. 4-6 were collected in a stare adjacent to the downwind tower (location indicated by the solid black line at constant range) over approximately one minute of the sample period in Fig. 4-5. The lidar detected multiple, highly-concentrated plumes at varying distances, only one of which appears to impact the tower. The bottom plot shows the average PM_{10} concentration with range during this time. The vertical scanning profiles used to monitor plumes emitted by the tillage activities allowed measurement of vertical and cross-beam horizontal plume extents. Monitored plumes reached elevations up to 150 m agl at the downwind lidar scanning plane, though most remained below 100 m. Plume widths also varied. Fig. 4-7 provides an example of two plumes captured in a single vertical scan on 5 June when two different tillage operations were performed in different areas of the field. The plume closer to the lidar is lower and denser than the plume farther away.

Comparisons between PM_k concentrations from MiniVol, OPC, and lidar data at upwind and downwind locations were performed for each sample period as a check on the use of the MCF_k and the lidar calibration procedure. Accurate estimates of PM_k are necessary for accurate estimates of PM emissions. The MiniVol, as it measures PM_k directly at each point, is assumed to be more representative of the actual PM_k than the OPC and lidar. Most inter-instrument comparisons revealed upwind values agreed fairly

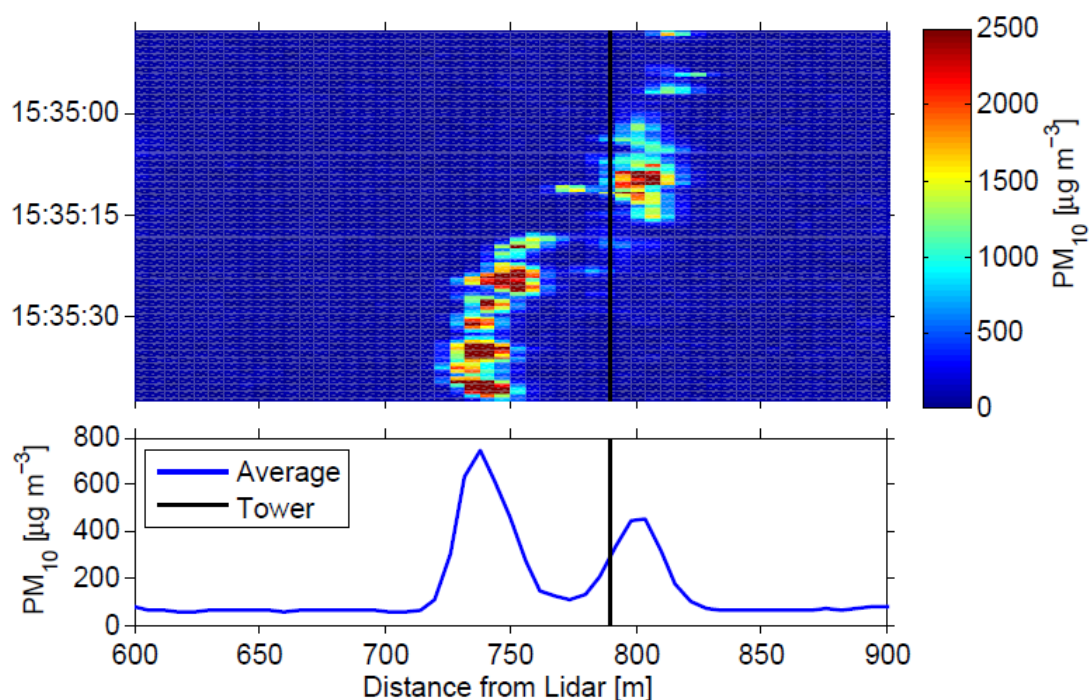


Figure 4-6. Lidar-derived PM₁₀ in a time versus distance from the lidar concentration map (top) and a time series average concentration versus distance from the lidar graph (bottom). Data were collected in a stare past the downwind tower during the 18 June sample period.

well, but greater differences were found in comparisons at downwind sample sites.

Potential reasons for the similarities and differences at both upwind and downwind point sampler locations will be discussed in the following paragraphs, with an example comparison provided as well.

The similarity of PM_k estimated by the OPC and lidar at the upwind site was expected as this is the calibration point in the lidar PM retrieval algorithm and both are converted to PM_k through the same MCF_k. The downwind sites, however, were not used as direct calibration points and, thus, may exhibit greater differences between lidar and

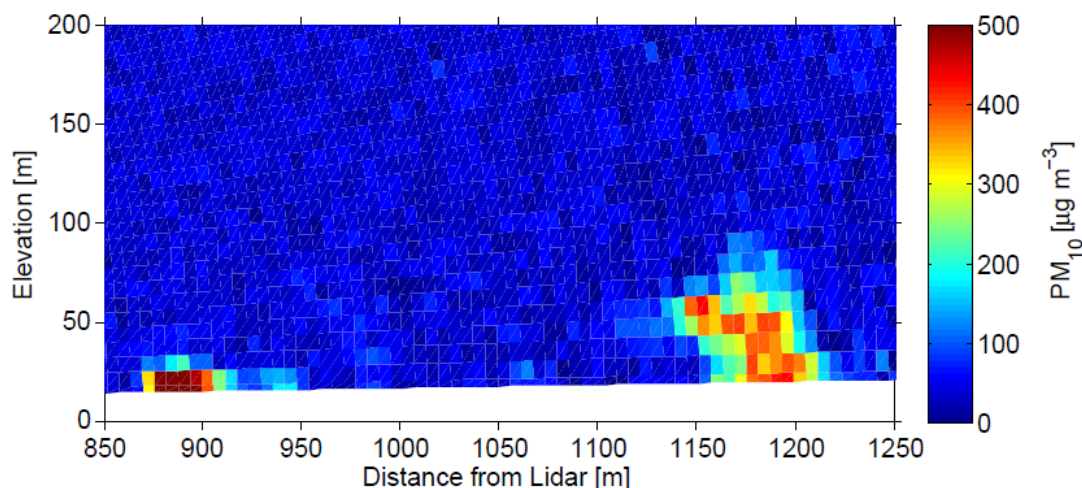


Figure 4-7. Image of plumes in a vertical scan on 5 June.

OPC period-averaged values. On a side note, the proximity of all upwind OPC and lidar PM_k demonstrates the selected time interval between lidar calibration stares was sufficient to adequately characterize changes in upwind PM. It also supports the assumption made in the flux calculations that upwind PM_k is relatively constant.

Differences in calculated PM_k between instruments may result from a variety of factors, including but not limited to, the following: sample volume differences (OPCs - 1 L min^{-1} ; MiniVols - 5 L min^{-1} ; lidar - 6 m bin length x ~ 1 m beam diameter sampled at 10 kHz with data averaged over 0.5 s); sampling frequency at the point sensor location (MiniVol and OPC - continuous; lidar - upwind: 3-5 min per 15 min, and downwind: 1-3 min per 15 min); lidar sample timing with respect to plume location (i.e., simultaneous presence of both the lidar beam and a transient plume impacting the instrumented tower versus the total time the plumes impacted the tower); and the differences

between the MCF_k values calculated at the comparison site and the average MCF_k across all measurement sites used to convert V_k to PM_k . Lidar stare time used in the comparison with continuously running, stationary OPCs and MiniVols was limited by the need to perform vertical scans for flux estimation. Better agreement is expected on the downwind side with an increasing proportion of time spent adjacent to downwind samplers.

The error introduced in this inter-instrument comparison associated with using a spatially-averaged MCF_k was generally less than $\pm 30\%$ during this study based on the 95% CIs reported in Table 4-3. Large differences in $PM_{2.5}$ between the filter- and optical-based methods were observed across all sample periods due to the use of a constant $MCF_{2.5}$ value that was not derived from on-site PM measurements. However, OPC and lidar $PM_{2.5}$ levels were close.

An example of an inter-instrument comparison is provided in Table 4-5 for the 18 June sample period, the period shown in Fig. 4-5. In this instance, average upwind OPC and lidar PM_{10} and TSP concentrations were within 15% and 7%, respectively, of the values reported by the MiniVol. Downwind lidar PM_{10} and TSP values were 73% and 64% of OPC levels, respectively, while the OPC PM_{10} was 6% higher than the PM_{10} concentration from the filter sample. The differences at the downwind location were likely caused, in large part, by the relatively small amount of time the lidar sampled adjacent to the point sensors. Longer stare periods at downwind locations are expected to yield better PM_k accuracy and are planned for future deployments.

Table 4-5. Comparison of period average PM mass concentrations as reported by collocated MiniVol filter samplers and OPCs, as well as the adjacent lidar bin, at measurement heights of 9 m agl at upwind and downwind tower locations for the 18 June sample period. Error values provided for OPC and lidar PM_k represent the 95% confidence interval (CI).

	$PM_{2.5}$ ($\mu\text{g m}^{-3}$)	PM_{10} ($\mu\text{g m}^{-3}$)	TSP ($\mu\text{g m}^{-3}$)
Upwind (T1)			
MiniVol PM sampler	30.1	56.5	195.4
OPC \pm 95% CI	4.9 ± 0.1	48.2 ± 1.1	185.4 ± 8.5
Lidar \pm 95% CI	5.1 ± 0.1	50.8 ± 1.3	200.0 ± 6.7
Downwind (T2)			
MiniVol PM sampler	63.2	87.5	---
OPC \pm 95% CI	6.4 ± 0.5	93.0 ± 15.1	442.3 ± 95.2
Lidar \pm 95% CI	6.3 ± 0.1	68.1 ± 2.1	284.5 ± 10.2

Estimated Emissions and Control Efficiencies

The PM_k data from the lidar, OPCs, and MiniVols were all used to calculate PM emissions using mass balance and inverse modeling techniques. Table 4-6 provides the results of these calculations, as well as the summed emissions from each tillage management practice. Stated uncertainties are the 95% confidence intervals (CIs) about the average and have been provided for cases where $n \geq 3$.

The summed conservation tillage sequence emissions (E_{ST}) consists of the following three passes: strip-till, plant, and herbicide application. The lidar did not detect plumes in downwind vertical scans during the herbicide application, as indicated by the no plumes observed (NPO) designation. However, downwind PM samplers

reported small increases in concentrations over background levels during this sample period, leading to small EFs relative to the other operations investigated. The herbicide application operation was performed by a small tractor pulling a spray applicator; as no subsurface disturbance occurred, the only active PM sources were the tractor and implement tires and the spray droplets.

The summed emissions for the conventional tillage method (E_{CT}) includes the following 13 passes in order: two break down in-field border passes, chisel, two disc passes, lister, two cultivator passes, roll, plant, fertilizer injection, and two more cultivator passes. The EFs for the break down in-field borders operation have been distributed over the entire field area (10.1 ha) instead of just the area worked (1.0 ha) to represent the emissions over the entire field in the E_{CT} calculation. As the lidar system was unavailable to take measurements during the last sample period for the third cultivator pass, the emissions of the last two cultivator passes were assumed to be equal to the observed emissions for the first two cultivator passes. The inverse modeling method found that the third cultivator pass emitted from 0.6 to 3.6 times as much PM as calculated for the first and second cultivator passes, with an average of 2.1.

Some of the lidar-derived EFs were much higher than those calculated by inverse modeling within an operation and PM size fraction, particularly for the chisel, disc 1, and lister passes. Others were not statistically different due to overlapping CIs. E_{CT} and E_{ST} EFs from the lidar dataset were significantly higher, based on the CIs, than those calculated through inverse modeling in all cases but the $PM_{2.5}$ E_{ST} . The lidar- and OPC-

Table 4-6. Average particulate matter (PM) emission factors and 95% confidence intervals (CI) estimated for the conventional and conservation tillage management practices. Emissions were calculated through applying a mass balance technique to mass calibrated lidar data and inverse modeling with AERMOD and both filter-based particle sampler (MiniVol) and mass calibrated OPC data. Control efficiency (η) results are also provided for the conservation tillage management practice. NPO = no plumes observed.

	Average Emission Factors \pm 95% CI (mg m ⁻²)										
	PM _{2.5}			PM ₁₀			TSP				
	Lidar	OPC	MiniVol	Lidar	OPC	MiniVol	Lidar	OPC	MiniVol	OPC	MiniVol
Conservation Tillage Method											
Strip-till	26.9 \pm 6.1	14.5 \pm 3.0	35.7 \pm 6.1	523.8 \pm 117.8	452.5 \pm 85.7	315.6 \pm 86.9	4,450.5 \pm 1,000.9	2,180.4 \pm 583.6	1,652.9 \pm 881.6		
Plant	50.2 \pm 15.0	6.6 \pm 3.3	133.5	175.6 \pm 52.6	173.5 \pm 36.8	123.3	567.6 \pm 169.9	881.8 \pm 234.5	857.4 \pm 523.2		
Herbicide Application	NPO	0.7 \pm 0.4	44.0	NPO	40.9 \pm 12.7	64.3	NPO	114.8 \pm 55.9	133.7 \pm 71.9		
Sum	77.1 \pm 16.2	21.8 \pm 4.5	213.2	699.4 \pm 129.0	666.9 \pm 94.1	503.2	5,018.1 \pm 1,015.2	3,177.0 \pm 631.5	2,644.0 \pm 1,027.7		
Conventional Tillage Method											
Break down in-field borders	3.0 \pm 1.8	0.7 \pm 0.1	---	33.6 \pm 20.8	51.2 \pm 7.9	---	152.3 \pm 94.4	617.6 \pm 79.8	5.8		
Chisel	101.1 \pm 11.1	18.3 \pm 5.4	---	1,132.8 \pm 123.9	647.4 \pm 181.0	---	4,997.9 \pm 546.8	3,828.2 \pm 758.5	---		
Disc 1	210.1 \pm 49.3	37.0 \pm 9.4	---	3,410.7 \pm 799.9	1,452.5 \pm 161.9	---	17,440.2 \pm 4,090.4	9,693.3 \pm 744.5	---		
Disc 2	58.9 \pm 16.2	36.4 \pm 13.3	---	1,066.4 \pm 293.2	1,797.5 \pm 703.1	---	6,023.4 \pm 1,655.8	10,483.4 \pm 2,976.9	---		
Lister	302.8 \pm 127.5	19.4 \pm 2.9	---	4,608.1 \pm 1940.8	849.5 \pm 150.5	---	23,375.6 \pm 9,845.2	4,918.9 \pm 1,169.8	---		
Break down ditches, Cultivator passes 1 and 2, & Roller	22.9 \pm 4.5	7.8 \pm 5.0	52.7 \pm 19.8	109.4 \pm 21.3	137.1 \pm 65.5	107.9 \pm 47.7	354.0 \pm 69.0	687.1 \pm 443.8	---		

Table 4-6 (continued).

		Average Emission Factors \pm 95% CI (mg m ⁻²)											
		PM _{2.5}				PM ₁₀				TSP			
		Lidar	OPC	MiniVol		Lidar	OPC	MiniVol		Lidar	OPC	MiniVol	
Plant	8.3 \pm 2.1	6.4 \pm 4.1	86.4		79.5 \pm 20.2	170.7 \pm 81.3	87.6		285.3 \pm 72.4	910.4 \pm 487.1	495.1		
Fertilizer Injection	9.4 \pm 6.2	21.5 \pm 17.6	67.1 \pm 63.1		139.4 \pm 91.9	642.5 \pm 380.3	515.9		684.1 \pm 451.3	4,602.1 \pm 2,370.2	3,686.7		
Cultivator Passes 3 & 4	---	11.1 \pm 4.0	31.9 \pm 4.1		---	369.8 \pm 157.7	234.5		---	2,459.4 \pm 894.9	2,063.5 \pm 436.7		
Sum	811.1 \pm 138.7	186.2 \pm 27.0	---		11,051.2 \pm 2,126.0	6,813.4 \pm 888.8	---		54,881.3 \pm 10,814.4	42,651.5 \pm 4,406.9	---		
CMP Control Effectiveness													
η , %	90.5	88.3	---		93.7	90.2	---		90.9	92.6	---		

based PM_{2.5} EFs were smaller than the MiniVol-based PM_{2.5} EFs in all cases, which is likely related to the use of the average soil density as the MCF_{2.5} in place of calculated values as discussed earlier.

While the EFs from published studies are generally not in close agreement, a high range of variability is expected from measurements made under different meteorological and soil conditions, as demonstrated in Ref. 5. Some of the PM₁₀ EF values calculated from this study were in agreement with those given by Ref. 5 and Ref. 10, such as the cultivate, roll, strip-till, conventional tillage planting, and conservation tillage planting passes. Other EFs were much larger than values previously reported, especially the disc 1, disc 2, chisel, and lister passes. The results from this campaign were, in general, not in as good agreement as previous studies have been.

The η values were also included in Table 4-6. They were calculated using the following formula based on a collection efficiency equation found in Ref. 30 and represents the PM emissions reduction of the conservation tillage compared to the conventional tillage:

$$\eta = \frac{E_{CT} - E_{ST}}{E_{CT}} \quad (4-5)$$

The strip-till conservation tillage reduced PM emissions in all size fraction by about 90%. The reduction in total tractor operation time per unit area of field was similar to PM reductions at 84% (see Table 4-6). The η results had a small range of < 6% across

methodologies and size fractions, despite large differences in summed emissions between methodologies.

Limitations of the PM sensors and AERMOD contribute to limitations and uncertainties in the estimated EFs. For instance, the scanning lidar system did not collect data below about 10 m agl at the range of the fields due to eye-safety concerns, which results in portions of plumes not being sampled and included in EF estimates. Vice versa, the inability to locate point sensors above 10 m limits their ability to characterize the plume depth. In this case, the lidar and point sensors complement each other in mapping the emitted plumes, as previously demonstrated by Ref. 6. In addition, measurements at a few points may or may not represent the plume characteristics sufficiently to accurately determine the EF, particularly for a roving source such as in agricultural tillage. This was mitigated by deploying as many samplers at different sites within the downwind plume as possible. Another limitation that was identified by Ref. 11 and was also present in this analysis is AERMOD's poor simulation of elevated plumes from agricultural tillage, particularly plumes completely detached from the ground.

Conclusions

A study was conducted in California's San Joaquin Valley to estimate the PM_k emissions η of a CMP relative to the conventional tillage practices. PM_k concentrations resulting from a spring tillage sequence transitioning from a winter wheat silage crop to a summer corn crop were monitored. The strip-till conservation tillage CMP, consisting

of three operations in three passes, was compared against the conventional tillage sequence, consisting of nine operations in 13 passes. The CMP reduced the amount of tractor operation time per unit area by 84%. Emissions were estimated through inverse modeling with filter-based PM_k and through a mass balance applied to mass-calibrated lidar PM_k .

A significant portion of the filter-based samples were rendered unusable for emissions calculations due to sampling irregularities and errors. The incompleteness of this PM_k dataset prevented the calculation of total EFs per management practice and the CMP η . However, the OPC- and lidar-based PM_k and EF datasets were sufficiently complete to calculate η values, which were all about 90%. Some of the calculated EFs were within the range found in the literature, but others were significantly higher. The total emissions per management practice and PM size fraction varied significantly, based on the 95% CIs, between the measurement and emissions estimation methodology combinations. This study demonstrated that the strip-till CMP can significantly reduce PM emissions and tractor operation time during the investigated spring tillage sequence.

Acknowledgments

We thank the individuals and groups whose efforts made this study and subsequent analysis possible. Funding was provided by the San Joaquin Valleywide Air Pollution Study Agency under contract 07-1 AG and the U.S. Department of Agriculture,

Cooperative Agreement # 58-3625-9-743. Cooperators include: the USDA ARS, National Laboratory for Agriculture and the Environment; Utah State University; EPA Region 9; EPA Office of Research and Development, National Exposure Research Laboratory; the San Joaquin Valley Ag Technical Group; the San Joaquin Valley Air Pollution Control District; the California Air Resources Board; and the cooperative agricultural producers and industry representatives. Mention of tradenames does not constitute endorsement by the USDA ARS, EPA, Space Dynamics Laboratory, or Utah State University.

References

1. Davidson, C.I., R.F. Phalen, and P.A. Solomon. 2005. Airborne particulate matter and human health: a review. *Aerosol Science and Technology* 39:737-749.
2. Environmental Protection Agency (EPA). 1991. Designations and classifications for initial PM-10 nonattainment areas. *Federal Register* 56(51):11101-11105.
3. EPA. 1993. Reclassification of moderate PM-10 nonattainment areas to serious area. *Federal Register* 58(5):3334-3342.
4. San Joaquin Valley Air Pollution Control District (SJVAPCD). 2006. Conservation Management Practices Program Report, San Joaquin Valley Air Pollution Control District (SJVAPCD). Available:
http://www.valleyair.org/farmpermits/updates/cmp_program_report_for_2005.pdf
. Accessed: 8 May 2013.

5. Flocchini, R.G., James, T.A., Ashbaugh, L.L., Brown, M.S., Carvacho, O.F., Holmen, B.A., Matsumura, R.T., Trezpla-Nabalgo, K., Tsubamoto, C. 2001. Interim Report: Sources and sinks of PM10 in the San Joaquin Valley. Crocker Nuclear Laboratory, UC-Davis, CA.
6. Holmén, B.A., Eichinger, W.E., Flocchini, R.G. 1998. Application of elastic LIDAR to PM10 emissions from agricultural nonpoint sources. *Environmental Science and Technology* 32:3068-3076.
7. Holmén, B.A., James, T.A., Ashbaugh, J.L., Flocchini, R.G. 2001a. LIDAR-assisted measurement of PM10 emissions from agricultural tilling in California's San Joaquin Valley—Part I. LIDAR. *Atmospheric Environment* 35:3251-2364.
8. Holmén, B.A., James, T.A., Ashbaugh, J.L., Flocchini, R.G. 2001b. LIDAR-assisted measurement of PM10 emissions from agricultural tilling in California's San Joaquin Valley—Part II: Emission factors. *Atmospheric Environment* 35:3265-3277.
9. Kasumba, J., Holmén, B.A., Hiscox, A., Wang, J., Miller, D. 2011. Agricultural PM10 emissions from cotton field disking in Las Cruces, NM. *Atmospheric Environment* 45:1668-1674.
10. Madden, N.M., Southard, R.J., Mitchell, J.P. 2008. Conservation tillage reduces PM10 emissions in dairy forage rotations. *Atmospheric Environment* 42:3795-3808.
11. Moore, K.D., M.D. Wojcik, R.S. Martin, C.C. Marchant, G.E. Bingham, R.L. Pfeiffer, J.H. Prueger, and J.L. Hatfield. 2013. Particulate emissions calculations from fall

- tillage operations using point and remote sensors. *Journal of Environmental Quality* 42:1029-1038. doi: 10.2134/jeq2013.01.0009.
12. Wang, J., Miller, D.R., Sammis, T.W., Hiscox, A.L., Yang, W., Holmen, B.A. 2010. Local dust emission factors for agricultural tilling operations. *Soil Science* 175:194-200.
 13. California Air Resources Board (ARB). 2003a. Area source methods manual, section 7.4: Agricultural land preparation. California ARB.
www.arb.ca.gov/ei/areasrc/fullpdf/full7-4.pdf (7 Nov. 2011).
 14. California ARB. 2003b. Area source methods manual, section 7.5: Agricultural harvest operations. California ARB. www.arb.ca.gov/ei/areasrc/fullpdf/full7-5.pdf (7 Nov. 2011).
 15. Williams, D., Hatfield, J., Sweet, J., Chilingaryan, S. 2014. Atmospheric LiDAR coupled with point measurement air quality samplers to measure fine particulate matter (PM) emissions from agricultural operations, Part 2 of the California 2007-2008 tillage campaigns: Spring 2008 data analysis. EPA/600/R-14/191. Washington, DC: EPA.
 16. U.S. Department of Agriculture, Natural Resources Conservation Service (USDA NRCS). 2009. Web Soil Survey 2.0. 2 January 2009.
<http://websoilsurvey.nrcs.usda.gov/app/>.
 17. Doran, J.W., Jones, A. 1996. Methods for assessing soil quality. SSSA Special Publication Number 49. Soil Science Society of America. Madison, Wisconsin.

18. Hill, J.S., P.D. Patel, and J.R. Turner. 1999. Performance characterization of the MiniVol PM_{2.5} Sampler. *Proceedings Air and Waste Management Association's 92nd Annual Meeting*. Paper 99-617. Pittsburgh, PA: Air and Waste Management Association.
19. Chow, J. C., Watson, J. G., Lowenthal, D. H., Chen, L.-W A., Tropp, R. J., Park, K., Magliano, K. A. 2006. PM_{2.5} and PM₁₀ Mass Measurements in California's San Joaquin Valley. *Aerosol Science and Technology* 40(10):796–810.
20. Chen, F.-L., Williams, R., Svendsen, E., Yeatts, K., Creason, J., Scott, J., Terrell, D., Case, M. 2007. Coarse particulate matter concentrations from residential outdoor sites associated with the North Carolina Asthma and Children's Environment Studies (NC-ACES). *Atmospheric Environment* 41:1200-1208.
21. Moore, K.D., R.S. Martin, W.J. Bradford, C.C. Marchant, D.S. Jones, M.D. Wojcik, R.L. Pfeiffer, J.H. Prueger, and J.L. Hatfield. 2014. Derivation and use of simple relationships between aerodynamic and optical particle measurements. *Journal of Environmental Engineering*, accepted [doi: 10.1061/(ASCE)EE.1943-7870.0000893].
22. Marchant, C.C., T.D. Wilkerson, G.E. Bingham, V.V. Zavyalov, J.M. Andersen, C.B. Wright, S.S. Cornelsen, R.S. Martin, P.J. Silva, J.L. Hatfield. Aglite lidar: A portable elastic lidar system for investigating aerosol and wind motions at or around agricultural production facilities. *Journal of Applied Remote Sensing* 3(1):033511 [doi: 10.1117/1.3097928].

23. Zavyalov, V. V., Marchant, C. C., Bingham, G. E., Wilkerson, T. D., Hatfield, J. L., Martin, R. S., Silva, P. J., Moore, K. D., Swasey, J., Ahlstrom, D. J., Jones, T. L. 2009. Aglite lidar: Calibration and retrievals of well characterized aerosols from agricultural operations using a three-wavelength elastic lidar. *Journal of Applied Remote Sensing* 3(1):033522 [doi: 10.1117/12.833365].
24. Marchant, C. 2008. Algorithm Development of the AGLITE-LIDAR Instrument. MS Thesis, Utah State University.
25. Jursa, A. S. 1985. Handbook of Geophysics and the Space Environment, Hanscom Air Force Base, Massachusetts: NTIS.
 - a. Klett, J.D. 1985. LIDAR inversion with variable backscatter/extinction ratio. *Applied Optics* 24: 1638-43.
26. Cimorelli, A.J., S.G. Perry, A. Venkatram, J.C. Weil, R.J. Paine, R.B. Wilson, R.F. Lee, W.D. Peters, and R.W. Brode. 2005. AERMOD: a dispersion model for industrial source applications. Part I: general model formulation and boundary layer characterization. *Journal of Applied Meteorology* 44:682-693.
27. EPA. 2008. AERSURFACE User's Guide. EPA-454/B-08-001. Research Triangle Park, N.C.: EPA Office of Air Quality Planning and Standards.
28. Arya, S.P. 1998. Air pollution meteorology and dispersion. Oxford University Press, New York.
29. Bingham, G.E., Marchant, C. C., Zavyalov, V. V., Ahlstrom, D. J., Moore, K. D., Jones, D. S., Wilkerson, T. D., Hipps, L. E., Martin, R. S., Hatfield, J. L., Prueger, J. H., Pfeiffer,

- R. L. 2009. Lidar based emissions measurement at the whole facility scale: Method and error analysis. *Journal of Applied Remote Sensing* 3(1):033510 [doi: 10.1117/12.829411].
30. Cooper, D.C., and Alley, F.C. 2002. *Air pollution control: A design approach*. Waveland Press Inc. Prospect Heights, Illinois.
31. USDA NRCS. 2007. *National Soil Survey Handbook, title 430-VI*. Available: <http://soils.usda.gov/technical/handbook/>.

CHAPTER 5

AMMONIA MEASUREMENTS AND EMISSIONS FROM A CALIFORNIA

DAIRY USING POINT AND REMOTE SENSORS¹**Abstract**

Ammonia (NH₃) is an important trace gas species in the atmosphere that can have negative impacts on human, animal, and ecosystem health. Agriculture has been identified as the largest source of NH₃, specifically livestock operations. NH₃ emissions from a commercial dairy in California were investigated during June 2008. Cattle were held in open lot pens, except for young calves in hutches with shelters. Solid manure was stored in the open-lot pens. Liquid manure from feed lanes was passed through a solids settling basin and stored in a holding pond. Passive sensors and open path Fourier transform infrared spectrometers (OP-FTIR) were deployed around the facility to measure NH₃ concentrations. Emissions from pens and the liquid manure system (LMS) were estimated using inverse modeling. Mean emission factors (EFs) for the entire facility were $140.5 \pm 42.5 \text{ g d}^{-1} \text{ animal}^{-1}$ from the passive sampler data and $199.2 \pm 22.0 \text{ g d}^{-1} \text{ animal}^{-1}$ from OP-FTIR data, resulting in the facility's summer time emissions calculated at $265.2 \pm 80.2 \text{ kg d}^{-1}$ and $375.4 \pm 27.1 \text{ kg d}^{-1}$, respectively. These EFs are within the range of values reported in the literature. Both concentrations and emissions

¹ Citation: Moore, K.D., E. Young, C. Gurell, M.D. Wojcik, R.S. Martin, G.E. Bingham, R.L. Pfeiffer, J.H. Prueger, J.L. Hatfield. 2014. Ammonia measurements and emissions from a California dairy using point and remote sensors. Transactions of the ASABE, 57:181-198.

exhibited a strong diurnal cycle, peaking in the late afternoon. Total facility emissions exhibited significant positive correlations with temperature and wind speed. The findings of this study show that NH_3 emissions from a commercial dairy 1) can vary by a factor of 10 or more throughout the day and 2) EFs can vary by two orders of magnitude when compared to other U.S. dairies, based on literature values.

Introduction

Gaseous ammonia (NH_3) is a significant basic species in the atmosphere and a compound of environmental concern based on two potentially major impacts. First, it may combine with nitric or sulfuric acids to form small particles that contribute to fine particulate matter (PM) concentrations, which has been shown to have adverse health effects in humans and animals and impacts on visibility and climate (Davidson et al., 2005). The second potential impact of NH_3 is through deposition, either dry or wet, to the land/water surface that may significantly contribute to local nitrogen budgets, which in turn affect ecosystem health and stability (Paerl, 1985; Duce, 1991).

Ammonia is a by-product of the microbial degradation of substances containing organic nitrogen, i.e. any plant or animal material. It is also manufactured for industrial and fertilizer uses. Various emissions inventories estimate that agriculture related activities contribute the largest portion of total NH_3 emissions, with 50 to 75% from livestock production (Battye et al., 2003; EPA, 2003). Livestock feed contains nitrogen (N) for conversion to animal product, but the utilization of that N is relatively inefficient

– between 50 to 80% of N intake is excreted in urea and manure. Gaseous NH_3 emissions originate from the excreted material, with substantial portions of it potentially volatilized as NH_3 within hours. Emission locations include animal housing, manure storage and treatment facilities, and manure land application. Many different factors have been shown to affect NH_3 emissions and include, but are not limited to: pH, temperature, wind speed, chemical and microbiological activities, total ammoniacal concentration (TAN), and transport and dispersion characteristics (Arogo et al, 2006).

Given the potential negative environmental effects of NH_3 and the large contribution to total emissions from agricultural livestock operations, focus has increased on quantifying emission rates (ERs) and emission factors (EFs) from a variety of livestock facilities. For the purposes of this discussion, EFs are emission values on a per animal or per animal unit (AU) and per unit time basis (i.e., $\text{g d}^{-1} \text{ animal}^{-1}$, $\text{kg yr}^{-1} \text{ AU}^{-1}$), while ERs are based on time but not per animal (i.e., kg d^{-1} , $\text{g m}^{-2} \text{ s}^{-1}$). This paper will focus on NH_3 emissions from a dairy cattle facility; dairies were estimated to contribute 24% of the total U.S. livestock NH_3 emissions in 2002 (EPA, 2005). There is a wide variety of climate, feeding, housing, facility operation, and manure management conditions in the dairy industry, all of which potentially affects NH_3 emissions and complicates estimating the industry's impacts on the environment. It is therefore important that emissions measurements be made under as many conditions as possible. Several published studies have investigated emissions from U.S. dairies under different conditions and over varying periods of time, with estimated EFs ranging over two orders

of magnitude (Schmidt et al., 2002; Cassel et al., 2005; Moore, 2007; Mukhtar et al., 2008; Rumburg et al., 2008a, 2008b; Bjorneberg et al., 2009; Flesch et al., 2009a; Adviento-Borbe et al., 2010; Leytem et al., 2011, 2013). Note that only one study, reported by Cassel et al. (2005) based on winter measurements, was conducted in California, the state with the largest milk cow population in the U.S. at 20% of the national population and with areas of significant air quality issues related to fine PM formed from NH_3 (Chow et al., 1993; USDA, 2009).

In an effort to contribute to the body of knowledge on air pollutants originating from California dairies and their potential environmental impacts, a study was conducted at a commercial dairy in the San Joaquin Valley to 1) characterize PM and NH_3 concentrations in and around the dairy using both point and remote sensors and 2) quantify summer time PM and NH_3 emissions from each source type present and from the facility as a whole. The results of the PM portion of the study have been published in Marchant et al. (2011). This paper reports on the NH_3 measurements and emissions calculations.

Materials and Methods

Ammonia concentrations and meteorological conditions were monitored in and around a dairy operation in the San Joaquin Valley of California in June 2008. ERs and EFs were estimated using an inverse modeling technique coupled with data from two sampling techniques: 1) passive NH_3 samplers, and 2) open path Fourier transform

infrared spectroscopy (OP-FTIR). The NH_3 emissions were estimated for two potential source groups, pens and a liquid manure system (LMS), and normalized by the number of animals in the facility.

Site Description

The dairy was located in northern Kings County, California and was surrounded by agricultural land. The dairy facility covered 24.7 hectares (ha), including all associated storage areas and access roads, which were mostly unpaved. A paved county road bordered the dairy on the east side, with crop land on the three other sides. Milking cows, dry milking cows, bulls, steers, and heifers uniformly distributed between birth and two years old were all housed on the dairy during the study period. Table 5-1 lists the number of animals, number of AU, and the average mass in each animal category. One AU is defined as one heifer, steer, or bull cattle and 0.7 milking or dry cattle (EPA, 2001), yielding a total of 2,335 AU on this dairy with 1,885 animals. The average size of a cattle farm in Kings County in 2007 was 1,021 animals, while the average dairy had 1,169 milk cows (USDA, 2009).

The youngest calves were housed in individual small hutches, each with a shelter. Milking cows, bulls, steers, dry cows, and heifers older than about four weeks old were housed in open lot pens with a dirt base. Stocking density during this study averaged $64.1 \text{ m}^2 \text{ animal}^{-1}$. Most open lot pens were equipped with a canopy shelter

Table 5-1. Animal count, average animal mass, average feed characteristics, and estimated manure and nitrogen excreted for cattle on this dairy during the study period. Excretion values were estimated based on information provided by Nennich et al. (2005) as part of standards revisions to ASAE D384.1 (2005), Manure Production and Characteristics.

<i>Animal Type</i>	<i>Animal Count</i>	<i>Animal Unit (AU)</i>	<i>Average Mass (kg)</i>	<i>Dry Matter Intake (kg d⁻¹ animal⁻¹)</i>	<i>Dietary Crude Protein (%)</i>	<i>Manure Excreted (kg d⁻¹ animal⁻¹)</i>	<i>Nitrogen Excreted (kg N d⁻¹ animal⁻¹)</i>
Milking Cow	950	1,357	748	25.2	18.4	75.7	0.537
Dry Cow	100	143	748	14.8	17	49.8	0.334
Bull ^[a]	30	30	857	14.8	17.7	49.8	0.353
Heifer	740	740					
Large (1-2 yrs old)	400	400	435	10.1	17	31.3	0.186
Small (< 1 yr old)	340	340	195	8.9	17	32.4	0.170
Steer ^[b]	5	5	435	10.1	17	31.3	0.186
Calf	60	60	64	4.8	17	16.4	0.091
<i>Farm Total</i>	<i>1,885</i>	<i>2,335</i>	<i>NA</i>	<i>33,308 kg d⁻¹</i>	<i>NA</i>	<i>103,103 kg d⁻¹</i>	<i>693 kg d⁻¹</i>

^[a] Dry matter intake and manure excreted for bulls was assumed to be equal to dry cows. Dietary crude protein for bulls represents an average between milk cow and heifer diets, based on the assumption bulls were evenly distributed between pens with milk cows and larger heifers, and nitrogen excretion was calculated based on the average crude protein content.

^[b] Steers were assumed to be fed the same ration as larger heifers and have equal dry matter intake, manure excretion, and nitrogen excretion.

consisting of a corrugated metal roof elevated about 6 m above ground level (agl) on poles. The total pen area was 13.0 ha, about 53% of the dairy footprint, with a total of 0.8 ha covered by shelters. The dairy layout is presented in Fig. 5-1, with the group of

pens for each animal category labeled and the locations of feed, equipment, and manure storage locations also shown. It should be noted that the five steers occupied only a quarter of the northwestern most pen.

The cows were milked twice a day, with a milking schedule from 08:00 h to 17:00 h and from 20:00 h to 05:00 h local time. Milk production averaged $34.1 \text{ kg d}^{-1} \text{ animal}^{-1}$ during June 2008. A feed truck delivered feed to all pens from 05:30 h to 12:00 noon and from 15:00 h to 17:00 h local time along concrete feed alleys adjacent to pens. Feed

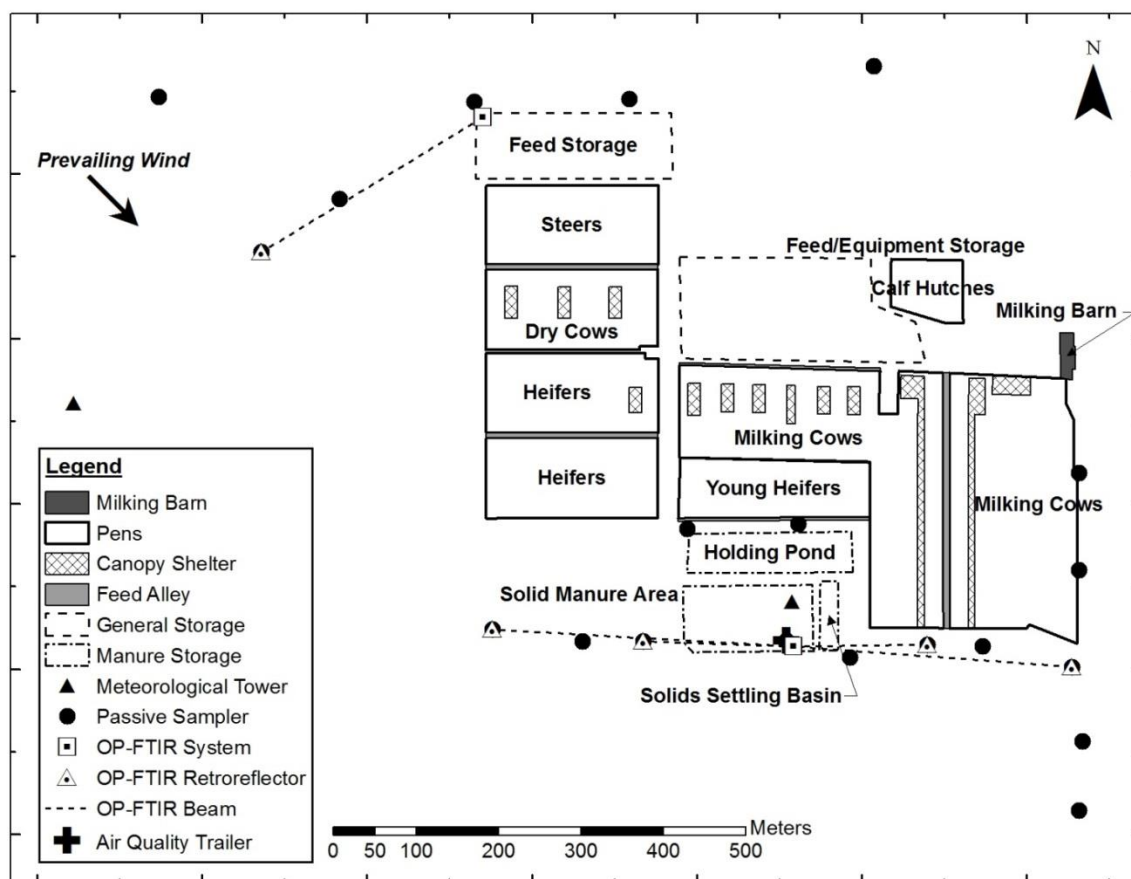


Figure 5-1. Map of dairy pens, storage, and sampling locations.

lanes, areas where the cattle stand while feeding and along which cattle are moved, were concrete and sloped for drainage. The remaining pen surfaces were unpaved. Feed lanes in pens holding milking cows were flushed several times per day, while feed lanes in the other open lots were scraped on a weekly basis with one scraping occurring during this study on 18 June. Unpaved pen surfaces were scraped on an as-needed basis; corral scraping occurred during equipment setup but not during the measurement period. Gathered manure from both the feed lane and pen area were stored in each pen for later removal. The liquids generated from both milk parlor washing and milking cow feed lane flushing were first passed through an earthen solids settling basin (0.1 ha) and was then stored in an earthen holding pond (0.6 ha). Separated solid manure was stored in windrows. The windrows present at the time of the study were in the southwest area of the solid manure handling area and dry at the surface. These windrows were not disturbed during the measurement period, nor were solids removed from the separator basin and windrowed.

Animal diets have been shown to be a significant factor in NH_3 emissions (Smits et al., 1995; Cole et al., 2005). As this study examined NH_3 emissions from all cattle on the dairy, the diets for each animal type should be considered. Cattle were fed different mixed ration diets based on gender, age, and milking status, though all diets were based on alfalfa and silage (green wheat silage for all animal types, with milking cows receiving corn silage as well) with additives to meet energy and nutrient targets. Dry matter fed (DM) and dietary crude protein content (CP) for each animal category are listed in Table

5-1. Milking cow DM and CP averaged higher than all others at 25.2 kg d⁻¹ animal⁻¹ and 18.4%, respectively, while CP for all others averaged 17%. Manure excreted (M_E) and nitrogen excreted (N_E) were estimated per animal based on equations for different categories of dairy cattle developed by Nennich et al. (2005) as part of standards revisions to ASAE D384.1 (2005), Manure Production and Characteristics, and summed over all cattle on the facility, as shown in Table 5-1. Due to a small dataset, Nennich et al. did not provide equations for dry cows. It is unlikely that the average excretion values provided by Nennich et al. would be representative for this dairy since the average DM and CP for dry cows on this dairy were 43% and 28% greater, respectively, than mean values reported by Nennich et al., though less than the maximum values reported. Therefore, M_E and N_E were calculated based on linear fits to the reported mean, minimum, and maximum values for M_E and N_E against the mean, minimum, and maximum values of DM and CP, respectively, resulting in the following equations:

$$M_E = 2.78 \times DM + 8.63, (R^2 = 0.9967) \quad (5-1)$$

$$N_E = 2.82 \times CP + 0.15, (R^2 = 1.000) \quad (5-2)$$

M_E and DM have units of kg d⁻¹ animal⁻¹, N_E has units of kg N d⁻¹ animal⁻¹, and CP has units of g of CP g⁻¹ of DM. Bulls were assumed to have similar DM intake and M_E and N_E excretion rates as dry cows, but with an average CP of 17.7% based on the assumption that bulls were evenly divided between pens with milking cows and older heifers. Steers were assumed to have intake and excretion rates equal to the larger heifers. All of the

dry dietary components were stored in the feed storage area in the northern portion of the dairy.

In order to meet PM₁₀ emissions reductions required to bring the San Joaquin Valley into compliance with PM₁₀ National Ambient Air Quality Standards, the San Joaquin Valley Air Pollution Control District (SJVAPCD) directed agricultural facilities above a threshold size to select and implement Conservation Management Practices (CMPs) designed to reduce PM₁₀ emissions (Siong and Sheikh, 2006). The SJVAPCD-accepted CMP plan for this dairy operation consisted of the following management practices: 1) manure from open corrals shall be frequently scraped and/or removed; 2) pull-type manure harvesting equipment shall be used; 3) shaded areas shall be provided for cattle in open corrals; 4) wet material shall be placed in the feed wagon prior to mixing; and 5) feed shall be wetted during mixing. While these target reducing direct PM₁₀ emissions, potential positive or negative impacts on NH₃ emissions may occur. For example, frequent scraping and or removal of manure in open corrals may produce short bursts of NH₃ releases due to the manure disturbance. Shaded areas provided for cattle may affect cattle behavior and result in greater inhomogeneity in excretion deposition across the pen surface. The CMPs dealing with feed mixing and the manure harvesting equipment type are not expected to affect NH₃ emissions.

Instrumentation

Historical wind measurements from June 2005-2007 were obtained from station #15 of the California Irrigation Management and Information System (CIMIS) near Stratford, California, as a representative site. These records showed that wind conditions during the month of June were very consistent, with winds coming dominantly from the northwest quadrant. Instruments were deployed to measure background concentrations north and northwest of the facility and emission plumes south and southeast of the dairy (Fig. 5-1). On-site measurements of wind direction during the experiment confirmed the dominant wind direction to be from the northwest. An air quality instrumentation trailer (dimensions approximately 5 m by 2.5 m by 2.5 m), located near the downwind OP-FTIR unit as shown in Figure 5-1, was used for sample preparation, collection, and storage as well as data storage.

Two 15.3 m towers were erected at the site to hold meteorological instruments. One was located 400 m west of the dairy and the other located just inside the southern boundary of the dairy. Each tower was equipped with five cup anemometers mounted at heights of 2.5, 3.9, 6.2, 9.7, and 15.3 m agl and five temperature and relative humidity sensors at heights of 1.0, 2.5, 3.9, 6.2, and 8.2 m agl. A wind vane was positioned on top of the towers at 15.3 m. Campbell Scientific (Logan, Utah) data-loggers were used to record and store the data from instruments on the towers as one minute averages. Incoming solar radiation, temperature, relative humidity, barometric

pressure, precipitation, wind speed, and wind direction were measured and reported as five minute averages by a weather station at 5.0 m agl at the air quality trailer near the downwind 15.3 m tower. Details for meteorological instruments used in this study are presented in Table 5-2. Reported meteorological values and hourly averaged data used for modeling were taken from measurements made downwind of the dairy. Due to an error discovered in post analysis in the wind direction averaging procedure for the wind vanes on the towers, wind directions reported by the weather station were used in all calculations and modeling.

Ammonia concentrations were measured with two methods. The first method was passive absorption onto citric acid-coated filters using passive samplers and pre-coated filters from Ogawa USA, Inc. (Pompano Beach, Fla.). An in-depth description of the sampler, the NH_3 concentration calculation procedure, and results from comparisons with an NH_3 scrubber during collocated deployments in ambient air and inside a poultry production house are provided by Roadman et al. (2003). Collection of NH_3 onto the pad is driven by a concentration gradient between the ambient air and the filter surface; the concentration at the filter surface is maintained at zero due to its reaction with the acid-coated filter surface and formation of a stable compound (ammonium citrate) for subsequent analysis. Total sorption of NH_3 is determined by the ambient concentration, the exposure time, and the mass transfer coefficient. Calculated concentrations represent the average concentration over the period of exposure. Roadman et al. conducted two saturation and deployment time studies and found that

Table 5-2. Meteorological instruments employed in this study.

<i>Instrument</i>	<i>Company, City, State/Country</i>	<i>Parameter Measured</i>	<i>Accuracy</i>
Gill 3-Cup Anemometer	R.M. Young Company, Traverse City, Mich.	Wind speed	± 0.2 m/s over 1 m/s, threshold speed 0.5 m/s
HMP45C	Vaisala, Oulu, Finland	Temperature	± 0.2 °C at 20 °C
		Relative Humidity	$\pm 2\%$ for values in the range 0-90%, $\pm 3\%$ for values in the range 90-100%
024A Wind Vane	Met One Instruments, Grants Pass, Ore.	Wind Direction	± 5 °
Pro2 Plus Weather Station	Davis Instruments, Hayward, Cali.	Temperature	± 0.5 °C for values greater than -7 °C, ± 1.0 °C for values less than -7 °C
		Relative Humidity	$\pm 3\%$ for values 0-90%, $\pm 4\%$ for values 90-100%
		Solar Radiation	$\pm 5\%$ of full scale
		Precipitation	$\pm 3\%$ or 0.02 mm per event, whichever is greater
		Barometric Pressure	± 0.8 mm Hg at 25°C
		Wind Speed	± 1 m/s or 5%, whichever is greater
		Wind Direction	± 3 °

the diffusion and sorption of NH₃ on the pad is linear for total collected masses up to 12.1 µg of NH₃, after which the mass transfer coefficient decreases with increasing mass collected. In cases where the total mass collected exceeded the 12.1 µg threshold, the estimated concentration would be lower than the actual average concentration.

The passive sampler exposure time selected for this study was 12 hours based on the optimum time ranges (see Figure 5-2 in Roadman et al. (2003)) for background concentrations assumed to be close to zero and instantaneous samples of up to 2 ppm during active pumping into and taken immediately downwind of the solids separator basin with a handheld NH₃ gas sensor (Toxi Pro Biosystems, Middleton, Connecticut; 0 – 100 ppm range, 1 ppm resolution). Passive sampler sites were arrayed upwind, downwind, and inside the dairy area as shown by the filled circles in Figure 5-1. Six were established as upwind sites and located to the north and northwest of the dairy with measurement heights of 1-2 m agl. The remaining 17 sites were placed at downwind locations, based on the prevailing winds, along the southern dairy border, the eastern dairy border, and between the pens with young heifers and the holding pond. Fourteen of the downwind sites sampled at 1-2 m agl heights and three were set at 9 m agl on towers at both ends of the southern dairy border and adjacent to the air quality trailer. Note that passive samplers were located at both 2 m and 9 m on the towers, leading to 23 deployed samplers and 20 sites shown in Figure 5-1.

Analysis of the mass of NH₃ collected on the pads as ammonium (NH₄⁺) was performed within the 28 day manufacturer suggested period of time after exposure. It was accomplished via extraction through sonication in 8 mL de-ionized water and quantification via ion chromatography (IC) at the Utah Water Research Laboratory (UWRL) in Logan, Utah. The IC instrument (Dionex Corporation) was equipped with an AS 40 Automated Sampler, CE20 Conductivity Detector, GP 40 Gradient Pump,

Membrane Suppressor, LC Chromatography Oven, IonPac® CS12A cation column, CG12A cation guard column, and a 500 μL sample loop. The IC method used a 0.03 N sulfuric acid (H_2SO_4) solution as eluent. Chemical standards, blanks, and continuous calibration verification (CCV) standards utilized de-ionized water and reagent grade chemical stocks. Blanks and CCVs were analyzed every 10 samples. A lab and field blank were collected for each sample period and analyzed in the same manner. The mass of NH_3 collected per sample and used to determine the period average concentration was calculated as the total detected mass minus the average mass detected on the corresponding lab and field blank. Duplicate analyses were run on 9% of the samples, with the two concentration values averaged for further calculations; the average differences between duplicate analyses, expressed as the percent of the average value, was 1.4% and the median was 0.0%. The average method detection limit (MDL) $\pm 1\sigma$ for the 12 h sample periods was 11.4 ± 0.4 ppbv ($7.8 \pm 0.4 \mu\text{g m}^{-3}$).

OP-FTIR was the second method of measuring ambient NH_3 concentrations utilized at the dairy. OP-FTIR is a real-time monitoring technique for remote detection and quantification of multiple compounds simultaneously. The principle of operation is based on the absorption of energy at different wavelengths by different compounds. The OP-FTIR unit projects an infrared (IR) beam of light through a volume to be analyzed and then captures this beam, generating a full infrared spectrum which can be used in conjunction with reference spectra to identify the gases present and allows for their concentration to be measured to ppb levels.

For this study, two OP-FTIR instruments were employed, with one located on each of the dominantly upwind and downwind sides. The upwind OP-FTIR instrument, manufactured by Industrial Monitoring and Control Corporation (IMACC, Round Rock, Texas), was operated in a monostatic mode in which a single unit containing the IR beam source, detector, and associated optics was used at one end of the path and a passive corner-cube array retroreflecting mirror was at the other end. It consisted of a 0.125 cm^{-1} FTIR modulator, a zinc selenium beam splitter, a mercury cadmium telluride detector cooled with liquid nitrogen, a helium neon laser for dynamic alignment control and a 25 cm diameter Cassegrain telescope. The upwind measurement path was 2 m agl along a transect from the northwest corner of the dairy over a field and totaling 250 meters (Fig. 5-1).

Spectra were collected at 1, 3, and 5 minute intervals and analyzed using the IMACC FTIR Software Suite, Ver. 01/2005. The IMACC software was used to define an analytical method for the selected analyte that was applied to each spectra to: 1) perform a point-by-point comparison with a reference spectra to determine the spectral line shift required to obtain the maximum correlation coefficient; 2) select portions of the spectra for further analysis that contains minimal impacts from compounds with potential interferences, based on comparisons between the collected spectra and reference spectra for potentially interfering compounds; 3) account for background levels of other compounds and dynamic changes in the measurement environment; and 4) calculate the path length concentration of the analyte of interest through a

calibration equation that accounts for response non-linearity over the full range of analyte concentrations through a best fit curve fitted to reference standard measurements across the full range. Background spectra were collected onsite during times the system was upwind of the dairy using a 25 m path length to minimize NH_3 absorption. The algorithm developed for NH_3 was applied to each recorded transmission spectra to generate a quantitative value of NH_3 concentration.

The OP-FTIR on the downwind side of the dairy was a monostatic unit manufactured by MDA (Atlanta, Ga., now Cerex Monitoring Solutions, LLC, Atlanta, Ga.) that utilized a Bomem Michelson 100 interferometer, a 25 cm telescope, and a mercury cadmium telluride detector cooled by a Stirling engine. Spectra were collected every 70 s. This OP-FTIR was set in a scanning system with multiple retroreflectors in order to determine NH_3 concentrations along multiple lines. The scanning system consisted of a covered set of scaffolding, a rack upon which the OP-FTIR was positioned with the output beam directed vertically through a hole in the roof and then onto a mirror capable of rotational (270°) and elevational (-5° to $+45^\circ$ from horizontal) movement. The mirror height was approximately 2.5 m agl. The IR beam was pointed toward each of 6 retroreflectors along the downwind side of the dairy using the steering mirror, with the OP-FTIR centrally located on the southern border of the facility as shown in Figure 5-1. Retroreflectors were located at about 140 m and 290 m away from the FTIR along an east-west line, with far retroreflectors stationed at both 2-3 m agl and 9 m agl and near retroreflectors at 2-3 m agl. Six spectra were collected at each position, with the first

two spectra collected not used due to interference from movement of the mirror between positions and to allow system stabilization. Therefore, four consecutive 70 s spectra were collected along each beam path on a 42 min cycle. Return signal strength, expressed as a percent of the outgoing signal, varied between 50% and 15%, depending on path length, alignment, and retroreflector cleanliness. Retroreflectors were cleaned every two to three days as needed. Spectra analysis and quantification of the path-length averaged NH_3 concentrations were performed using a data analysis software created by Dr. Peter Griffiths at the University of Idaho utilizing a partial least squares regression technique (Griffiths et al., 2009; Shao et al., 2010) with instrument-specific calibration parameters.

During the setup period, the OP-FTIR units were placed adjacent to each other at the upwind OP-FTIR location for a collocated comparison test using adjacent beam paths. Two tests, each 1.5 to 2.0 h in duration, were conducted. The units measured incoming background levels during one test, averaging (\pm SD) 39.0 ± 7.7 ppb and 35.7 ± 4.7 ppb for the upwind and downwind units, respectively. Incoming background levels were spiked by exposed liquid ammonium for the other test, resulting in average concentrations of 120.3 ± 28.8 ppb and 121.1 ± 23.5 ppb for the upwind and downwind units, respectively. These tests show that the units agreed very well at the higher level and slightly less well at the lower background level.

Data Treatment and Filtering

Concentrations measured by the OP-FTIR instruments were averaged over 2 h intervals throughout the measurement period for EF estimation. This averaging time was selected to minimize the smoothing of potential trends in emissions while providing two or more groups of samples on which to base a period average. Due to the low cumulative sampling of the downwind scanning system along a given path (~4.5 min every 42 min), the representativeness of an average value for the entire 2 h period was of concern. Representativeness was assessed based on a period's relative standard deviation (RSD). Exclusion of data due to RSD levels > than 25%, 33%, 40%, 50%, and 75% was examined. Average values with a RSD > 33% were excluded from EF calculations because the 33% level provided a conservative assessment of representativeness. This resulted in the removal of $\leq 30\%$ of the averaged data in six of the seven employed OP-FTIR measurement paths from emissions calculations.

As previously stated, the sampler layout during this experiment was designed to measure the dairy facility's impact on downwind concentrations to the south and east. However, winds from directions other than the prevailing northwest sector would diminish the effectiveness of this setup. Dairy and sample layout geometry indicated that periods with wind directions outside of -70 to $+50^\circ$ from North should be excluded from EFs calculations. Hourly averaged wind direction measured on-site was used to screen data periods. While wind direction may vary considerably over an hour and

render the hourly averaged wind direction insufficient for screening purposes, the wind directions recorded during this study were very consistent over time spans of several hours with periods of higher variability almost always resulting in hourly averages outside of the optimal range. Therefore, hourly averaged wind direction values were sufficient for screening in this instance. Additionally, determination of the upwind or downwind status of each sample location/path was made based on hourly averaged wind direction.

Values reported at upwind sites were averaged to calculate the background NH_3 levels (C_B) entering the facility. Concentrations resulting from the dairy activities (C_{meas}) were calculated on a location-by-location basis by subtracting C_B from the measured downwind concentration. This difference was determined to be significant if C_{meas} was greater than the 67% confidence interval (CI) about C_B , corresponding to one SD. Only C_{meas} values found to be significant in this way were used in emissions calculations. About 18% of the downwind OP-FTIR measurements lacked a corresponding OP-FTIR C_B value. In these cases, the average passive sampler C_B and corresponding 67% CI were used to estimate C_{meas} .

Emissions Calculations

A dispersion model requires a user-input emission rate for a source in order to predict downwind concentration values. However, this study seeks to determine the dairy emission rate that resulted in the measured impact on downwind NH_3

concentrations. This was accomplished through inverse modeling, a process of comparing a measured impact on concentration (C_{meas}) at a downwind site with a model predicted impact on concentration (C_{sim}) based on an initial emission rate supplied to the model (Q_{sim}) in order to estimate the actual emission rate (Q_{meas}). As given by Faulkner et al. (2007) and Flesch et al. (2009b), the relationship for deriving Q_{meas} from a single source, assuming a proportionally linear response between Q_{sim} and C_{sim} in the model, may be mathematically expressed as:

$$Q_{meas} = \frac{C_{meas}}{(C/Q)_{sim}} \quad (5-3)$$

Note that the ratio of $(C/Q)_{sim}$ is dependent upon both the source-receptor spatial relationship and the meteorological conditions over the modeled period, and, therefore, is only valid for the modeled scenario.

In the case where multiple sources are active and additive properties between the impacts of the different sources on the total concentration at a given location may be assumed, the multi-source inverse modeling technique described by Flesch et al. (2009b) may be used to simultaneously estimate the emissions from each source. In summary, a system of linear algebraic equations is created to estimate the emission rate of each source i by calculating the modeled proportional impact on the total predicted concentration at each receptor j . A system of linear equations with three sources and three measurements is given in Equation 5-4 as an example, with number subscripts

representing different sources and letter subscripts representing different measurement/receptor locations:

$$\begin{bmatrix} (C_{A,1}/Q_1)_{sim} & (C_{A,2}/Q_2)_{sim} & (C_{A,3}/Q_3)_{sim} \\ (C_{B,1}/Q_1)_{sim} & (C_{B,2}/Q_2)_{sim} & (C_{B,3}/Q_3)_{sim} \\ (C_{C,1}/Q_1)_{sim} & (C_{C,2}/Q_2)_{sim} & (C_{C,3}/Q_3)_{sim} \end{bmatrix} \begin{bmatrix} Q_{meas,1} \\ Q_{meas,2} \\ Q_{meas,3} \end{bmatrix} = \begin{bmatrix} C_{meas,A} \\ C_{meas,B} \\ C_{meas,C} \end{bmatrix} \quad (5-4)$$

If there are fewer measurements than sources ($j < i$), the system is under-determined and a unique solution cannot be found. If more measurements exist than contributing sources ($j > i$), the system is over-determined and the solution may be found through an optimization approach. See Flesch et al. (2009b) for a more detailed description, as well as a discussion on the effect of source-receptor spatial relationships on emission estimates.

There are a variety of atmospheric dispersion models available for use in inverse modeling. The one selected to carry out this inverse modeling exercise was the American Meteorological Society/US Environmental Protection Agency Regulatory Model (AERMOD) software, executable file Version 12345. It was chosen because it is a current U.S. EPA recommended regulatory model, it has a proportionally linear relationship between Q_{sim} and C_{sim} (see Cimorelli et al., 2005), and to maintain continuity within the study (Marchant et al., 2011). Some recent agricultural NH_3 emissions studies utilizing an inverse modeling methodology have used WindTrax (Thunder Beach Scientific, www.thunderbeachscientific.com), a backward Lagrangian stochastic model (Bjorneberg et al., 2009; Flesch et al., 2009a; Todd et al., 2008; Leytem

et al., 2011, 2013). Faulkner et al. (2008) utilized both AERMOD and WindTrax, in addition to two other air dispersion models, to estimate NH₃ emissions from a beef cattle feedyard. They found that ERs and EFs were model specific, and that a simple relationship did not exist between the estimated emissions. However, Bonifacio et al. (2013) found strong linear correlations between AERMOD and WindTrax in estimating PM emissions from a beef cattle feedyard and calculated AERMOD/WindTrax conversion factors ranging between 1.3 to 1.6, depending on meteorological inputs.

The AERMOD model operates in one hour time steps and assumes steady-state conditions, continuous emissions, conservation of mass, and concentrations predicted at a receptor resulting from different sources are additive. Pollutant distribution is modeled as Gaussian in the stable boundary layer in both the horizontal and vertical directions and in the horizontal direction in the convective boundary layer; vertical pollutant distribution in the convective boundary layer is modeled as bi-Gaussian (Cimorelli et al., 2005). The interface used to run this model was the commercially available AERMOD View package by Lakes Environmental Software (Waterloo, Ontario).

AERMOD requires hourly averaged meteorological data such as wind speed, wind direction, temperature, and solar radiation. These data were supplied by measurements made just south of and predominantly downwind of the dairy. Wind direction and incoming solar radiation data recorded at 5.0 m agl by the Davis weather station were utilized, along with wind speed data collected by the cup anemometer mounted at 6.2 m on the nearby tower, the closest level corresponding to the wind

direction measurements at 5.0 m. Temperature data were taken from the 2.5 m agl level on the tower. Cloud cover was set at zero for the entire study period, as there were clear skies throughout the measurement campaign.

The meteorological preprocessor for AERMOD, AERMET, also requires that values for Bowen ratio (β), noon-time albedo (α), and surface roughness length (z_0) be specified by the user. The average z_0 was calculated from vertical wind speed profiles measured downwind of the dairy using the following equation which relates wind speeds (u_1, u_2 in m s^{-1}) at two heights (z_1, z_2 in m) and was derived from the integrated logarithmic wind speed profile equation:

$$\frac{u_2}{u_1} = \frac{\ln\left(\frac{z_2}{z_0}\right)}{\ln\left(\frac{z_1}{z_0}\right)} \quad (5-5)$$

A least sum of squares of residuals methodology was used to determine the value of z_0 that best fit measured wind speeds at the higher elevation of two paired wind speed time series over the study period. A z_0 value of 0.09 m was calculated as the arithmetic average of the values that best fit six pairings of hourly averaged wind speeds measured at 3.9 m, 6.2 m, 9.7 m, and 15.3 m agl, i.e. 3.9 m and 6.2 m, 3.9 m and 9.7 m, 3.9 m and 15.3 m, 6.2 m and 9.7 m, 6.2 m and 15.3 m, and 9.7 m and 15.3 m.

Unlike z_0 , data were not collected that could be used to calculate the β and α values. Instead, summer-time values were selected from tables with seasonal values

provided in EPA (2008). The selected β value was 4.0, the suggested summer-time value for bare rock/sand/clay in an arid region under average soil moisture conditions. Despite soil moisture measurements from pen and road surfaces revealing dry conditions at the sample locations, the deposition of urine to pen surfaces by cattle and the presence of the LMS were used as justification for selecting the suggested value for average soil moisture conditions. The suggested noon-time α value of 0.20 for bare rock/sand/clay in an arid region was used in this study.

Faulkner et al. (2008) found that maximum C_{sim} as predicted by AERMOD from a ground level area source were sensitive to, among other input parameters, α and z_0 but it was not sensitive to β . The lack of sensitivity to β was theorized to be due to the dominance of mechanical mixing in the planetary boundary layer in their application. Based on these findings, the sensitivity of C_{sim} and the resulting Q_{meas} estimates in this inverse modeling application to variations in α and β was investigated. The sensitivity to z_0 was not tested as it was calculated from measured data. Summer α values selected were 0.18, the suggested value for fallow fields and supported by Hansen (1993) for light colored, dry soil such as that in fields surrounding the dairy, and 0.25, the suggested value for shrublands in an arid region. Two summer values for β were selected as 1.5, suggested for both wet conditions in a bare rock/sand/clay surface in an arid region and for fallow fields under dry conditions, and 6.0 for dry conditions in a bare rock/sand/clay surface in an arid region (EPA, 2008).

Four consecutive passive sampler measurement periods, two morning and two afternoon, were selected for the comparison. Changes in C_{sim} and Q_{meas} were calculated as a percentage of C_{sim} and Q_{meas} calculated at the base case of $\alpha = 0.20$, $\beta = 4.0$. Values of C_{sim} at all downwind sites varied between -3% and +5% from the base case, though most were within $\pm 1\%$. Estimates of Q_{meas} under the different values of α and β varied most for the LMS (-6% to +4%), while the changes in pen and combined EFs estimates were about equal at -2% to +1%. Values of C_{sim} increased, resulting in decreased Q_{meas} estimates, with increasing α at constant values of β . Holding α constant while increasing β had the opposite effect, leading to lower C_{sim} values, and thus higher Q_{meas} estimates. Therefore, in the case of this dairy and sampling layout, neither the C_{sim} nor the Q_{meas} estimated through inverse modeling with AERMOD were sensitive to the selected ranges of α and β .

AERMOD requires the source type, size, location, and emission rate be specified, as well as sampler/receptor locations. The pens, settling basin, and holding pond were specified as ground level area sources with areal extents equal to their respective dimensions and with an initial plume height of 0 m. The vertices of the sources and the receptor locations were taken from multiple hand-held GPS measurements made during the study and available satellite imagery. Pens not occupied by cattle were not included in the model; for example, only the quarter of the northern-most group of pens that was occupied by steers was specified as an active source.

Note that the value of the $(C/Q)_{sim}$ ratio in Equation 5-3 is the same across all ranges of Q_{sim} when using a model with a proportionally linear response in C_{sim} to changes in Q_{sim} ; this also applies to the ratio of each source/receptor pairing in Equation 5-4. This means that the ratio describes the slope of a straight-line relationship without local maxima or minima and eliminates the dependency of the results on the input Q_{sim} values. However, the method used to determine the initial Q_{sim} values for each source i for this study is important to note as it was integrated into the optimization procedure. An initial estimate of the pen EF (f) of $1.5 \text{ mg animal}^{-1} \text{ s}^{-1}$, the yearly average NH_3 EF reported for an open lot dairy by Leytem et al. (2011), was combined with animal occupancy (m , number of cattle) and area (A , m^2) as shown in Equation 5-6 to calculate $Q_{sim,i}$ values ($\text{g s}^{-1} \text{ m}^{-2}$) for the pens:

$$Q_{sim,i} = \frac{fm_i}{A_i} \quad (5-6)$$

The emission rates of the solids settling basin and the holding pond were assumed to be equal and given an initial value of $0.1 \text{ mg m}^{-2} \text{ s}^{-1}$, an average of the lower and upper ranges reported by Rumburg et al. (2008b). The initial estimates of Q_{sim} for each source were supplied to AERMOD, which was then run for each sample period. Calculated hourly C_{sim} values were averaged over a sample period, for instance from 12 noon until 12 midnight to correspond with a p.m. passive sample period, for comparison with C_{meas} .

The presence of the trailer on the downwind side of the dairy may have affected measurements at that location due to flow disruption. However, the potential effects on

dispersion and nearby concentrations could not be modeled within AERMOD because the software does not allow the modeling of building effects with area sources. In addition, NH_3 is known to deposit readily to most surfaces. Deposition likely occurred during this study, to some degree, in the short distance between the sources and measurement locations and resulted in lower C_{meas} than if some NH_3 had not deposited. However, deposition was neither measured nor simulated in this study. As a lower C_{meas} results in a lower Q_{meas} , any depositional loss occurring between the source and the measurement location that is not accounted for in emissions calculations would lead to estimated EFs and ERs being lower than the actual values. In such cases, the calculated EFs and ERs should be considered as effective ERs and EFs.

A total of 10 active sources were specified in the model. A sufficient number of downwind passive sampler measurements existed to calculate an emission rate for each individual source, but a maximum of six downwind OP-FTIR measurement paths yielded an under-determined system. Simplification of the system was performed and reduced the total number of emission rates solved for in the system to two based on the following: 1) as the solids settling basin and the holding pond Q_{sim} were assumed to be equal, the change in C_{sim} at a given location resulting from the entire LMS was assumed to be linear compared to the change in the sum of the LMS emissions per area per unit time ($Q_{sim,LMS}$); and 2) as m and A in Equation 5-6 are constants for a given pen source i , leaving only changes in f to change $Q_{sim,i}$, and the same value of f was applied to each pen, a linear change in C_{sim} resulting from all the pens at a given location to a change in

the sum of the pen $Q_{sim,i}$ per unit area per unit time was assumed. Both assumptions were verified to be true through modeling with different f and $Q_{sim,LMS}$ values.

Therefore, the system of linear algebra equations used to estimate the dairy NH_3 ERs was designed to solve for f_{meas} and $Q_{meas,LMS}$, yielding an over-determined system for both passive and OP-FTIR sampling configurations. The optimization method employed to solve these systems was a least sum of squares of residuals comparing C_{sim} and C_{meas} . Reported EFs on a per animal basis were calculated for the LMS by relating the estimated ERs to the number of contributing animals, which was assumed to be limited to those in the milking cow pens due to the lack of feed lane flushing in other pens. The EF per animal for those in the milking cow pens was calculated as the sum of the pen EF and the LMS EF. The average NH_3 EF across the facility was calculated as a weighted average of the pen EF and the summed EF for cattle in the milking cow pens, with weights assigned based on the number of cattle in the two categories. In addition, the overall study average EFs were calculated as weighted averages according to the number of EF estimates during each sample period time throughout a day. For example, the reported OP-FTIR based averages represent the sum of the estimated emissions over a 24 h period using the average EFs for each 2 h block.

Results and Discussion

The measurement campaign began at 12:00 noon Pacific Standard Time (PST) on 13 June 2008, and ended at 00:00 h PST on 21 June 2008. A total of thirteen sample

periods, approximately 12 h each, were conducted using the passive samplers, with all previous samples being collected and the next samples being deployed within 30 min of 00:00 h and 12:00 noon PST. The upwind OP-FTIR unit operated nearly continuously from 14 June 04:20 h to 19 June 08:30 h. Data were collected by the downwind OP-FTIR unit from 13 June 13:30 h to 21 June 00:00 h, operating for 118.9 h out of 178.5 total hours (66.6%).

Meteorological conditions throughout the field study were hot and dry, with diurnally consistent wind patterns. Low wind speeds with highly variable direction were recorded each morning shortly before sunrise. The wind speed at 6.2 m agl from 05:00-06:00 h varied between 0.6-1.5 m s⁻¹ with a campaign average \pm 1 SD of 1.1 \pm 0.2 m s⁻¹. The SD is reported in this paper for all measurements unless otherwise noted to show the variability in the reported values. During the remainder of the day winds came from the northwest. Figure 5-2 shows the dominance of winds from the northwest sector throughout the study, accounting for 74% of recorded values. Cloud cover was either absent or extremely light and at high altitudes throughout with no recorded precipitation events. Samples of the soil on unpaved roads and in dry-lot pens were collected on 16 June and analyzed for percent moisture, resulting in averages of 0.56% \pm 0.50% ($n = 3$) and 5.3% \pm 5.1% ($n = 7$) for the unpaved roads and pens, respectively.

Campaign average meteorological conditions measured on-site are presented in Table 5-3, as well as average conditions measured at the Stratford CIMIS site during the study period, for all of June 2008, and for the month of June from 1998-2007. Average

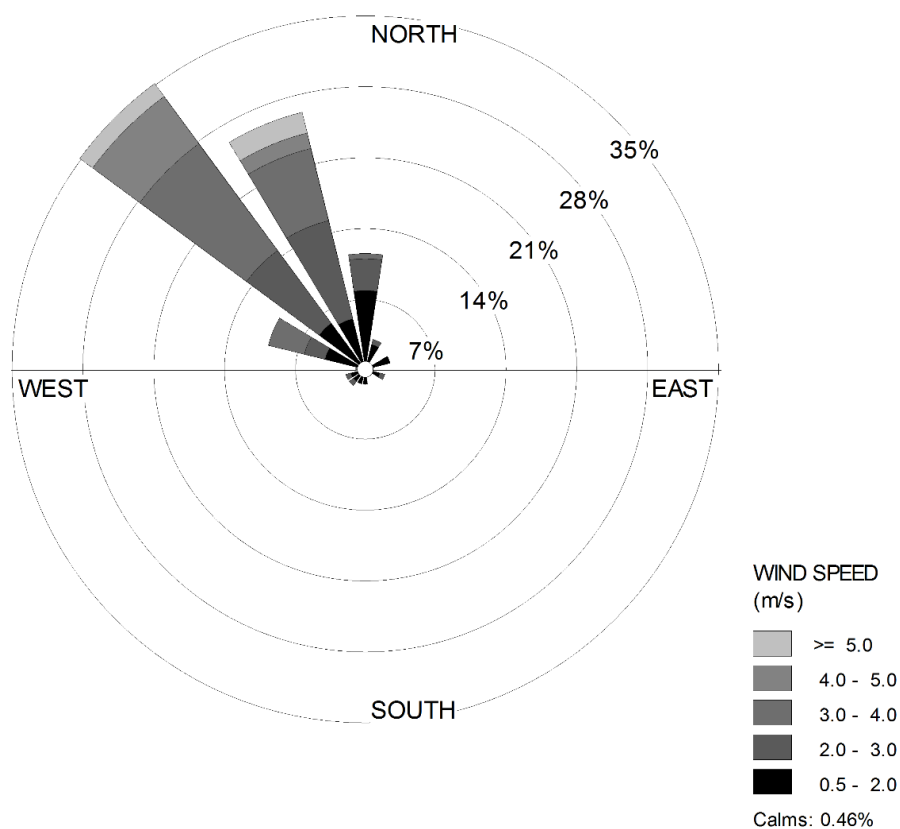


Figure 5-2. Hourly average wind conditions measured at the dairy during the measurement periods, 13-20 June 2008.

Table 5-3. Comparison of average meteorological conditions (± 1 SD) measured at the dairy from 13-20 June 2008 and at a site in Kings County for the same period, the full month of June 2008, and June from 1998-2007.

	On-site 13-20 June 2008	Off-site 13-20 June 2008	Off-site June 2008	Off-site June of 1998-2007
Temperature (C)	26.5 \pm 6.7	26.7 \pm 7.4	24.8 \pm 7.2	24.2 \pm 6.7
Relative Humidity (%)	41 \pm 18	30 \pm 16	33 \pm 17	45 \pm 18
Wind Speed (m/s)	2.4 \pm 1.1	2.9 \pm 1.2	3.2 \pm 1.7	2.8 \pm 1.3
Wind Direction ($^{\circ}$)	325 \pm 42	326 \pm 42	329 \pm 42	330 \pm 45
Total Precipitation (mm)	0.0	0.0	0.3	16.2

conditions on-site were indistinguishable from those measured at Stratford for

temperature, wind direction, and precipitation; wind speeds were slightly lower and

relative humidity values were higher at the dairy, with little difference between upwind (data not shown) and downwind measurements. Comparison of the study period conditions at Stratford with the remainder of the month and during previous years reveals this period was slightly warmer and drier than monthly averages, but with similar wind conditions. June 2008 was similar to past years in temperature and wind direction, with slightly higher average wind speeds and lower relative humidity values. It should be noted that the total precipitation in each column is a summation of all data considered and that the sum of 16.2 mm comes from three recorded events from 1998-2007 during the month of June and is strongly driven by a single event totaling 14.0 mm.

Concentration Measurements

A total of 298 samples were successfully collected upwind, downwind, and within the dairy using the passive samplers deployed at 23 locations. The average upwind concentration was 84.5 ± 19.2 ppbv ($57.4 \pm 13.4 \mu\text{g m}^{-3}$, $n = 86$) with a range of 52.9 to 128.3 ppbv. Concentrations measured downwind varied much more, with a range of 69.3 to 1879.2 ppbv and an average of 412.4 ± 281.1 ppbv ($280.0 \pm 188.6 \mu\text{g m}^{-3}$, $n = 209$). No passive samples exceeded the 12.1 μg collected NH_3 threshold, after which the collection efficiency becomes non-linear. There was a significant difference in NH_3 concentrations measured between morning (sampled from roughly 0:00 h to 12:00 noon) and afternoon (sampled from roughly 12:00 noon to 0:00 h) periods. Average morning levels were 99.3 ± 16.5 ppbv ($n=25$) at upwind sites and 308.5 ± 181.0 ppbv

($n=89$) at downwind sites. Afternoon concentrations averaged 78.7 ± 16.9 ppbv ($n=60$) and 489.4 ± 315.3 ppbv ($n=120$) at upwind and downwind locations, respectively. The highest concentrations in each period were measured between the holding pond and the young heifer pens and downwind of the milking cow pens. These concentrations were in the range of values reported by Cassel et al. (2005), Bjorneberg et al. (2009), and Leytem et al. (2009) at open lot dairies in California and Idaho.

Ammonia concentrations recorded by the OP-FTIR units were more frequent than the passive sampler measurements, thus providing more information about the diurnal pattern and temporal variation in concentrations. However, these values are volumetrically averaged concentrations across the beam area (diameter ≈ 0.3 m) and along the length of the beam path (140 to 290 m, depending on pointing position). Thus, the OP-FTIR units provide less spatial information than the passive samplers. Figure 5-3 presents a five-day time series of data collected at 2 to 2.5 m agl along five different beam paths (see Figure 5-1 for beam path locations). Reported levels of NH_3 are in the same range as those calculated from passive sampler measurements, as well as measurements given in literature from dairies with similar housing and manure management systems (Cassel et al., 2005; Bjorneberg et al., 2009; Leytem et al., 2009). Note that the highest NH_3 concentrations throughout the period were detected to the east of the centrally-located downwind OP-FTIR unit, which is immediately downwind of both the LMS area and milking cow pens. Additionally, the highest concentrations detected downwind of the dairy were recorded in the evening and shortly after

midnight while the lowest NH_3 levels were measured from dawn until at mid-day. Sharp increases and decreases in NH_3 levels at the upwind beam path correspond with the 05:00-06:00 h periods of light winds of variable direction discussed previously.

The concentrations reported at upwind sites from both measurement methodologies are high for ambient levels not immediately adjacent to a source, which is indicative of the size and density of NH_3 sources in the region. Kings County, the county in which this dairy is located, and Fresno County, the county north and northwest of Kings County, had a combined 2007 animal population (with animal density given in parenthesis) of 789,612 cattle (41.1 km^{-2}), including 278,368 milk cows

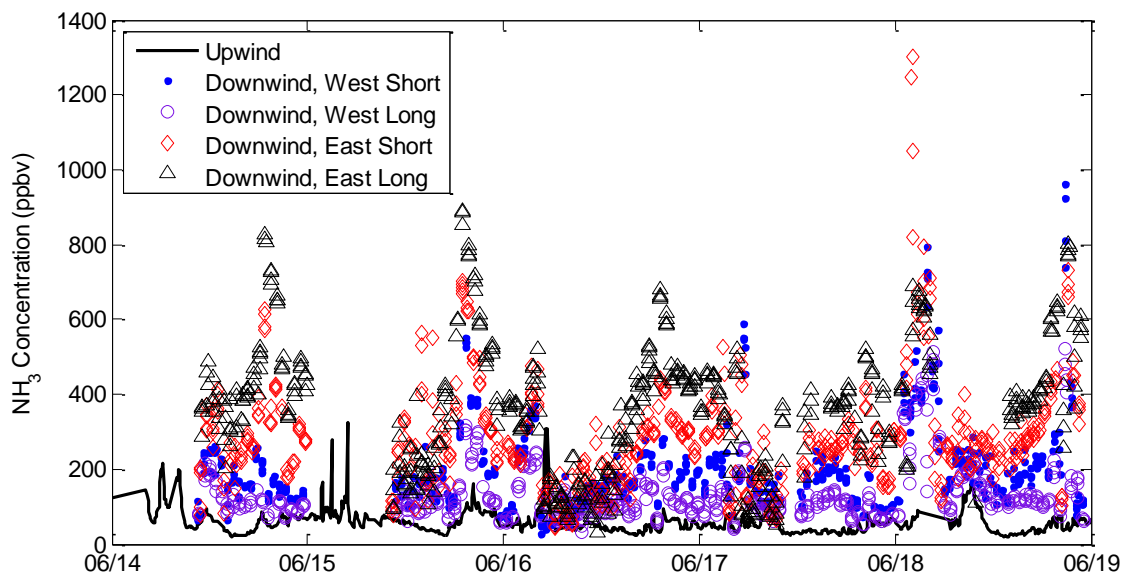


Figure 5-3. NH_3 concentration (ppbv) measured by both the upwind and downwind OP-FTIR instruments at $\sim 2\text{m}$ agl. Downwind beam paths are described by the direction from the monostatic unit to the retroreflector and the relative distance to the retroreflector.

(14.5 km²) and 26,999 beef cows (1.4 km²); 9,809 hogs (0.5 km²); and 89,860,417 broiler chickens, all in Fresno County (4,682.9 km²) (USDA, 2009). Battye et al. (2003) provided a summary of three NH₃ emissions inventories for the Fresno County area, all of which estimated livestock's contribution at 50 to 75% of the total emissions, which ranged from 71,000 to 99,000 Mg yr⁻¹. Winter time background NH₃ measurements in the San Joaquin Valley of California ranged from 16 to 96 µg m⁻³ (Cassel et al., 2005). Robarge et al. (2002) reported a summer average NH₃ concentration of 10.5 µg m⁻³ from measurements taken in the agriculture-rich Inner Coastal Plain of North Carolina. Walker et al. (2004) summarized literature values collected in agricultural, non-agricultural, and urban land use settings from 11 studies, with average concentrations ranging from 0.02 µg m⁻³ at high elevation during summer to 10.48 µg m⁻³ during fall at a swine facility. Moore (2007) reported winter and summer average concentrations throughout the Cache Valley, a heavily agricultural valley along the Utah/Idaho border with significant dairy cattle and layer hen populations, of 28.8 and 24.7 µg m⁻³. Leytem et al. (2009) reported background NH₃ levels ranging from 10 to 60 µg m⁻³ in another area of Idaho with a high dairy density.

On a path-by-path comparison, passive sampler NH₃ levels were higher than OP-FTIR measurements by an average of 1.38 ± 0.15 ($n=50$). One possible explanation for the difference between the reported concentrations in the passive and OP-FTIR datasets is the difference in methodology. Another possible cause is the effectiveness of a limited number of discrete sampling points to represent a concentration field in close proximity

to strong sources, which is somewhat related to the first possible explanation. To conduct these comparisons, the two to four passive samplers located along each OP-FTIR beam path were used to calculate the path length average passive sampler concentration, and OP-FTIR measurements were averaged over the passive sampler deployment time to calculate the period average OP-FTIR concentration. The sample heights of the passive samplers were set as close to the height of the OP-FTIR beam path as possible, although some were up to 1 m lower. The crosswind scale of the source in relation to the distance between sampling points, as well as the distance from the source to the sampling points, could have significant impacts on how representative the measured concentration field derived from a few sample points is compared to the actual concentration field. While the spatial scales of most of the sources on the dairy are large compared to the distances between samplers, the homogeneity of the emissions from the pen and LMS surfaces may vary significantly on scales smaller than the distance between sampling points and create emissions hotspots. The result is a non-uniform concentration profile across the plume that may or may not be effectively sampled by the point samplers. The path-integrated sample of the OP-FTIR has the advantage in that it can sample the entire width of the plume, but spatial information available from an adequate number of point sensors is sacrificed.

Going et al. (2008) found that passive sampler measurements were on average 55% greater than OP-FTIR measurements when the passive samplers were deployed as directed by the manufacturer. Meng et al. (2011) compared seven-day NH_3

concentration averages reported by Ogawa passive samplers and an active NO_x/NH_3 analyzer and found a strong correlation, yielding a linear fit slope of 1.21 with the active analyzer as the independent variable and the passive sampler as the dependent variable. Puchalski et al. (2011) compared two and three week long average NH_3 concentrations from Ogawa passive samplers against other passive samplers and an active analyzer over a 0.5 to 9.0 $\mu\text{g m}^{-3}$ range and found that the Ogawa sampler reported values not statistically different from the other passive samplers in one study and 36% lower than the active sampler in another study.

Estimated Emissions

The ERs and EFs for this study were estimated through inverse modeling. Screening of the datasets to identify periods in which the wind direction was outside of the optimal range of -70 to $+50^\circ$ from North yielded a total of 12 hours (8%) during 5 of the 13 passive sampler deployment periods. One period, June 14 a.m. had six hourly average wind direction values outside the optimal range; the remaining four periods had 1 to 2 hours each. The June 14 a.m. period was removed from ER and EF calculations, while the other four passive sampler periods were not removed due to the limited amount of time in each period that the sites were not impacted by the dairy and the ability of the model to simulate the effects of these non-ideal wind directions on period average concentrations.

The C_{meas} values calculated for the two locations between the young heifer pens and the holding pond, the locations with the largest reported concentration values during all sample periods, were excluded from emissions estimation calculations because of doubt that they were only influenced by the pens. It is hypothesized that the feed lane fencing on the south side of the pen immediately upwind likely presented a flow disturbance sufficient to allow some of the holding pond plume to be circulated in the upwind direction. The samplers were located within a few meters of the northern edge of the holding pond and had a sample height of 1 m. Removal of these two points resulted in EF estimates with better fits to the remaining C_{meas} data.

There were 78 potential OP-FTIR sample periods during the field study based on 2 h averages. Irregularities with instrument operation, alignment, and retroreflector cleanliness reduced the number of periods with valid data from two or more downwind beam paths to 48, or 62%. Of these, six were removed due to wind directions outside of the optimal range, yielding a total of 42 sample periods from which to calculate ERs and EFs. These irregularities and non-optimal wind directions disproportionately affected the morning blocks (00:00 h through 12:00 noon), which had only two or three valid datasets in most 2 h blocks for ER and EF calculations, about half as many as in the afternoon. This likely contributed to the greater RSD in the average emissions from the pens and the entire facility for morning blocks when compared to the afternoon blocks. As previously mentioned, light and variable winds were observed each day during 05:00-06:00 h, resulting in no valid data points for the block ending at 06:00 h. To provide an

emissions estimate for this period, a gap filling technique was used based on the average of the 04:00 h and 08:00 h blocks.

The unconstrained least squares optimization method initially used in estimating ERs and EFs generally performed well, but it yielded negative emissions from either the pens or the LMS in a few instances. This phenomenon was neither observed in measured data nor is it considered to be real. It is instead assumed to be an artifact of the optimization method. Flesch et al. (2009b) suggests setting a minimum ER value in such cases. This recommendation was applied to our emissions calculations, using a minimum pen f_{meas} value of $0.5 \text{ g d}^{-1} \text{ animal}^{-1}$ and a minimum $Q_{meas,LMS}$ value of $0.5 \text{ mg m}^{-2} \text{ d}^{-1}$, which were estimated from minimum values shown in Leytem et al. (2011), an NH_3 and greenhouse gas emissions study conducted at an open lot dairy.

Flesch et al. (2009b) also suggests designing sampling layouts for multiple sources in such a way that each measurement location is impacted by only one source. If that ideal situation is not possible, as in the case of this dairy, and assuming at least the same number of measurements as sources, they suggest that the measurement sites be located such that the first site be impacted by only one source, the second site by the first source plus the second source, the third site by the first, second, and third sources, and so on. Emissions can then be estimated in a progressive manner. This sequential ER estimation methodology was applied to the passive sampler dataset. Some sites were impacted only by pens, while others were impacted by both pens and the LMS, allowing first the pen f_{meas} and then the $Q_{meas,LMS}$ to be calculated.

Determination of the sources impacting a given sample was made based on the range of hourly average wind directions measured during the sample period. The number of sites used to estimate the pen f_{meas} ranged from 3 to 7, while 6 to 13 sites were used to estimate $Q_{meas,LMS}$. This sequential method was not applied to the OP-FTIR dataset because the downwind OP-FTIR unit in the center of the configuration was rarely not downwind of the LMS, resulting in all beam paths being impacted by both the pens and the LMS most of the time.

Another important point discussed by Flesch et al. (2009b) concerns the matrix conditioning number (κ), which is a measure of the sensitivity of the estimated Q_{meas} vector in Equation 5-4 to changes in the $(C/Q)_{sim}$ ratios. If a change in Q_{meas} is proportional to the change in a $(C/Q)_{sim}$ value, the system is referred to as well-conditioned and has a low κ value (minimum $\kappa = 1.0$). A system is said to be ill-conditioned if a large change in Q_{meas} is found from a small change in $(C/Q)_{sim}$, which would result in a large κ value. The value of κ also is related to the relative error in estimates of Q_{meas} . The reader is referred to Flesch et al. (2009b) for an in depth discussion with examples. An important conclusion was that accurate emissions estimates in controlled release experiments with various source/receptor configurations were strongly dependent on κ . Good ensemble averaged estimates of the total amount released were calculated for $(C/Q)_{sim}$ matrices with κ values less than 50 and good estimates of the individual source contributions were found for matrices with κ values less than 10-20. Values of κ calculated for the matrices in this dairy emissions study

based on passive sampler data ranged from 1.5 to 2.7, suggesting good confidence in the emissions estimates. Values of κ calculated for matrices based on OP-FTIR data ranged from 4.5 to 25.6, again suggesting good confidence in the emissions estimates.

The averages, SDs, minimums, and maximums of the EFs calculated using the three optimization methods discussed above for both datasets are presented in Table 5-4. Average EF values estimated from the passive dataset for the unconstrained and constrained values were very similar, but greater differences were found between methodologies in the EF values based on OP-FTIR data. All reported statistics for the pen and whole facility EFs predicted by the progressive methodology based on passive sampler data were lower than for the other two methods; average estimated LMS EFs were higher for the progressive method and had a greater range in individual values. Average EFs based on OP-FTIR data for the pens, LMS, and the whole facility were higher than those based on passive sampler data and had a wider range between minimum and maximum values. One factor likely contributing to the larger range between maximum and minimum values based on OP-FTIR data is the greater temporal resolution in the OP-FTIR dataset, 2 h averages versus 12 h averages for passive samplers, allowing it to show greater diurnal variation in estimated EFs with smaller minimum values and larger maximum values that are smoothed out in the passive sampler EFs.

As previously stated, negative EFs were calculated from both passive sampler and OP-FTIR data using the unconstrained methodology. Negative EFs values are not

Table 5-4. Statistics of emission factors (EFs) calculated for both NH₃ measurement datasets using the following three optimization procedures: Unconstrained – EF values for pen and liquid manure system (LMS) are unconstrained; Constrained – constraints are imposed on the minimum values for pen and LMS EFs, based on minimum values found in literature; and Sequential – pen EF estimated first from samples impacted only by pens, then the LMS EF is estimated from samples impacted by both pens and LMS.

	Pen EF ^[a] (g d ⁻¹ animal ⁻¹)				LMS EF (g d ⁻¹ animal ⁻¹)				Facility EF (g d ⁻¹ animal ⁻¹)			
	Avg	SD	Min	Max	Avg	SD	Min	Max	Avg	SD	Min	Max
<i>Passive Sampler Data</i>												
Unconstrained	134	41.		313.	12.				140.	42.		324.
	.2	4	32.5	0	7	9.9	-3.6	63.1	7	5	33.4	2
Constrained ^[b]	133	41.		313.	13.				140.	42.		324.
	.3	5	30.1	0	6	9.9	0.0	63.1	2	6	30.1	2
Sequential							-					
	106	25.		230.	18.	14.	12.		116.	26.		251.
	.4	5	8.4	8	8	5	1	85.7	1	6	13.2	2
<i>OP-FTIR Data</i>												
Unconstrained	158	37.	-	661.	53.	23.	-	521.	186.	28.	-	661.
	.7	6	213.	4	3	1	40.	2	0	7	109.	6
			7				2				4	
Constrained ^[b]	177	27.	0.5	661.	41.	17.	0.0	455.	199.	21.	8.4	661.
	.8	3	5	5	6	7	7	7	2	9		6
Sequential	NA	NA	NA	NA	NA	NA	NA	NA	NA	NA	NA	NA

^[a] EF = emission factor, Avg = average, SD = standard deviation, Min = minimum, Max = maximum, NA = not applicable.

^[b] Optimization methodology selected as yielding the best EF estimates from this facility

considered to be real and are assumed to be an artifact of the optimization method.

Therefore, the EFs estimated through the constrained methodology were considered to be better estimates despite having imposed minimum values, a conclusion supported by the findings of Flesch et al., 2009b. Surprisingly, negative LMS EF values were also given by the progressive methodology based on passive sampler data. These results may suggest shortcomings in this inverse modeling procedure, including the following: 1) the assumption of homogenous source strength across a pen or liquid surface is not valid for this case; 2) the assumption of equal emissions per animal is not valid for this case; 3)

the combined dairy and sample layout employed in this study are not conducive to estimating NH_3 emissions from individual components; or 4) another factor not accounted for in this analysis influenced NH_3 emissions. The first assumption is required without prior knowledge of the magnitude and spatial patterns of the inhomogeneity. The second assumption is also required as this study seeks to determine emissions from the entire facility and it is impractical to examine emissions from individual cattle. The third shortcoming may have merit, though the low calculated κ values suggest the systems of linear algebraic equations are, for the most part, very well-conditioned and should yield good estimates of the total and individual source emissions. It is likely that not all factors affecting NH_3 emissions are accounted for in this analysis as there are many factors that contribute (e.g., Arogo et al., 2006 and Rumburg et al., 2008a, 2008b). Future NH_3 emissions experiments should be designed to account for as many factors as feasibly possible.

The negative results for individual components may cast doubt on the ability of the present modeled scenario to quantify the emissions from individual sources. However, as shown by Flesch et al. (2009b), application of a minimum EF limit can significantly improve the ER estimation of individual components. In addition, the ER of the facility as a whole can be estimated well even when negative ERs are calculated for individual components. Therefore, the optimization methodology selected to best represent the actual EFs from the individual components and from the dairy as a whole was the constrained methodology. This resulted in an estimated summer time total

facility NH_3 emission of $265.2 \pm 80.2 \text{ kg d}^{-1}$ and an average EF of $140.7 \pm 42.5 \text{ g d}^{-1}$ animal⁻¹ based on the passive sampler dataset. Calculated values based on the OP-FTIR dataset were 40% higher with a total facility emission of $375.4 \pm 27.1 \text{ kg d}^{-1}$ and an EF of $199.2 \pm 21.9 \text{ g d}^{-1}$ animal⁻¹. These EF values are listed in Table 5-5, along with EF values reported in other dairy NH_3 emissions studies. The type of facility, geographical location, methodology used to estimate EFs, and season of the year and ambient temperatures in which measurements were made are also provided to allow for comparison between the different housing, climate, and manure storage and treatment conditions that may affect NH_3 EFs. Seasonal EFs, specifically summer time EFs, are provided where available for comparison against the values derived from the limited summer time dataset herein described.

The summer time facility EFs calculated for this dairy based on data collected over seven days are near the top of the range of EFs found in the literature, which spans 2 orders of magnitude, but within the range of values reported for facilities with open lot pens and holding pond configurations (Mukhtar et al., 2008; Bjorneberg et al., 2009; Leytem et al., 2011). Specifically, the summer EFs derived herein are close to the summer EFs reported by Bjorneberg et al. (2009) and Leytem et al. (2011) from open lot dairies, but generally higher than summer EFs reported for other housing and manure management configurations. Not all studies found in the literature estimate emissions from the entire dairy facility (housing, exercise area, manure storage and treatment system) as was measured in this study, which is necessary in order to estimate

Table 5-5. Comparison of dairy NH₃ emission factors (EFs) estimated from this study with EFs reported in literature. When necessary, conversions between reported emissions units and those used in this table were made.

<i>Source</i>	<i>Facility Type Studied</i>	<i>Location</i>	<i>Methodology</i>	<i>Measurement Period</i>	<i>Average T_{Amb} (°C)^[a]</i>	<i>EF (g d⁻¹ animal⁻¹)</i>
Arogo et al., 2006	Literature review of published EFs (n=11)	Europe	Various	Average	--- ^[b]	22.7
				Minimum		18.0
				Maximum		28.5
Ngwabie et al., 2009	Free stall barn with manure gutter under a slatted floor	Sweden	Ventilation rate (barn only)	Winter and Spring	1 to 16	29
Schrade et al., 2012	6 with similar facilities: barn and outdoor exercise area	Switzerland	Tracer method (barn and outdoor exercise areas only)	Range of annual values	---	28.9 to 32.6
Schmidt et al., 2002	Free stall barn	Minnesota, U.S.	Ventilation rate (barn only)	Winter Summer	-1.8 14	4.2 9.1
Cassel et al., 2005	Open lots with free stall and lagoon	California, U.S.	Micrometeorological integrated horizontal flux	Winter	8 to 15	50
	Free stall barn with corrals and open lots with lagoon				7 to 18	103
Moore, 2007	Free stall barn and open pens with covered free stall with lagoon	Utah, U.S.	Inverse modeling (ISCST3) with passive sampler measurements	Late Fall	1.0	193.0

Table 5-5 (continued)

<i>Source</i>	<i>Facility Type Studied</i>	<i>Location</i>	<i>Methodology</i>	<i>Measurement Period</i>	<i>Average T_{Amb} (°C)^[a]</i>	<i>EF (g d⁻¹ animal⁻¹)</i>
	Mixed concrete and soil surface pens with partial covers and straw bedding	Utah, U.S.			1.0	235.0
Mukhtar et al., 2008	Open lots with lagoon	Texas, U.S.	Flux chamber	Winter	6 to 11.6 ^[c]	17.0
				Summer	27 to 33.7	31.8
				Annual	---	25.8
Rumburg et al., 2008a	Free stall barn only	Washington, U.S.	Nitrogen balance model verified with Summer remote sensor measurements	Annual simulation	---	109.6
Rumburg et al., 2008b	Anaerobic lagoon only	Same dairy	Nitrogen balance model verified with Summer remote sensor measurements	Annual simulation	---	150.7
			<i>Sum of Rumburg et al., 2008a and 2008b</i>			260.3
Bjorneberg et al. 2009	Open lot pens with lagoon and composting	Idaho, U.S.	Inverse modeling (WindTrax) with remote sensor measurements	Winter	-8.3 to 9.3	40
				Spring	-1.3 to 15.5	250
				Summer	7.7 to 43.3	190
				Fall	0.8 to 25.9	150
				Annual	---	156
Bluteau et al., 2009	Tie-stall barn	Quebec, Canada	Ventilation rate (barn only)	Winter	nd ^[b]	5.5
	Tie-stall barn			Summer	nd	14.3

Table 5-5 (continued)

<i>Source</i>	<i>Facility Type Studied</i>	<i>Location</i>	<i>Methodology</i>	<i>Measurement Period</i>	<i>Average T_{Amb} ($^{\circ}C$)^[a]</i>	<i>EF ($g\ d^{-1}\ animal^{-1}$)</i>
Flesch et al., 2009a	Free stall barn with lagoon	Wisconsin, U.S.	Inverse modeling (WindTrax) with remote sensor measurements	Annual	---	54.8
				Summer	17.5 to 19.7 ^[c]	93
				Annual	---	52.1
Flesch et al., 2009a	Free stall barn with lagoon	Wisconsin, U.S.	Inverse modeling (WindTrax) with remote sensor measurements	Summer	21.2 to 22.0	93
				Annual	---	54.8
				Summer	20.2	100
Adviento-Borbe et al., 2010	Free stall barn	Pennsylvania, U.S.	Flux chamber (barn only)	Winter/Spring	nd	22.1
				Summer/Fall		35.5
Leytem et al., 2011	Open lot pens with lagoon and composting	Idaho, U.S.	Inverse modeling (WindTrax) with remote sensor measurements	Winter	-4.0 to 4.8	136
				Spring	5.0 to 20.6	157
				Summer	20.8 to 24.4	146
				Fall	8.4 to 15.3	162
				Annual	---	150
Leytem et al., 2013	Free stall barn with exercise lots, anaerobic digester, and lagoons	Idaho, U.S.	Inverse modeling (WindTrax) with point and remote sensor measurements	Winter	-8.3 to -1.4 ^[c]	27
				Spring	8.2 to 13.2	266
				Summer	16.1 to 23.8	332
				Fall	1.8 to 10.8	181
				Annual	---	201
<i>This study</i>	Open lot pens with lagoon	California, U.S.	Inverse modeling (AERMOD) with point and remote sensor measurements	Summer	26.5	<i>Passives</i> 141 <i>OP-FTIR</i> 199

^[a] Average ambient temperature (T_{amb}) or temperature range only given for seasonal measurement periods if provided by the source

^[b] nd = no data or insufficient data, --- = data not provided for annual periods

^[c] Ranges provided for all seasons represent the range of sample period average T_{amb} .

emissions for an entire facility. If this dairy's summer time emissions were calculated based on literature EFs from the U.S. that reported EFs for the entire facility without regard for housing, climate, and manure management system, it would range from 59.9 kg d⁻¹ (from Mukhtar et al., 2008) to 625.8 kg d⁻¹ (from Leytem et al., 2013). Note that Mukhtar et al. utilized a flux chamber, a methodology that yields results for the environment within the chamber and may not represent actual ambient conditions, as well as being susceptible to insufficient sampling of the high variability in urine and manure deposition, soil moisture, soil temperature, and other influential surface conditions such as typically found in an open lot dairy configuration.

Pen emissions estimated during this study accounted for 95% of the total emissions based on passive sampler data and 89% of the total based on OP-FTIR data. This result is supported by both C_{meas} datasets. Ammonia levels were consistently highest immediately downwind of the milking cow pen areas on the eastern side of the measurement layout and C_{meas} from sites downwind of the LMS were also impacted by the pen areas. As the optimization methods were designed to yield the best fit of C_{sim} to C_{meas} , this led to pen emissions accounting for a large portion of the facility's emissions. (C_{meas} values from between the young heifer pens and the holding pond were excluded from ER/EF calculations as previously described; however, if they were included the pens had a higher contribution to total emissions.) As stated previously, NH₃ emissions originate from N excreted in the manure and urine (Arogo et al., 2006). The dominance of the pens in total NH₃ emissions may be explained by reviewing where manure and

urine are deposited and stored in this open lot system. Feces from about half of the cattle on the facility, basically all but the milk cows, remain in the pen for up to one year and do not enter the LMS. Only the feed lanes in the milk cow pens and the milking parlor floors are flushed, which is a very small percentage of the potential feces deposition area in the milking cow pen area. In addition, the feed lanes are not shaded, which may affect cattle behavior by decreasing time spent in the feed lane eating and increasing time spent in the shade on the open lot area of the pen, especially during the summer. Direct solar radiation on the feed lane increases available energy at the surface and likely increases emissions from deposited feces. Furthermore, intermittent flushing throughout the day allows for the accumulation of feces in the feed lane and may provide sufficient time for a significant portion of the N in the urine to volatilize as NH_3 before being flushed into the LMS (Arogo et al., 2006).

Bjorneberg et al. (2009) and Leytem et al. (2011) also found that pen areas produced most of the NH_3 emissions on dairies with open lots and holding ponds, with summer contributions of 88% and 70%, respectively. However, Rumburg et al. (2008a, 2008b), Flesch et al. (2009a), and Leytem et al. (2013) found that summer emissions were generally dominated by the LMS for dairy systems using barns and holding ponds/treatment lagoons and, in the case of Leytem et al. (2013), an anaerobic digester. The difference in the manure management between the dairy systems would help explain the difference in dominant sources between these groups. Manure is usually

stored in the open lot pens, with removal occurring once or twice yearly, while manure is generally removed daily from the barns and stored or treated elsewhere.

The LMS ERs estimated from this dairy averaged $1.7 \pm 1.3 \text{ g d}^{-1} \text{ m}^{-2}$ and $5.5 \pm 2.3 \text{ g d}^{-1} \text{ m}^{-2}$ based on the passive sampler and OP-FTIR datasets, respectively, as calculated from the daily total emissions. Both calculated ERs are within the range of values found for dairy lagoons in literature. Mukhtar et al. (2008) measured a summer average ER of $0.45 \text{ g d}^{-1} \text{ m}^{-2}$ and a winter average of $0.03 \text{ g d}^{-1} \text{ m}^{-2}$. The range of NH_3 ERs for an anaerobic dairy lagoon reported by Rumburg et al. (2008b) was from $2.6 \text{ g d}^{-1} \text{ m}^{-2}$ to $13.0 \text{ g d}^{-1} \text{ m}^{-2}$. Flesch et al. (2009a) measured no emissions from lagoons that were frozen over during winter and reported a range of $2.3 \text{ g d}^{-1} \text{ m}^{-2}$ to $8.7 \text{ g d}^{-1} \text{ m}^{-2}$ during summer and fall. Moore (2007) calculated ERs for two holding ponds in series during late fall to be $4.1 \text{ g d}^{-1} \text{ m}^{-2}$ and $1.3 \text{ g d}^{-1} \text{ m}^{-2}$ for the first and second ponds, respectively. An average emission of $8.8 \text{ g d}^{-1} \text{ m}^{-2}$ was reported by Sheffield and Louks (2006). Zhao et al. (2007) measured an average ER of $6.2 \text{ g d}^{-1} \text{ m}^{-2}$, a minimum of $0.5 \text{ g d}^{-1} \text{ m}^{-2}$, and a maximum of $15.1 \text{ g d}^{-1} \text{ m}^{-2}$ from measurements collected one day per month over 10 months.

Similar to NH_3 concentrations measured downwind of the dairy, a diurnal profile was evident in the estimated emissions from both datasets. Figure 5-4 shows the estimated emissions diurnal profile for the pens, the LMS, and the entire facility based on the OP-FTIR data. Note that no 2 h block periods ending at 06:00 h were available and the values shown in this figure for that time of day were calculated as the average

of the mean emissions values from the periods ending at 04:00 h and 08:00 h. Average calculated facility NH_3 emissions during early morning hours were 15 times lower than peak emissions in the late afternoon and early evening. LMS emissions peaked during mid-day and contributed a greater amount of the total hourly emissions during those hours relative to the rest of the day. Cassel et al. (2005), Flesch et al. (2009a), and Leytem et al. (2011, 2013) also reported diurnal NH_3 emissions patterns, but with peaks occurring during early afternoon and with emissions remaining high through the late afternoon and early evening. Bjorneberg et al. (2009) reported peak pen emissions during the evening in the spring and during late afternoon in the summer.

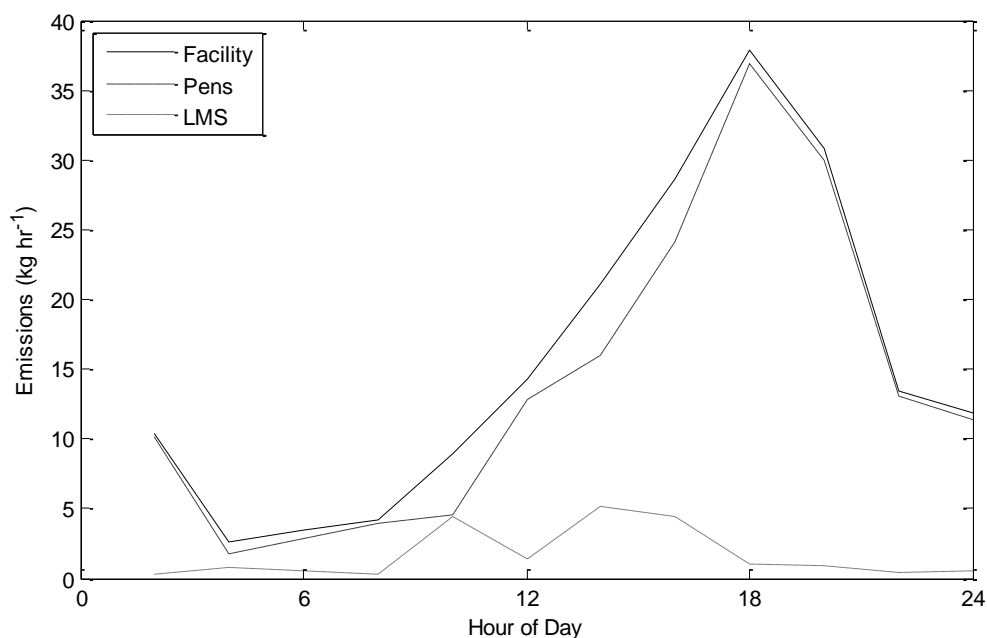


Figure 5-4. Estimated diurnal emissions profiles for the pens, liquid manure system (LMS), and the entire facility based on 2 h averaged OP-FTIR data.

Good temporal correlations were found between facility NH_3 emissions and 2 h block averaged ambient temperature ($r=0.65$) and wind speed ($r=0.63$), based on the Pearson correlation coefficient (r). The LMS emissions did not have significant correlations with temperature and wind speed, but it had a moderate correlation with incoming solar radiation ($r = 0.45$). As incoming solar radiation directly affects several surface and atmospheric properties, it is likely that this correlation exists because of solar radiation's effect on a property that more directly influences NH_3 volatilization but was not monitored, such as, for example, liquid surface temperature. Assuming that the emissions calculated for individual source types are representative, these results suggest different diurnal emissions cycles between the pens and LMS during this study. The temporal emissions patterns and correlations found at this dairy may or may not hold under different seasonal patterns – measurements at this dairy during other seasons are needed to investigate the applicability of these patterns and correlations throughout the year.

Air temperature and wind speed have been shown to be significant factors, among others, that affect NH_3 volatilization (Beauchamp et al., 1982; Sommer et al., 1991; Sommer et al., 2003; Cassel et al., 2005; Arogo et al., 2006). Temperature is also a factor in estimating volatilization based on Henry's Law. The demonstrated effect of temperature on NH_3 emissions raises the question of the representativeness of the EFs and total emissions calculated during this short period in June as representative for the summer period. Daily and weekly temperature averages and ranges during the months

of July and August may be higher than those measured during this study. However, the mean monthly average values reported by the CIMIS station near Stratford, California for July and August 1998-2007 for the average temperature, average daily maximum temperature, and average daily minimum temperature were each within 2° C of the corresponding statistical values calculated from on-site measurements made during this study. Therefore, the facility emissions and EFs herein presented are assumed to be representative of monthly average summer values.

Conclusions

Summer gaseous NH₃ concentrations were measured upwind, downwind, and within an open lot dairy over seven days using passive samplers and OP-FTIR units to estimate the facility's total emissions and EFs. These are the first reported summer time NH₃ emissions measurements for California, the state with the nation's largest dairy cattle population. Background NH₃ concentrations measured during this study were high relative to ambient concentrations found in the literature, suggesting the San Joaquin Valley is a very rich source area for NH₃ which is supported by agricultural livestock statistics reported in the 2007 Census of Agriculture (USDA, 2009). Emissions from both the pens and the LMS were estimated from both concentration datasets using inverse modeling with AERMOD and least squares optimization methods. Average emissions ± one SD for the entire facility were calculated as 140.7 ± 42.5 g d⁻¹ animal⁻¹ (113.5 ± 34.3 g d⁻¹ AU⁻¹) from the passive sampler data and 199.2 ± 22.0 g d⁻¹ animal⁻¹ (160.8 ± 17.8 g

$\text{d}^{-1} \text{AU}^{-1}$) from OP-FTIR data. The facility's calculated summer emissions were $265.2 \pm 80.2 \text{ kg d}^{-1}$ and $375.4 \pm 27.1 \text{ kg d}^{-1}$ based on EFs calculated from passive and OP-FTIR datasets, respectively. The pens were estimated to contribute 95% and 89% of the total facility emissions for the passive sampler and OP-FTIR based EFs, respectively. Derived EFs were within the range of EF values from U.S. dairies found in literature, a range which spans two orders of magnitude. Mean LMS ERs were $1.7 \pm 1.3 \text{ g d}^{-1} \text{ m}^{-2}$ based on passive sampler data and $5.5 \pm 2.3 \text{ g d}^{-1} \text{ m}^{-2}$ based on OP-FTIR data, which are within the range of literature values from other dairy lagoons and holding ponds. A strong diurnal cycle was observed in both concentrations and emissions datasets, with the highest values occurring in the late afternoon and evening. Calculated daily maximum emissions were 15 times greater than daily minimum values based on OP-FTIR data. Good correlations between facility emissions and temperature and wind speed were found with the 2 h block averaged OP-FTIR emissions data, while LMS emissions had a moderate correlation with incoming solar radiation.

Acknowledgments

This material is based upon work supported by the U.S. Department of Agriculture, Cooperative Agreement # 58-3625-9-743. Any opinions, findings, conclusions, or recommendations expressed in this publication are those of the authors and do not necessarily reflect the view of the U.S. Department of Agriculture. The authors thank the producers for their cooperation, the team involved in conducting the

field work, and the reviewers, whose feedback has greatly enhanced the quality of this manuscript. Mention of a trademark, proprietary product, or vendor is for information purposes only and does not constitute an endorsement by the U.S. Department of Agriculture, Utah State University, or Space Dynamics Laboratory.

References

- Adviento-Borbe, M.A.A., E.F. Wheeler, N.E. Brown, P.A. Topper, R.E. Graves, V.A. Ishler, and G.A. Varga. 2010. Ammonia and greenhouse gas flux from manure in freestall barn with dairy cows on precision fed rations. *Trans. ASABE* 53:1251-1266.
- Arogo, J., P.W. Westerman, A.J. Heber, W.P. Robarge, and J.J. Cassen. 2006. Ammonia emissions from animal feeding operations. In *Animal Agriculture and the Environmental: National Center for Manure and Animal Waste Management White Papers*, 41-88. J.M. Rice, D.F. Caldwell, and F.J. Humenik, eds. St. Joseph, Mich.: American Society for Agricultural and Biological Engineers.
- Battye, W., V.P. Aneja, P.A. Roelle. 2003. Evaluation and improvement of ammonia emissions inventories. *Atmospheric Environ.* 37:3873-3883.
- Beauchamp, E.G., G.E. Kidd, and G. Thurtell. 1982. Ammonia volatilization from liquid dairy cattle manure in the field. *Can. J. Soil Sci.* 62:11-19.
- Bjorneberg, D.L., A.B. Leytem, D.T. Westermann, P.R. Griffiths, L. Shao, and M.J. Pollard. 2009. Measurement of atmospheric ammonia, methane, and nitrous oxide at a concentrated dairy production facility in southern Idaho using open-path FTIR spectrometry. *Trans. ASABE* 52:1749-1756.
- Bluteau, C.V., D.I. Massé, and R. Leduc. 2009. Ammonia emission rates from dairy livestock buildings in Eastern Canada. *Biosyst. Eng.* 103:480-488.
- Bonifacio, H.F., R.G. Maghirang, E.B. Razote, S.L. Trabue, and J.H. Prueger. 2013. Comparison of AERMOD and WindTrax dispersion models in determining PM₁₀ emission rates from a beef cattle feedlot. *J. Air and Waste Manage. Assoc.* 63:545-556.

- Cassel, T., L. Ashbaugh, and R. Flocchini. 2005. Ammonia emission factors for open-lot dairies: direct measurements and estimation by Nitrogen intake. *J. Air and Waste Manage. Assoc.* 55:826-833.
- Chow, J.C., J.G. Watson, D.H. Lowenthal, P.A. Solomon, K.L. Magliano, S.D. Ziman, and L.W. Richards. 1993. PM₁₀ and PM_{2.5} compositions in California's San Joaquin Valley. *Aerosol Sci. Technol.* 18:105-128.
- Cimorelli, A.J., S.G. Perry, A. Venkatram, J.C. Weil, R.J. Paine, R.B. Wilson, R.F. Lee, W.D. Peters, and R.W. Brode. 2005. AERMOD: a dispersion model for industrial source applications. Part I: general model formulation and boundary layer characterization. *J. Applied Meteor.* 44:682-693.
- Cole, N.A., R.N. Clark, R.W. Todd, C.R. Richardson, A. Gueye, L.W. Greene, and K. McBride. 2005. Influence of dietary crude protein concentration on potential ammonia emissions from beef cattle manure. *J. Animal Sci.* 83(3): 722-731.
- Davidson, C.I., R.F. Phalen, and P.A. Solomon. 2005. Airborne particulate matter and human health: a review. *Aerosol Sci. & Tech.* 39:737-749.
- Duce, R.A. 1991. The atmospheric input of trace species to the world's oceans. *Global Biogeochem. Cycles* 5:193-259.
- EPA. 2001. National pollutant discharge elimination system permit regulation and effluent limitation guidelines and standards for concentration animal feeding operations. *Fed. Reg.* 66(9): 2960-3138. Washington, D.C.: GPO.
- EPA. 2003. National air quality and emissions trends report: 2003 special studies edition. EPA-454/R-03-005. Research Triangle Park, N.C.: EPA Office of Air Quality Planning and Standards.
- EPA. 2005. National emission inventory – ammonia emissions from animal agricultural operations: revised draft report. Washington, D.C. Available at: ftp://ftp.epa.gov/EmisInventory/2002finalnei/documentation/nonpoint/nh3inventory_draft_042205.pdf. Accessed 17 October 2012.
- EPA. 2008. AERSURFACE User's Guide. EPA-454/B-08-001. Research Triangle Park, N.C.: EPA Office of Air Quality Planning and Standards.

- Faulkner, W.B., J.M. Lange, J.J. Powell, B.W. Shaw, and C.B. Parnell. 2007. Sampler placement to determine emission factors from ground level area sources. *Atmospheric Environ.* 41:7672-7678.
- Faulkner, W.B., B.W. Shaw, and T. Grosch. 2008. Sensitivity of two dispersion models (AERMOD and ISCST3) to input parameters for a rural ground-level area source. *J. Air and Waste Manage. Assoc.* 58:1288-1296.
- Flesch, T.K., L.A. Harper, J.M. Powell, and J.D. Wilson. 2009a. Inverse-dispersion calculation of ammonia emissions from Wisconsin dairy farms. *Trans. ASABE* 52:253-265.
- Flesch, T.K., L.A. Harper, R.L. Desjardins, A. Gao, and B.P. Crenna. 2009b. Multi-source emission determination using an inverse-dispersion technique. *Boundary Layer Meteorol.* 132:11-30.
- Griffiths, P.R., L. Shao, and A.B. Leytem. 2009. Completely automated open-path FT-IR spectrometry. *Anal. Bioanal. Chem.* 393:45-50.
- Going, C., G.B. Bingham, N.S. Pougatchev, E. Day, K. Moore, R. Martin, E. Reese. 2008. Multi path FTIR agricultural air pollution measurement system. ASABE Paper No. 084080. St. Joseph, Mich., USA: ASABE.
- Hansen, F. V. 1993. Albedos. ARL-TR-57: Army Research Laboratory. Available at: www.dtic.mil/cgi-bin/GetTRDoc?AD=ADA268255. Accessed 15 November 2012.
- Leytem, A.B., R.S. Dungan, and D.L. Bjorneberg. 2009. Case study: Seasonal and spatial distribution of ambient ammonia concentrations measured at a large open-lot dairy. *Prof. Anim. Sci.* 25:786-793.
- Leytem, A.B., R.S. Dungan, D.L. Bjorneberg, and A.C. Koehn. 2011. Emissions of ammonia, methane, carbon dioxide, and nitrous oxide from dairy cattle housing and manure management systems. *J. Environ. Quality* 40:1383-1394. doi:10.2134/jeq2009.0515.
- Leytem, A.B., R.S. Dungan, D.L. Bjorneberg, and A.C. Koehn. 2013. Greenhouse gas and ammonia emissions from an open-freestall dairy in southern Idaho. *J. Environ. Qual.* 42:10-10.

- Marchant, C. C., K. D. Moore, M. D. Wojcik, R. S. Martin, R. L. Pfeiffer, J. H. Prueger, and J. L. Hatfield. 2011. Estimation of dairy particulate matter emission rates by lidar and inverse modeling. *Trans. ASABE* 54:1453-1463.
- Meng, Z.Y., W.L. Lin, X.M. Jiang, P. Yan, Y. Wang, Y.M. Zhang, X.F. Jia, and X.L. Yu. 2011. Characteristics of atmospheric ammonia over Beijing, China. *Atmos. Chem. Phys.* 11:6139-6151.
- Moore, K.D. 2007. Derivation of agricultural gas-phase ammonia emissions and application to the Cache Valley. MS thesis. Logan, Utah: Utah State University, Department of Civil and Environmental Engineering.
- Mukhtar, S., A. Mutlu, S.C. Capareda, and C.B. Parnell. 2008. Seasonal and spatial variations of ammonia emissions from an open-lot dairy operation. *J. Air and Waste Manage. Assoc.* 58:369-376.
- Nennich, T.D., J.H. Harrison, L.M. VanWieringen, D. Meyer, A.J. Heinrichs, W.P. Weiss, N.R. St-Pierre, R.L. Kincaid, D.L. Davidson, and E. Block. 2005. Prediction of manure and nutrient excretion from dairy cattle. *J. Dairy Sci.* 88:3721-3733.
- Ngwabie, N.M., K.-H. Jeppsson, S. Nimmermark, C. Swensson, G. Gustafsson. 2009. Multi-location measurements of greenhouse gasses and emission rates of methane and ammonia from a naturally-ventilated barn for dairy cows. *Biosystems Engineering* 103:68-77.
- Paerl, H.W. 1985. Enhancement of marine primary productivity by nitrogen enriched rain. *Nature* 315:747-749.
- Pulchalski, M.A., M.E. Sather, J.T. Walker, C.M.B. Lehmann, D.A. Gay, J. Mathew, and W.P. Robarge. 2011. Passive ammonia monitoring in the United States: comparing three different sampling devices. *J. Environ. Monit.* 13:3156-3167.
- Roadman, M. J., J. R. Scudlark, J. J. Meisinger, and W. J. Ullman. 2003. Validation of Ogawa passive samplers for the determination of gaseous ammonia concentrations in agricultural settings. *Atmospheric Environ.* 37:2317-2325.
- Robarge, W.P., J.T. Walker, R.B. McCulloch, and G. Murray. 2002. Atmospheric concentrations of ammonia and ammonium at an agricultural site in the southeast United States. *Atmospheric Environ.* 36:1661-1674.

- Rumburg, B., G.H. Mount, J. Filipy, B. Lamb, H. Westberg, D. Yonge, R. Kincaid, and K. Johnson. 2008a. Measurement and modeling of atmospheric flux of ammonia from dairy milking cow housing. *Atmospheric Environ.* 42:3364-3379.
- Rumburg, B., G.H. Mount, D. Yonge, B. Lamb, H. Westberg, M. Neger, J. Filipy, R. Kincaid, and K. Johnson. 2008b. Measurements and modeling of atmospheric flux of ammonia from an anaerobic dairy waste lagoon. *Atmospheric Environ.* 42:3380-3393.
- Schmidt, D. R., L. D. Jacobsen, and K. A. Janni. 2002. Continuous monitoring of ammonia, hydrogen sulfide and dust emissions from swine, dairy, and poultry barns. ASAE Paper No. 024060. St. Joseph, Mich.: ASAE.
- Schrade, S., K. Zeyer, L. Gygax, L. Emmenegger, E. Hartung, and M. Keck. 2012. Ammonia emissions and emission factors of naturally ventilated dairy housing with solid floors and an outdoor exercise area in Switzerland. *Atmospheric Environ.* 47:183-194.
- Shao, L., P.R. Griffiths, and A.B. Leytem. 2010. Advances in data processing for open-path fourier transform infrared spectrometry of greenhouse gases. *Anal. Chem.* 82:8027-8033.
- Sheffield, R.E., and B. Louks. 2006. Diurnal variations of ammonia and hydrogen sulfide flux from a dairy manure storage pond in Idaho, 1131. In P.A. Viney et al., ed., *Proceedings: Workshop on Agricultural Air Quality: State of the Science*. Raleigh, N.C.: Department of Communication Services, North Carolina State University.
- Siong, P. and S. Sheikh. 2006. Conservation Management Practices Program Report, San Joaquin Valley Air Pollution Control District (SJVAPCD). Available: http://www.valleyair.org/farmpermits/updates/cmp_program_report_for_2005.pdf. Accessed: 8 May 2013.
- Smits, M.C.J., H. Valk, A. Elzing and A. Keen. 1995. Effect of protein nutrition on ammonia emission from a cubicle house for dairy cattle. *Livestock Prod. Sci.* 44(2): 147-156.
- Sommer, S.G., S. Générumont, P. Cellier, N.J. Hutchings, J.E. Olesen, and T. Morvan. 2003. Processes controlling ammonia emission from livestock slurry in the field. *Europ. J. Agron.* 19:465-486.

- Sommer, S.G., J.E. Oleson, and B.T. Christensen. 1991. Effects of temperature, wind speed, and air humidity on ammonia volatilization from surface applied cattle slurry. *J. Agric. Sci.* 117:91-100.
- Todd, R.W., N.A. Cole, R.N. Clark, T.K. Flesch, L.A. Harper, and B.H. Baek. 2008. Ammonia emissions from a beef cattle feedyard on the southern High Plains. *Atmospheric Environ.* 42:6797-6805.
- United States Department of Agriculture (USDA). 2009. 2007 Census of Agriculture: United States Summary and State Data. AC-07-A-51.
- Walker, J.T., D.R. Whitall, W. Robarge, and H.W. Paerl. 2004. Ambient ammonia and ammonium aerosol across a region of variable ammonia emission density. *Atmospheric Environ.* 38:1235-1246.
- Zhao, L.Y., M. Darr, X. Wang, R. Manuzuo, M. Brugger, E. Imerman, G. Arnold, H. Keener, and A.J. Heber. 2007. Temporal variations in gas and odor emissions from a dairy manure storage pond. ASABE Paper No. 701P0507e. St. Joseph, Mich.: ASABE.

CHAPTER 6

USING A DEPOSITION-ENABLED BACKWARD LAGRANGIAN STOCHASTIC

MODEL TO ESTIMATE PARTICULATE MATTER AREA SOURCE

EMISSIONS THROUGH INVERSE MODELING¹

Abstract

Inverse modeling is a commonly used technique for estimating air pollutant emissions (Q) from large area and volume sources, such as agricultural operations. This method calculates Q based on pollutant measurements and atmospheric dispersion modeling. Models frequently employed in inverse modeling are not capable of simulating dry deposition or pollutant trajectory deviations from the carrier fluid trajectory, both of which are common for particles with diameters (d_p) $> 1 \mu\text{m}$. This work presents a modified 3D Lagrangian stochastic (LS) model that accounts for particle settling velocity (v_s) and deposition in dispersion calculations. It can be run either forward (fLS) or backward (bLS) in time, setting it apart from other LS models accounting for v_s and deposition that are fLS only; the advantage of a bLS is greatly reduced computational time.

¹ Citation: Moore, K.D., R.S. Martin, M.D. Wojcik, B. Auvermann, J.H. Prueger, J.L. Hatfield. Using a deposition-enabled backward Lagrangian stochastic model to estimate particulate matter area source emissions through inverse modeling. Atmospheric Environment, submitted.

In non-depositional mode, the modified bLS was evaluated against a validation dataset for the original bLS and reported nearly equal results. Application of the bLS and fLS models to data collected at a commercial feedlot demonstrated the following: 1) the similarity of the bLS deposition results to those of the fLS for $d_p \leq 10 \mu\text{m}$ was dependent on the proximity of their particle release heights (z_{rel}); 2) the bLS:fLS ratio for Q was consistently 1.15 to 1.3 during operational testing for $d_p \leq 10 \mu\text{m}$, including the non-depositional case of $d_p = 0.0 \mu\text{m}$; 3) Q for $d_p < 5 \mu\text{m}$ were equal to the value of Q at $d_p = 0.0 \mu\text{m}$ in both bLS and fLS; and 4) the upper d_p limit for consistent bLS:fLS ratios in this test scenario was $20 \mu\text{m}$. These results suggest that for $d_p < 20 \mu\text{m}$, the modified bLS may be used to simulate the dispersion of particles, which is the range of interest for $\text{PM}_{2.5}$ and PM_{10} .

The modified bLS was used to estimate $Q_{\text{PM}_{10}}$ for the feedlot in both deposition and non-deposition modes. The Deposition $Q_{\text{PM}_{10}}$ was $62.5 \pm 12.4 \text{ g animal}^{-1} \text{ day}^{-1}$, 12% larger than the $55.9 \pm 11.2 \text{ g animal}^{-1} \text{ day}^{-1}$ for Non-deposition $Q_{\text{PM}_{10}}$. These are higher than literature values based on year-round sampling, but are similar to that reported for another summer-only sample period. The diurnal $Q_{\text{PM}_{10}}$ profiles show Deposition $Q_{\text{PM}_{10}}$ was always larger than Non-deposition $Q_{\text{PM}_{10}}$, with a range from 8% to 20%.

Introduction

Greater focus on agricultural air quality impacts over the past two decades has yielded a dramatic increase in the number of studies examining emission source

characteristics from various agricultural operations. Quantifying emission rates (Q) for the large area and volume agricultural sources has generally been carried out using inverse modeling, flux profile, eddy covariance, or flux chamber techniques. The first three methods are similar in that each requires one or more measurements of the source's impact on ambient downwind concentrations of the pollutant/molecule of interest (C), but they differ in the methodology for relating C to Q . The fourth encloses multiple small areas within the source to measure Q from each location in order to characterize Q of the entire system. Each method has strengths and weaknesses, as well as limitations for proper use. In this paper, we will use the inverse modeling method. Specifically, we examine inverse modeling of particulate matter (PM) Q from an agricultural area source on a near-source scale (100s m).

Inverse modeling uses an atmospheric dispersion model to relate C measured near a facility/operation of interest ($C_{downwind}$, C_{upwind}) to Q (Cowherd, 2005). An initial Q estimate is provided to the model (Q_{sim}) in order to predict the C (C_{sim}) at a given location. The $(C/Q)_{sim}$ ratio can then be used with measured C to estimate Q_{calc} :

$$Q_{calc} = \frac{C_{downwind} - C_{upwind}}{(C/Q)_{sim}} \quad (6-1)$$

In cases where the dispersion model used yields a linear response in C_{sim} to changes in Q_{sim} , the initial estimate of Q_{sim} will not affect Q_{calc} because the $(C/Q)_{sim}$ ratio describes the slope of the line relating the two terms and has neither local maxima nor minima. Careful selection and testing of Q_{sim} is required for models without such a linear

response. The $(C/Q)_{sim}$ ratio is unique to a given spatial source-receptor relationship and must be calculated for each unique meteorological condition.

There are several air dispersion models that have been used in near-source inverse modeling in agricultural settings (AERMOD, ISCST3, WindTrax, and other custom models), but most have not been validated. However, Flesch et al. (1995, 2004) described a 3D Lagrangian stochastic (LS) model that can be run forward (fLS) or backward (bLS) in time and validated the bLS form for near-source inverse modeling for a ground level area source with gaseous emissions. This is the basis of the modeling software WindTrax (www.thunderbeachscientific.com). An LS model is intended to mimic atmospheric transport and dispersion by simulating movement of tiny carrier fluid parcels or marked fluid elements (MFE), each with a different path due to the stochastic term. Running the LS model for many thousands of MFEs provides a statistically robust simulation of the dispersion and yields the $(C/Q)_{sim}$ ratio required to calculate Q_{calc} . LS models have been successfully used in a wide array of applications and at a variety of scales (Lin et al., 2012).

Many agricultural ER studies of both gaseous and PM emissions have used the 3D WindTrax bLS model in inverse modeling (Bjorneberg et al., 2009; Bonifacio et al., 2012, 2013a; Flesch et al., 2007, 2009; Leytem et al., 2009, 2011, 2013; Todd et al., 2008, 2015; and others). Others have proposed 2D fLS formulations to model heavy particle transport and dispersion for spores and pollen (Aylor et al., 2006; Aylor and Ferrandino, 1989; Aylor and Flesch, 2001; Boehm and Aylor, 2005; Boehm et al., 2008;

Wilson, 2000). Particles may behave differently than the surrounding fluid due to a gravity-induced settling velocity (v_s). This may result in lower vertical positions relative to the carrier MFE associated with the particle at the beginning of a given time step, which may also change horizontal position based on changing wind speed with height above ground level (agl). In addition, particles may deposit out of the flow. Neither v_s nor deposition are accounted for in the bLS from Flesch et al. (2004). McGinn et al. (2010) included modifications for heavy particles from Wilson (2000) in the Flesch et al. (2004) 3D fLS formulation to estimate PM₁₀ (PM with aerodynamic equivalent diameters $\leq 10 \mu\text{m}$) emissions from feedlots. The fLS model was run for a single particle diameter (d_p) of $7 \mu\text{m}$, which was used as the mass median diameter of the plume based on literature. Wang et al. (2008) estimated PM₁₀ emissions from agricultural tillage operations using a 3D fLS that accounted for v_s and deposition. They modeled particle transport for a particle with $d_p = 2 \mu\text{m}$ by calculating the 3D downwind C for that size and then estimating the cumulative PM₁₀ concentration contribution of particles with d_p from 0.007 to $10 \mu\text{m}$ by their respective number density relative to the $2 \mu\text{m}$ particle density. In effect, these models accounted for v_s and deposition for a single particle and assumed it was representative of all $d_p \leq 10 \mu\text{m}$.

The bLS model has a significant computational efficiency advantage over the fLS model, as reported by Flesch et al. (1995). However, a 3D bLS with modifications for modeling particle dispersion is not found in the literature. In this paper, we present a modified LS to account for v_s and deposition of particles for use in inverse modeling that

can be run as both fLS and bLS. The results of the modified bLS are compared with the fLS results for d_p ranging from 1 μm to 50 μm . The modified bLS model is then used to estimate $\text{PM}_{10} Q (Q_{\text{PM}_{10}})$ based on summer time measurements at a commercial beef feedlot.

Model Formulation

The 3D LS model selected for modification in this work is that described in Flesch et al. (1995, 2004). A brief summary is provided here; the reader is referred to Flesch et al. (1995, 2004) for an in-depth derivation and discussion. The discretized LS model equations are the same for both fLS and bLS, as follows:

$$\begin{aligned} \Delta x &= (U(z) + u)\Delta t & \Delta y &= v\Delta t & \Delta z &= w\Delta t \\ \Delta u &= a_u\Delta t + b_u R & \Delta v &= a_v\Delta t + b_v R_v & \Delta w &= a_w\Delta t + b_w R_w, \end{aligned} \quad (6-2)$$

where u , v , and w are the instantaneous wind velocities in the x , y , and z directions, respectively; $U(z)$ is the period average wind velocity at height z ; U is aligned with the $+x$ axis; Δt is the model time step; R_u , R_v , and R_w are independent random numbers chosen from a Gaussian distribution with a mean of zero and a variance of Δt ; and a_u , a_v , a_w , b_u , b_v , and b_w are functions of position, instantaneous velocity, and properties of the flow. It is assumed that the mixing/turbulent state of the atmosphere can be described from observations using Monin-Obukov similarity theory (MOST) through the friction velocity (u^*), Obukov length (L), surface roughness length (z_0), and wind direction (θ)

parameters. While this assumption does not always hold, the application of this LS model should be limited to conditions in which MOST is valid.

Forward Model

Unique equations for the a and b values in Eq. 6-2 do not yet exist for multidimensional models and generally constitute the largest differences between proposed LS models. Flesch et al. (2004) use the following equations for the fLS model, which are derived for an ideal atmospheric surface layer and based on the well-mixed LS model for Gaussian turbulence given by Thomson (1987):

$$\begin{aligned}
 a_u &= -\frac{1}{2(\sigma_u^2\sigma_w^2 - u_*^4)} b_u^2 [\sigma_w^2(u - U) + u_*^2 w] + w \frac{\partial U}{\partial z} \\
 a_v &= -\frac{1}{2} b_v^2 \frac{v}{\sigma_v^2} \\
 a_w &= -\frac{1}{2(\sigma_u^2\sigma_w^2 - u_*^4)} b_w^2 [u_*^2(u - U) + u_*^2 w] + \frac{1}{2} \frac{\partial \sigma_w^2}{\partial z} + \frac{1}{2(\sigma_u^2\sigma_w^2 - u_*^4)} \left[u_*^2 \frac{\partial \sigma_w^2}{\partial z} (u - U) w + \sigma_u^2 \frac{\partial \sigma_w^2}{\partial z} w^2 \right]
 \end{aligned}
 \tag{6-3}$$

and

$$b_u = b_v = b_w = b = \sqrt{C_0 \varepsilon}.
 \tag{6-4}$$

σ_u^2 (σ_v^2, σ_w^2) is the standard variance of the u (v, w) wind component. The variables ε and C_0 in Eq. 6-4 are, respectively, the turbulent kinetic energy dissipative rate and a constant with reported values that range between 2 and 9. Flesch et al. (2004) calculated $C_0 = 4.41$ for their model. Δt is calculated as a fraction of the velocity decorrelation time scale for a MFE, also known as the Lagrangian time scale τ_L , and varies with z and the turbulent state of the atmosphere,

$$\Delta t = 0.025\tau_L \text{ where } \tau_L = \frac{2\sigma_w^2}{C_0\varepsilon}. \quad (6-5)$$

Assumptions made in deriving Eqs. 6-3 and 6-4 include: horizontally homogeneous turbulence in which the MOST parameters are valid throughout the modeled domain; a stationary atmosphere with average vertical wind component velocity $W = 0$; $\overline{u'w'} = -u_*^2$, where u' (w') is the instantaneous deviation from U (W) and $\overline{u'w'}$ is the covariance; and $\overline{u'v'} = \overline{v'w'} = 0$ because y is perpendicular to U . As formulated, this model assumes no changes in elevation within the domain.

In the fLS, the $(C/Q)_{sim}$ ratio was calculated using the following equations:

$$(C/Q_{vol})_{sim} = \frac{V_{src}}{V_{sens}} \frac{1}{N} \sum_{i=1}^n (t_{res})_{V_{sens},i} \quad (6-6)$$

for a volume source, where V_{src} is the volume of the source; and

$$(C/Q_{area})_{sim} = \frac{A_{src}}{V_{sens}} \frac{1}{N} \sum_{i=1}^n (t_{res})_{V_{sens},i} \quad (6-7)$$

for an area source with area A_{src} . In both Eqs. 6-6 and 6-7, V_{sens} is the volume of air sampled by the sensor, N is the total number of MFEs released, n is the number of MFEs that passed through V_{sens} , and $(t_{res})_{V_{sens},i}$ is the residence time of MFE i within V_{sens} . The units for Q_{vol} are mass length⁻³ time⁻¹ and the units for Q_{area} are mass length⁻² time⁻¹.

Note that both the fLS and bLS models have linear responses in C_{sim} to changes in Q_{sim} .

Backward Model

As per Flesch et al. (2004), the bLS model equations differ from the fLS in only two ways: 1) Δt is negative; and 2) the signs on the first terms on the RHS of Eq. 6-3 are reversed. In addition, the $(C/Q)_{sim}$ ratio calculation in Eq. 6-7 is simplified to

$$(C/Q)_{sim} = \frac{1}{N} \sum_{i=1}^n \left| \frac{z}{w_i} \right| \quad (6-8)$$

when a ground level area source is assumed. In this case, the model tracks particles backward in time and records instances when $z < z_0$, i.e., the particle crosses the level at which $u = 0.0 \text{ m s}^{-1}$. This is referred to as a touchdown. The x , y , and w values are recorded for each touchdown, after which the particle is reflected above the z_0 plane and the model continues tracking it backwards in time. In Eq. 6-8, n is the total number of touchdowns within the source area and the w_i term is the w value recorded for touchdown i within the source area. Touchdowns occur in the fLS and are reflected in the same way, but their locations are not used to calculate $(C/Q)_{sim}$.

Modeling Particle Motion

The LS model in Eqs. 6-2 through 6-4 describes the flow of a fluid, and applying this formulation to model movement of emissions into the atmosphere requires the assumption that the substance of interest adheres to the behavior of the fluid. However, solid and liquid particles may behave differently than the carrier gas in the atmosphere due to greater mass, inertia, and gravitational effects. Therefore,

adjustments to the model formulation were required to account for a particle's deviation from the fluid movement. Wilson (2000) and Aylor and Flesch (2001) accounted for these effects by making several changes to the LS model formulation. These same changes were applied to the Flesch et al. (2004) 3D model and the result will be referred to as the modified LS model hereafter.

First, the v_s (m s^{-1}), as calculated in Hinds (1999), of a particle of diameter d_p and particle density ρ_p was added to the Δz calculation in Eq. 6-2, becoming

$$\Delta z = (w - v_s)\Delta t. \quad (6-9)$$

Second, Δt was reduced to minimize errors associated with differences between the carrier fluid flow characteristics at the particle's final z position and the final z position of the MFE with which the particle was initially associated. Following Sawford and Guest (1991) and Aylor and Flesch (2001), the new time step, Δt_p , was calculated as:

$$\Delta t_p = f\Delta t$$

$$f = 1/\sqrt{1 + (\beta v_s/\sigma_w)^2}. \quad (6-10)$$

β is an empirical constant with a value of 1.5. The magnitude of f for a constant v_s varies with z based on σ_w and reaches a minimum near $z=0$.

The final change was to allow the particle to be removed from the flow to simulate deposition. Flesch et al. (2004) assume each MFE that crosses the z_0 boundary is reflected back into the atmosphere and continues within the domain. Aylor and Flesch (2001) allowed dry deposition within a plant canopy and to the ground, as well as washout by rain. In this application, only dry deposition to the ground as simulated

following Aylor and Flesch (2001) and Aylor and Ferrandino (1989) was employed. When a particle's z position dropped below the z_0 plane, the probability of deposition (G) was calculated as

$$G = \begin{cases} \frac{2v_s}{v_s - w} & \text{for } w < -v_s \\ 1 & \text{for } |w| < v_s \end{cases} \quad (6-11)$$

G was then compared to a random number selected from a uniform distribution between 0 and 1. If G is greater than the random number, the particle is deposited. If not, the particle is reflected and the particle position and surrounding air velocity were modified through

$$\begin{aligned} z_{new} &= z_{old} - 2v_s\Delta t \\ u_{new} &= -(u_{old} - U(z_{old})) + U(z_{new}) \\ w_{new} &= -w_{old} \end{aligned} \quad (6-12)$$

where the "old" subscript represents the values before crossing the z_0 plane and "new" is for the values after reflection. Note that this is a different reflection method than used by Flesch et al. (2004).

The modified fLS model stops simulating a particle's movement if it is deposited, logging the deposition in addition to x , y , and w . Deposition, therefore, potentially limits the number of released particles that can pass through the downwind sensor volume, which would decrease the $(C/Q)_{sim}$ ratio for a constant N and lead to a higher Q_{calc} . An increase in N may be required to maintain the same level of confidence in the simulation results.

However, the modified bLS model must reflect the particle in order to determine the previous path and origin of the deposited particle. The deposition is logged and Eq. 6-12 is used to calculate the particle's new position and instantaneous velocities. Regardless of the number of depositions, a particle's movement in the modified bLS is simulated until it reaches an upwind distance beyond the area of interest.

Accounting for the effect of deposition in the bLS on Q was performed through the use of a unitless scalar multiplier (a_{dep}) to the Q_{calc} estimated in Eq. 6-1,

$$Q_{calc,dep} = a_{dep}Q_{calc}. \quad (6-13)$$

The reasoning behind this approach is as follows: each MFE/particle trajectory in a bLS simulation represents a path that one or more gas molecules or particles could have followed to arrive at the sampling volume of the sensor. The use of many thousands of MFEs/particles in the bLS provides a statistically robust representation of the pathways and/or origins of those detected by the sensor. As a result, the $(C/Q)_{sim}$ ratio calculated with Eq. 6-8 and the corresponding Q_{calc} from Eq. 6-1 are representative of those particles. When the bLS simulates a deposition, it is not simulating the deposition of the particle that passed through the sensor volume but of a different particle with a similar trajectory that did not pass through the sensor volume due to being deposited. Therefore, the number of depositions associated with trajectories of particles having touchdowns within the source volume must be examined for use in adjusting Q_{calc} to $Q_{calc, dep}$. In this application, a_{dep} is calculated as:

$$a_{dep} = 1 + \frac{n_{dep}}{n_{td}} \quad (6-14)$$

where n_{td} is the number of touchdowns within the source area and n_{dep} is the number of depositions recorded after (in time) a touchdown within the source area. As $a_{dep} \geq 1.0$, $Q_{calc, dep}$ will be $\geq Q_{calc}$.

Emissions Calculations

The use of the modified models to estimate the emission rate of a PM mass fraction of interest k , where $k = 2.5$ for $PM_{2.5}$ or 10 for PM_{10} , requires information about the particle size distribution (PSD) and ρ_p in addition to Q_{calc} for fLS or $Q_{calc, dep}$ for bLS applications. These are used to estimate particle count emissions for each particle size bin m ($Q_{m, count}$), calculated with a variation of Eq. 6-1 in which C has units of particles volume⁻¹ instead of mass volume⁻¹ and Q has units of particles volume⁻¹ (or area⁻¹) time⁻¹ instead of mass volume⁻¹ (or area⁻¹) time⁻¹. The $(C/Q)_{sim}$ values calculated from Eqs. 6-6 through 6-8 remain valid as the units for Q can be either mass or count. Then, Q_{PMk} is calculated using the total particle volume in each size bin up to M , the bin containing $d_p = k$.

$$Q_{PMk} = \rho_p \sum_{m=1}^M \left(\frac{4}{3} \pi \frac{GMD_m^3}{8} Q_{m, count} \right). \quad (6-15)$$

Model Testing

Site Description

The modified LS models were tested using PM measurements collected at a commercial cattle feedyard operation located in the panhandle of Texas, USA (Figure 6-1). The feedyard had a capacity of 45,000 head with approximately 40,000 head on-site during data collection. The entire facility had an area of 2.0 km² with 0.9 km² for the pens, a rectangle of about 800 m x 1200 m with the long sides oriented roughly along longitudinal lines. Feed was mixed onsite and distributed by truck twice daily. Manure management practices consisted of scraping pens to move accumulated manure into one mound in each pen, with mound removal occurring annually. Liquid runoff was stored in an on-site evaporation pond, located to the east of the pens in Figure 6-1. Historical meteorological observations have shown dominant wind directions in this area are from the southern quadrant in summer, with most deviations related to low pressure systems. Previous gaseous ammonia *Q* studies at this site were reported by Flesch et al. (2007) and Todd et al. (2008), both of which used the bLS WindTrax software. In addition, an open-path PM study at this site was reported by Upadhyay et al. (2008).

Data Collection and Processing

Multiple sensors to measure particle and meteorological variables were deployed around the facility, as shown in Figure 6-1. PM and meteorological data were collected June 3-12, 2015. Seven tapered-element oscillating microbalance (TEOM) units, Model 1400a from Thermo Scientific, Inc., were set on the northern (downwind) and southern (upwind) sides of the feedlot to measure PM₁₀ concentrations. The TEOMs were deployed at sampling sites 1-7. An Optical Particle Sizer (OPS), Model 3330 from TSI, Inc., was collocated with a TEOM at Site 3 on the northern side and used to measure the PSD. The OPS was deployed from June 10-12 during an intensive operation period (IOP). TEOM data were recorded as 5-minute averages from June 3 through mid-day June 9, then as 1-minute averages through the end of collection early on June 12; the OPS data were recorded as 1-minute averages. All inlets were located at approximately 2 m agl. TEOM and OPS data were aggregated into 30 minute averages for this analysis.

Meteorological variables were measured by two integrated weather stations and a 3D sonic anemometer. One weather station and the 3D sonic anemometer were located at 10 m agl on the northern side of the feedyard adjacent to Site 4. The second weather station was deployed 800 m to the west of Site 4 at 2 m agl during the IOP. Both weather stations provided values for barometric pressure, precipitation, air temperature, relative humidity, solar radiation, wind speed, and wind direction. The sonic anemometer reported the average and standard deviation of the sonic



Figure 6-1. Satellite image of the feedlot under study with particle and meteorological measurement locations shown, as well as the facility and pen borders.

temperature, u , v , and w components of the wind, wind speed, and wind direction.

Weather station data were archived as 1-minute averages throughout the study. Sonic data were recorded as averages and standard deviations over 30 minutes for June 3 through early June 10 and over 1 minute for early June 10 through June 12 during the intensive operating period. These values were averaged into 30 minute periods for further calculations and analysis.

Meteorological inputs required by the LS model include period average wind speed (U), wind direction (θ), surface roughness (z_0), Monin-Obukov length (L), and the shear velocity (u^*). Raw, high frequency sonic anemometer data is typically used to calculate this set of parameters using the eddy covariance method. Unfortunately, the raw data were not saved during this experiment and these parameters were not calculated by the datalogger, resulting in only U and θ being provided for a given sample period and averaged over 30 minutes. Therefore, alternative methods for calculating u^* , z_0 , and L were required that did not require high frequency sonic anemometer data.

First, $z_0 = 0.08$ m was set as a constant based on z_0 values from Figure 7 in Flesch et al. (2007), which presents a five-day time series of z_0 , u^* , and L for this same facility in June 2004. In addition, a displacement value of zero was assumed following Flesch et al. (2007). Next, u^* was calculated using Eq. 6-16 derived from the diabatically corrected logarithmic wind profile equation with U from the sonic anemometer height of 10 m

$$u^* = \frac{Uk}{\ln\left(\frac{z}{z_0}\right) + \psi\left(\frac{z}{L}\right)} \quad (6-16)$$

where k is the von Karman constant with a value of 0.4, z is the measurement height (m), and $\psi(z/L)$ is the correction term for stability. $\psi(z/L)$ was calculated based on the following equations from Dyer (1974) for stable conditions ($L > 0$) and Dyer and Hicks (1970) for unstable conditions ($L < 0$).

$$\begin{aligned} \psi\left(\frac{z}{L}\right) &= 1 + 5\frac{z}{L} && \text{for } L > 0 \\ \psi\left(\frac{z}{L}\right) &= \left(1 - 16\frac{z}{L}\right)^{1/4} && \text{for } L < 0 \end{aligned} \quad (6-17)$$

L was calculated with the following equation, which is dependent on the heat flux (H , W m^{-2}), among other parameters,

$$L = -\frac{T_a u^{*3} \rho C_p}{kgH}. \quad (6-18)$$

T_a , ρ , and C_p are mean ambient temperature (K), air density (kg m^{-3}), and specific heat of air at constant pressure ($\text{J kg}^{-1} \text{K}^{-1}$). The average sonic temperature (T_s) was used in place of T_a , and ρ and C_p were calculated using T_s and the data collected by the weather station. H , which may be calculated through the eddy covariance method using raw sonic data, is the last unknown parameter in Eq. 6-18. Prueger and Kustas (2005) summarized a method to calculate H during daytime, convective conditions using the variance of potential temperature θ (σ_θ):

$$H = \rho C_p \left(\frac{\sigma_\theta}{c}\right)^{3/2} \left(\frac{kgz}{T_s}\right)^{1/2}, \quad (6-19)$$

where c is an empirical constant assigned a value of 0.95 and g is the constant acceleration due to gravity (m s^{-2}).

As H is always positive when calculated using Eq. 6-19, an additional method for calculating negative values of H was required for periods with low insolation. First, the distinction between periods with positive and negative H values was made. The solar elevation angle (β) was calculated at the center time of each sample period. These were compared with the critical solar elevation angle (β_{cr}), the point at which the changing incoming solar radiation causes the heat flux to change signs. This was calculated as:

$$\sin(\beta_{cr}) = \left(\frac{1}{990} \right) \left(\frac{-c_1 T^6 + \sigma_{SB} T^4 + c_2 N_{cc}}{(1-r_\alpha)(1-3/4 N_{cc}^{3.4})} + 30 \right) \quad (6-20)$$

$$r_\alpha = \alpha + (1 - \alpha)e^{a\beta+b}$$

where β and β_{cr} have units of degrees, c_1 is a constant with value $5.31 \text{ W m}^{-2} \text{ K}^{-6}$, c_2 is a constant with value 60 W m^{-2} , T has units of Kelvin and T_a is used here, σ_{SB} is the Stefan-Boltzmann constant with a value of $5.67 \times 10^{-8} \text{ W m}^{-2} \text{ K}^{-4}$, N_{cc} is fraction of cloud cover, α is albedo as a fraction, a is a constant with a value of -0.1 deg^{-1} , and $b = -(1-\alpha^2)/2$. Cloud cover was not measured on-site. Instead, observations from two meteorological stations 50-65 km away in opposite directions were averaged and assumed to be valid at the 30-minute time scale in this application.

The methodology outlined in Eqs. 6-16 through 6-18 for calculating u^* and L was used for those sample periods for which $\beta \geq \beta_{cr}$. For sample periods with $\beta < \beta_{cr}$, these parameters were calculated with the method used for stable boundary layers in AERMET, the meteorological preprocessor for the regulatory air dispersion model AERMOD, as described by Cimorelli et al. (2005) and Hanna and Chowdhury (2014).

First, the turbulent temperature scale (θ^* , K) was calculated based on N_{cc} as follows as

$$\theta^* = 0.09(1 - 0.5N_{cc}^2). \quad (6-21)$$

The θ^* value was used to calculate u^* according to Eq. 6-22, and both are used to calculate L and H using the following equations derived from a combination of Eqs. 6-18, 6-19, and 6-21:

$$u^* = \left(\frac{u\sqrt{C_{DN}}}{2} \right) \left(1 + \sqrt{1 - \left(\frac{2u_0/u}{\sqrt{C_{DN}}} \right)^2} \right) \quad (6-22)$$

$$C_{DN} = (k/\ln(z/z_0))^2$$

$$u_0 = \sqrt{\beta_m g z \theta^* / T}$$

$$H = -\theta^* \rho c_p u^* \quad (6-23)$$

$$L = \frac{T_s u^{*2}}{kg\theta^*} \quad (6-24)$$

The period wind speed scale (u_0) was then compared against the critical wind speed (u_{cr}), the minimum wind speed needed to maintain turbulence in a stable atmosphere and below which MOST is not applicable (Hanna and Chowdhury, 2014).

$$u_{cr} = \frac{2u_0}{\sqrt{C_{DN}}} \quad (6-25)$$

If $u_0 < u_{cr}$ for a given sample period, u^* and θ^* were recalculated using the following ratio equations and the H and L were then recalculated.

$$u^* = u^* \left(\frac{u_{ref}}{u_{cr}} \right) \quad (6-26)$$

$$\theta^* = \theta^* \left(\frac{u_{ref}}{u_{cr}} \right)$$

Weather station data collected downwind of the feedlot and adjacent to Site 4 were used in the calculations above, except for a period of six hours on June 10 due to a data gap. This gap was filled using data from the second weather station.

Extreme values for L , u^* , and z_0 have been shown to indicate potential for an inaccurate description of atmospheric conditions under the MOST assumptions, leading to potentially large model errors. Therefore, the following criteria were used to identify

and exclude such periods following the methodology of Flesch et al. (2004, 2007). Sample periods were removed from the ER calculation if $u^* \leq 0.15 \text{ m s}^{-1}$ (low wind conditions) or $|L| \leq 10 \text{ m}$ (strongly stable/unstable atmosphere). The measured wind direction was used to identify sample periods in which the pens did not likely impact the PM instrumentation sufficiently to yield a good ER estimate. To be designated a sample period with sufficient upwind fetch within the source area, θ had to be such that the ray drawn from a given sample site in the upwind direction ($\theta - 180^\circ$) was required to intersect the east (west) edge of the overall pen area $\geq 250 \text{ m}$ south of the northeast (northwest) corner, approximately $\frac{1}{4}$ the length of the eastern/western edges. Therefore, θ had to be between 112° and 251° . This criterion for θ differs from Flesch et al. (2007) due to different C measurement types (point vs. line C measurement).

Modified LS Model Application

The modified LS models were run with the measured and calculated U , θ , L , and u^* values for the 10 m sonic anemometer height. The v_s for each d_p of interest was calculated for use in the model using the following assumptions: the particles are spherical; particles have a ρ_p of 1.71 g cm^{-3} following Sweeten et al. (1998) and McGinn et al. (2010); and, if using data from the OPS, the geometric mean diameter (GMD_i) is representative of the mean d_p for a given bin i . The modified models were run for each d_p of interest and for the non-depositional case of $d_p = 0.0 \text{ }\mu\text{m}$ ($v_s = 0.0 \text{ m s}^{-1}$) to provide a reference $(C/Q)_{sim}$ value.

LS Model Sources. Homogeneous surface and meteorological conditions at a given height z of 10 m were assumed throughout the area of interest. Therefore, the modeled touchdowns from the bLS and the 3D t_{res} matrix output by the fLS were translatable in the $[x,y]$ plane. This significantly increased computational efficiency by allowing both models to be run for a single, small release volume per sample period. The results were then copied and translated horizontally for application to each source/receptor relationship. In the fLS, this allowed great flexibility in source number (S) and location, allowing for a test of the minimum value of S that achieves the same results as using a source covering the full pen extents. In the case of the bLS model, the single generic configuration was run while logging touchdown and deposition positions relative to the particle release point. This dataset was then applied to each sampling site with valid TEOM data.

When running the bLS model, the MFEs were released from a cube with a center located at $[x,y,z] = [0.0,0.0,2.0]$ m, with the z value set to the PM sensor inlet heights. Each side of the cube was 0.25 m in length and initial MFE locations within the cube were set randomly using normal distributions in each direction. Particles were tracked backwards in time until the x position was $< -1,400$ m to ensure the entire feedlot pen surface area was contained within the modeled upwind fetch.

The source used with the fLS model had several similarities with the bLS application: a cube with each side measuring 0.25 m in length; MFEs randomly placed throughout the volume based on normal distributions in each direction; and particles

were tracked until $x > 1,400$ m. However, the cube was centered at $[x,y,z] = [0.0,0.0,0.205]$ m to represent the near-ground dust created by animal hoof action assumed to be the main feedlot PM source. The bottom of the cube was placed at the z_0 plane.

Emissions Quantification. The emission area for the feedlot facility was specified as the pen areas. The pen vertices were determined using satellite imagery. The sensor locations were measured with a hand-held GPS unit during the field study and adjusted with values taken from Google Earth satellite imagery to ensure correct source-receptor spatial relationships in the emissions quantification procedure. The feedlot pens were divided into nine rows, each separated by feed lanes, as shown in Figure 6-1. The emissions from on-site support activities, such as feed mixing, feed distribution, wind-blown dust, and unpaved road emissions, were attributed to the animals and included in this emissions calculation as their impact on downwind PM_{10} was indistinguishable from the pen emissions.

As stated previously, the bLS and fLS model results were translatable in the $[x,y]$ plane, allowing a simulation with a small sensor or source volume to be applied throughout the domain. The use of multiple fLS sources required the following modification to Eq. 6-6 to calculate the $(C/Q)_{sim}$ ratio:

$$(C/Q_{vol})_{sim} = \frac{V_{src} S}{V_{sens} NS} \sum_{j=1}^S \left(\sum_{i=1}^n (t_{res})_{V_{sens,i}} \right)_{V_{sens,j}} \quad (6-27)$$

where N is the total number of particles released per source, S is the total number of small volume sources spread throughout the pen area, and n is the number of particles that passed through V_{sens} from source s_j . Unlike the fLS, no changes were required to calculate the $(C/Q)_{sim}$ ratio for the bLS. However, accounting for deposition simulation in the bLS required the use of α_{dep} and Eq. 6-13 to yield $Q_{calc, dep}$.

Information on the PSD during each sample period was required in order to estimate $Q_{PM_{10}}$. As the OPS was deployed from only June 10 through June 12, the PSD was estimated for the remaining sample periods by assuming the measured PSDs were representative of PSDs throughout the study. Relationships were found to relate changes in OPS channel counts to changes in PM_{10} . Both first order and second order polynomial fits were calculated using TEOM data from sites 2 and 4. Site 3 TEOM data, the TEOM collocated with the OPS, were invalid due to an inlet obstruction found at the end of the study. Changes in particle counts in channels 1 and 2 varied relatively little compared to changes observed in other channels and were very weakly correlated with changes in PM_{10} levels. Therefore, particle counts in the first two channels were attributed entirely to background aerosol and were not included in the emission estimate. Second order polynomials provided better fits for channels 3 through 17, particularly for $PM_{10} < 1,000 \mu\text{g m}^{-3}$, and were selected instead of the first order polynomials. These relationships were applied at each location, including the upwind Site 7, to estimate the PSD based on measured PM_{10} .

The PSDs were used to calculate Q_{PM10} using two slightly different methods. First, values for $Q_{m, count}$ and Q_{PM10} were calculated as described in above and will be referred to as the Deposition Q_{PM10} . Second, Q_{PM10} was estimated through the typical method used with a model that does not account for v_s or deposition in inverse modeling calculations. The $(C/Q)_{sim}$ ratios for $d_p = 0.0 \mu\text{m}$ from the modified model and PM_{10} calculated from the estimated PSDs were used in Eq. 6-1. The PSD-derived PM_{10} was calculated by multiplying the volume per particle, based on the GMD of each size bin, by the number of particles emitted by the facility in the respective size bin, and then multiplied by ρ_p . The PSD-derived PM_{10} and the modified model results for $d_p = 0.0 \mu\text{m}$ were employed in order to examine differences in Q solely due to account for v_s and deposition in the model and to avoid additional confounding factors introduced by a different model or PM_{10} dataset. This second emission rate is termed the Non-deposition Q_{PM10} .

Results and Discussion

Particulate Matter and Meteorological Characteristics

The wind and stability values measured and calculated for use in the models are presented in Figure 6-2. Note that the full time series of these variables is shown, including the extreme values of u^* and L and θ outside of the limits required for sufficient plume impact on the downwind TEOM sensors, as described above. Note that many sample periods had u^* below the criteria level of 0.15 m s^{-1} . A total of 121 sample

periods passed all the meteorological filter specifications, 77 in unstable conditions ($L < 0$) and 44 in stable conditions ($L > 0$).

The PM_{10} time series reported by five of the seven deployed TEOMs are shown in Figure 6-3. Sites 1, 2, 4, and 6 were generally downwind of the feedlot and Site 7 was upwind, except early on June 8 when winds were briefly from the northern quadrant. Concentrations at Site 7 averaged $10.1 \mu\text{g m}^{-3}$ throughout the study, with a standard

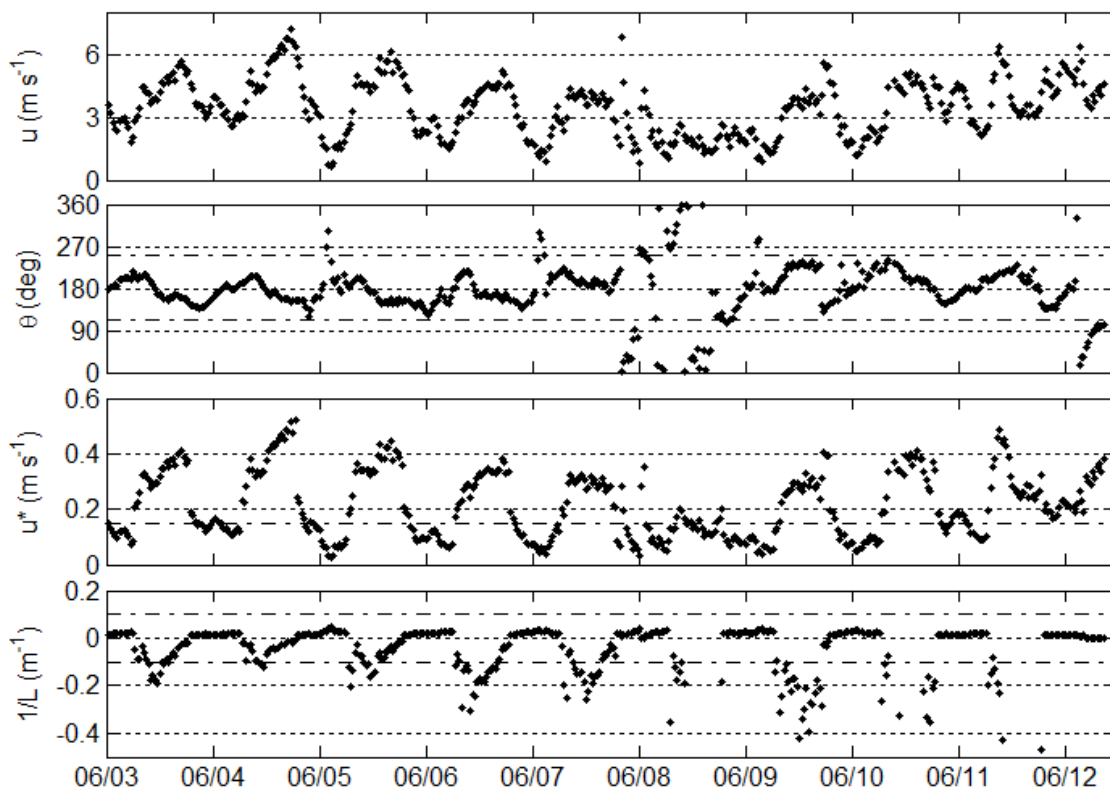


Figure 6-2. Measured values for wind speed (u) and direction (θ) and calculated values for shear velocity (u^*) and the inverse of Monin-Obukov length ($1/L$) as 30 min averages throughout the collection period. Note that the dash-dot lines (---) parallel to the x-axis in the θ , u^* , and $1/L$ graphs represent the criteria levels used to filter out periods for modeling with either insufficient impact on the sensors due to θ or meteorological periods with extreme values of u^* and L .

deviation of $11.8 \mu\text{g m}^{-3}$. Examining the 121 sample periods that passed all the meteorological filters, Site 7 averaged $14.1 \pm 13.3 \mu\text{g m}^{-3}$. However, seven of those periods did not have an upwind PM_{10} measurement, leaving 114 sample periods (70 with $L < 0$, 44 with $L > 0$) over which to calculate $Q_{\text{PM}_{10}}$. As has been reported by others at feedlots, downwind PM_{10} levels show a consistent diurnal pattern, peaking in the evening and at a minimum in the early morning (Bonifacio et al., 2012, 2013a, 2013b; McGinn et al., 2010; Purdy et al., 2007; Upadhyay et al., 2008; and others). Irregularities found in data from TEOMs at Sites 3 and 5, related to a sample line obstruction and instrument health invalidating the calibration, respectively, resulted in their exclusion from calculations. Site 6 PM_{10} generally tracked other downwind levels until early

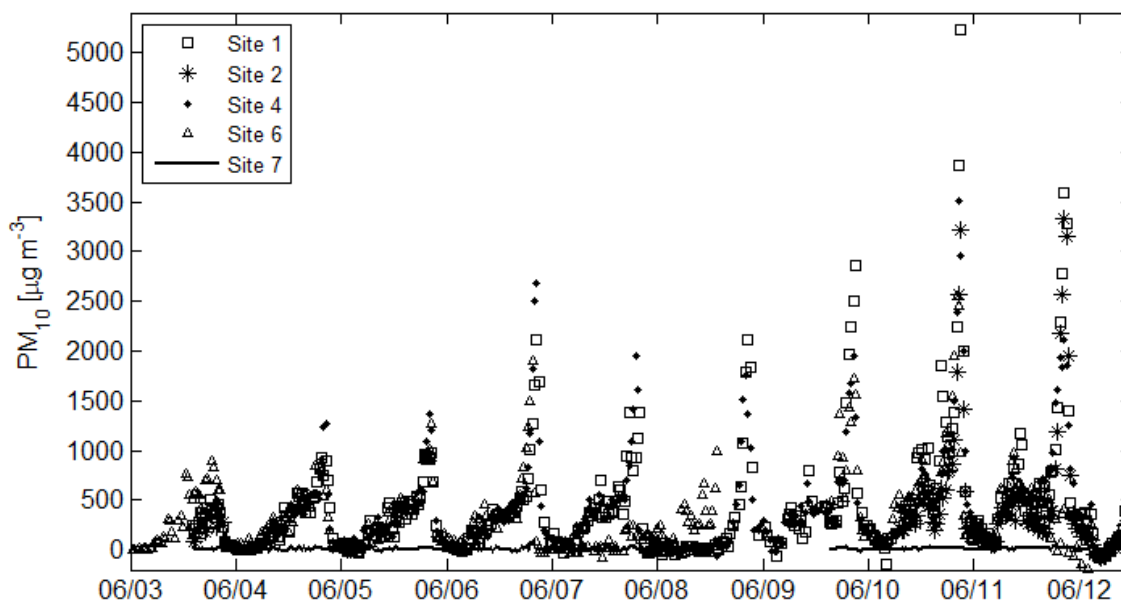


Figure 6-3. PM_{10} concentrations measured at the feedlot by the upwind (Site 7) and downwind (Sites 1, 2, 4, and 6) TEOMs as 30 min averages.

evening on June 11, after which it deviated substantially. Site 6 data after this point were not used to estimate Q_{PM10} .

Several PSDs measured during the June 10-12 OPS deployment are presented in Figure 6-4 (a), selected to represent the PSDs across a range of PM_{10} concentrations as observed in the time series plot in (b). The greatest changes in particle counts with increasing PM_{10} were in the channels with larger GMDs; also, counts in channels 1 and 2, with the smallest GMDs, did not appear correlated to changes in PM_{10} . Note that Site 2 and Site 4 were used for comparison against the OPS-derived PM_{10} in Figure 6-4 (b). The OPS PM_{10} follows the TEOM trends and matches the concentrations from the adjacent sites fairly well throughout the OPS data record.

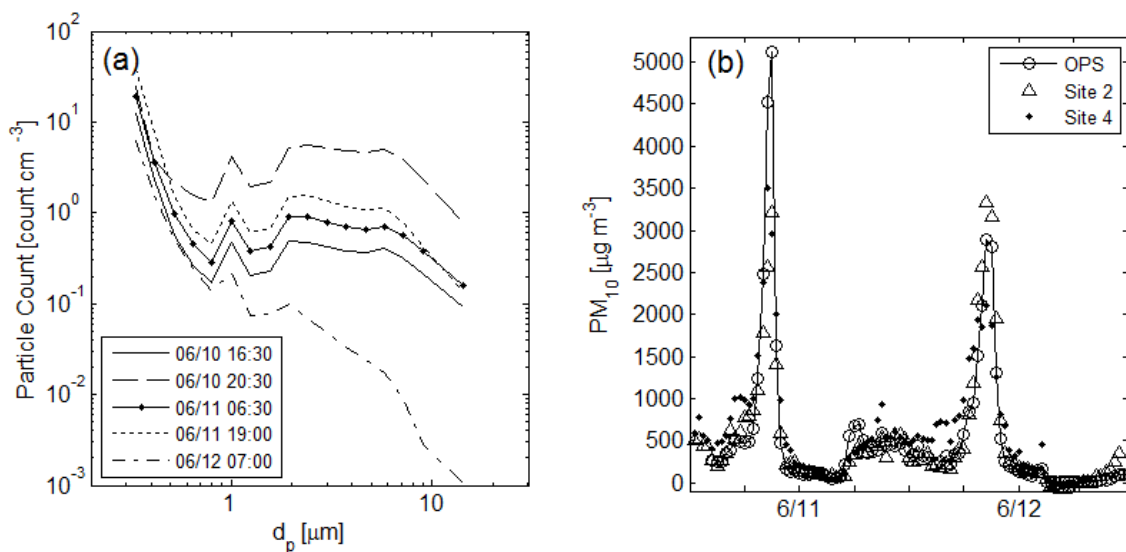


Figure 6-4. (a) Example particle size distributions (PSDs) measured by the OPS at Site 3 averaged over 30 min periods and (b) the PM_{10} concentration calculated from the OPS PSD measured at Site 3 compared with TEOM PM_{10} from adjacent sites 2 and 4.

Modified LS Model Testing

Testing of the modified LS model was conducted to: 1) test if the non-depositional mode of the model yielded results similar to Flesch et al. (2004); 2) examine the impact of including deposition on model results; and 3) determine optimal configurations regarding application to the feedlot.

The first test was to determine if the modified bLS yielded similar results as the bLS in Flesch et al. (2004) for a common dataset. A subset of their published data, the TA3-5 sample run with eight 15-minute sample periods, was selected. Flesch et al. report an average $Q_{calc}:known\ Q$ ratio of 0.96 with a standard deviation of 0.10. The modified bLS yielded a slightly higher average ratio of 1.15 but with the same standard deviation of 0.10. While these results are slightly different, they provide evidence the modified bLS does a good job at estimating emissions. Few differences exist between the model formulations, the largest likely being how the new position of a particle that crosses the z_0 boundary is calculated. The significance of this and other differences were not investigated but could be part of future work.

The remaining tests were conducted using a subset of 30 sample periods from the full Texas feedlot dataset described above. Fifteen sample periods were randomly selected from both stable ($L > 0$) and unstable ($L < 0$) conditions. Both bLS and fLS models were run for each period with $N = 50,000$ and using the d_p values in Table 6-1. A range of d_p were selected to test the models' response across a range of v_s . The v_s values

shown in Table 6-1 are the average of the 30 sample periods and change by four orders of magnitude between 1 and 50 μm .

One test examined the number of particle touchdowns and depositions for bLS and fLS results as a function of d_p . In addition to the formula differences between bLS and fLS models, there was a difference in the height agl of the release point (z_{rel}) under normal operation. As shown in Figure 6-5, a difference of a factor of approximately 2 was found between touchdown counts averaged across the sample period subset at $d_p < 10 \mu\text{m}$ for fLS with $z_{rel} = 0.205\text{m}$ and bLS with $z_{rel} = 2.0\text{m}$. Note that the touchdown and deposition results for $d_p = 0.0 \mu\text{m}$ are shown in the graphs at $0.5 \mu\text{m}$ since a value of 0.0 cannot be shown on a log scale. If the bLS model is run with $z_{rel} = 0.205 \text{m}$, the number of average touchdowns is essentially equal to the fLS model for d_p from 0 to $5 \mu\text{m}$, but then approaches the lower values of bLS with $z_{rel} = 2.0 \text{m}$ as d_p increases.

The relative results between models for average deposition counts are very similar to average touchdowns for $d_p < 10 \mu\text{m}$, including the counts for fLS and bLS, with $z_{rel} = 0.205 \text{m}$ being roughly twice as much as depositions for bLS with $z_{rel} = 2.0 \text{m}$. The behavior of deposition counts for $d_p > 10 \mu\text{m}$ is markedly different between the bLS and fLS results. The fLS deposition counts approach 50,000, the maximum number of depositions possible in the fLS model runs because a total of 50,000 particles were

Table 6-1. The d_p and the average v_s values used in configuration testing of the LS models.

d_p (μm)	0	1	2.5	5	10	20	30	40	50
v_s (m s^{-1})	0	6.4×10^{-5}	3.5×10^{-4}	1.3×10^{-3}	5.2×10^{-3}	2.0×10^{-2}	4.6×10^{-2}	8.1×10^{-2}	1.3×10^{-1}

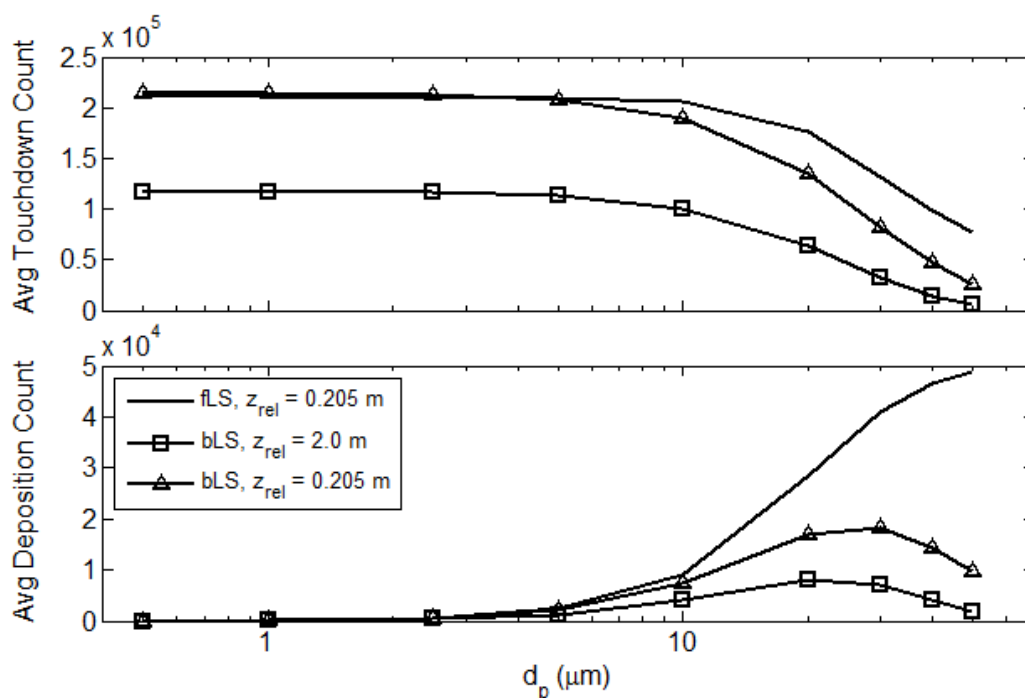


Figure 6-5. Touchdown and deposition counts as a function of d_p for the fLS model and two bLS model runs with different particle release heights (z_{rel}). Note that results at $d_p = 0.5$ μm are actually those for non-depositional case of $d_p = 0.0$ μm as 0.0 μm is not shown on a logarithmic axis.

released. The v_s values at higher d_p become sufficient to overcome nearly all w values and lead to general downward particle movement and near-total deposition with fewer total touchdowns. The same cause leads to slightly different results from the bLS. As v_s increases with increasing d_p , the particles generally move upward due to the use of a $-\Delta t$ in Eq. 6-9, resulting in the bLS number of touchdowns and depositions at $d_p > 10$ μm decreasing relative to the fLS results.

In addition to total counts, the number of touchdowns and depositions as a function of distance from the release point were examined for similarity between the fLS and bLS models. Figure 6-6 presents the average counts as a function of radius,

binned in 100 m intervals, for $d_p = 10 \mu\text{m}$. Note that the left figures give the total touchdown and deposition counts while the right figures show the counts per bin relative to the counts in the 0-100 m bin. The fLS logged more touchdowns and depositions than both bLS models at all radii; both bLS models had similar counts per bin at distances > 100 m and the number of fLS touchdowns was within 10% of the bLS counts for distances > 800 m. Looking at the counts per bin relative to the first bin for both touchdowns and deposition, the bLS and fLS with $z_{rel} = 0.205$ m showed very similar levels. The bLS with $z_{rel} = 2.0$ m had the lowest counts per bin, but recorded higher relative values. Histograms for $d_p < 10 \mu\text{m}$ (not shown) have better agreement between the bLS with $z_{rel} = 0.205$ m and the fLS results, while those for $d_p > 10 \mu\text{m}$ (not shown) have greater divergence between the fLS and bLS models.

The results of these two analyses on touchdown and deposition patterns suggest small differences between touchdowns and depositions from fLS and bLS models with the same z_{rel} for $d_p \leq 10 \mu\text{m}$ and non-depositional cases. In addition, for cases with different z_{rel} values, the touchdown and deposition counts have a similar ratio for $d_p < 10 \mu\text{m}$ and the differences between the two models are strongly influenced by differences in z_{rel} . As d_p increases above $10 \mu\text{m}$, the logarithmically increasing v_s rapidly gains influence on particle motion to yield varying differences between bLS and fLS model results. Therefore, the use of a fLS is recommended for modeling particles with v_s approaching or greater than the magnitude of w . In the case of the feedlot measurements, this effect was noticeable at $d_p = 10 \mu\text{m}$ and strong for $d_p \geq 20 \mu\text{m}$.

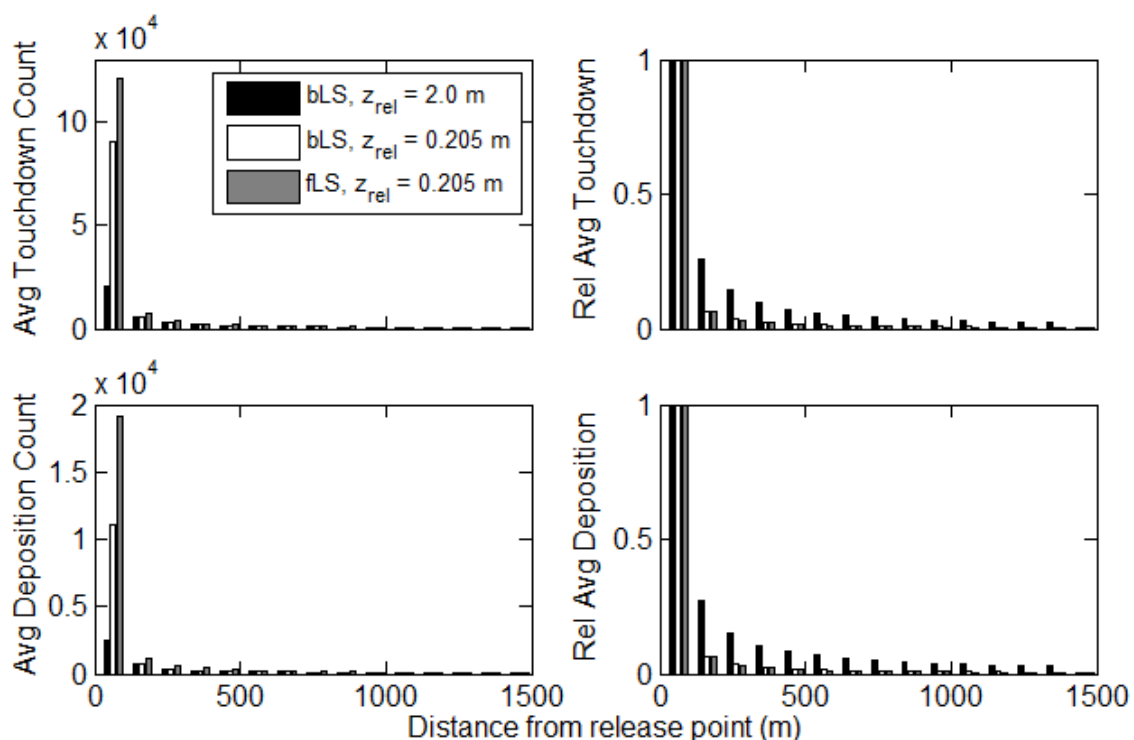


Figure 6-6. Histograms of touchdowns and depositions versus distance from the source volume at $[0,0,z_{rel}]$ for bLS models with $z_{rel} = 2.0$ m and 0.205 m and the fLS with $z_{rel} = 0.205$ m for $d_p = 10$ μm and a bin width of 100 m. The left two graphs show average counts across the subset and the right two figures show average counts per bin relative to the 0-100 m bin.

Another test investigated the number of small, surface-based volume sources (S) needed in the feedlot fLS application to represent the pens like one large source covering each pen. As stated previously, the fLS model was run for a single volume source at $[x,y,z] = [0,0,0.205]$, the resulting t_{res} matrix was applied at each source location, and the overall $(C/Q_{Vol})_{sim}$ value for a given sampler location was calculated using Eq. 6-6. The metric used for this test was the spread of the relative individual $(C/Q_{Vol})_{sim}$ values between the 30 sample periods using a range of source densities (sources per 100 m^2 of pen area) for each d_p . The relative $(C/Q_{Vol})_{sim}$ values for each

sample period were found by dividing the $(C/Q_{Vol})_{sim}$ calculated at each source density by the value from the greatest density tested; a relative value of 1.0 would provide the same answer at the lower source density as at the highest density. Sources were approximately equally spaced within the total source area, with tested densities varying from 0.01 to 33 sources per 100 m². The results are presented in Figure 6-7. Note that the average $(C/Q_{Vol})_{sim}$ ratio approaches 1.0 as source density increases and the density at which all individual sample period ratios are within 10% of 1.0 increases with increasing d_p . For $d_p \leq 20 \mu\text{m}$, all sample period ratios are within 5% of 1.0 by 1.1 sources per 100 m² and within 2% of 1.0 by 6.6 sources per 100 m². Based on this, remaining feedlot applications of the fLS were conducted at a source density value of about 5 sources per 100 m², corresponding to an S value of 38,411, evenly distributed throughout the pen areas.

The final test was to determine how well the bLS $Q_{m, count}$ solution matched the fLS $Q_{m, count}$ solution for the feedlot across the test d_p using the 30 sample subset. The modified fLS was used as the standard based on the good agreement with measured spore concentration profiles and accurate calculated emissions by the fLS in Aylor and Flesch (2001), and all other applications of an LS accounting for v_s and deposition having been fLS formulations (Aylor and Ferrandino, 1989; Aylor and Flesch, 2001; Boehm et al., 2008; McGinn et al., 2010; Wilson, 2000; and others). The $Q_{m, count}$ values were calculated using a particle concentration of 1.0 particles m⁻³ for each d_p .

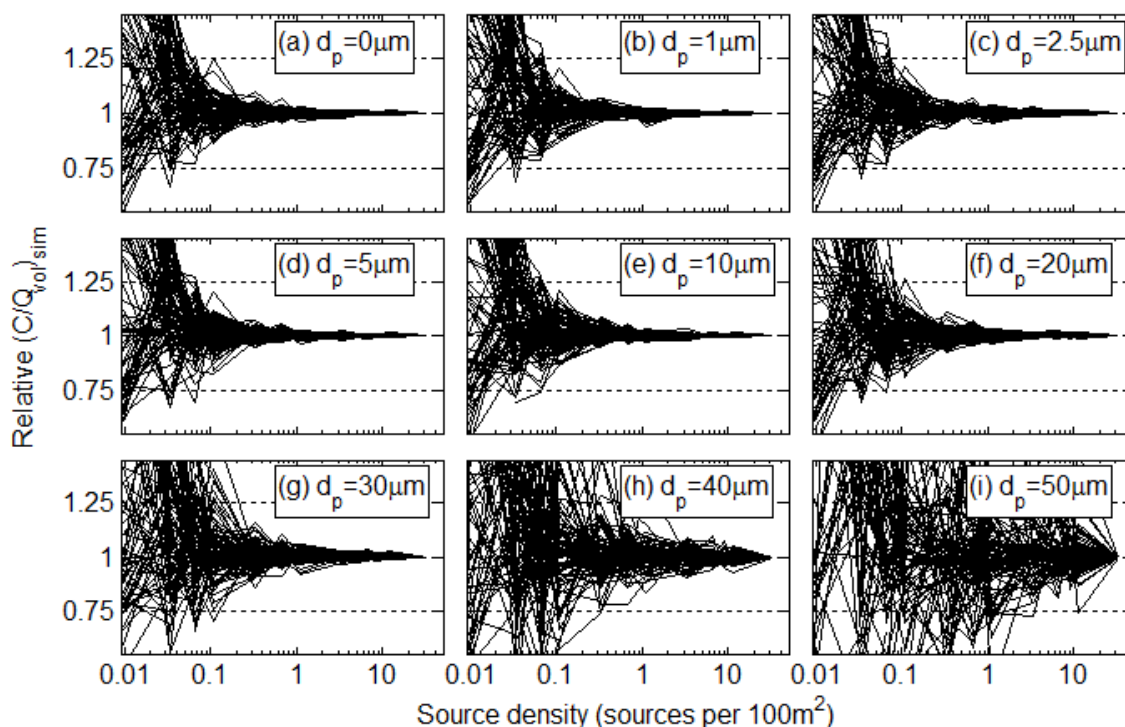


Figure 6-7. The relative fLS $(C/Q_{Vol})_{sim}$ values for randomly selected sample periods for particles with d_p of (a) $0 \mu\text{m}$, (b) $1 \mu\text{m}$, (c) $2.5 \mu\text{m}$, (d) $5.0 \mu\text{m}$, (e) $10 \mu\text{m}$, (f) $20 \mu\text{m}$, (g) $30 \mu\text{m}$, (h) $40 \mu\text{m}$, and (i) $50 \mu\text{m}$. The relative $(C/Q_{Vol})_{sim}$ values were calculated by dividing by the $(C/Q_{Vol})_{sim}$ at each source density by the $(C/Q_{Vol})_{sim}$ at the highest density for each sample period.

The results in plots (a) and (b) of Figure 6-8 show $Q_{m, count}$ for $d_p \leq 10 \mu\text{m}$ nearly equal to $Q_{m, count}$ for the non-depositional case at $d_p = 0.0 \mu\text{m}$ (shown at $0.5 \mu\text{m}$ due to the lack of a zero value on a log scale). The bLS results begin to show departures from the non-depositional values at slightly lower d_p than the fLS. It is interesting to note that $Q_{m, count}$ as Q_{calc} from Eq. 6-1 for the bLS is more similar in shape to the fLS $Q_{m, count}$ than the $Q_{m, count}$ as $Q_{calc, dep}$ from Eq. 6-13 as shown here. This due to the use of the scalar a_{dep} to account for deposition adjustment, which increased logarithmically from 1.00 at $d_p = 2.5 \mu\text{m}$ to average values of 1.01, 1.04, 1.11 and 1.17 at $d_p = 5, 10, 20,$ and $30 \mu\text{m}$,

respectively. Despite the more similar shape of the bLS Q_{calc} , the $Q_{m, count}$ as $Q_{calc, dep}$ is reported in order to directly account for the effects of deposition. $Q_{m, count}$ lines at all d_p were grouped into stable and unstable atmospheric conditions, with the average value lying between them.

The bLS $Q_{m, count}$ were divided by the fLS $Q_{m, count}$ to yield the unitless ratios in Figure 6-8 (c). The ratios were stable between 1.15 and 1.3 for $d_p \leq 10 \mu\text{m}$ and increased in both mean and spread thereafter. The ratio statistics show the bLS model, as herein applied in this subset, yields $Q_{m, count}$ consistently 15-20% higher than the fLS $Q_{m, count}$ for all $d_p \leq 5 \mu\text{m}$, including the non-depositional case. The bLS $Q_{m, count}$ for $d_p = 10 \mu\text{m}$ and 20

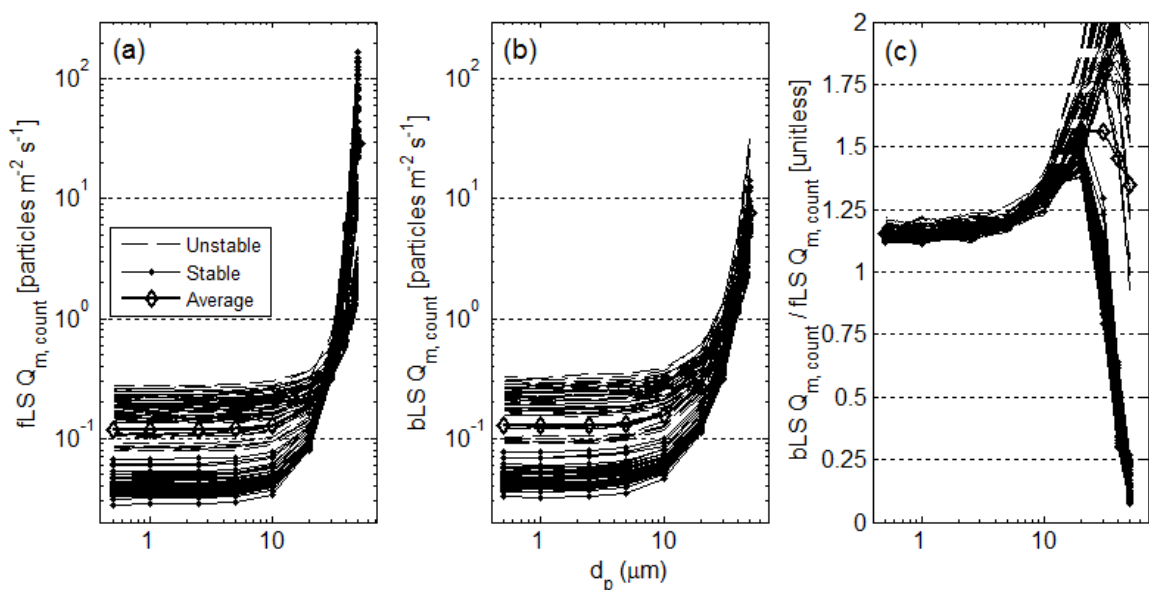


Figure 6-8. Emission rates ($Q_{m, count}$) calculated from the (a) fLS and (b) bLS models as applied to the Texas feedlot for a subset of 30 sample periods and assuming a particle concentration of $1.0 \text{ particles m}^{-3}$ for each d_p . The ratios of the $Q_{m, count}$ are presented in (c) to show comparability for this dataset. Note that results for $d_p = 0.0 \mu\text{m}$ ($v_s = 0.0 \text{ m s}^{-1}$) are shown at $0.5 \mu\text{m}$.

μm were 31% and 56% higher than fLS $Q_{m, count}$. The ratio behavior changes drastically for $d_p > 20 \mu\text{m}$ between the two stability classifications, diverging significantly and bLS results differing from the fLS by factors of up to 10. This could be attributed, at least in part, to the relative sizes of w and v_s at those d_p and the general downward and upward particle movement induced in the fLS and bLS models, respectively, as noted previously in regard to total touchdown and deposition count. The use of the fLS is, therefore, suggested for modeling larger d_p . The upper d_p at which the modified bLS can be effectively used will vary based on particle and meteorological characteristics, as well as other potential factors not investigated here. Based on these results, the bLS is assumed to be valid for $d_p < 20 \mu\text{m}$ for the Texas feedlot used for this study.

Feedlot PM₁₀ Emissions

The Deposition Q_{PM10} and Non-deposition Q_{PM10} values were estimated for each downwind sampling site with an estimated PSD in the 114 sample periods. These values were then grouped by sample period position in a 24-hour day to calculate the diurnal profiles of Q_{PM10} , as shown in Figure 6-9. The bars represent the number of data points in each 30-minute sample period. These were aggregated into 2-hour averages for display and further calculations. Deposition Q_{PM10} was larger at all times, with averaged values ranging from 8% higher around midday to 20% higher in the late evening and middle of the night. Accounting for v_s and deposition is most influential on Q_{PM10} at the highest number concentrations of large particles.

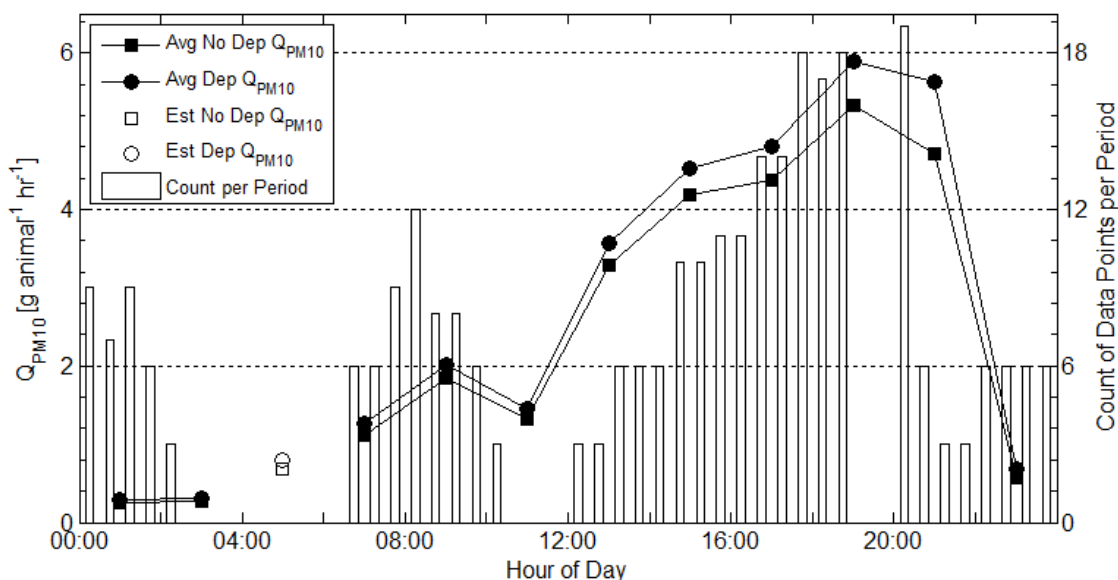


Figure 6-9. Diurnal pattern of calculated Deposition feedlot PM₁₀ emissions (Q_{PM10}) and Non-deposition Q_{PM10} as two hour averages (left axis) and the number of Q_{PM10} values in each half hour sampling period throughout the day (right axis). The empty markers represent the values estimated to fill the 04:00-06:00 data gap.

Diurnal patterns are present in the Q_{PM10} datasets, as was observed in the TEOM PM₁₀ levels during this study and reported in both PM concentrations and Q in other published studies. The maximum values in the evening are approximately a factor of 20 greater than the minimum values estimated in the early morning. The dip present at 10:00-12:00 in both profiles is atypical of smoother patterns reported by others. This may be due to a small sample size ($n = 3$) from a single sample period on June 4. Unfortunately, the meteorological filter removed most, if not all, of the sample periods for early morning (02:00-06:00), midday (10:30-13:00), and during the evening atmospheric transition period from unstable to stable conditions (19:00-20:00), limiting the robustness of the dataset on which these diurnal profiles are based. However, the

pattern consistency with other studies, coupled with the similarity to the measured PM_{10} concentrations, justify its use in calculating an integrated daily emission. The lack of data for the 04:00-06:00 period required estimates to complete the diurnal profile. Using the PM_{10} concentrations shown in Figure 6-3 as a guide, missing values for both the Deposition $Q_{PM_{10}}$ and Non-deposition $Q_{PM_{10}}$ were estimated as the average of the two adjacent data points in each respective dataset. These values are shown in Figure 6-9 as the hollow markers.

The daily summer emissions calculated for this feedlot were 62.5 ± 12.4 g animal⁻¹ day⁻¹ for Deposition $Q_{PM_{10}}$ and 55.9 ± 11.2 g animal⁻¹ day⁻¹ for Non-deposition $Q_{PM_{10}}$. The corresponding surface fluxes were 3.23 ± 0.65 g m⁻² day⁻¹ for Deposition and 2.89 ± 0.58 g m⁻² d⁻¹ for Non-deposition. The integrated Deposition values were 12% higher than the Non-deposition ones. These $Q_{PM_{10}}$ and surface flux values are higher than most found in the literature, as shown in Table 6-2. Note that those from Bonifacio et al. are for 17 or 24 month datasets. The $Q_{PM_{10}}$ at the same level was measured during summer conditions at one of the feedlots investigated by McGinn et al. (2010), which had a $Q_{PM_{10}}$ of 60 g animal⁻¹ d⁻¹. Note that both $Q_{PM_{10}}$ and surface fluxes can vary based on, among other characteristics, measurement technique, emissions estimation technique, stocking density, surface moisture content, feedlot surface type, and manure management.

The uncertainty values in the reported daily $Q_{PM_{10}}$ represent the standard deviation of the spread of the data about the average. The uncertainty of the inverse modeling method using the modified LS model was not quantified. It is not expected to

Table 6-2. Comparison of feedlot PM₁₀ emissions (Q_{PM10}) and surface fluxes calculated in this study with some found in literature.

Source	Q_{PM10} [g animal ⁻¹ d ⁻¹]	Flux [g m ⁻² d ⁻¹]	Notes
<i>This study</i>	62.5 ± 12.4	3.23 ± 0.65	Texas, USA; Summer 2015; Deposition (± 1σ)
	55.9 ± 11.2	2.89 ± 0.58	Texas, USA; Summer 2015; Non-deposition (± 1σ);
McGinn et al., 2010	Feedlot 1 - 60 ± 100 Feedlot 2 - 31 ± 52	Feedlot 1 – 1.45 Feedlot 2 – 1.61	Queensland, Australia; Feb-Mar 2008, Summer; Method – Inverse Modeling with fLS with deposition
Bonifacio et al., 2012	Median Values: Feedlot 1 - 27 Feedlot 2 - 30	Median Values: Feedlot 1 - 1.60 Feedlot 2 - 1.10	Kansas, USA; Jan 2007 – Dec 2008; Method – Inverse Modeling with AERMOD
Bonifacio et al., 2013a	Median Values: 26.0 to 41.3	Median Values: 1.32 to 2.10	Kansas, USA; May 2010 – Sept 2011; Method – Inverse Modeling with AERMOD and WindTrax
Bonifacio et al., 2013b	Median Values: 35.6	Median Values: 1.81	Kansas, USA; May 2010 – Sept 2011; Method – Flux-Gradient

be better than the ±20% standard deviation values from the dataset due the uncertainty contributed by meteorological and PM measurements, parameter calculations, and deviations of modeled dispersion from actual conditions, any one of which could be larger than 20%. Specifically, issues regarding the accuracy of and errors in reported values from typical PM sensors measuring ambient PM near sources with significant mass fractions at $d_p > 5 \mu\text{m}$, such as the TEOM and OPS deployed here, has not been taken into account (for examples, see Auvermann et al., 2006; Buser et al., 2007; and Wanjura et al., 2008). This is beyond the scope of this analysis and could be pursued in future work. Another potential subject of future work is the use of this modified model to test the simulation of dry deposition of gasses.

Conclusions

This manuscript presents the formulation and initial test results of a 3D LS model modified to account for v_s and deposition of particles in order to estimate area/volume source emissions through inverse modeling. The base model is that presented by Flesch et al. (1995, 2004), with changes based on the fLS models of Aylor and Ferrandino (1989), Wilson (2000), and Aylor and Flesch (2001). The modified LS model allows for simulating the dispersion and deposition for particles across a range of d_p , including the non-depositional case of $d_p = 0.0 \mu\text{m}$ ($v_s = 0.0 \text{ m s}^{-1}$). The novel contribution of this work is the development and use of the modified LS in a backward-in-time simulation, including developing an emissions quantification method to account for deposition estimates. The bLS is preferred over the fLS when possible due to significant computational and memory-usage savings.

The modified bLS formulation was run in a non-depositional mode for a subset of the validation dataset from by Flesch et al. (2004). The modified bLS yielded an average emission estimate for the subset that was slightly larger than Flesch et al. but still in close proximity to the actual value and with the same standard deviation. This demonstrated its ability to estimate emissions based on the near-field dispersion simulation.

An initial application of the modified LS model to data collected during the summer at a commercial feedlot also yielded promising results. For a 30 sample subset,

the bLS model yielded similar touchdown and deposition counts to those of the modified fLS for the same z_{rel} and $d_p \leq 10 \mu\text{m}$. Touchdown and deposition counts were reduced relative to the fLS when the bLS release height was set at the higher operational z_{rel} . The bLS consistently yielded emission estimates 1.15 to 1.30 times higher than the fLS model for all tested $d_p \leq 10 \mu\text{m}$, including $d_p = 0.0 \mu\text{m}$. The $Q_{m, count}$ values for $d_p < 5 \mu\text{m}$ in both bLS and fLS were nearly equal to the value at $d_p = 0.0 \mu\text{m}$, suggesting that v_s and deposition were not significant for smaller particles. In addition, the upper d_p limitation for behavioral consistency between bLS and fLS results was found to be about $20 \mu\text{m}$ in this test scenario, above which they produced very different results. The test results suggest that for $d_p < 20 \mu\text{m}$ the bLS may be used to simulate dispersion of particles. This is the range of interest when estimating Q of $\text{PM}_{2.5}$ or PM_{10} .

The daily summer mean $Q_{\text{PM}_{10}}$ values were estimated using both deposition-enabled and non-depositional model runs. The Deposition $Q_{\text{PM}_{10}}$ was $62.5 \pm 12.4 \text{ g animal}^{-1} \text{ day}^{-1}$, 12% larger than the $55.9 \pm 11.2 \text{ g animal}^{-1} \text{ day}^{-1}$ calculated for Non-deposition $Q_{\text{PM}_{10}}$. These are higher than $Q_{\text{PM}_{10}}$ in the literature based on year-round sampling but are similar to that reported for another summer-only sample period. The diurnal profiles show Deposition $Q_{\text{PM}_{10}}$ was always larger than Non-deposition $Q_{\text{PM}_{10}}$, with a range of 8% to 20%. Calculated diurnal profiles were similar to those previously reported.

Acknowledgments

The research reported in this paper is partially based upon work supported by the USDA, Cooperative Agreement No. 58-3625-9-743 and by a project under Texas A&M AgriLife Research titled "Measuring Path-Averaged PM Concentrations Over Intermediate Path Lengths." Both funding sources contributed to part of the technical development, data analysis, and manuscript preparation, with Texas A&M AgriLife Research funding data collection. Any opinions, findings, conclusions, or recommendations expressed in this paper are those of the writers and do not necessarily reflect the view of the USDA, Texas A&M AgriLife Research, or Space Dynamics Laboratory. The writers thank the team involved in conducting field work and the cooperating producers for permission to perform the study. Mention of a trademark, proprietary product, or vendor is for information purposes only and does not constitute an endorsement by the USDA, Utah State University, Texas A&M AgriLife Research, or Space Dynamics Laboratory.

References

- Auvermann, B., R. Bottcher, A. Heber, D. Meyer, C.B. Parnell, B. Shaw, and J. Worley. 2006. "Particulate matter emissions from animal feeding operations," p 435-468, in: Rice, J.M., D.F. Caldwell, and F.J. Humenik, eds., *Animal Agriculture and the Environment: National Center for Manure and Animal Waste Management White Papers*. St. Joseph, Michigan: American Society of Agricultural and Biological Engineers, Pub. Number 913C0306.
- Aylor, D.E., M.T. Boehm, and E.J. Shields. 2006. Quantifying aerial concentrations of maize pollen in the atmospheric surface layer using remote-piloted airplanes and

- Lagrangian stochastic modeling. *Journal of Applied Meteorology and Climatology*, 45:1003-1015.
- Aylor, D.E., and F.J. Ferrandino. 1989. Dispersion of spores released from an elevated line source within a wheat canopy. *Boundary-Layer Meteorology*, 46:251-273.
- Aylor, D.E., and T.K. Flesch. 2001. Estimating spore release rates using a Lagrangian stochastic simulation model. *Journal of Applied Meteorology*, 40:1196-1208.
- Bjorneberg, D.L., A.B. Leytem, D.T. Westermann, P.R. Griffiths, L. Shao, and M.J. Pollard. 2009. Measurement of atmospheric ammonia, methane, and nitrous oxide at a concentrated dairy production facility in southern Idaho using open-path FTIR spectrometry. *Transactions of the ASABE*, 52:1749-1756.
- Boehm, M.T., and D.E. Aylor. 2005. Lagrangian stochastic modeling of heavy particle transport in the convective boundary layer. *Atmospheric Environment*, 39:4841-4850.
- Boehm, M.T., D.E. Aylor, and E.J. Shields. 2008. Maize pollen dispersal under convective conditions. *Journal of Applied Meteorology and Climatology*, 47:291-307.
- Bonifacio, H.F., R.G. Maghirang, B.W. Auvermann, E.B. Razote, J.P. Murphy, and J.P. Harner III. 2012. Particulate matter emission rates from beef cattle feedlots in Kansas – reverse dispersion modeling. *Journal of the Air & Waste Management Association*, 62:350-361.
- Bonifacio, H.F., R.G. Maghirang, E.B. Razote, S.L. Trabue, and J.H. Prueger. 2013a. Comparison of AERMOD and WindTrax dispersion models in determining PM10 emission rates from a beef cattle feedlot. *Journal of the Air and Waste Management Association*, 63:545-556.
- Bonifacio, H.F., R.G. Maghirang, S.L. Trabue, L.L. McConnell, J.H. Prueger, and E.B. Razote. 2013b. Particulate emissions from a beef cattle feedlot using the flux-gradient technique. *Journal of Environmental Quality*, 42:1341-1352.
- Buser, M.D., C.B. Parnell, B.W. Shaw, and R.E. Lacey. 2007. Particulate matter sampler errors due to the interaction of particle size and sampler performance characteristics: background and theory. *Transactions of ASABE*, 50:221-228.
- Cimorelli, A.J., S.G. Perry, A. Venkatram, J.C. Weil, R.J. Paine, R.B. Wilson, R.F. Lee, W.D. Peters, and R.W. Brode. 2005. AERMOD: A dispersion model for industrial source

applications. Part I: General model formulation and boundary layer characterization. *Journal of Applied Meteorology*, 44:682-693.

- Cowherd, C. 2005. Chapter 28: Fugitive dust emissions. In *Aerosol Measurement: Principles, Techniques, and Applications*, 845-858. 2nd ed. P. A. Baron and K. Willeke, eds. Hoboken, N.J.: John Wiley and Sons.
- Dyer, A.J. 1974. A review of flux-profile relationships. *Quarterly Journal of the Royal Meteorological Society*, 96:715-721.
- Dyer, A.J., and B.B. Hicks. 1970. Flux-gradient relationships in the constant flux layer. *Quarterly Journal of the Royal Meteorological Society*, 96:715-721.
- Flesch, T.K., J.D. Wilson, and E. Yee. 1995. Backward-time Lagrangian stochastic dispersion models and their application to estimate gaseous emissions. *Journal of Applied Meteorology*, 34:1320-1332.
- Flesch, T.K., J.D. Wilson, L.A. Harper, B.P. Crenna, and R.R. Sharpe. 2004. Deducing ground-to-air emissions from observed trace gas concentrations: a field trial. *Journal of Applied Meteorology*, 43: 487-502.
- Flesch, T.K., J.D. Wilson, L.A. Harper, R.W. Todd, N.A. Cole. 2007. Determining ammonia emissions from a cattle feedlot with an inverse dispersion technique. *Agricultural and Forest Meteorology*, 144:139-155.
- Flesch, T.K., L.A. Harper, J.M. Powell, and J.D. Wilson. 2009. Inverse-dispersion calculation of ammonia emissions from Wisconsin dairy farms. *Transactions of the ASABE*, 52:253-265.
- Hanna, S.R., and B. Chowdhury. 2014. Minimum turbulence assumptions and u^* and L estimation for dispersion models during low-wind stable conditions. *Journal of the Air & Waste Management Association*, 64:309-321.
- Hinds, W. C. 1999. *Aerosol Technology: Properties, Behavior, and Measurement of Airborne Particles*, 2nd Edition. John Wiley & Sons, New York. Pp. 233-242.
- Leytem, A.B., R.S. Dungan, and D.L. Bjorneberg. 2009. Case study: Seasonal and spatial distribution of ambient ammonia concentrations measured at a large open-lot dairy. *Professional Animal Science*, 25:786-793.

- Leytem, A.B., R.S. Dungan, D.L. Bjorneberg, and A.C. Koehn. 2011. Emissions of ammonia, methane, carbon dioxide, and nitrous oxide from dairy cattle housing and manure management systems. *Journal of Environmental Quality*, 40:1383-1394.
- Leytem, A.B., R.S. Dungan, D.L. Bjorneberg, and A.C. Koehn. 2013. Greenhouse gas and ammonia emissions from an open-freestall dairy in southern Idaho. *Journal of Environmental Quality*, 42:10-20.
- Lin, J., D. Brunner, C. Gerbig, A. Stohl, A. Luhar, and P. Webley. 2012. Lagrangian Modeling of the Atmosphere, Geophysical Monograph Series 200. American Geophysical Union, Washington, DC.
- McGinn, S.M., T.K. Flesch, D. Chen, B. Crenna, O.T. Denmead, T. Naylor, D. Rowell. 2010. Coarse particulate matter emissions from cattle feedlots in Australia. *Journal of Environmental Quality*, 39:791-798.
- Prueger, J.H., and W.P. Kusta. 2005. Aerodynamic methods for estimating turbulent fluxes, p. 407-436, in: J.L. Hatfield and J.M. Baker, eds., *Micrometeorology in Agricultural Systems*, Agronomy Monograph 47; American Society of Agronomy, Crop Science Society of Agronomy, Soil Science Society of America, Madison, WI, USA.
- Purdy, C.W., R.N. Clark, and D.C. Straus. 2007. Analysis of aerosolized particulates of feedyards located in the Southern High Plains of Texas. *Aerosol Science and Technology*, 41:497-509.
- Sawford, B.L., and F.M. Guest. 1991. Lagrangian statistical simulation of the turbulent motion of heavy particles. *Boundary Layer Meteorology*, 54:147-166.
- Sweeten, J.M., C.B. Parnell, Jr., V.W. Shaw, and B.W. Auvermann. 1998. Particle size distribution of cattle feedlot dust emission. *Transactions of the ASAE*, 41:1477-1481.
- Thomson, D.J. 1987. Criteria for the selection of stochastic models of particle trajectories in turbulent flows. *Journal of Fluid Mechanics*, 180:529-556.
- Todd, R.W., N.A. Cole, R.N. Clark, T.K. Flesch, L.A. Harper, and B.H. Baek. 2008. Ammonia emissions from a beef cattle feedyard on the southern High Plains. *Atmospheric Environment*, 42:6797-6805.

- Todd, R.W., N.A. Cole, G.R. Hagevoort, K.D. Casey, and B.W. Auvermann. 2015. Ammonia losses and nitrogen partitioning at a southern High Plains open lot dairy. *Atmospheric Environment*, 110:75-83.
- Upadhyay, J.K., B.W. Auvermann, A.N. Paila, and N. Hiranuma. 2008. Open-path transmissometry to determine atmospheric extinction efficiency associated with feedyard dust. *Transactions of the ASABE*, 51:1433-1441.
- Wang, J., A.L. Hiscox, D.R. Miller, T.H. Meyer, T.W. Sammis. 2008. A dynamic Lagrangian, field-scale model of dust dispersion from agricultural tilling operations. *Transactions of the ASABE*, 51:1763-1774.
- Wanjura, J.D., B.W. Shaw, C.B. Parnell, R.E. Lacey, and S.C. Capareda. 2008. Comparison of continuous monitor (TEOM) and gravimetric sampler particulate matter concentrations. *Transactions of the ASABE*, 51:251-257.
- Wilson, J.D. 2000. Trajectory models for heavy particles in atmospheric turbulence: comparisons with observations. *Journal of Applied Meteorology*, 39:1894-1912.

CHAPTER 7

CONCLUSIONS

The purposes of this dissertation work were to enhance the methods and tools available for measuring air pollution emissions from large agricultural sources and to quantify emissions for different agricultural processes/operations. These were accomplished through work presented in a collection of five chapters that were papers submitted to peer-reviewed scientific journals for publication. Each paper makes a contribution to methodology, reports emissions estimates based on field data, or both. This work was carried out through the Ag Program at the Space Dynamics Laboratory and Utah State University, in part accomplishing two of the program's purposes of improving emissions quantification methods and determining the effectiveness of management practices and control technologies to reduce air emissions.

The first paper described the mass conversion factor (MCF) and demonstrated its usefulness in Ag Program activities. The MCF is a simple, empirical relationship between collocated optical and mass concentration measurements that can be used to convert optical measurements to PM concentrations. The MCF allows PM concentration dynamics to be investigated at the optical instrument's finer sampling resolution. The MCF also enables the use of an elastic backscatter lidar, like Aglite, to quantify PM mass concentrations and emissions over a much greater spatial extent (100s to 1,000s of m), both horizontally and vertically, and at both finer spatial and temporal scales than

possible with point sensors alone. This paper provides examples of how the MCF and lidar together provide greater insight into PM concentration and emission dynamics.

The next two papers utilize the MCF to produce PM mass-calibrated OPC and Aglite lidar, which are used to estimate the emissions control efficiency of agricultural tillage management practices that are designed to reduce total emissions, referred to as Conservation Management Practices (CMP). The first field study measured emissions from fall tillage operations after a row crop harvest for the traditional management practice and the combined operations CMP. The traditional method made six passes across the field and the CMP made two passes. Emissions were calculated using a mass balance applied to the PM-calibrated lidar data and inverse modeling in combination with filter based PM measurements. The results showed the combined operations CMP reduced PM_{2.5} emissions by 29%, PM₁₀ emissions by 60%, and TSP emissions by 25%. The lidar provided a full set of emissions estimates even when the point sensors were unable to resolve downwind impacts in a couple of instances. In addition, the lidar observed plumes far above the sampling heights of the point sensors, plumes not reproduced by in inverse modeling.

The other tillage study compared operations in spring tillage after harvest of a winter wheat and in preparation for planting corn. The traditional method consisted of nine different operations with a total of 13 passes over the field. The conservation tillage CMP, designed to reduce the field area disturbed through tillage by >80%, was comprised of three operations in three passes. Issues with sampler maintenance after

exposure to some high-intensity plumes and windblown dust contaminated nearly one third of the downwind filter samples. Therefore, PM emissions were estimated using the PM-calibrated lidar and OPC datasets through the mass balance and inverse modeling approaches, respectively. The conservation tillage CMP reduced emissions by approximately 90% for PM_{2.5}, PM₁₀, and TSP. The lidar provided more evidence of the temporally and spatially non-homogeneous nature of tillage plumes.

The third emissions study was for summer time NH₃ from an open-lot dairy in the SJV of California. Despite having 20% of the national dairy herd, only one previous NH₃ emissions study had previously been conducted in the state of California, and that study was performed during winter months on a dairy with similar management practices. NH₃ does not have a NAAQS, but it reacts with other gases in the atmosphere to form particles and has been shown to be an important factor in SJV PM. Concentration measurements were collected using passive samplers and open path-Fourier transform infrared spectrometers (OP-FTIR). The OP-FTIR on the downwind side of the facility measured NH₃ along multiple paths in a repeating series with a scanning system, the first known implementation of such a system with OP-FTIR. Inverse modeling was performed with AERMOD to estimate atmospheric dispersion, which was then combined with the two NH₃ concentration datasets to estimate the emissions using a least sum of squares optimization approach. This approach yielded NH₃ emissions of $140.7 \pm 42.5 \text{ g d}^{-1} \text{ animal}^{-1}$ ($113.5 \pm 34.3 \text{ g d}^{-1} \text{ AU}^{-1}$) from the passive

sampler data and $199.2 \pm 22.0 \text{ g d}^{-1} \text{ animal}^{-1}$ ($160.8 \pm 17.8 \text{ g d}^{-1} \text{ AU}^{-1}$) from OP-FTIR data, both within the range of summer time values reported for other open lot U.S. dairies.

The last paper presented the formulation and initial testing of a Lagrangian stochastic (LS) atmospheric dispersion model that accounts for a particle's deviation from the behavior of the carrier fluid due to settling velocity and deposition. While the modified model was based on work by others, this is the first instance in published literature where a deposition-enabled LS was run in both forward-in-time (fLS) and backward-in-time (bLS) configurations – all other such models are exclusively fLS. Initial testing of the modified bLS demonstrated its ability to estimate emissions through inverse modeling, yielding an average estimated-to-known emission ratio of 1.15 for a validation dataset when run in a non-deposition mode. Testing of the fLS and bLS on a subset of a PM dataset collected at a commercial beef feedlot revealed the bLS has an upper particle size limitation of about $20 \mu\text{m}$ for results to be consistent with the fLS. Behaviors between the model configurations diverged dramatically above this diameter. The impact of accounting for settling velocity and deposition in the bLS was an enhancement of between 8% and 20% throughout the diurnal PM_{10} emissions profile over the non-depositional run. The deposition-enabled daily emissions were $62.5 \pm 12.4 \text{ g animal}^{-1} \text{ day}^{-1}$, 12% larger than the $55.9 \pm 11.2 \text{ g animal}^{-1} \text{ day}^{-1}$ calculated for the non-deposition case.

In summary, contributions to the knowledge and practice of the science of measuring emissions from large area sources made in this dissertation include the

description and examples of applying the MCF, a demonstration of the ability of the lidar to observe and measure tillage emissions plumes not reproduced in the air dispersion model, the use of a scanning system with the OP-FTIR to measure NH_3 levels downwind of a dairy, and the results showing the deposition-enabled bLS yielded similar results as the fLS for particles $\leq 20 \mu\text{m}$. In addition, the tillage study papers present two more examples of the application of the mass balance method to PM-calibrated lidar data to estimate emissions. The lidar produced a full dataset when the deployed point sensors were unable to do so. These papers also contributed emissions estimates of agricultural operations to literature. The fall tillage study yielded the first set of emissions reduction measurements for the combined operations CMP and the spring tillage study confirmed results from a similar study; both herein reported showed significant reductions in PM emissions by the investigated CMPs. The NH_3 emissions value were the first reported for a California dairy during the summer, helping to provide a better picture of yearly emissions. The last paper reported summer time emissions from a beef feedlot in Texas, contrasting calculated emissions when particle behavior is taken into account versus when it is not.

CHAPTER 8

ENGINEERING SIGNIFICANCE

The work described in this dissertation advances scientific knowledge in the field of emissions measurement and estimation, particularly for large area sources. The use of the MCF allows PM_k to be calculated with optical instruments, including an elastic lidar system. This was key to developing the mass balance approach to estimate emissions with the Aglite elastic backscatter lidar, as applied in the papers examining emissions from agricultural tillage operations. The tillage PM emission control efficiency studies provided measurements of the reductions in PM emissions, which can replace estimated values previously used in CMP rule development. The dairy NH_3 emissions study represents the first peer-reviewed publication of the scanning OP-FTIR system, as well as presenting significant improvements over previous Ag Program analyses in the inverse modeling methodology (data filtering; optimization of data fitting using least sum of squares; and using multiple sources). In addition, this was the first published summer time NH_3 emissions study from the state of California; combined with the winter time value from literature, an estimate of the yearly average NH_3 emissions can be calculated. The last paper presents the first bLS model found in literature that accounts for settling velocity and deposition – other LS models accounting for these terms in order to model particle dispersion are fLS models. In addition, the results of evaluating the modified bLS with a validation dataset have shown it estimates emissions

well in near-field inverse modeling. Another important finding of testing the modified bLS was that the modified bLS may be used in inverse modeling for $d_p < 20 \mu\text{m}$. Accounting for deposition in the feedlot dataset increased emissions by 8% to 20% in the diurnal emissions cycle, with the daily emission rate being 12% greater than the non-depositional case.

APPENDICES

Appendix A: Data

The data supporting the published papers is not supplied in this document due to the enormous amount collected. In addition, some datasets require approval for release from the Space Dynamics Laboratory. Interested parties should contact the author, Kori Moore, at kori.moore@sdl.usu.edu.

Appendix B: Journal Copyright Releases

Paper #1: Response from Journal of Environmental Engineering

July 3, 2017

Kori Moore

To the Permissions Editor:

I am in the process of preparing my dissertation in the Department of Civil and Environmental Engineering at Utah State University. I hope to complete my degree program in August 2017.

The article "Derivation and use of simple relationships between aerodynamic and optical aerosol measurements," of which I am first author, and which appeared in the Journal of Environmental Engineering in 2015, Volume 141 and document number 04014078, reports an essential part of my dissertation research. I would like permission to reprint it as a chapter in my dissertation, which may require some revision. Please note that USU sends every dissertation to ProQuest to be made available for reproduction.

I will include acknowledgment to the article on the first page of the chapter, as shown below. Copyright and permission information will be included in a special appendix. Please let me know if you would like a different acknowledgment.

Please indicate your approval of this request by signing in the space provided, and attach any other form necessary to confirm permission. If you charge a reprint fee for use of an article by the author, please indicate that as well.

If you have any questions, please contact me at the phone number or email below. Thank you for your assistance.

Kori Moore

kori.moore@sdl.usu.edu

(435) 890-8306

I hereby give permission to Kori Moore to reprint the requested article in his dissertation, with the following acknowledgment:

"Citation: Moore, K.D., R.S. Martin, W.J. Bradford, C.C. Marchant, D.S. Jones, M.D. Wojcik, R.L. Pfeiffer, J.H. Prueger, and J.L. Hatfield. 2015. Derivation and use of simple relationships between aerodynamic and optical ^{aerosol} ~~particle~~ measurements. Journal of Environmental Engineering, 141:04014078."

Signed: _____

Date: 7/5/17

Fee: N/A

Leslie Connelly, ASCE
Marketing Coordinator
703-295-6169
PERMISSIONS@asce.org
<http://ascelibrary.org/page/rightsrequests>

Paper #2: Response from Journal of Environmental Quality

June 14, 2017

Kori Moore

To the Permissions Editor:

I am in the process of preparing my dissertation in the Department of Civil and Environmental Engineering at Utah State University. I hope to complete my degree program in August 2017.

The article "Particulate emissions calculations from fall tillage operations using point and remote sensors," of which I am first author, and which appeared in the Journal of Environmental Quality in 2013, Volume 42, pages 1029-1038, reports an essential part of my dissertation research. I would like permission to reprint it as a chapter in my dissertation, which may require some revision. Please note that USU sends every dissertation to ProQuest to be made available for reproduction.

I will include acknowledgment to the article on the first page of the chapter, as shown below. Copyright and permission information will be included in a special appendix. Please let me know if you would like a different acknowledgment.

Please indicate your approval of this request by signing in the space provided, and attach any other form necessary to confirm permission. If you charge a reprint fee for use of an article by the author, please indicate that as well.

If you have any questions, please contact me at the phone number or email below. Thank you for your assistance.

Kori Moore
kori.moore@sdl.usu.edu
(435) 890-8306

I hereby give permission to Kori Moore to reprint the requested article in his dissertation, with the following acknowledgment:

"Citation: Moore, K.D., M.D. Wojcik, R.S. Martin, C.C. Marchant, G.E. Bingham, R.L. Pfeiffer, J.H. Prueger, and J.L. Hatfield. 2013. Particulate emissions calculations from fall tillage operations using point and remote sensors. Journal of Environmental Quality, 42:1029-1038."

Signed: Abby Morrison

Date: 6/14/17

Fee: _____

Paper #3: Response from Journal of Applied Remote Sensing

June 14, 2017

Kori Moore

To the Permissions Editor:

I am in the process of preparing my dissertation in the Department of Civil and Environmental Engineering at Utah State University. I hope to complete my degree program in August 2017.

The article "Particulate matter emission estimates from agricultural Spring tillage operations using lidar and inverse modeling," of which I am first author, and which appeared in the Journal of Applied Remote Sensing in 2015, Volume 9 and document number 096066, reports an essential part of my dissertation research. I would like permission to reprint it as a chapter in my dissertation, which may require some revision. Please note that USU sends every dissertation to ProQuest to be made available for reproduction.

I will include acknowledgment to the article on the first page of the chapter, as shown below. Copyright and permission information will be included in a special appendix. Please let me know if you would like a different acknowledgment.


Please indicate your approval of this request by signing in the space provided, and attach any other form necessary to confirm permission. If you charge a reprint fee for use of an article by the author, please indicate that as well.

If you have any questions, please contact me at the phone number or email below. Thank you for your assistance.

Kori Moore
kori.moore@sdl.usu.edu
(435) 890-8306

I hereby give permission to Kori Moore to reprint the requested article in his dissertation, with the following acknowledgment:

"Citation: Moore, K.D., M.D. Wojcik, R.S. Martin, C.C. Marchant, D.S. Jones, W.J. Bradford, G.E. Bingham, R.L. Pfeiffer, J.H. Prueger, and J.L. Hatfield. 2015. Particulate-matter emission estimates from agricultural spring-tillage operations using LIDAR and inverse modeling. Journal of Applied Remote Sensing, 9: 096066."

Signed:  SPE Publisher's permission is hereby granted under the following conditions: (1) you obtain permission of the author(s); (2) the material to be used has appeared in our publication without credit or acknowledgment to another source; and (3) you credit the original SPIE publication. Include the authors' names, title of paper, volume title, SPIE volume number, and year of publication in your Fee: _____ credit statement.

Director of Publications
SPIE
PO Box 10, Bellingham, WA 98227-0010 USA
360/676-3290 (Pacific Time) eric@spie.org

Eric Peppers, Director of Publications

Date

6/14/17

Paper #4: Response from Transactions of the ASABE

July 3, 2017

Kori Moore

To the Permissions Editor:

I am in the process of preparing my dissertation in the Department of Civil and Environmental Engineering at Utah State University. I hope to complete my degree program in August 2017.

The article "Ammonia measurements and emissions from a California dairy using point and remote sensors," of which I am first author, and which appeared in the Transactions of ASABE journal in 2014, Volume 57, pages 181-198, reports an essential part of my dissertation research. I would like permission to reprint it as a chapter in my dissertation, which may require some revision. Please note that USU sends every dissertation to ProQuest to be made available for reproduction.

I will include acknowledgment to the article on the first page of the chapter, as shown below. Copyright and permission information will be included in a special appendix. Please let me know if you would like a different acknowledgment.

Please indicate your approval of this request by signing in the space provided, and attach any other form necessary to confirm permission. If you charge a reprint fee for use of an article by the author, please indicate that as well.

If you have any questions, please contact me at the phone number or email below. Thank you for your assistance.

Kori Moore

kori.moore@sdl.usu.edu

(435) 890-8306

I hereby give permission to Kori Moore to reprint the requested article in his dissertation, with the following acknowledgment:

"Citation: Moore, K.D., E. Young, C. Gurell, M.D. Wojcik, R.S. Martin, G.E. Bingham, R.L. Pfeiffer, J.H. Prueger, J.L. Hatfield. 2014. Ammonia measurements and emissions from a California dairy using point and remote sensors. Transactions of the ASABE, 57:181-198."

Signed: Glenn Laing

Date: 5 July 2017

Fee: None

Paper #5: Response from Atmospheric Environment

July 3, 2017

Kori Moore

To the Permissions Editor:

I am in the process of preparing my dissertation in the Department of Civil and Environmental Engineering at Utah State University. I hope to complete my degree program in August 2017.

The article "Using a deposition-enabled backward Lagrangian stochastic model to estimate particulate matter area source emissions through inverse modeling," of which I am first author, and which was submitted to the Atmospheric Environment journal in April 2017 and given the manuscript reference number ATMENV-D-17-00675, reports an essential part of my dissertation research. I would like permission to reprint it as a chapter in my dissertation, assuming it is eventually accepted and printed in Atmospheric Environment. Inclusion in my dissertation may require some revision. Please note that USU sends every dissertation to ProQuest to be made available for reproduction.

I will include acknowledgment to the article on the first page of the chapter, as shown below. Copyright and permission information will be included in a special appendix. Please let me know if you would like a different acknowledgment.

Please indicate your approval of this request by signing in the space provided, and attach any other form necessary to confirm permission. If you charge a reprint fee for use of an article by the author, please indicate that as well.

If you have any questions, please contact me at the phone number or email below. Thank you for your assistance.

Kori Moore

kori.moore@sdl.usu.edu

(435) 890-8306

I hereby give permission to Kori Moore to reprint the requested article in his dissertation, with the following acknowledgment, and assuming it will be accepted and printed in Atmospheric Environment:

"Citation: Moore, K.D., R.S. Martin, M.D. Wojcik, B. Auvermann, J.H. Prueger, J.L. Hatfield. Using a deposition-enabled backward Lagrangian stochastic model to estimate particulate matter area source emissions through inverse modeling. Atmospheric Environment, submitted."

Signed: _____

Date: _____

Fee: _____

From: oxfordcopyrights (ELS)
To: [Kori Moore](#)
Subject: RE: permissions request for dissertation
Date: Wednesday, July 12, 2017 4:00:04 AM

Dear Kori Moore,

Thank you for your query. It has been forwarded to me as my team handles copyrights at Elsevier.

I understand your article is yet to be accepted for publication, this would mean that Elsevier would yet to have any rights transferred regards to your manuscript. We do not generally consider thesis to constitute prior publication of a kind that would prohibit our acceptance of an article. However this is subject to individual editorial policy, and therefore you should check with the journal you have submitted your article to, if you are planning to publish the article in your thesis before you have received confirmation regards to your submission.

If your article is accepted for publication, Elsevier author rights would apply. Please see the following link to the retained author rights:

<https://www.elsevier.com/about/company-information/policies/copyright>

If you click "personal use" a pop-up window will appear.

- It would be your author retained right to include your article in a thesis or dissertation (provided that this is not to be published commercially)

If you are including the manuscript in your thesis we would recommend you to acknowledge that the article is currently "submitted to" particular Elsevier journal. Later on, if your article is accepted for publication, this information is advised to be updated with an appropriate acknowledgement to the publication.

Please do not hesitate to contact me should you require any further assistance in this matter.

Sergio Oreni Gordillo

Right Associate - Global Rights Department | ELSEVIER |
The Boulevard | Langford Lane | Kidlington | Oxford OX5 1GB |
Tel: [+44 1865 843325](tel:+441865843325) Fax: [+44 1865 853333](tel:+441865853333)
s.orenigordillo@elsevier.com

From: Kori Moore [<mailto:Kori.Moore@sdl.usu.edu>]
Sent: Monday, July 03, 2017 6:23 PM
To: Permissions Helpdesk
Subject: permissions request for dissertation

Appendix C: Permission-to-Use Letters from Coauthors

Brent Auvermann

November 30, 2017

Brent Auvermann, PhD
Center Director
Texas A&M AgriLife Research and Extension Center at Amarillo
6500 Amarillo Boulevard West
Amarillo, TX 79106

Dear Dr. Auvermann,

I am writing to request permission to use the journal article published by our group and identified below as a piece of my dissertation. As per Utah State University policy, all coauthors must grant permission to use each manuscript in a thesis/dissertation. If you agree, please sign below and return this document to me via email. Thank you for your time.

Kori

Kori Moore
Scientist
Space Dynamics Laboratory
1695 North Research Park Way
North Logan, UT 84341
kori.moore@sdl.usu.edu

I hereby grant permission to Kori Moore to use the following published journal article as part of his dissertation:

- Moore, K.D., R.S. Martin, M.D. Wojcik, B. Auvermann, J.H. Prueger, J.L. Hatfield. Using a deposition-enabled backward Lagrangian stochastic model to estimate particulate matter area source emissions through inverse modeling. Atmospheric Environment, submitted.

X

Dr. Brent Auvermann

Gail Bingham

November 30, 2017

Gail Bingham, PhD
SDL Chief Scientist (Ret)

Dear Dr. Bingham,

I am writing to request permission to use the journal articles published by our group and identified below as pieces of my dissertation. As per Utah State University policy, all coauthors must grant permission to use each manuscript in a thesis/dissertation. If you agree, please sign below and return this document to me via email. Thank you for your time.

Kori

Kori Moore
Scientist
Space Dynamics Laboratory
1695 North Research Park Way
North Logan, UT 84341
kori.moore@sdl.usu.edu

I hereby grant permission to Kori Moore to use the following published journal articles as part of his dissertation:

- Moore, K.D., M.D. Wojcik, R.S. Martin, C.C. Marchant, G.E. Bingham, R.L. Pfeiffer, J.H. Prueger, and J.L. Hatfield. 2013. Particulate emissions calculations from fall tillage operations using point and remote sensors. *Journal of Environmental Quality*, 42:1029-1038.
- Moore, K.D., E. Young, C. Gurell, M.D. Wojcik, R.S. Martin, G.E. Bingham, R.L. Pfeiffer, J.H. Prueger, J.L. Hatfield. 2014. Ammonia measurements and emissions from a California dairy using point and remote sensors. *Transactions of the ASABE*, 57:181-198.
- Moore, K.D., M.D. Wojcik, R.S. Martin, C.C. Marchant, D.S. Jones, W.J. Bradford, G.E. Bingham, R.L. Pfeiffer, J.H. Prueger, and J.L. Hatfield. 2015b. Particulate-matter emission estimates from agricultural spring-tillage operations using LIDAR and inverse modeling. *Journal of Applied Remote Sensing*, 9:096066.

X

Dr. Gail Bingham

William Bradford

November 30, 2017

William Bradford
Campbell Scientific, Inc.
815 West 1800 North
Logan, UT 84321

Dear Mr. Bradford,

I am writing to request permission to use the journal articles published by our group and identified below as pieces of my dissertation. As per Utah State University policy, all coauthors must grant permission to use each manuscript in a thesis/dissertation. If you agree, please sign below and return this document to me via email. Thank you for your time.

Kori

Kori Moore
Scientist
Space Dynamics Laboratory
1695 North Research Park Way
North Logan, UT 84341
kori.moore@sdl.usu.edu

I hereby grant permission to Kori Moore to use the following published journal articles as part of his dissertation:

- Moore, K.D., R.S. Martin, W.J. Bradford, C.C. Marchant, D.S. Jones, M.D. Wojcik, R.L. Pfeiffer, J.H. Prueger, and J.L. Hatfield. 2015a. Derivation and use of simple relationships between aerodynamic and optical aerosol measurements. *Journal of Environmental Engineering*, 141:04014078.

- Moore, K.D., M.D. Wojcik, R.S. Martin, C.C. Marchant, D.S. Jones, W.J. Bradford, G.E. Bingham, R.L. Pfeiffer, J.H. Prueger, and J.L. Hatfield. 2015b. Particulate-matter emission estimates from agricultural spring-tillage operations using LIDAR and inverse modeling. *Journal of Applied Remote Sensing*, 9:096066.

12/1/2017

X

William Bradford

Signed by: bbradford@campbellsci.com

Cassi Gurell

November 30, 2017

Cassi Gurell

Dear Mrs. Gurell,

I am writing to request permission to use the journal article published by our group and identified below as a piece of my dissertation. As per Utah State University policy, all coauthors must grant permission to use each manuscript in a thesis/dissertation. If you agree, please sign below and return this document to me via email. Thank you for your time.

Kori

Kori Moore
Scientist
Space Dynamics Laboratory
1695 North Research Park Way
North Logan, UT 84341
kori.moore@sdl.usu.edu

I hereby grant permission to Kori Moore to use the following published journal article as part of his dissertation:

- Moore, K.D., E. Young, C. Gurell, M.D. Wojcik, R.S. Martin, G.E. Bingham, R.L. Pfeiffer, J.H. Prueger, J.L. Hatfield. 2014. Ammonia measurements and emissions from a California dairy using point and remote sensors. Transactions of the ASABE, 57:181-198.

X

Cassi Gurell

Jerry Hatfield

November 30, 2017

Jerry Hatfield, PhD
Laboratory Director
National Laboratory for Agriculture and the Environment
2110 North University Boulevard
Ames, IA 50011

Dear Dr. Hatfield,

I am writing to request permission to use the journal articles published by our group and identified below as pieces of my dissertation. As per Utah State University policy, all coauthors must grant permission to use each manuscript in a thesis/dissertation. If you agree, please sign below and return this document to me via email. Thank you for your time.

Kori

Kori Moore
Scientist
Space Dynamics Laboratory
1695 North Research Park Way
North Logan, UT 84341
kori.moore@sdl.usu.edu

I hereby grant permission to Kori Moore to use the following published journal articles as part of his dissertation:

- Moore, K.D., M.D. Wojcik, R.S. Martin, C.C. Marchant, G.E. Bingham, R.L. Pfeiffer, J.H. Prueger, and J.L. Hatfield. 2013. Particulate emissions calculations from fall tillage operations using point and remote sensors. *Journal of Environmental Quality*, 42:1029-1038.
- Moore, K.D., E. Young, C. Gurell, M.D. Wojcik, R.S. Martin, G.E. Bingham, R.L. Pfeiffer, J.H. Prueger, J.L. Hatfield. 2014. Ammonia measurements and emissions from a California dairy using point and remote sensors. *Transactions of the ASABE*, 57:181-198.

- Moore, K.D., R.S. Martin, W.J. Bradford, C.C. Marchant, D.S. Jones, M.D. Wojcik, R.L. Pfeiffer, J.H. Prueger, and J.L. Hatfield. 2015a. Derivation and use of simple relationships between aerodynamic and optical aerosol measurements. *Journal of Environmental Engineering*, 141:04014078.
- Moore, K.D., M.D. Wojcik, R.S. Martin, C.C. Marchant, D.S. Jones, W.J. Bradford, G.E. Bingham, R.L. Pfeiffer, J.H. Prueger, and J.L. Hatfield. 2015b. Particulate-matter emission estimates from agricultural spring-tillage operations using LIDAR and inverse modeling. *Journal of Applied Remote Sensing*, 9:096066.
- Moore, K.D., R.S. Martin, M.D. Wojcik, B. Auvermann, J.H. Prueger, J.L. Hatfield. Using a deposition-enabled backward Lagrangian stochastic model to estimate particulate matter area source emissions through inverse modeling. *Atmospheric Environment*, submitted.

JERRY
X HATFIELD

Digitally signed by JERRY
HATFIELD
Date: 2017.12.05 20:05:31
-06'00'

Dr. Jerry Hatfield

Derek Jones

November 30, 2017

Derek Jones
Campbell Scientific, Inc.
815 West 1800 North
Logan, UT 84321

Dear Mr. Jones,

I am writing to request permission to use the journal articles published by our group and identified below as pieces of my dissertation. As per Utah State University policy, all coauthors must grant permission to use each manuscript in a thesis/dissertation. If you agree, please sign below and return this document to me via email. Thank you for your time.

Kori

Kori Moore
Scientist
Space Dynamics Laboratory
1695 North Research Park Way
North Logan, UT 84341
kori.moore@sdl.usu.edu

I hereby grant permission to Kori Moore to use the following published journal articles as part of his dissertation:

- Moore, K.D., R.S. Martin, W.J. Bradford, C.C. Marchant, D.S. Jones, M.D. Wojcik, R.L. Pfeiffer, J.H. Prueger, and J.L. Hatfield. 2015a. Derivation and use of simple relationships between aerodynamic and optical aerosol measurements. *Journal of Environmental Engineering*, 141:04014078.

- Moore, K.D., M.D. Wojcik, R.S. Martin, C.C. Marchant, D.S. Jones, W.J. Bradford, G.E. Bingham, R.L. Pfeiffer, J.H. Prueger, and J.L. Hatfield. 2015b. Particulate-matter emission estimates from agricultural spring-tillage operations using LIDAR and inverse modeling. *Journal of Applied Remote Sensing*, 9:096066.

X

Derek Jones

Christian Marchant

November 30, 2017

Christian Marchant, PhD

Dear Dr. Marchant,

I am writing to request permission to use the journal articles published by our group and identified below as pieces of my dissertation. As per Utah State University policy, all coauthors must grant permission to use each manuscript in a thesis/dissertation. If you agree, please sign below and return this document to me via email. Thank you for your time.

Kori

Kori Moore
Scientist
Space Dynamics Laboratory
1695 North Research Park Way
North Logan, UT 84341
kori.moore@sdl.usu.edu

I hereby grant permission to Kori Moore to use the following published journal articles as part of his dissertation:

- Moore, K.D., M.D. Wojcik, R.S. Martin, C.C. Marchant, G.E. Bingham, R.L. Pfeiffer, J.H. Prueger, and J.L. Hatfield. 2013. Particulate emissions calculations from fall tillage operations using point and remote sensors. *Journal of Environmental Quality*, 42:1029-1038.
- Moore, K.D., R.S. Martin, W.J. Bradford, C.C. Marchant, D.S. Jones, M.D. Wojcik, R.L. Pfeiffer, J.H. Prueger, and J.L. Hatfield. 2015a. Derivation and use of simple relationships between aerodynamic and optical aerosol measurements. *Journal of Environmental Engineering*, 141:04014078.
- Moore, K.D., M.D. Wojcik, R.S. Martin, C.C. Marchant, D.S. Jones, W.J. Bradford, G.E. Bingham, R.L. Pfeiffer, J.H. Prueger, and J.L. Hatfield. 2015b. Particulate-matter emission estimates from agricultural spring-tillage operations using LIDAR and inverse modeling. *Journal of Applied Remote Sensing*, 9:096066.

X

Dr. Christian Marchant

Analyst
US Dept. of Defense

Richard Pfeiffer

November 30, 2017

Richard Pfeiffer, PhD
Chemist, Retired
National Laboratory for Agriculture and the Environment
2110 North University Boulevard
Ames, IA 50011

Dear Dr. Pfeiffer,

I am writing to request permission to use the journal articles published by our group and identified below as pieces of my dissertation. As per Utah State University policy, all coauthors must grant permission to use each manuscript in a thesis/dissertation. If you agree, please sign below and return this document to me via email. Thank you for your time.

Kori

Kori Moore
Scientist
Space Dynamics Laboratory
1695 North Research Park Way
North Logan, UT 84341
kori.moore@sdl.usu.edu

I hereby grant permission to Kori Moore to use the following published journal articles as part of his dissertation:

- Moore, K.D., M.D. Wojcik, R.S. Martin, C.C. Marchant, G.E. Bingham, R.L. Pfeiffer, J.H. Prueger, and J.L. Hatfield. 2013. Particulate emissions calculations from fall tillage operations using point and remote sensors. *Journal of Environmental Quality*, 42:1029-1038.
- Moore, K.D., E. Young, C. Gurell, M.D. Wojcik, R.S. Martin, G.E. Bingham, R.L. Pfeiffer, J.H. Prueger, J.L. Hatfield. 2014. Ammonia measurements and emissions from a California dairy using point and remote sensors. *Transactions of the ASABE*, 57:181-198.

- Moore, K.D., R.S. Martin, W.J. Bradford, C.C. Marchant, D.S. Jones, M.D. Wojcik, R.L. Pfeiffer, J.H. Prueger, and J.L. Hatfield. 2015a. Derivation and use of simple relationships between aerodynamic and optical aerosol measurements. *Journal of Environmental Engineering*, 141:04014078.
- Moore, K.D., M.D. Wojcik, R.S. Martin, C.C. Marchant, D.S. Jones, W.J. Bradford, G.E. Bingham, R.L. Pfeiffer, J.H. Prueger, and J.L. Hatfield. 2015b. Particulate-matter emission estimates from agricultural spring-tillage operations using LIDAR and inverse modeling. *Journal of Applied Remote Sensing*, 9:096066.

John Prueger

November 30, 2017

John Prueger, PhD
Research Soil Scientist
National Laboratory for Agriculture and the Environment
2110 North University Boulevard
Ames, IA 50011

Dear Dr. Prueger,

I am writing to request permission to use the journal articles published by our group and identified below as pieces of my dissertation. As per Utah State University policy, all coauthors must grant permission to use each manuscript in a thesis/dissertation. If you agree, please sign below and return this document to me via email. Thank you for your time.

Kori

Kori Moore
Scientist
Space Dynamics Laboratory
1695 North Research Park Way
North Logan, UT 84341
kori.moore@sdl.usu.edu

I hereby grant permission to Kori Moore to use the following published journal articles as part of his dissertation:

- Moore, K.D., M.D. Wojcik, R.S. Martin, C.C. Marchant, G.E. Bingham, R.L. Pfeiffer, J.H. Prueger, and J.L. Hatfield. 2013. Particulate emissions calculations from fall tillage operations using point and remote sensors. *Journal of Environmental Quality*, 42:1029-1038.
- Moore, K.D., E. Young, C. Gurell, M.D. Wojcik, R.S. Martin, G.E. Bingham, R.L. Pfeiffer, J.H. Prueger, J.L. Hatfield. 2014. Ammonia measurements and emissions from a California dairy using point and remote sensors. *Transactions of the ASABE*, 57:181-198.

- Moore, K.D., R.S. Martin, W.J. Bradford, C.C. Marchant, D.S. Jones, M.D. Wojcik, R.L. Pfeiffer, J.H. Prueger, and J.L. Hatfield. 2015a. Derivation and use of simple relationships between aerodynamic and optical aerosol measurements. *Journal of Environmental Engineering*, 141:04014078.
- Moore, K.D., M.D. Wojcik, R.S. Martin, C.C. Marchant, D.S. Jones, W.J. Bradford, G.E. Bingham, R.L. Pfeiffer, J.H. Prueger, and J.L. Hatfield. 2015b. Particulate-matter emission estimates from agricultural spring-tillage operations using LIDAR and inverse modeling. *Journal of Applied Remote Sensing*, 9:096066.
- Moore, K.D., R.S. Martin, M.D. Wojcik, B. Auvermann, J.H. Prueger, J.L. Hatfield. Using a deposition-enabled backward Lagrangian stochastic model to estimate particulate matter area source emissions through inverse modeling. *Atmospheric Environment*, submitted.

X

Dr. ~~John~~ Prueger

Emyrei Young

November 30, 2017

Emyrei Young

Dear Mrs. Young,

I am writing to request permission to use the journal article published by our group and identified below as a piece of my dissertation. As per Utah State University policy, all coauthors must grant permission to use each manuscript in a thesis/dissertation. If you agree, please sign below and return this document to me via email. Thank you for your time.

Kori

Kori Moore
Scientist
Space Dynamics Laboratory
1695 North Research Park Way
North Logan, UT 84341
kori.moore@sdl.usu.edu

I hereby grant permission to Kori Moore to use the following published journal article as part of his dissertation:

- Moore, K.D., E. Young, C. Gurell, M.D. Wojcik, R.S. Martin, G.E. Bingham, R.L. Pfeiffer, J.H. Prueger, J.L. Hatfield. 2014. Ammonia measurements and emissions from a California dairy using point and remote sensors. Transactions of the ASABE, 57:181-198.

Emyrei Young

Appendix D: List of Acronyms and Symbols

3D	Three dimensional
α	Noon-time albedo, unitless fraction
β	Bowen ratio, unitless ; solar elevation angle above the horizon
β_{cr}	Critical solar elevation angle
Δt	Time step in LS, sec
Δt_p	Time step in LS for particles, sec
ϵ	Turbulent kinetic energy dissipative rate
η	Control efficiency, unitless
θ	Average wind direction, °; potential temperature
θ^*	Turbulent temperature scale, K
κ	Matrix conditioning number
λ	Wavelength, units vary
ρ, ρ	Air density, kg m ⁻³
ρ_p, ρ_p	Particle density, kg m ⁻³
σ (also SD)	Standard deviation, units vary
σ_θ	Standard deviation of potential temperature
σ_{SB}	Stefan-Boltzmann constant, 5.67 x 10 ⁻⁸ W m ⁻² K ⁻⁴
$\sigma_u, \sigma_v, \sigma_w$	Standard deviation of instantaneous wind velocity in x, y, and z directions
τ_L	Lagrangian time scale, sec
$\varphi(z/L)$	Correction term for stability in wind speed profile equation
μg	Microgram = 1x10 ⁻⁶ g
μm	Micrometer = 1x10 ⁻⁶ m
°	Degrees
a	Constant, -0.1 K ⁻¹
A_i	Area of pen i
a_i	Variables for $i = u, v,$ and w in the LPDM equations
a_{dep}	Scalar multiplier for Q_{calc} to account for depositions in bLS
A_{src}	Area of an area source
AERMET	Meteorological preprocessor for AERMOD
AERMOD	American Meteorological Society/EPA Regulatory Model
AGL, agl	Above ground level
AQ, AQT	Air quality trailer

ARB	State of California, Air Resources Board
ARS	Agricultural Research Service, USDA
ASAE, ASABE	American Society of Agricultural and Biological Engineers
AU	Animal unit
Avg	Average
b	Calculated based on fraction of α , unitless
b_i	Variables for $i = u, v$, and w in the LPDM equations
bLS	backward Lagrangian stochastic dispersion model
BMP	Best management practice
$C, ^\circ\text{C}$	Degrees Celsius
C	Concentration of a pollutant
C_0	Constant in equation for b in LS model
c_1	Constant, $5.31 \text{ W m}^{-2} \text{ K}^{-6}$
c_2	Constant, 60 W m^{-2}
$C_{downwind}, C_{meas}$	Concentration measured downwind of a source
C_p	Specific heat of air at constant pressure, $\text{J kg}^{-1} \text{ K}^{-1}$
C_{sim}	Concentration predicted by an air dispersion model
C_{upwind}, C_B	Concentration measured upwind of a source
CCF	Counting correction factor
CCV	Continuous calibration verification sample
CFR	U.S. Code of Federal Regulations
CH_4	Methane
CI	Confidence interval
CIMIS	California Irrigation Management Information System
cm	Centimeter = $1 \times 10^{-2} \text{ m}$
CMP	Conservation management practice
CO	Carbon monoxide
CO_2	Carbon dioxide
CP	Crude protein, in a dairy cattle diet
d	Day
d_a, d_a	Aerodynamic particle diameter
d_k, d_k	Particle diameter of size k
d_{op}, d_{op}	Optical particle diameter
d_p	Physical particle diameter
DM	Dry matter

EC	Elemental carbon
EF	Emission factor, various units
EF_{CMP}	Summed EF for a CMP
EF_{COT}	Summed EF for combined operations tillage CMP
EF_{CT}	Summed EF for conventional tillage management practice
EF_{ST}	Summed EF for strip-till tillage CMP
EPA	U.S. Environmental Protection Agency
ER	Emission rate, various units
f	Initial estimate of pen NH ₃ emissions; Δt adjustment factor for particles
fLS	Forward Lagrangian stochastic dispersion model
FRM	Federal Reference Method
G	Probability of particle deposition
g	Gram
g, g	Constant acceleration due to gravity, $m\ s^{-2}$
GMD	Geometric mean diameter, μm
GPS	Global positioning system
H	Heat flux, $W\ m^{-2}$
ha	Hectare = $1 \times 10^4\ m^2$
Hg	Mercury
H ₂ SO ₄	Sulfuric acid
h, hr	Hour
hr _{tractor}	Hour of tractor operation
H ₂ S	Hydrogen sulfide
IC	Ion chromatography
IMPROVE	Interagency Monitoring of Protected Visual Environments
IOP	Intensive operating period
IQR	Interquartile range
IR	infrared
J	Joule,
k	Placeholder for various particle diameters
K	Degrees Kelvin
kg	kilogram
kHz	kilohertz = $1 \times 10^{-3}\ sec$
km	Kilometer = $1 \times 10^3\ m$

L	Monin-Obukov length, m
L	Liter
lidar	Light detection and ranging
LMS	Liquid manure system
LS	Lagrangian stochastic dispersion model
M	Upper size bin for calculating volume from a PSD
m	Size bin indicator
m_i	Animal occupancy in pen i
m	Meter
M_E	Manure excreted
Max	Maximum
MCF	Mass conversion factor
MCF_k	MCF for k size fraction
MDL	Method detection limit
MFE	Marked fluid element
mg	Milligram = 1×10^{-3} g
Min	Minimum
min	Minute
mm	Millimeter = 1×10^{-3} m
$N, n(d)$	Number concentration, units vary
N	Number of particles/MFEs released in LS model
\bar{N}	Average number concentration over a sample period
n	Number of samples
N	Nitrogen
N_{cc}	Fraction of cloud cover
N_E	Nitrogen excreted
NA	Not applicable
NAAQS	National Ambient Air Quality Standards
NAEMS	National Agriculture Emissions Monitoring Study
nd	No data
n_{dep}	Number of depositions recorded downwind of a touchdown within a source
Nd:YAG	Neodymium-doped yttrium aluminium garnet
NERL	National Exposure Research Laboratory
NH_3	Ammonia

NH_4NO_3	Ammonium nitrate
$(\text{NH}_4)_2\text{SO}_4$	Ammonium sulfate
nm	Nanometer = 1×10^{-9} m
NMHC	Non-methane hydrocarbon
NO_2	Nitrogen dioxide
NO_x	Oxides of nitrogen
N_2O	Nitrous oxide
NPO	No plumes observed
NRC	National Research Council
NRCS	National Resource Conservation Service, USDA
ns	Not significant, nonsignificant
n_{td}	Number of touchdowns logged within the source area of an LS
O_3	Ozone
OC	Organic carbon
OPC	Optical particle counter
OP-FTIR	Open path-Fourier transform infrared spectrometer
ρ	Dimensionless constant in wind speed power law
p_{ij}	Raw particle counts provided by OPC i for size channel j
Pb	Lead
PM	Particulate matter
PM_1	PM with $d_a \leq 1 \mu\text{m}$
$\text{PM}_{2.5}$	PM with $d_a \leq 2.5 \mu\text{m}$
PM_{10}	PM with $d_a \leq 10 \mu\text{m}$
PM_k	Cumulative PM for particles with $d_a \leq k$
ppb, ppbv	Parts per billion volume
PSD	Particle size distribution
PSL	Polystyrene latex sphere
PST	Pacific standard time
q	Flow rate, units vary
Q	Emission rate, emissions
Q_{area}	ER from an area source
$Q_{calc}, Q_{meas},$ $Q_{calc,dep}$	Calculated ER
QLMS	
$Q_{m, count}$	ER per PSD bin m , counts per volume or area per time

$Q_{PM2.5}$	ER for $PM_{2.5}$
Q_{PM10}	ER for PM_{10}
Q_{PMk}	ER for PM_k
Q_{sim}	ER used in an air dispersion model
Q_{vol}	ER from a volume source
QA	Quality assurance
QC	Quality control
r	Correlation coefficient
R	Lidar range bin
R_i	Independent random numbers in LPDM equations for $i = u, v,$ and w
R^2	Coefficient of determination
RARE	Regionally Applied Research Effort
R_c	Calibration range for lidar
RH	Relative humidity, %
RSD	Relative standard deviation, %
S	Number of LS sources used to model emissions from an operation
s, sec	Seconds
SD (also σ)	Standard deviation
SDL	Space Dynamics Laboratory
SJV	San Joaquin Valley
SJVAPCD	SJV Air Pollution Control District
SO_2	Sulfur dioxide
SO_x	Oxides of sulfur
t	Sample time, units vary
T, T_a, T_{amb}	Ambient temperature, C
TAN	Total ammonical nitrogen concentration
TSP	Total suspended particulate
u'	Instantaneous wind velocity in x direction or measured wind velocity
u^*	Shear velocity, $m\ s^{-1}$
u_0	Period wind speed scale
ucr	Critical wind speed
$\bar{u}(z), U(z)$	Period average wind speed at height z
UDAQ	State of Utah, Division of Air Quality
USDA	U.S. Department of Agriculture

USEPA, U.S. EPA	U.S. Environmental Protection Agency
USU	Utah State University
UWRL	Utah Water Research Laboratory
V	Particle volume concentration; period average wind velocity in y direction
v'	Instantaneous velocity in y direction
V_k	Cumulative volume of particles with $d_{op} \leq k$
v_s	Particle settling velocity, $m\ s^{-1}$
V_{sens}	Volume of the sensors in LS model
V_{src}	Volume of the source in LS model
VOC	Volatile organic compounds
W	Period average vertical wind velocity
w'	Instantaneous vertical wind velocity
w_i	Instantaneous vertical wind velocity of MFE/particle i that touched down within a source area
x	Along-wind position
y	Cross-wind position
yr	Year
z	Vertical position
z_0	Surface roughness
z_{rel}	Particle/MFE release height in LS model

Appendix E: Vitae

KORI D. MOORE

August 2017

CURRENT POSITION*Scientist*Space Dynamics Laboratory
North Logan, UT 84341Phone: (435) 713-3848
Mobile: (435) 890-8306
Email: kori.moore@sdl.usu.eduEDUCATION

- | | | |
|-----------|---|------|
| Ph.D. | Civil and Environmental Engineering
UTAH STATE UNIVERSITY, Logan, UT
2010 Utah State University Research Foundation Ph.D. Tomorrow Fellowship
<u>Dissertation</u> : Measurement of Agriculture Related Air Pollutant Emissions using Point and Remote Sensors | 2017 |
| M.S./B.S. | Civil and Environmental Engineering (Concurrent Program)
UTAH STATE UNIVERSITY, Logan, UT
M.S. Thesis: Derivation of Agricultural Gas-Phase Ammonia Emissions and Application to the Cache Valley
B.S. Design Projects
Senior Thesis: Feasibility Study of Constructing a Spawning and Rearing Channel on the Virgin River for Woundfin Minnow Population Restoration
Air Quality Management: Feasibility Study of Implementing a Vehicle Inspection and Maintenance Program in Cache County, UT | 2007 |

RELEVANT EMPLOYMENT HISTORY

- 2007 - Pres. Space Dynamics Laboratory and Energy Dynamics Laboratory
Utah State University Research Foundation
North Logan, UT
Scientist, Civil/Environmental Engineer

- 2005 - 2007 Utah Water Research Laboratory
Utah State University
Logan, UT
Research Assistant
- 2003 - 2005 Summer Undergraduate Research Experience (SURE)
Global Change Education Program
Summers 2004, 2005 Aerodyne Research, Inc.
Billerica, MA
Summer 2003 Pacific Northwest National Laboratory
Richland, WA
SURE Fellow
- 2002 - 2005 Utah Water Research Laboratory
Utah State University
Logan, UT
Research Technician

TEACHING EXPERIENCE

- Air Pollution Control – 23 lectures
Environmental Impacts of Agriculture Systems – 1 lecture
Environmental Management – 4 lectures

AWARDS

- 2011 Utah State University Research Foundation Achievement Award
2010 Rocky Mountains Section, Air & Waste Management Association, Scholarship
2010 Utah State University Research Foundation Ph.D. Tomorrow Fellowship
3rd Place, 2011 ASABE International Symposium on Erosion and Landscape Evolution,
Student Poster Competition.
1st Place, Annual AWMA Undergraduate Paper and Poster Competition, 2004 and 2005
Utah State University Blue Light Award, October 2004

SOFTWARE/CODING LANGUAGES

ArcGIS	MODTRAN	Windows	MS Office
MATLAB	AERMOD View	Linux	CAMx
Simulink	CALPUFF View	C/C++	GrADS

CERTIFICATES/TRAINING

Atmospheric Codes (MODTRAN, FASCODE, and HITRAN) for Sensor Development and Evaluation, SPIE Short Course, April 2015

Atmospheric Lidar Engineering, Georgia Tech Research Institute, 2014

Hazardous Waste Operations and Emergency Response, May 2013

CAMx Training, ENVIRON, June 2012

Technical Management Institute, Krannert School of Management, Purdue University, Oct. 2011

AERMOD Dispersion Modeling Course, Lakes Environmental, May 2009

CALPUFF Dispersion Modeling Course, Lakes Environmental, May 2009

AFFILIATIONS

Air and Waste Management Association, since 2004

American Association for Aerosol Research, since 2007

American Geophysical Union, since 2009

American Society of Agricultural and Biological Engineers, since 2007

Cache County PM_{2.5} SIP Development Workgroup, 2011-12

SPIE, since 2015

PEER REVIEWER

Archives of Agronomy and Soil Science

Atmospheric Environment

Journal of Atmospheric and Oceanic Technology

Journal of Environmental Quality

Journal of Environmental Sciences

PEER REVIEWED ARTICLES

- Moore, K.D., R.S. Martin, M.D. Wojcik, B. Auvermann, J.H. Prueger, J.L. Hatfield. Using a deposition-enabled backward Lagrangian stochastic model to estimate particulate matter area source emissions through inverse modeling. *Atmos. Environ.*, submitted.
- Moore, K.D., M.D. Wojcik, R.S. Martin, C.C. Marchant, D.S. Jones, W.J. Bradford, G.E. Bingham, R.L. Pfeiffer, J.H. Prueger, and J.L. Hatfield. 2015. Particulate-matter emission estimates from agricultural spring-tillage operations using LIDAR and inverse modeling. *J. Appl. Remote Sens.*, 9:096066.
- Moore, K.D., R.S. Martin, W.J. Bradford, C.C. Marchant, D.S. Jones, M.D. Wojcik, R.L. Pfeiffer, J.H. Prueger, and J.L. Hatfield. 2015. Deriving simple empirical relationships between aerodynamic and optical particulate matter measurements and their application. *J. Environ. Eng.*, 141:04014078.
- Moore, K.D., E. Young, C. Gurell, M.D. Wojcik, R.S. Martin, G.E. Bingham, R.L. Pfeiffer, J.H. Prueger, and J.L. Hatfield. 2014. Ammonia measurements and emissions from a California dairy using point and remote sensors. *Trans. ASABE*, 57:181-198.
- Williams, L.R., L.A. Gonzalez, J. Peck, D. Trimborn, J. McInnis, M.R. Farrar, K.D. Moore, J.T. Jayne, W.A. Robinson, D.K. Lewis, T.B. Onasch, M.R. Canagaratna, A. Trimborn, M.T. Timko, G. Magoon, R. Deng, D. Tang, E. de la Rosa Blanco, A.S.H. Prévôt, K.A. Smith, and D.R. Worsnop. 2013. Characterization of an aerodynamic lens for transmitting particles greater than 1 micrometer in diameter into the Aerodyne aerosol mass spectrometer. *Atmos. Measur. Tech.*, 6:3271-3280.
- Moore, K.D., M.D. Wojcik, R.S. Martin, C.C. Marchant, G.E. Bingham, R.L. Pfeiffer, J.H. Prueger, and J.L. Hatfield. 2013. Particulate emissions calculations from fall tillage operations using point and remote sensors. *J. Environ. Qual.*, 42:1029-1038.
- Marchant, C.C., K.D. Moore, M.D. Wojcik, R.S. Martin, R.L. Pfeiffer, J.H. Prueger, and J.L. Hatfield. 2011. Estimation of dairy particulate matter emission rates by lidar and inverse modeling. *Trans. ASABE*, 54:1453-1463.
- Rogers, P.C., K.D. Moore, and R.J. Ryel. 2009. Aspen succession and nitrogen loading: a case for epiphytic lichen as bioindicators in the Rocky Mountains, USA. *J. Veg. Sci.*, 20: 498-510.

- Bingham, G.E., C.C. Marchant, V.V. Zavyalov, D.J. Ahlstrom, K.D. Moore, D.S. Jones, T.D. Wilkerson, L.E. Higgs, R.S. Martin, P.J. Silva, and J.L. Hatfield. 2009. Lidar based emissions measurements at the whole facility scale: method and error analysis. *J. Appl. Remote Sens.*, 3: 033510.
- Zavyalov, V.V., C.C. Marchant, G.E. Bingham, T.D. Wilkerson, J.L. Hatfield, R.S. Martin, P.J. Silva, K.D. Moore, J. Swasey, D.J. Ahlstrom, and T.L. Jones. 2009. Aglite lidar: calibration and retrievals of well characterized aerosols from agricultural operations using a three-wavelength elastic lidar. *J. Appl. Remote Sens.*, 3: 033522.
- Martin, R.S., P.J. Silva, K. Moore, M. Erupe, and V.S. Doshi. 2008. Particle composition and size distributions in and around a deep pit swine operation, *J. Atmos. Chemistry*, 59:135-150.
- Liu, P.S.K., R. Deng, K.A. Smith, L.R. Williams, J.T. Jayne, M.R. Canagaratna, K. Moore, T.B. Onasch, D.R. Worsnop, and T. Deshler. 2007. Transmission efficiency of an aerodynamic focusing lens system: comparison of model calculations and laboratory measurements for the Aerodyne aerosol mass spectrometer. *Aerosol Sci. & Tech.*, 41:721-733.

PROCEEDINGS/REPORTS

- Moore, K., A. Bird, M. Wojcik, and R. Lemon. 2015. "Compact Eyesafe Lidar System (CELiS), rapid detection and quantification of fugitive particulate emissions using a 1.5 μm wavelength lidar," Paper #58, presented at the A&WMA 108th Annual Conference and Exhibition, Raleigh, NC, June 2015.
- Bird, A., K. Moore, M. Wojcik, R. Lemon, and A. Weibe. 2015. "Single-wavelength lidar retrieval algorithm of particulate matter concentration using CELiS (compact eyesafe lidar system) a 1.5 μm elastic lidar system," Paper #9455-18, presented at the 2015 SPIE DSS Conference, Baltimore, MD, April 2015.
- Moore, K., M. Wojcik, R. Martin, R. Pfeiffer, J. Prueger, J. Hatfield. 2013. "Application of a backwards Lagrangian stochastic model to Lidar data to estimate particulate matter emissions," Paper EW1A.5 in Renewable Energy and the Environment, OSA Technical Digest (online), Optical Society of America.
- Wojcik, M.D., R.S. Martin, K. Moore, J.L. Hatfield, J.H. Prueger. 2012. "Lidar based particulate flux measurements of agricultural field operations," Paper # EM4C.3

in *Renewable Energy and the Environment Optics and Photonics Congress*, Eindhoven, Netherlands, November 2012.

- Moore, K.D., M.D. Wojcik, C.C. Marchant, R.S. Martin, E. Young, R.L. Pfeiffer, J.H. Prueger, J.L. Hatfield. 2012. "Emissions calculated from particulate matter and gaseous ammonia measurements from a commercial dairy in California, USA," Paper #ILES12-2246 in *9th International Livestock Environment Symposium*, Valencia, Spain, July 2012.
- Wojcik, M., J. Hatfield, R. Martin, K. Moore, R. Pfeiffer, J. Prueger. 2012. Aglite: A 3-wavelength lidar system for quantitative assessment of agricultural air quality and whole facility particulate emissions," Paper #ILES12-1538 in *9th International Livestock Environment Symposium*, Valencia, Spain, July 2012.
- Wojcik, M.D., R.S. Martin, K. Moore, J.L. Hatfield, J.H. Prueger. 2012. "Lidar based particulate flux measurements of agricultural field operations," Paper # 83790G in M.D. Turner and G.W. Kamerman (eds.), *Proceedings of SPIE 8379, Laser Radar Technology and Applications XVII*, Baltimore, Maryland, April 2012.
- Moore, K.D., M.D. Wojcik, C.C. Marchant, R.S. Martin, R.L. Pfeiffer, J.H. Prueger, J.L. Hatfield. 2011. "Comparisons of measurements and predictions of PM concentrations and emission rates from a wind erosion event," Paper, Presentation, and Poster #11020, ASABE International Symposium on Erosion and Landscape Evolution, Anchorage, AK, September, 2011. – *3rd Place, Student Poster Competition*.
- Martin, R., K. Moore, M. Mansfield, S. Hill, K. Harper, H. Shorthill. Final Report: Uinta Basin Winter Ozone and Air Quality Study. EDL/11-039. Submitted to Uintah Impact Mitigation Special Service District.
- Wojcik, M.D., K.D. Moore, R.S. Martin, J. Hatfield. 2010. "Strategies for lidar characterization of particulates from point and area sources," in: C.M.U. Neale and A. Maltese (Ed.), *Proceedings of SPIE, Vol. 7824: Remote Sensing for Agriculture, Ecosystems, and Hydrology XII*. SPIE, Bellingham, WA. doi: 10.1117/12.865079.
- Zavyalov, V.V., G.E. Bingham, M. Wojcik, J.L. Hatfield, T.D. Wilkerson, R.S. Martin, C. Marchant, K. Moore, W. Bradford. 2010. "Integration of remote lidar and in-situ measured data to estimate particulate flux and emission from tillage operations," in : U.N. Singh and G. Pappalardo, (Ed.), *Proceedings of SPIE, Vol. 7832: Lidar Technologies, Techniques, and Measurements for Atmospheric Remote Sensing VI*. SPIE, Bellingham, WA. doi: 10.1117/12.865140.

- Wojcik, M.D., K.D. Moore, R.S. Martin. 2010. "Successful strategies for using lidar for particle characterization of point and diffuse area sources", Paper # 352, AWMA International Specialty Conference on Leapfrogging Opportunities for Air Quality Improvement, Xi'an, Shaanxi Province, China.
- Wojcik, M.D., G.E. Bingham, C.C. Marchant, V.V. Zavyalov, D.J. Ahlstrom, K.D. Moore, T.D. Wilkerson, L.E. Hipps, R.S. Martin, J.L. Hatfield, and J.H. Prueger. 2008. "Lidar based particulate flux measurements" Proceedings of the IEEE, IGARSS, Boston, MA: pp. IV, 263-266.
- Going, C., G. Bingham, N. Pougatchev, E. Day, K. Moore, R. Martin, and E. Reese. 2008. "Multi path FTIR agriculture air pollution measurement system," Paper Number 08, 2008 ASABE Annual International Meeting, Providence, RI, June, 2008.
- Martin, R.S., V.S. Doshi, and K. Moore. 2006. Determination of particulate (PM₁₀ and PM_{2.5}) and gas-phase ammonia (NH₃) emissions from a deep-pit swine operation using arrayed field measurements and inverse Gaussian plume modeling, pp. 890-894, in: Aneja, V.P. *et al.* (Ed.), Proceedings: Workshop on Agricultural Air Quality: State of the Science. Dept. of Communication Services, North Carolina State University, Raleigh, NC.
- Silva, P., R.S. Martin, V.S. Doshi, K. Moore, and M. Erupe. 2006. Variations in particle composition and size distributions in and around a deep pit swine operation, pp. 584-585, in: Aneja, V.P. *et al.* (Ed.), Proceedings: Workshop on Agricultural Air Quality: State of the Science. Dept. of Communication Services, North Carolina State University, Raleigh, NC.

PRESENTATIONS

- Moore, K., A. Bird, M. Wojcik, R. Lemon, A. Weibe, and J. Hatfield. 2015. "Compact Eyesafe Lidar System (CELiS), rapid detection and quantification of fugitive particulate emissions using a 1.5 μm wavelength lidar," paper #58, presented at the ASABE 2015 Annual International Meeting, New Orleans, LA, July 2015.
- Moore, K., M. Wojcik, R. Martin, J. Prueger, and J. Hatfield. "Application of a modified Lagrangian stochastic model to estimate particulate matter emissions from a dairy," paper #153, presented at A&WMA 108th Annual Conference and Exhibition, Raleigh, NC, June 2015.

- Moore, K. 2014. "Contributions of co-curricular summer research programs to my professional growth," poster #ED23E-3515, presented at the 2014 AGU Fall Meeting, San Francisco, CA, December 2014.
- Moore, K., A. Bird, M.D. Wojcik, R. Lemon, J. Hatfield. 2014. "CELiS (Compact Eyesafe Lidar System), a portable 1.5 μm elastic lidar system for rapid aerosol concentration measurement: Part 2, retrieval of particulate matter concentration," poster #A21D-3062, presented at the 2014 AGU Fall Meeting, San Francisco, CA, December 2014.
- Bird, A., M.D. Wojcik, K.D. Moore, R. Lemon, A. Weibe. 2014. "CELiS (Compact Eyesafe Lidar System), a portable 1.5 μm elastic lidar system for rapid aerosol concentration measurement: Part 1, instrument design and operation," poster # A21D-3061, presented at the 2014 AGU Fall Meeting, San Francisco, CA, December 2014.
- Moore, K., E. Young, C. Gurell, M. Wojcik, R. Martin, G. Bingham, R. Pfeiffer, J. Prueger, and J. Hatfield. "Ammonia measurements and emissions estimates from a California, USA dairy using both point and remote sensors," presentation #256-1, presented at the 2014 Agronomy Society of America, Crop Science Society of America, and Soil Science Society of America International Annual Meetings, Long Beach, CA, November 2014.
- Moore, K., M. Wojcik, A. Bird, R. Lemon. 2014. "CELiS: Compact Eyesafe Lidar System, a 1.5 μm elastic lidar system for aerosol measurement," presentation #12.IM.1, presented at the 33rd Annual AAAR Conference, Orlando, FL, October 2014.
- Martin, R., and K. Moore. "Wintertime Indoor and Outdoor $\text{PM}_{2.5}$ in Northern Utah's Cache Valley," poster #2.IA.11, presented at the 33rd Annual AAAR Conference, Orlando, FL, October 2014.
- Moore, K., M. Wojcik, R. Martin, R. Pfeiffer, J. Prueger, J. Hatfield. 2014. "Application of a modified backwards Lagrangian stochastic model to estimate particulate matter emissions from a dairy," presentation #141913971, 2014 ASABE Annual International Meeting, Montreal, Quebec, July, 2014.
- Moore, K., M. Wojcik, R. Martin, R. Pfeiffer, J. Prueger, J. Hatfield. 2013. "Application of a backwards Lagrangian stochastic model to estimate particulate matter emissions from Lidar data," poster #A31C-0065, 2013 AGU Fall Meeting, San Francisco, CA, December 2013.

- Moore, K., R. Martin, K. Harper, S. Lyman. 2012. "Wintertime distributed ozone measurements in Utah's Uintah Basin during UBWOS 2012," poster #A23B-0224, presented at the 2012 AGU Fall Meeting, San Francisco, CA, December 2012.
- Merkley, W., M. Wojcik, R. Martin, K. Moore. 2012. "Development and Validation of an Isokinetic Calibration System for Cross Correlation of Differing Aerosol Measurement Methodologies," poster #8.IM.7, presented at the 31st Annual AAAR Conference, Minneapolis, MN, October 2012.
- Banta, R.M., W.A. Brewer, R.S. Martin, K. Moore, G. Petron, C. Sweeney, A. Karion, D. Helmig, E.J. Williams, C.J. Senff, S.P. Sandberg, R.J. Alvarez, A.M. Weickmann, A.O. Langford, R.M. Hardesty, J.M. Roberts, A. Conley. 2012. "Wintertime high O₃ and local within-basin flows in the Uintah Basin in eastern Utah," presented at the 15th AMS Conference on Mountain Meteorology, Steamboat Springs, CO, August 2012.
- Moore, K.D., E. Young, R.S. Martin, M.D. Wojcik, R.L. Pfeiffer, J.H. Prueger, J.L. Hatfield. 2012. "Gaseous ammonia emissions estimated from measurements taken at a commercial dairy in California, USA," presentation #121337635, 2012 ASABE Annual International Meeting, Dallas, TX, July, 2012.
- Wojcik, M., J. Hatfield, R. Martin, K. Moore, R. Pfeiffer, J. Prueger. 2012. "Aglite: A 3-wavelength lidar system for quantitative assessment of agricultural air quality and whole facility particulate emissions," presentation #121337637, 2012 ASABE Annual International Meeting, Dallas, TX, July, 2012.
- Moore, K.D., C. Marchant, R.S. Martin, M.D. Wojcik, R.L. Pfeiffer, J.H. Prueger, J.L. Hatfield. 2012. "Particulate matter emission estimates for a commercial dairy in California, USA," presentation #121337636, 2012 ASABE Annual International Meeting, Dallas, TX, July, 2012.
- Martin, R.S., K.D. Moore, S. Hill, K. Harper. 2011. "Elevated wintertime ozone in Utah's Uinta Basin," presentation #A14B-08, AGU 2011 Fall Meeting, San Francisco, CA, December 2011.
- Wojcik, W., J. Hatfield, R. Martin, K. Moore, J. Prueger, C. Marchant. 2011. "Using multi-wavelength elastic lidar to quantify whole-facility PM emission rates," poster #A41B-0074, AGU 2011 Fall Meeting, San Francisco, CA, December 2011.
- Moore, K.D., R.S. Martin, S. Hill, H. Shorthill. 2011. "O₃, VOC, NO_x, PM_{2.5}, and meteorological measurements during an inversion episode in Utah's Uinta

- Basin,” poster #A51A-0261, 2011 AGU Fall Meeting, San Francisco, CA, December 2011.
- Wojcik, M., K. Moore, R. Martin, J. Hatfield. 2011. “Whole-facility particulate emissions measurement of a process water treatment facility using Aglite: A 3-wavelength elastic lidar,” presented at Optical Society of America Renewable Energy and the Environment Congress, Austin, TX, November 2011.
- Wojcik, M.D., K. Moore, C.C. Marchant, V.V. Zavyalov, R.S. Martin, J.L. Hatfield, J.H. Prueger. 2011. “Lidar based particulate flux measurement of agricultural field operations,” presented at Air Quality VIII International Conference on Carbon Management, Mercury, Trace Substances, Sox, NOx, and Particulate Matter, Washington, DC, October, 2011.
- Moore, K., R. Martin, M. Wojcik, R. Pfeiffer, J. Prueger, J. Hatfield. 2011. “Effects of various representations of temporally and spatially variable agricultural processes in air quality dispersion modeling,” presentation #1111847, 2011 ASABE Annual International Meeting, Louisville, KY, August, 2011.
- Wojcik, W., J. Hatfield, J. Prueger, R. Pfeiffer, K. Moore, R. Martin. 2010. “Aglite: A 3-wavelength lidar system for assessment of agricultural air quality, whole facility emission rates and fluxes,” poster # B33C-0422, AGU 2010 Fall Meeting, San Francisco, CA, December 2010.
- Moore, K., M. Wojcik, J. Jin, J. Hatfield. 2010. “High-Resolution WRF-Chem simulations of particulate matter emitted by different agricultural tillage under different weather conditions,” poster #A31C-0076, AGU 2010 Fall Meeting, San Francisco, CA, December 2010.
- Moore, K., R. Martin, W. Bradford, C. Marchant, M. Wojcik. 2010. “Deriving empirical relationships between aerodynamic and optical aerosol measurements”, poster #2.F.29, AAAR 29th Annual Conference, Portland, OR, October 2010.
- Moore, K., E. Reese, R. Martin, C. Marchant, M. Wojcik, C. Going, R. Pfeiffer, J. Prueger, J. Hatfield. 2010. “Preliminary ammonia measurements and emission calculation results from a California dairy”, poster #12, ASABE International Symposium on Air Quality and Manure Management for Agriculture, Dallas, TX.
- Marchant, C., K. Moore, M. Wojcik, R. Martin, R. Pfeiffer, J. Prueger, J. Hatfield. 2010. “Preliminary particulate matter measurements and emission calculation results from a California dairy”, poster #13, ASABE International Symposium on Air Quality and Manure Management for Agriculture, Dallas, TX.

- Moore, K., M. Wojcik, R. Martin, C. Marchant, D. Jones, J. Hatfield, R. Pfeiffer, J. Prueger, W. Bradford, V. Zavyalov, D. Ahlstrom, T. Jones, P. Silva, G. Bingham. 2010. "Particulate emissions from fall tillage operations as determined via inverse modeling and lidar mass balance techniques", presentation # 1009283, 2010 ASABE Annual International Meeting, Pittsburgh, PA.
- Moore, K., R. Martin, W. Bradford, D. Jones, M. Wojcik. 2009. "Comparisons and relationships between aerodynamic and optical aerosol measurements", poster # 3G.6, AAAR 28th Annual Conference, Minneapolis, MN, October, 2009.
- Price, D.J., R.S. Brown, K.D. Moore, P.J. Silva. 2009. "Measurement of particulate matter during dairy operations in California", poster # 3C.23, AAAR 28th Annual Conference, Minneapolis, MN, October, 2009.
- G.E. Bingham, R.S. Martin, V.V. Zavyalov, T.D. Wilkerson, C.C. Marchant, K. Moore, D. Jones, P. Silva, C. Going, J. Bowman, and N. Pougatchev. 2007. "Agricultural pollutant emissions determined via standard emission rate estimation methods and lidar techniques," presentation #17A.2, AAAR 26th Annual Meeting, Reno, NV, September, 2007.
- Bingham, G.E., T. Wilkerson, V. Zavyalov, J. Bowman, C. Marchant, K. Moore, R. Martin, P. Silva, L. Hipps, and J. Hatfield. 2007. "Integrated whole facility aerosol fluxes," presented at Western Dairy Air Quality Symposium, Las Vegas, NV, April, 2007.
- Martin, R.S., and K. Moore. 2006. "Seasonal and spatial distributions of ambient ammonia in the Cache Valley of northern Utah and southeastern Idaho," poster #A31C-0919, 2006 AGU Fall Meeting. San Francisco, CA, December, 2006.
- Moore, K. & V. Doshi. 2005. "Indoor/Outdoor particulate matter concentration and composition at four schools in the Cache Valley," presented at the Air & Waste Management Association's 98th Annual Conference, Student Poster/Paper Competition. Minneapolis, MN, June, 2005. - *1st Place, Undergraduate Division*
- Moore, K. 2004. Monitoring vertical temperature inversions in Utah's Cache Valley using HOBO[®] Temperature Sensors/Dataloggers. Presented at the Air & Waste Management Association's 97th Annual Conference, Student Poster/Paper Competition. Indianapolis, IN, June, 2004. - *1st Place, Undergraduate Division*